Characterization of the Chemical Properties of Intermediates in Furan Metabolism

A DISSERTATION
SUBMITTED TO THE FACULTY OF THE GRADUATE SCHOOL
OF THE UNIVERSITY OF MINNESOTA
BY

Martin Blake Phillips

IN PARTIAL FULFILLMENT OF THE REQUIREMENTS
FOR THE DEGREE OF
DOCTOR OF PHILOSOPHY

Dr. Lisa A. Peterson, Adviser

September 2012

Acknowledgments

I would like to acknowledge my parents, Seth Phillips and Lorraine Blake, for their examples and for their unending support of my educational pursuits; my twin brother Bevan for his humor and for the perseverance he's demonstrated in his own life; my sister Dara for our shared experience of finishing our dissertations together; and the rest of my family for their love and support. I would also like to acknowledge my best friends, Kathryn Haigh, Jennifer Nguyen, and Kendric Moore, for grounding and centering me.

Thanks go to Dr. Lisa A. Peterson, who guided me in my research and shared her expertise with me, and to my committee members for their generous time and encouragement: Dr. Stephen S. Hecht, Dr. Elizabeth A. Amin, and Dr. William A. Toscano. I would like to thank Dr. John Lipscomb and his graduate student Michael Mbughuni, along with Dr. Alon McCormick for assistance with the kinetic analysis. Many thanks go to Dr. Beverly Ostrowski, Dr. Youlin Xia, Dr. Letitia Yao, Todd Rappe, and all of the excellent NMR staff who helped me learn everything I know about these wonderfully powerful instruments. Thanks go also to Dr. Peter Villalta and Brock Matter for helping me with the mass spectrometers – I think I used every single one of them at one point or another. I'd like to give special acknowledgments to my fellow graduate students Ania Urban, Valerie Kramlinger, and Nicole Skinner, who were the best role models I could have asked for. Mathilde Sullivan also deserves special thanks, as she trained me on most of the techniques I used in my graduate career.

Finally, I'd like to thank my co-workers for making the Peterson Lab such an enjoyable place to work, the other researchers in the 7th floor of the Cancer Center for their extensive knowledge on every possible subject, and the University of Minnesota for serving as my home for the past nine years.

Chapter-Specific Acknowledgments

Chapter 2: We thank Patrick Kinney, Dr. Fekadu Kassie, and Dr. Michael Byrns for their assistance with the animal studies, Dr. Peter Villalta and Brock Matters for their assistance with the mass spectral analyses, Choua Vu for the synthesis of [$^{13}C_4$]furan and Meredith Cummings and Iman Hassan for their assistance in the preliminary characterization of the furan metabolites. We also thank Dr. Howard Towle, Dr. Douglas Mashek and their laboratories for their generous gift of Sprague-Dawley rat hepatocytes. The mass spectral analyses were performed in the Analytical Biochemical Core at the Masonic Cancer Center, University of Minnesota, which is funded by National Cancer Institute Center Grant CA-77598. This research is funded by ES-10577 from the National Institutes of Health.

Chapter 3: We thank Anna Urban, Patrick Kinney, Dr. Fekadu Kassie, and Dr. Michael Byrns for their assistance with the animal studies, Dr. Peter Villalta and Brock Matter for their assistance with the mass spectral analyses, Choua Vu for the synthesis of [$^{13}C_4$]furan, and Meredith Cummings and Iman Hassan for their assistance in the

preliminary characterization of the furan metabolites. The mass spectral analyses were performed in the Analytical Biochemical Core at the Masonic Cancer Center, University of Minnesota, which is funded by National Cancer Institute Center Grant CA-77598. NMR instrumentation was provided with funds from the NSF (BIR-961477), the University of Minnesota Medical School, and the Minnesota Medical Foundation. This research is funded by ES-10577 from the National Institutes of Health.

Chapter 4: We thank Dr. Beverly Ostrowski, Dr. Youlin Xia, Dr. Letitia Yao, and Todd Rappe for assistance with NMR. We also thank Dr. Peter Villalta and Brock Matter for help with mass spectrometry. Dr. John Lipscomb, Dr. Alon McCormick, and Michael Mbughuni provided invaluable advice regarding the kinetic analysis.

Chapter 5: We thank Dr. Peter Villalta for his assistance with the LTQ-Orbitrap Velos mass spectrometer and Thomas Krick for his assistance with the Bruker BioFlex III mass spectrometer. Dr. Peter Villalta and Valerie Kramlinger provided an invaluable orientation to the Proteome Discoverer software. We thank Jingjing Shen for her assistance with cytochrome *c* reaction and tryptic digestion

Dedication

This dissertation is dedicated to the members of my family who have fought cancer: my grandmother Kathryn, my aunt Carla, my uncles Rowland and Leland, my sister-in-law Angie, and my father Seth. You are the inspiration for what I do.

Table of Contents

List of Tables

List of Figures

List of Schemes

List of Abbreviations

BDA: *cis*-2-butene-1,4-dial; BDA hydrate: 2,5-dihydrofuran-2,5-diol; *bis*-2-GSH: L-*γ*-glutamyl-L-cysteinylglycine (2→1′)-sulfide with *N*-[4-carboxy-4-(2-mercapto-1*H*-pyrrol-1-yl)-1-oxobutyl]-L-cysteinylglycine; *bis*-3-GSH: L-*γ*-glutamyl-L-cysteinylglycine (2→1′)-sulfide with *N*-[4-carboxy-4-(3-mercapto-1*H*-pyrrol-1-yl)-1-oxobutyl]-L-cysteinylglycine; CHO: Chinese hamster ovary; CID: collision-induced dissociation; CNL: constant neutral loss; DCE: 1,1-dichloroethylene; DDE: *trans*,*trans*-2,4-decadienal; DTT: dithiothreitol; D_2O: deuterium oxide; GSH-BDA: 2-(*S*-glutathionyl)succinaldehyde; GSH pyrrolinone: *N*-[4-carboxy-4(*S*)-(2-oxo-2,5-dihydro-1*H*-pyrrol-1-yl)-1-oxobutyl]-L-cysteinylglycine; HNE: 4-hydroxy-2-nonenal; HRMS: High resolution mass spectrometry; LC-ESI^+-MS/MS: high performance liquid chromatography electrospray ionization (positive mode) tandem mass spectrometry; MALDI-TOF-MS: matrix-assisted laser desorption/ionization time-of-flight mass spectrometry; mCPBA: *m*-chloroperbenzoic acid; *mono*-GSH: *N*-[4-carboxy-4-(3-mercapto-1*H*-pyrrol-1-yl)-1-oxobutyl]-L-cysteinylglycinecyclic sulfide; NAC: *N*-acetyl-L-cysteine; NAL: N^{α}-acetyl-L-lysine; NOAEL: no observable adverse effect level; ONE: 4-oxo-2-nonenal; 3-4 NALpy: L-2-(acetylamino)-6-(2,5-dihydro-2-oxo-1*H*-pyrrol-1-yl)-1-hexanoic acid; 4-5 NALpy: L-2-(acetylamino)-6-(2,3-dihydro-2-oxo-1*H*-pyrrol-1-yl)-1-hexanoic acid; SRM: selective reaction monitoring; TFA: trifluoroacetic acid; THF: tetrahydrofuran; *trans*-BDA: (*E*)-4,4-dihydroxybut-2-enal; VDC: vinylidene chloride

Chapter 1: Introduction

Overview

Environmental carcinogens are a major public health concern and have received significant attention from scientists with a wide range of backgrounds. My graduate research has focused on one particular environmental carcinogen: furan. Furan is a known animal carcinogen.[1,2] Humans are exposed to furan from many sources, including cigarette smoke, other combustion sources, and food.[1] The United States National Toxicology Program (NTP) and the International Agency for Research on Cancer (IARC) have classified furan as a possible human carcinogen (Group IIB).[2,3] The human health effects of furan are currently unknown.[2] Furan itself is not a direct-acting carcinogen, as evidence suggests metabolism is required for its toxic effects.[4] The precise mechanism of action through which furan exerts its toxic and carcinogenic effects is still to be determined.

The primary target organ in rats and mice with furan treated by oral gavage is the liver.[1] Furan is metabolized by cytochrome P450 2E1 to *cis*-2-butene-1,4-dial (BDA), an α,β-unsaturated dialdehyde.[5] This *bis*-electrophile can react in many combinations with cellular nucleophiles, for instance by reacting in two sequential steps with a thiol and an amine to create a pyrrole cross-link.[6] Thirteen percent of a radiolabeled dose administered by gavage to rats was associated with liver protein after 24 hours, suggesting that furan covalently modifies liver proteins.[7] Another radiolabel study identified 83 distinct proteins that were modified by furan *in vivo*.[8] Analysis of the urine of furan-treated rats has identified the structures of degraded protein adducts including *N*-acetyl-*S*-[1-(5-amino-5-carboxypentyl)-1*H*-pyrrol-3-yl]-L-cysteine (a cross-link of *N*-

acetylcysteine and lysine via a pyrrole ring derived from the four carbons of BDA).[9] Protein adducts could potentially occur on any nucleophilic sidechain; BDA-only adducts such as lysine pyrrolinones are also possible.[10] Furan's carcinogenic and toxic effects are directly related to the chemical properties of its metabolites, as these properties dictate the target and establish the sequence of events between exposure and toxicity and/or carcinogenesis. Scheme 1-1 shows one hypothesized pathway of furan metabolism. This scheme shows the central position that BDA occupies in the various biotransformations that occur after furan exposure.

Understanding the complete mechanism of action of through which furan exerts its toxicological effects will require the identification and characterization of metabolites of furan. Since BDA has long been considered the principal reactive intermediate of furan in biological systems, study of its chemical properties will aid in identifying cellular targets. Further characterization of BDA and other metabolites will lead to a mechanism of action.

The rate of reaction of the bioactivated form of a xenobiotic has a direct influence on the types of toxicological events that are seen in biological systems. In the case of furan, Figure 1-1 shows a visual summary of current hypothesis of furan's route through the cell. At its core, it states that the site of damage is directly dependent on the kinetics and dynamics of the furan/hepatocyte system. These factors are a natural consequence of the chemical properties of the various intermediates. For instance, BDA is believed to react quickly with nucleophiles; however, there is no evidence that there is a significant level of mechanism-based inactivation of P450s that catalyze the furan-to-BDA oxidation step. BDA is thought to be released from the P450 active site, but is likely to be rapidly

intercepted by GSH in the cytosol.

Being a *bis*-electrophile, a single reaction between GSH and BDA to form a GSH-BDA intermediate is not sufficient to neutralize all of the reactive centers. This new electrophile has fewer sites at which it can react, moving it to a lower position when referring to Figure 1-1. If this new intermediate is only slightly less reactive than BDA, it is likely that most of this intermediate reacts with proteins or other cellular molecules such as the free amines. If it is less reactive, it has the possibility to migrate to other organelles like the nucleus, the mitochondria, or the endoplasmic reticulum. If it is even less reactive, the possibility exists that the GSH-BDA intermediate might be able to escape the cell of origin and be distributed to sites distant from its formation. The GSH conjugates of structurally similar electrophiles, such as 4-hydroxy-2-nonenal (HNE), are exported from the cell via membrane transporters such as RLIP76.[11] GSH-BDA conjugates retaining their ability to modify nucleophiles could be exported by the same system to the bile canaliculi, which would be consistent with furan's adverse effects on cholangiocytes that lead to cholangiocarcinomas in rats. The impact of the chemical properties of furan and its intermediates on the kinetics of reaction are expected to have a major impact on the dynamics of the intermediates and the end products of metabolism. This impact is likely to be intimately related to the targets of furan toxicity and carcinogenic transformation.

Health Effects of Furan in Animals

Before it can be established how the chemical properties of furan and its intermediates lead to the health effects seen after exposure, it is first necessary to establish what these effects are. Furan has been classified as a known rodent carcinogen,

but its human health effects are still unknown.[2] Because of the lack of a clear occupational exposure cohort, the first step in establishing the potential human health effects of furan was to determine its health effects in other mammals. In 1993, the NTP published the results of its rodent studies on furan.[1] Studies of different durations were performed: 16 days, 13 weeks, and 2 years.[1] In the 16 day study, furan was found to be acutely toxic to both rats and mice; however, only rats in the highest dose groups showed furan-related liver lesions upon necropsy.[1] Toxic lesions of the liver were seen in the 13 week study in rats and mice of both sexes.[1] Rats were more sensitive than mice to the deleterious effects of furan.[1] The liver lesions included degeneration of the hepatocytes, cholangiofibrosis, and bile duct hyperplasia, among others.[1] These results show that furan is an acute and sub-chronic hepatotoxicant.

Rats in the two year study had dose-dependent increases in hepatocellular adenomas and carcinomas as well as mononuclear cell leukemias.[1] Additionally, all rats of both sexes showed a 100% incidence of cholangiocarcinomas at all doses tested (2, 4, and 8 mg/kg) and 0% in the control group (rates adjusted for intercurrent mortality).[1] Mice in the two year study also had dose-dependent increases in hepatocellular adenomas and carcinomas, as well as benign pheochromocytomas in their adrenal glands.[1] The report concluded that there is clear evidence that furan causes cancer in F344/N rats and $B6C3F_1$ mice of both sexes.[1]

The International Agency for Research on Cancer (IARC) included furan in their series "Monographs on the Evaluation of Carcinogenic Risk to Humans" volume #63 published in 1995.[2] They agreed with the conclusions of the NTP report two years prior, but the lack of any substantial evidence for a carcinogenic effect in humans prevented

furan from being listed as a known human carcinogen.[2] Nevertheless, because of the great potential for human exposure and the strong carcinogenic effect in rodents, furan was listed by both the NTP and IARC as a member of Group IIB, a possible human carcinogen.[2,3] The liver was identified as the primary target.[1,2] The IARC ranking system classifies chemicals and other potential carcinogens (such as radiation) on a scale from I to IV. Members of Group I are known human carcinogens, Group IIA contains probable human carcinogens, Group IIB (which includes furan) contains possible human carcinogens, Group III contains agents where there is inadequate or limited evidence of carcinogenity that prevents further classification, and Group IV contains agents that are probably not human carcinogens.

Recent carcinogenicity studies, some still in progress, have focused on lower doses of furan in rats.[12,13] One study looked at four doses: 0, 0.1, 0.5, and 2 mg/kg for 28 days.[12] The authors found no increase in oxidative damage as determined in an LC/MS assay of 8-oxo-2´-deoxyguanosine (8-oxo-dG), a DNA adduct and marker of oxidative stress.[12] Additionally, they found no changes in the metabolome as determined by either principal component analysis (PCA) or orthogonal projection to latent structure – discriminant analysis (OPLS-DA) of urine samples analyzed by NMR, no marked histopathological changes as determined by H&E stain or the TUNEL assay, and only small dose-dependent increases in unconjugated bile acids and serum cholesterol levels.[12] There was a dose-dependent increase in 5-bromo-2´-deoxyuridine incorporation in the subcapsular areas of the left and caudate lobes of the liver that reached statistical significance at the highest dose tested, suggesting that increased cell proliferation may contribute to the carcinogenic mechanism of action of furan.[12] The NTP has stated its

plan to perform another carcinogenesis assay of furan at lower doses than the original 1993 study.[13]

Another study focused on the carcinogenicity of lower doses of furan in mice.[14] The authors tested 1, 2, 4, and 8 mg/kg, as compared to 8 and 15 mg/kg in the NTP study.[1,14] They found furan-induced liver toxicity at all four doses tested, but a significant increase in tumors over the control animals was seen only at the 4 and 8 mg/kg levels.[14] This result suggests that there may be a threshold dose for tumorigenesis, which is usually associated with non-genotoxic or indirect genotoxic mechanisms of action.[14]

Furan exposure leads to toxicity and carcinogenesis in rodents, with the principal target being the liver.[1] Extending the dose/response curve to lower doses in both rats and mice will improve our understanding of its effects at more physiologically relevant exposures.

Exposure to Furan

A critical difference between hazard assessment and risk assessment is the extent to which humans are exposed to the substance of interest. Human exposure to furan is unavoidable and comes from a variety of sources. Furan is present as a by-product of incomplete combustion and is therefore present in wood smoke, automobile exhaust, cigarette smoke, and emissions from a deep-fat fryer.[2,3] It is also formed naturally in foods from precursors including reducing sugars and amino acids (alone or in combination), ascorbic acid, polyunsaturated fatty acids, and carotenoids.[15] The most efficient precursors at forming furan at 250 °C are (from most to least efficient): L-ascorbic acid, dehydroascorbic acid (pyrolysis temperature: 350 °C), and the combination

of glycolaldehyde/L-alanine.[16] Because these precursors are ubiquitous, furan is formed in almost all foods that are heat-treated.

The concentration of furan in foodstuffs may be accurately determined using gas chromatographic techniques.[17,18] Concentrations are highest in food that is heat-treated in closed containers, which prevents the furan from evaporating after it is formed. In adult food, the highest concentrations of furan were found in vegetable beef soup (88.0 ng/g), baked beans (84.2 ng/g), and brewed coffee (51.7 ng/g).[17] In infant food, the highest concentrations were found in sweet potatoes (80.3 ng/g), garden vegetables (75.5 ng/g), and squash (49.3 ng/g).[17] Adult exposure was estimated to be greatest from brewed coffee, at 0.15 μg/kg body weight/day.[17] Mean exposure from all food sources for men and women over two years of age was estimated to be 0.25 μg/kg body weight/day.[17] Infants who subsist entirely on formula may have relatively greater exposure because the concentration of furan in ready-to-feed formula averages 7.2 ng/g. A study by the European Food Safety Authority (EFSA) estimated the mean exposure for infants between 3-12 months old at 0.27-1.01 μg/kg body weight/day.[19] The results of the studies clearly show that humans are exposed to measureable levels of furan in their diet.

The level of exposure is not a simple weighted sum of the concentrations in various foodstuffs. Furan has a very high vapor pressure at room temperature of 700 mmHg (0.92 atm).[20] While the concentration of furan in food declines over time when placed in an open container, it remains detectable.[18] The concentration of furan in baby food was still about 50% of the starting concentration after 5.5 h when unheated, and was still approximately 15% of the starting concentration after 5.5 h when heated to about 75 °C.[18] While the concentration of furan in brewed coffee showed a sudden decrease when

simulating the act of pouring from a coffee pot into a cup, it was still well above the limit of detection.[18] The concentration of furan in food increased when heating the food in a closed container; however, it did not increase significantly when heating the food in an open container.[21] This is consistent with furan's high volatility. Because it is difficult to calculate exposure due to the wide variability between various foodstuffs and furan's tendency to evaporate, a biomarker-based approach would be very useful for calculating actual exposure levels.

Because of the attenuating factors involved in oral exposure from food, inhalation of cigarette smoke may be a significant route of exposure for many people. The average concentration in cigarettes was found to be 35.8 ± 6.4 μg/cigarette.[22] A pack-a-day smoker can therefore be expected to be exposed to 716 ± 128 μg furan/day. Unlike with food, smokers intentionally inhale the volatile components of cigarette smoke, presumably making the high vapor pressure less of an issue. Furan has been detected in the exhaled breath of both non-smokers (at 0-28 μg/hr) and smokers (at 0-98 μg/hr), indicating that this compound is eliminated through the lungs in humans exposed to it.[2]

Occupational exposure to furan is expected to be low, based on the National Occupational Hazard Survey (1972-1974) and the National Occupational Exposure Survey (1981-1983).[20] Furan is isolated in closed systems away from workers in industrial situations.[20] The lack of an easily identifiable high-exposure cohort makes it necessary to develop biomarkers before correlating pre-existing levels of exposure with adverse health effects.

Humans are exposed to furan via food and air. The mean levels adults are exposed to are approximately 10,000-fold less than a known carcinogenic dose of furan

in rats. A margin of exposure of this magnitude is generally considered concerning enough to justify additional research into the toxicological effects of a substance.[13]

Distribution and Metabolism

Furan's distribution and metabolism are a direct result of its kinetic and dynamic properties that are expected to play the central role in determining the targets of toxicity and carcinogenicity. Radiolabeled furan was used to determine the distribution of furan administered to rats by gavage. [2,5-^{14}C]Furan was administered to male F344/N rats by gavage and the elimination of the radiolabel was tracked for 24 h.[7] Forty percent of the radioactive dose was eliminated through the lungs, 26% as carbon dioxide and 14% as the parent compound.[7] Elimination through the urine and feces were roughly equal: 20% and 22%, respectively.[7] Nineteen percent of the dose had not been eliminated by the end of 24 h, 13% associated with the liver and the remaining 6% associated with other organs.[7]

The tissue-bound radioactivity was almost exclusively associated with the protein fraction, with no significant percentage of the dose associated with DNA.[7] The results of this study are consistent with the NTP carcinogenesis studies, with the primary target organ being the liver. Scheme 1-1 shows one possible pathway for furan biotransformation that is consistent with the results of the metabolism study. The results provide evidence that metabolism is a key step in determining furan's toxicity and carcinogenicity, since at least 67% of the radioactive dose was excreted as metabolites in the urine and feces or as carbon dioxide.

The metabolism of furan in the liver is considered to be crucial for understanding the toxicological effects of furan *in vivo*. This was originally hypothesized because 13%

of a radioactive dose of furan is still associated with the liver after 24 h, most of which was covalently associated with proteins, suggesting stable protein modifications are formed upon furan treatment.[7] As mentioned previously, furan is metabolized in the liver by cytochrome P450 2E1 (CYP2E1)[4] to form BDA.[5,23] BDA is an α,β-unsaturated dialdehyde that quickly forms a cyclic hydrate in aqueous solutions.[23] Metabolism is induced by acetone-pretreatment and inhibited by 1-phenylimidazole, supporting a role for the 2E1 isoform.[4,24] SKF525A, an inhibitor of many P450s but a poor inhibitor of 2E1, did not significantly reduce the extent of furan metabolism.[9,25]

The metabolism of furan has been extensively studied and has been strongly implicated in the toxicity of furan *in vitro*.[4-6,26-29] Bioactivation of furan in the liver by CYP2E1 is widely regarded as the initial step in furan metabolism and crucial for cytotoxicity and carcinogenesis.[20,23,24] Further metabolites are formed as a result of the intrinsic reactivity of BDA, which can react with nucleophiles in 1,2-addition (direct addition) or 1,4-addition (conjugate addition) (Scheme 1-2).[10] Sulfhydryl groups, such as those in GSH and *N*-acetyl-L-cysteine (NAC), prefer the 1,4-addition mode.[10] Primary amino groups, such as those in semicarbazide and lysine, prefer the 1,2-addition mode, most likely passing through an imine intermediate.[10,23] Reaction of BDA with an amine leads to the formation of a pyrrolinone ring, the thermodynamically favored isomer of which has the double bond conjugated with the carbonyl bond.[10,26] Initial reaction of BDA with a sulfhydryl, followed by a second reaction with a primary amine leads to products with a characteristic pyrrole ring structure.[6,10,26,29] We hypothesize, however, that additional metabolites of furan may exist as many metabolites will have either the pyrrolinone or pyrrole structure, with free polyamines and amino acids as well as lysine

residues in proteins serving as the primary amine donor. One of the principal goals of this work is to identify these additional metabolites.

An oral route of exposure directs furan directly to the liver, its principal toxicological target. The liver contains high levels of CYP2E1, the enzyme responsible for the furan-to-BDA transformation.[4] The reactive nature of BDA means that initial reaction with a nucleophile such as GSH leads to additional intermediates that are still electrophilic in character. These intermediates can go on to modify proteins, which may play a role in toxicity and cellular dysregulation.[9]

Chemistry of α,β-Unsaturated Carbonyl Compounds

Because the chemistry of furan's reactive intermediates plays an important role in determining its mechanism of action, it is useful to compare these intermediates to other substances with similar chemical properties. BDA is an α,β-unsaturated carbonyl compound, where the double bond of the alkene is conjugated to the double bond of two carbonyl oxygens. These compounds are extremely electrophilic. The most important nucleophiles in the cellular environment are amines and sulfhydryls because of their presence in proteins and amino acids.[30] GSH is the most abundant non-protein thiol in the cell.[31] It serves the role as the first line of defense against electrophilic compounds, both of xenobiotic and endogenous origin.[31] The sulfhydryl group of GSH reacts quickly at the β-position of α,β-unsaturated carbonyls (1,4-conjugate or Michael-type addition).[32] This reaction is further promoted by the "soft" nature of both the sulfhydryl nucleophile and the β-carbon electrophile as predicted by hard-soft acid-base theory (HSAB).[32]

Lipid peroxidation, an endogenous process, forms a variety of α,β-unsaturated carbonyl compounds, including 4-hydroxy-2(*E*)-nonenal and 4-oxo-2(*E*)-nonenal.[33]

Other compounds in this class are found in cigarette smoke, such as acrolein.[34] These electrophiles are known to react with the primary amino groups on the lysine side chains of proteins, forming covalent protein adducts.[33] Lipid peroxidation products are also able to modify DNA and lead to the formation of a variety of miscoding DNA adducts.[35]

Even after BDA reacts with GSH, which is usually considered a detoxification step, it will still retain its dialdehyde moiety (Scheme 1-1). This could react with primary amino groups in DNA and proteins to form adducts, most likely containing the pyrrole ring seen in previously characterized metabolites of furan. For these reasons, the chemistry of BDA is likely to play a major role in the types of cellular molecules and macromolecules that become modified as a result of furan exposure.

Possible Mechanism of Action: Genotoxic

A chemical's mechanism of action has a profound effect on the risk assessment process. Chemicals with a genotoxic mechanism of action are assumed to lack a NOAEL (no observable adverse effect level) or threshold dose for toxicity, changing the way they are regulated.[36] Furan and BDA have genotoxic potential.[1] Genotoxic mechanisms of carcinogenesis are well-established in both hazard assessment and cancer etiology fields. Furan was negative in the Ames mutagenesis assay with and without S9 in all strains tested.[1,37] Furan was positive for gene mutations in L5178Y $tk^{+/-}$ mouse lymphoma cells *in vitro* in the absence of S9.[1,38] It was also positive for sister chromatid exchanges and chromosomal aberrations in Chinese hamster ovary (CHO) cells both with and without S9.[1] An earlier study had found that furan was positive only for clastogenicity in CHO cells, and that this activity required S9.[39] In contrast, it was positive for chromosomal aberrations but negative for sister chromatid exchanges in $B6C3F_1$ mouse bone marrow

cells *in vivo* when administered by injection.[1] It was negative in the sex-linked recessive lethal mutation test in *Drosophila melanogaster* both when administered in feed and by injection.[1,40] A phage T7 inactivation test found that furan had the lowest, but still quantifiable, genotoxic activity of the 28 furan and arenofuran derivatives tested at 6.8 M*min (range of all compounds: $7.5x10^{-3}$ – 6.8 M*min).[41] The overall results of all these genotoxicity studies are mixed; furan has tested both positive and negative in the presence and absence of metabolic activation, depending on which test is considered. Some of these tests were performed with poor experimental design (treating with extremely high doses of furan, not treating in a closed container, etc.), suggesting that more physiologically relevant studies may be called for.

DNA damage often triggers specific downstream events that can be identified using established assays. Furan treatment of male F344/N rats and male $B6C3F_1$ mice by gavage was not found to induce unscheduled DNA synthesis *in vivo*.[42] Cellular necrosis and a corresponding increase in cellular proliferation (measured by the uptake of ^{3}H-thymidine, giving the fraction of cells in S-phase) was seen in the livers of treated rats and mice.[42] Furan was found to cause hepatotoxicity and compensatory cell replication in a dose-dependent manner in a two-year study in female $B6C3F_1$ mice given 1-8 mg/kg furan.[14] Additionally, it was noted that evidence of necrosis was greatest on the visceral surface of the left and caudate lobes of the liver, suggesting that furan may be transported by passive diffusion through the lining of the stomach.[42] Other studies have confirmed that the greatest toxicity occurs in the subcapsular areas[12], lending credence to this hypothesis. Cytotoxicity and a compensatory increase in cell proliferation has been hypothesized to play an important role in the mechanism of carcinogenesis of furan.[12,42]

These results do not eliminate other possible mechanisms of action, but may indicate that DNA damage is occurring.

BDA has been tested in several standard mutagenesis assays. It tested positive in the Ames assay using *S. typhimurium* strain TA 104, a strain that is known to be sensitive to aldehydes.[43] Another study also found that BDA was positive in both the comet assay (looking for DNA strand breaks) and the mouse lymphoma thymidine kinase gene mutation assay in L5178Y $tk^{+/-}$ cells, however in this case the interpretation of the genotoxicity data was complicated by the acute cytotoxicity of BDA that limited the range of conditions that could be tested.[44] Previously characterized DNA adducts of BDA were isolated from Ames assay strain TA104; this and other studies have shown that BDA is able to alkylate DNA *in vitro*.[45-47] These adducts have the potential to lead to mutations and play a role in carcinogenesis,[45] however there are no literature reports of BDA adducts being detected *in vivo*. Overall, the combined data indicate that a) furan is not genotoxic without metabolic activation, b) BDA is genotoxic, and c) furan exposure *in vivo* has the potential to cause DNA damage due to the oxidation of furan to BDA.

Recent studies in our lab using the Big Blue™ mouse model to detect mutations *in vivo* have suggested that furan treatment does not increase the frequency of mutations, but may cause a shift in the types of mutations detected.[48] A published study in Big Blue™ rats similarly showed that furan does not cause an increase in mutations.[49] It is unlikely considering the evidence that furan exerts its carcinogenic effect solely through a genotoxic mechanism, although this pathway may contribute in part to the overall toxicity and carcinogenicity of furan. The results seen may indicate that furan and/or its metabolites (including BDA) may not be able to access the nuclear compartment, re-

emphasizing the necessity to more fully understand the kinetics and dynamics of the system as a whole.

Possible Mechanism of Action: Non-Genotoxic

Since it is unlikely that furan is acting exclusively through a genotoxic mechanism, non-genotoxic mechanisms must be considered. Several studies have shown that furan treatment leads to protein adduction.[7,9] Since BDA is a Michael acceptor, this suggests that furan may share a similar cytotoxic mechanism of action with the hepatotoxicant acetaminophen, which is metabolized by CYP2E1 to the Michael acceptor *N*-acetyl-*p*-benzoquinone imine (NAPQI) and also causes protein adduction.[50,51] Both BDA and NAPQI are α,β-unsaturated carbonyl compounds with somewhat overlapping chemistry including three proteins that are covalently modified by both compounds: peroxiredoxin, aldehyde dehydrogenase, and Ppa1 protein.[8,50] Furan treatment has been shown to deplete glutathione (GSH) in rat hepatocytes in suspension culture.[4] GSH depletion can leave the hepatocyte open to damage from other electrophiles of endogenous and xenobiotic origin.[4]

Damage to DNA may not be from furan or one of its metabolites *per se*, but rather through an exposure-dependent increase in reactive oxygen species (ROS). Furan treatment of Sprague-Dawley rats at 30 mg/kg via gavage has been shown to increase hepatic levels of 8-oxo-dG, an indicator of oxidative DNA damage, as measured by immunofluorescence.[52] The increase in 8-oxo-dG was shown to persist in areas of cholangiofibrosis.[52] Loss of connexin 32 was seen by immunofluorescence and has been hypothesized to play a role in converting DNA damage to fixed mutations.[52] Another study using 0.1 mg/kg, 0.5 mg/kg, and 2 mg/kg furan saw no increase in 8-oxo-dG as

measured by a sensitive LC/MS method.[12] Oxidative stress and subsequent DNA damage may therefore be dependent on very high hepatotoxic doses. One recent study proposed that furan acts primarily through a secondary genotoxic mechanism (i.e. an increase in oxidative stress and inflammation).[53]

Differences in gene expression, rather than in the sequence of genes themselves, are also known to lead to carcinogenesis. Furan is known to cause changes in expression of genes crucial to cell cycle control, oxidative stress, apoptosis, and DNA damage.[52,54] A preliminary study on the effect of furan treatment on DNA methylation patterns suggested that changes in gene/protein expression caused by furan treatment are not related to DNA methylation.[54] A later study by the same research group showed that furan treatment is associated with mRNA expression changes that persist for at least one month after the last dose of furan.[55] Tissue from tumors showed hypomethylation when compared to the healthy tissue.[55] Epigenetic changes induced by furan exposure therefore constitute a possible non-genotoxic mechanism of action.[55]

Of the possible non-genotoxic mechanisms that have been tested and reported in the literature, the ones considered most likely are: a) cytotoxicity leading to compensatory cellular proliferation that eventually becomes dysregulated;[12,42] b) adduction of proteins leading to changes in structure/function that facilitates transformation;[27] and/or c) increases in oxidative stress leading to DNA damage.[52] The failure to see mutagenesis *in vivo* using the Big Blue™ rodent studies puts these non-genotoxic mechanisms further up the list.

Thesis Objective and Hypothesis

The long term objective of the laboratory is to establish the human health effects

of furan exposure. Research on this topic by the laboratory began when BDA was established to be the primary reactive intermediate in furan metabolism. The chemical properties of this compound led to further hypotheses about the potential reactions in which it could participate. This in turn led to the systematic characterization of hepatocyte and urinary metabolites in rodent models, which have potential future use as biomarkers for furan exposure. In order to achieve the long term goal of determining human health effects, it will be necessary to establish a mechanism of action – genotoxic, non-genotoxic, or both – through which furan exerts its toxic and carcinogenic effects. In order to establish a mechanism, the cellular targets must first be identified. After a mechanism has been established, it will be possible to design experiments that test the translatability of this mechanism from rodent to human physiology.

The objective of this thesis is to continue to explore the link between the chemical structure and properties of the known intermediates of furan metabolism with the known targets of furan toxicity, as well as to expand this analysis to include additional intermediates and the stable end-products of metabolism. The chemical structure and reactivity profile of each of the intermediates will directly influence the targets of furan-dependent modification, and therefore the mechanism of action.[10] The reactivity profile includes kinetic and dynamic factors relating the speed at which reactions take place to the possible targets for modification. Chemical transformation of furan in biological systems leads to a variety of intermediates whose chemical properties and intrinsic reactivity are crucial to the development of a mechanism of action for the toxic and carcinogenic effects of furan.

Investigation of the impact that the chemical properties of furan and its

intermediates and end-products have on the cell took place over a series of experiments that were a natural continuation of work already in progress in our laboratory. The first experiments were aimed at characterizing the predominant end-products of furan metabolism in rat hepatocytes. It was determined that GSH-BDA-lysine cross-links and their derivatives make up the majority of end-products as determined by ion trap LC/MS. GSH-BDA-polyamine cross-links were also significant end-products. In an attempt to rationalize the distribution of products, experiments were designed to determine the effect of intrinsic reactivity of primary amino groups toward BDA in the presence of GSH. Next, the distribution of protein lysine adducts was investigated using cytochrome *c* as a model protein and the results compared to other protein-modifying agents, especially structurally related α,β-unsaturated carbonyl compounds. Finally, the kinetics of BDA and its downstream reaction products with both GSH and N^{α}-acetyl-L-lysine (NAL) were measured *in situ* using NMR. The structures of the uncharacterized intermediates were assigned based on detailed structural information gathered using additional targeted NMR experiments. These experiments provide valuable insight into the cellular targets of furan.

The results of these experiments will allow future studies to be properly framed within the known chemistry of not only furan and BDA, but also of the other intermediates, specifically GSH-BDA. The characterization of stable end-products of furan metabolism is not only an important step in the development of biomarkers of furan exposure, but also will allow the direct comparison of metabolites between species. Since it is likely that furan acts through a non-genotoxic mechanism, these metabolites are candidates for bioactive compounds directly involved in the depletion of cellular GSH

and dysregulation of cell proliferation and cell cycle control, especially the GSH-BDA-polyamine cross-links. The ability to compare the metabolism of rodents, in which furan is known to be toxic and carcinogenic, with the metabolism of humans is a crucial step in establishing the human health effects of furan exposure. Since much of the chemistry that has been examined through the experiments delineated above is dependent only on the chemical properties of the various reactants and intermediates, it appears more likely that the same mechanism of action is active across all species that have the ability to perform the initial oxidation of furan to BDA.

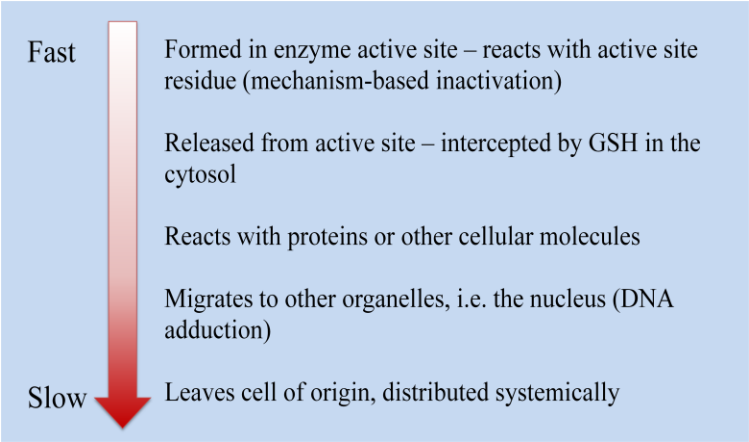

Figure 1-1: Toxicokinetic/dynamic hypothesis

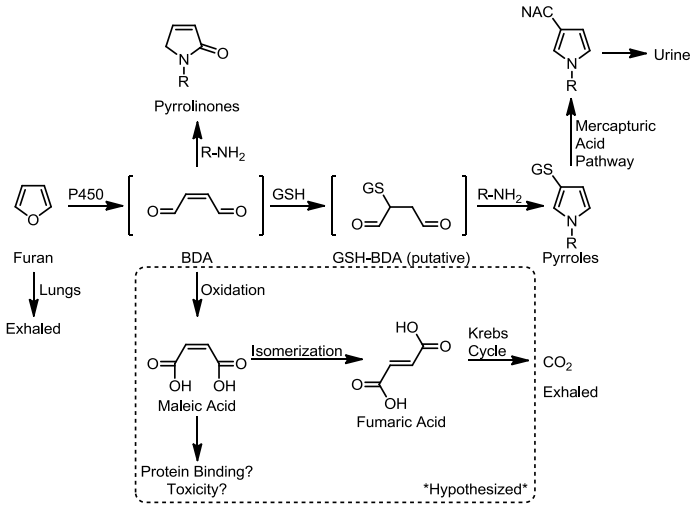

Scheme 1-1: Hypothesized pathway of furan metabolism.

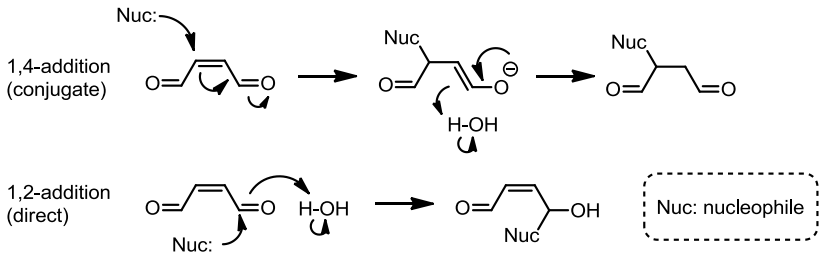

Scheme 1-2: Conjugate vs. direct addition to BDA

Chapter 2: Degraded protein adducts of *cis*-2-butene-1,4-dial are urinary and hepatocyte metabolites of furan

Summary – This chapter describes the characterization of several urinary and hepatocyte metabolites of furan and identifies a portion of these as degraded protein adducts.

Rationale – The structures of the metabolites of a compound provide insight into the biotransformation process, the chemical properties of the parent substance and the nature of its reactive intermediates, and the toxicological mechanism. This work demonstrates a common reactive intermediate as the source of many metabolites of furan as well as indicating that this intermediate can modify proteins, which are subsequently degraded and excreted in the urine. This suggests that protein adduction may play a role in furan toxicity and/or carcinogenicity

My contribution to this work – I synthesized *S*-[1-[5-(acetylamino)-5-carboxypentyl]-1*H*-pyrrol-3-yl]-glutathione, the GSH-BDA-N^{α}-acetyl-L-lysine cross-link. I characterized this product through co-elution by LC/MS with the authentic metabolite, by fragmentation in an ion trap mass spectrometer, by retention time on HPLC, and by proton NMR. I also assisted in the preparation and revision of the manuscript.

Degraded protein adducts of *cis*-2-butene-1,4-dial are urinary and hepatocyte metabolites of furan

Ding Lu,[1] Mathilde M. Sullivan,[1] Martin B. Phillips[2] and Lisa A. Peterson[1,2,3]

Division of Environmental Health Sciences, Department of Medicinal Chemistry and Masonic Cancer Center, University of Minnesota, Mayo Mail Code 806, 420 Delaware Street SE, Minneapolis, Minnesota 55455

[1]Masonic Cancer Center

[2]Department of Medicinal Chemistry

[3]Division of Environmental Health Sciences

Reprinted with permission from Lu, D., Sullivan, M. M., Phillips, M. B., and Peterson, L. A. (2009) Degraded protein adducts of *cis*-2-butene-1,4-dial are urinary and hepatocyte metabolites of furan. *Chem. Res. Toxicol. 22*, 997-1007.

SUMMARY

Furan is a liver toxicant and carcinogen in rodents. Based on these observations and the large potential for human exposure, furan has been classified as a possible human carcinogen. The mechanism of tumor induction by furan is unknown. However, the toxicity requires cytochrome P450 catalyzed oxidation of furan. The product of this oxidation, *cis*-2-butene-1,4-dial (BDA), reacts readily with glutathione, amino acids and DNA and is a bacterial mutagen in Ames assay strain TA104. Characterization of the urinary metabolites of furan is expected to provide information regarding the structure(s) of the reactive metabolite(s). Recently, several urinary metabolites have been identified.

We reported the presence of a mono-glutathione-BDA reaction product, *N*-[4-carboxy-4-(3-mercapto-1*H*-pyrrol-1-yl)-1-oxobutyl]-L-cysteinylglycine cyclic sulfide. Three additional urinary metabolites of furan were also characterized: *R*-2-acetylamino-6-(2,5-dihydro-2-oxo-1*H*-pyrrol-1-yl)-1-hexanoic acid, *N*-acetyl-*S*-[1-(5-acetylamino-5-carboxypentyl)-1*H*-pyrrol-3-yl]-L-cysteine and its sulfoxide. It was postulated that these three metabolites are derived from degraded protein adducts. However, the possibility that these metabolites result from reaction of BDA with free lysine and/or cysteine was not ruled out. In this latter case, one might predict that the reaction of thiol-BDA with free lysine would not occur exclusively on the ε-amino group. Reaction of BDA with *N*-acetylcysteine or GSH in the presence of lysine indicated that both the α- and ε-amino groups of lysine can be modified by thiol-BDA. The *N*-acetylcysteine-BDA-*N*-acetyllysine urinary metabolites were solely linked through the ε-amino group of lysine. A GSH-BDA-lysine crosslink was a significant hepatocyte metabolite of furan. In this case, the major product resulted from reaction with the ε-amino group of lysine, however, small amounts of the α-amino reaction product were also observed. Western analysis of liver and hepatocyte protein extracts using anti-GSH antibody indicated that GSH was covalently linked to proteins in tissues or cells exposed to furan. Our data support the hypothesis that GSH-BDA can react with either free lysine or protein lysine groups. These data suggest that there are multiple pathways by which furan can modify cellular nucleophiles. In one pathway, BDA reacts directly with proteins to form cysteine-lysine reaction products. In another, BDA reacts with GSH to form GSH-BDA conjugates which then reacts with cellular nucleophiles like free lysine or lysine moieties in proteins. Both pathways will give rise to *N*-acetyl-*S*-[1-(5-acetylamino-5-carboxypentyl)-1*H*-

pyrrol-3-yl]-L-cysteine. Given the abundance of these metabolites in urine of furan-treated rats, these pathways appear to be major pathways of furan transformation *in vivo*.

INTRODUCTION

Furan is an important industrial compound that is used both as a solvent and as a synthetic intermediate.[2] It is also present in the environment. It has been detected in many foods and beverages[56] as well as in smog, engine exhaust, wood smoke and cigarette smoke.[2,57] The levels in food are estimated to range from 10 to 5000 μg/kg.[58] In rodents, furan is toxic to liver and kidney and induces cholangiocarcinoma and hepatocellular neoplasms.[1] Its human health effects are unknown. However, its toxicological properties, as well as the potential for significant human exposure, led the National Toxicology Program and the International Agency for Research on Cancer (IARC) to list furan as a possible human carcinogen (Group 2B).[2,59]

While the mechanistic details of furan-induced toxicity and carcinogenicity are unknown, experimental evidence indicated that metabolism plays a critical role in these processes. Furan is converted into a protein binding intermediate via a P450-dependent process both *in vitro* and *in vivo*.[7,60] Its toxic effects are inhibited by P450 inhibitors such as 1-phenylimidazole and induced by acetone pretreatment (induction of CYP2E1), paralleling the effects of P450 inhibitors and P450 inducers on furan metabolism.[24] The initial product of P450 catalyzed oxidation, *cis*-2-butene-1,4-dial (BDA), is a reactive molecule and could be responsible for the toxic and carcinogenic products of furan.[6,23,61] BDA reacts readily with glutathione and amino acids.[6,10] This metabolite also reacts with DNA and is mutagenic in the Ames assay.[43,45-47] All these data suggest that BDA is a good candidate for the ultimate reactive metabolite(s) responsible for furan's toxicities.

However, it is possible that metabolites of BDA also contribute to the toxicological properties of this chemical.

Our understanding of furan metabolism is incomplete. Furan is extensively metabolized in rats.[7] Forty percent of an 8 mg/kg dose of radiolabeled furan was eliminated in exhaled air as either unchanged furan (14%) or carbon dioxide (26%). The pathway to carbon dioxide is likely initiated by oxidation of furan to BDA (Scheme 2-1). In addition, a significant amount of radioactivity was excreted in urine (22%) and feces (20%). Recently, several urinary metabolites have been identified. We reported the presence of a BDA-glutathione reaction product, *N*-[4-carboxy-4-(3-mercapto-1*H*-pyrrol-1-yl)-1-oxobutyl]-L-cysteinylglycine cyclic sulfide (**1**, Scheme 2-1) in the urine of furan-treated rats.[29] A downstream metabolite of this product, *S*-[1-(5-acetylamino-5-carboxypentyl)-1*H*-pyrrol-3-yl]methanethiol (**2**, Scheme 2-1) has also been identified.[26] Three additional urinary metabolites of furan were also characterized: *R*-2-acetylamino-6-(2,5-dihydro-2-oxo-1*H*-pyrrol-1-yl)-1-hexanoic acid (**3**), *N*-acetyl-*S*-[1-(5-acetylamino-5-carboxypentyl)-1*H*-pyrrol-3-yl]-L-cysteine (**4a**) and its sulfoxide (**5a**).[26] Metabolite **3** results from the reaction of BDA with lysine whereas metabolites **4a** and **5a** result from the crosslinking of cysteine and lysine by BDA.[10]

It was postulated that these three metabolites are derived from degraded protein adducts.[26] This is possible since a large percentage of an 8 mg/kg dose of [^{14}C]furan becomes covalently bound to liver protein.[7] However, these metabolites could also result from reaction of BDA with free lysine and/or cysteine. In this latter case, one might predict that the reaction of thiol-BDA with free lysine would not occur exclusively on the ε-amino group. Some reaction would be expected with the α-amino group, leading to the

formation of *S*-[1-(5-amino-1-carboxypentyl)-1*H*-pyrrol-3-yl]-cysteine. Acetylation of this metabolite would generate *N*-acetyl-*S*-[1-(5-acetylamino-1-carboxypentyl)-1*H*-pyrrol-3-yl]-L-cysteine (**4b**). This possibility was not considered in the previous report.[26]

To gain more information about the possible precursors to the cysteine-BDA-lysine crosslink metabolites in rat urine, we determined the regioselectivity of the reaction between BDA and free lysine in the presence of *N*-acetylcysteine or GSH *in vitro*. We then determined if both regioisomers of this reaction appear as metabolites in the urine of furan-treated rats or as furan metabolites in rat hepatocytes. As described below, we demonstrate that the lysine-derived metabolites of furan result primarily from reaction of a BDA-thiol conjugate with the epsilon nitrogen of lysine. In addition, we provide evidence that GSH is likely a major source of the cysteine in metabolites derived from cysteine-BDA-lysine crosslinks. Combined, these data strongly support a hypothesis in which GSH conjugates with BDA to form a reactive intermediate which further reacts with cellular nucleophiles.

EXPERIMENTAL PROCEDURES

Caution: *BDA is toxic and mutagenic in cell systems. Furan is toxic and carcinogenic in laboratory animals. Both chemicals should be handled with proper safety equipment and precautions.*

Chemicals. [$^{13}C_4$]Furan, BDA, **1**, **4a** and the *bis*-GSH-BDA conjugates and their metabolites were prepared as previously described.[6,10,29,46,62] Furan and trifluoroacetic acid were purchased from Acros Organics (Pittsburgh, PA). Cocktail protease inhibitors were purchased from Sigma (St. Louis, MO). All other reagents were purchased from

Aldrich Chemical (Milwaukee, WI) unless stated otherwise. All solvents used for HPLC were of chromatography grade.

Instrumentation. HPLC was carried out on a Shimadzu LC-10AD system coupled to a Shimadzu SCL-10A UV-Vis detector, using a Phenomenex (Torrence, CA) Synergi 4µ Hydro-RP column (250 × 10.00 mm, 4 micron) with a flow rate of 4 mL/min. Two different HPLC methods were employed. In Method 1, solvent A was 50 mM ammonium formate, pH 2.8, and solvent B was 50% acetonitrile in H_2O. After 10 min at 100% A, the column was eluted with a 26 min linear gradient to 75% A, 25% B, followed by a 10 min linear gradient to 50% A, 50% B and a subsequent 4 min linear gradient to 100% B. In Method 2, solvent A was 20 mM ammonium acetate, pH 6.8, and solvent B was methanol with 5% water. The column was eluted with a linear gradient from 100% A to 50% A, 50% B over 30 min followed by a second linear gradient to 100% B over 20 min.

Collision-induced mass spectra of standards were obtained from an Agilent 1100 series LC/MSD Trap SL mass spectrometer operating in either positive or negative ion mode by direct infusion of the sample dissolved in 10 mM ammonium formate, pH 2.8, into the ion source. Helium was the nebulizing and drying gas (15 psi, 5 L/min) which had a temperature set at 200 °C. High resolution mass spectral data for the metabolites were obtained on a Thermo Ultra AM Triple Quadrupole mass spectrometer. High resolution mass spectral data for the synthetic standards were obtained on a Bruker BioTOF II mass spectrometer in the Department of Chemistry, University of Minnesota.

^{1}H NMR, ^{13}C NMR and 2D-NMR (COSY and HMQC) spectra were recorded on a Varian Inova spectrometer operating at 300, 500 or 600 MHz. Chemical shifts are reported in parts per million as referenced to the residual solvent peak.

***N*-Acetyl-*S*-[1-(5-acetylamino-5-carboxypentyl)-1*H*-pyrrol-3-yl]-L-cysteine sulfoxide, 5a.** *m*CPBA (35.8 µmol) was added to a stirred solution of **4a** (35.8 µmol) in methanol-dichloromethane (1:1) at -78 °C. After 1 h, the reaction was warmed to room temperature. HPLC analysis with HPLC Method 1 demonstrated the presence of two major UV-absorbing products eluting at 34.8 min and 38.3 min. The products were isolated by semi-preparative HPLC. The organic solvent was removed under reduced pressure and the buffer salts were removed by solid phase extraction using Strata-X cartridges (Phenomenex, Torrance, CA). The compound eluting at 34.8 min was identified as *N*-acetyl-*S*-[1-(5-acetylamino-5-carboxypentyl)-1*H*-pyrrol-3-yl]-L-cysteine sulfoxide (**5a**). ^{1}H NMR analysis showed the presence of two diastereomers in an 11:9 ratio. The major diastereomer: ^{1}H NMR (600 MHz, CD_3OD): δ 7.30 (s, 1H, H2'), 6.92-6.91 (m, 1H, H5'), 6.55-6.53 (m, 1H, H4'), 4.32-4.27 (m, 2H, Cys α-CH, Lys α-CH), 3.97-3.94 (m, 2H, Lys ε-CH_2), 3.61-3.44 (m, 1H, Cys β-CH_a), 3.43-3.38 (m, 1H, Cys β-CH_b), 1.93 (s, 3H, CH_3), 1.92 (s, 3H, CH_3), 1.83-1.76 (m, 3H, Lys β-CH_a, Lys δ-CH_2), 1.70-1.63 (m, 1H, Lys β-CH_b), 1.35-1.31(m, 2H, Lys γ-CH_2). The minor diastereomer: ^{1}H NMR (600 MHz, CD_3OD): δ 7.30 (s, 1H, H2'), 6.89-6.88 (m, 1H, H5'), 6.52-6.51 (m, 1H, H4'), 4.32-4.27 (m, 2H, Cys α-CH, Lys α-CH), 3.97-3.94 (m, 2H, Lys ε-CH_2), 3.61-3.44 (m, 1H, Cys β-CH_a), 3.43-3.38 (m, 1H, Cys β-CH_b), 1.93 (s, 3H, CH_3), 1.92 (s, 3H, CH_3), 1.83-1.76(m, 3H, Lys β-CH_a, Lys δ-CH_2), 1.70-1.63 (m, 1H, Lys β-CH_b), 1.35-

1.31(m, 2H, Lys γ-CH_2). ^{13}C NMR (150 MHz, $CDCl_3$): δ 124.9, 124.0, 105.8, 57.5, 52.6, 49.8, 49.5, 31.1, 30.6, 22.6, 21.3. The mass spectral data are presented in Table 2-1.

The compound eluting at 38.3 min was characterized as *N*-acetyl-*S*-[1-(5-acetylamino-5-carboxypentyl)-1*H*-pyrrol-3-yl]-L-cysteine sulfone. ^{1}H NMR (600 MHz, DMSO-d_6): δ 7.84 (d, 1H, *J*=8.4 Hz, NH), 7.66 (d, 1H, *J*=7.2 Hz, NH), 7.28 (s, 1H, H2'), 6.83 (s, 1H, H5'), 6.24 (s, 1H, H4'), 4.21 (t, 1H, *J*=9.0 Hz, Cys α-CH), 3.97-3.94 (m, 1H, H5), 3.90-3.84 (m, 2H, H1), 3.55 (d, 1H, *J*=13.2 Hz, Cys β-CH_a), 3.29 (dd, 1H, *J*=10.2, 15.0 Hz, Cys β-CH_b), 1.77 (s, 3H, $COCH_3$), 1.63 (s, 3H, $COCH_3$), 1.60-1.56 (m, 2H, H2), 1.53-1.48 (m, 2H, H4), 1.14-1.08 (m, 2H, H3); ^{13}C NMR (150 MHz, DMSO-d_6): δ 126.2, 123.1, 109.1, 59.6, 53.9, 50.6, 49.7, 32.1, 30.8, 23.5, 22.7. ESI-MS *m*/*z* 432 [M+H], 414, 390, 344, 327, 285.

Derivatization of 5a with acidic methanol. Compound **5a** (5 mg, 12 μmol) or HPLC fractions of furan-treated urine containing **5a** were dissolved in 1 mL of 3N methanolic HCl solution. The reaction was incubated in water bath (50 ºC) for 20 min. HPLC coupled with MS analysis of reaction mixture indicated the formation of multiple products with the major product having a retention time of 43.7 min. The compound was purified by semi-preparative HPLC and identified as *N*-acetyl-*S*-[1-(5-acetylamino-6-oxo-6-methoxyhexyl)-1*H*-(2-methoxy)pyrrol-3-yl]-L-cysteine methyl ester (**8**). ^{1}H NMR (500 MHz, $CDCl_3$): δ 6.28 (d, 1H, *J*=2.5 Hz, H4'), 6.27 (t, 2H, *J*=6.0 Hz, NH), 5.29 (d, 1H, *J*=2.0 Hz, H5'), 4.78-4.75 (m, 1H, Cys α-CH), 4.63-4.59 (m, 1H, H5), 3.81-3.68 (m, 2H, H1), 3.79 (s, 3H, OCH_3), 3.75 (s, 3H, OCH_3), 3.67 (s, 3H, OCH_3), 3.11-3.07 (m, 1H, Cys β-CH_a), 3.01-2.98 (m, 1H, Cys β-CH_b), 2.02 (s, 3H, $COCH_3$), 1.99 (s, 3H, $COCH_3$),

1.82-1.65 (m, 4H, H2 and H4), 1.34-1.24 (m, 2H, H3). HRMS $C_{20}H_{31}N_3NaO_7S$ [M+Na] calculated 480.1771, observed 480.1775.

Reaction of L-lysine and *N*-acetyl-L-cysteine with BDA. *N*-Acetyl-L-cysteine (130 µmol) and *cis*-2-butene-1,4-dial (130 µmol) were incubated in 1 M sodium phosphate buffer, pH 7.4, at 37 ºC for 15 min before adding L-lysine (130 µmol; total volume: 1.5 mL). The reaction was shaken for 15 hours. HPLC analysis with HPLC Method 1 demonstrated the presence of two major UV-absorbing products eluting at 32.8 min and 40.1 min in a ratio of 2:1. The first peak was identified as *N*-acetyl-*S*-[1-(5-amino-1-carboxypentyl)-1*H*-pyrrol-3-yl]-L-cysteine (**6b**). ^{1}H NMR (600 MHz, DMSO-d_6): δ 7.83 (d, 1H, *J*=8.0 Hz, NH), 6.87 (s, 1H, H2'), 6.73 (s, 1H, H5'), 5.99 (s, 1H, H4'), 4.39-4.36 (m, 1H, H1), 4.11-4.06 (m, 1H, Cys α-CH), 2.92 (dd, 1H, *J*=4.5, 13.5 Hz, Cys β-CH_a), 2.74 (dd, 1H, *J*=8.0, 13.5 Hz, Cys β-CH_b), 2.68-2.67 (m, 2H, H5), 1.97-1.95 (m, 1H, $H2_a$), 1.85 (s, 3H, $COCH_3$), 1.82-1.78 (m, 1H, $H2_b$), 1.50-1.36 (m, 2H, H4), 1.23-1.09 (m, 2H, H3); ^{13}C NMR (150 MHz, DMSO-d_6): δ 126.2, 122.2, 113.7, 54.6, 53.6, 49.5, 39.9, 31.2, 23.4, 22.6. The mass spectral data are presented in Table 2-1.

The second peak was identified as *N*-acetyl-*S*-[1-(5-amino-5-carboxypentyl)-1*H*-pyrrol-3-yl]-L-cysteine (**6a**). ^{1}H NMR (500 MHz, DMSO-d_6): δ 7.99 (d, 1H, *J*=7.8 Hz, NH), 6.79 (s, 1H, H2'), 6.67 (s, 1H, H5'), 5.97 (s, 1H, H4'), 4.09-4.06 (m, 1H, Cys α-CH), 3.78-3.76 (m, 1H, H5), 3.18-3.16 (m, 2H, H1), 2.94 (dd, 1H, *J*=5.4, 13.2 Hz, Cys β-CH_a), 2.65 (dd, 1H, *J*=7.8, 13.2 Hz, Cys β-CH_b), 1.80 (s, 3H), 1.63-1.55 (m, 4H, H2 and H4), 1.22-1.13 (m, 2H, H3); ^{13}C NMR (150 MHz, DMSO-d_6): δ 126.0, 122.1, 112.9, 64.2, 54.0, 40.3, 39.7, 33.5, 27.6, 24.0, 23.5. The mass spectral data are presented in Table 2-1.

Reaction of N^{ε}-acetyl-L-lysine and *N*-acetyl-L-cysteine with BDA. *N*-Acetyl-L-cysteine (130 µmol) and *cis*-2-butene-1,4-dial (130 µmol) were incubated in 1.5 mL of 1 M sodium phosphate buffer, pH 7.4, at 37 ºC for 15 min before adding N^{ε}-acetyl-L-lysine (130 µmol). The reaction was kept shaking for 15 hours. HPLC analysis with HPLC Method 1 demonstrated the presence of one major UV-absorbing product eluting at 46.0 min. After preparative isolation of the reaction product by HPLC, the organic solvent was removed under reduced pressure and the buffer salts were removed by solid phase extraction using a Strata-X cartridge. The product was identified as *N*-acetyl-*S*-[1-(5-acetylamino-1-carboxypentyl)-1*H*-pyrrol-3-yl]-L-cysteine (**4b**). ^{1}H NMR (600 MHz, $CDCl_3$): δ 7.93-7.92 (m, 1H, NH), 7.76 (s, 1H, NH), 6.84 (s, 1H, H2'), 6.72 (d, 1H, *J*=1.8 Hz, H5'), 5.98 (s, 1H, H4'), 4.37-4.34 (m, 1H, H1), 4.18-4.16 (m, 1H, Cys α-CH), 2.91-2.89 (m, 3H, H5, Cys β-CH_a), 2.70 (t, 1H, *J*=9.6 Hz, , Cys β-CH_b), 1.93-1.89 (m, 2H, H2), 1.83 (s, 3H, $COCH_3$), 1.72 (s, 3H, $COCH_3$), 1.35-1.28 (m, 2H, H4), 1.09-0.99 (m, 2H, H3); ^{13}C NMR (75 MHz, DMSO-d_6): δ 173.7, 173.5, 169.7, 165.3, 125.2, 122.0, 112.7, 110.0, 64.0, 53.2, 40.1, 38.9, 33.3, 29.3, 23.9, 23.3. The mass spectral data are presented in Table 2-1.

Air oxidation of **4b** resulted in the formation of *N*-acetyl-*S*-[1-(5-acetylamino-1-carboxypentyl)-1*H*-pyrrol-3-yl]-L-cysteine sulfoxide (**5b**) as indicated by the presence of a peak in the LC mass chromatogram at *m/z* 416 eluting at 45.1 min. The mass spectral data are in Table 2-1.

Reactions between GSH, BDA and amino acids. L-Lysine, glutamine or N^{α}-acetyl-L-lysine (67.5 µmol) and glutathione (67.5 µmol) were added to a solution of *cis*-2-butene-1,4-dial (67.5 µmol) in 1 M sodium phosphate, pH 7.4 (total volume of 2 mL). The

reaction was incubated at 37 °C for 2 hours. Products were separated by semi-preparative HPLC employing HPLC Method 1. The solvent was removed under reduced pressure and the buffer salts were removed by solid phase extraction using Strata-X cartridges.

When the reaction was performed with lysine, the resulting reaction mixture was complex. However, there were only two UV-absorbing products which had molecular ions at *m/z* 502, consistent with the cross link of L-lysine to GSH via BDA. The compound eluting at 28.0 min was identified as *S*-[1-(5-amino-1-carboxypentyl)-1*H*-pyrrol-3-yl]-glutathione (**7b**). ^{1}H NMR (600 MHz, D_2O): δ 6.79 (s, 1H, H2'), 6.70 (s, 1H, H5'), 6.08 (d, 1H, *J* = 2.5 Hz, , H4'), 4.43-4.35 (m, 1H, H1), 4.22-4.14 (m, 1H, Cys α-CH), 3.68-3.62 (m, 1H, Glu α-CH), 3.62(s, 2H, Gly α-CH_2), 3.05-2.99 (m, 1H, Cys β-CH_a), 2.82-2.75 (m, 2H, H5), 2.74-2.68 (m, 1H, Cys *β*-CH_b), 2.43-2.30 (m, 2H, Glu *γ*-CH_2), 2.04-1.98 (m, 2H, Glu *β*-CH_2), 1.98-1.93 (m, 1H, $H2_a$), 1.89-1.80 (m, 1H, $H2_b$), 1.57-1.43 (m, 2H, H4), 1.21-1.09 (m, 1H, $H3_a$), 1.07-1.03 (m, 1H, $H3_b$); ^{13}C NMR (150 MHz, D_2O): δ 125.8, 122.9, 113.3, 64.7, 54.4, 53.6, 42.9, 39.8, 38.9, 32.1, 31.6, 26.5, 26.4, 22.8. The mass spectral data are presented in Table 2-1.

The compound eluted at 32.7 min was characterized as *S*-[1-(5-amino-5-carboxypentyl)-1*H*-pyrrol-3-yl]-glutathione (**7a**). ^{1}H NMR (600 MHz, D_2O): δ 6.90 (s, 1H, H2'), 6.72 (s, 1H, H5'), 6.11 (s, 1H, H4'), 4.22-4.18 (m, 1H, Cys α-CH), 3.82-3.73 (m, 2H, H1), 3.64-3.60 (m, 1H, Glu α-CH), 3.60-3.58 (m, 2H, Gly α-CH_2), 3.58-3.53 (m, 1H, H5), 3.06-2.96 (m, 1H, Cys *β*-CH_a), 2.78-2.71 (m, 1H, Cys *β*-CH_b), 2.43-2.30 (m, 2H, *γ* Glu-CH_2), 2.04-1.95 (m, 2H, Glu *β*-CH_2), 1.76-1.68 (m, 2H, H4), 1.66-1.61 (m, 2H, H2), 1.23-1.09 (m, 2H, H3); ^{13}C NMR (150 MHz, D_2O): δ 127.0, 125.7, 115.7, 56.0,

51.7, 56.9, 45.6, 57.4, 46.4, 34.2, 29.0, 32.8, 33.0, 24.4. The mass spectral data are presented in Table 2-1.

The GSH-BDA-glutamine reaction mixture was similarly complex. There were two UV-absorbing products which had the expected molecular ion, *m/z* 502, for the GSH-BDA-glutamine reaction products. These products eluted at 29.1 min and 29.7 min displayed a ratio of 1:14 when HPLC Method 1 was employed. The major isomer that eluted at 29.7 min was identified as *S*-[1-(4-amino-1-carboxy-4-oxobuty)-1*H*-pyrrol-3-yl]-glutathione (**9b**). ^{1}H NMR (500 MHz, D_2O): δ 6.74 (s, 1H, H2'), 6.64 (d, 1H, *J* = 2.5 Hz, H5'), 6.04 (d, 1H, *J* = 2.5 Hz, H4'), 4.41 (dd, 1H, *J* = 4.5, 10.5 Hz, H1), 4.17 (dd, 1H, *J* = 4.5, 10 Hz, Cys α-CH), 3.65 (s, 2H, Gly α-CH), 3.57 (t, 1H, *J* = 6.5 Hz, Glu α-CH), 2.95 (dd, 1H, *J* = 4.0, 14.0 Hz, Cys *β*-CH_a), 2.67 (dd, 1H, *J* = 10.0, 14.0 Hz, Cys *β*-CH_b), 2.35-2.29 (m, 1H, $H3_a$), 2.29-2.25 (m, 1H, $H3_b$), 2.23-2.17 (m, 1H, Glu γ-CH_a), 2.08-2.04 (m, 1H, Glu γ-CH_b), 2.03-1.99 (m, 1H, $H2_a$), 1.98-1.96 (m, 1H, $H2_b$), 1.97-1.95 (m, 2H, Glu β-CH_2). ^{13}C NMR (125 MHz, D_2O): δ 122.3, 113.1, 63.0, 54.1, 53.3, 42.1, 37.9, 31.7, 31.4, 28.3, 26.3. The mass spectral data are presented in Table 2-1.

The minor isomer eluting at 29.1 min was tentatively identified as *S*-[1-(4-amino-4-carboxy-1-oxobutyl)-1H-pyrrol-3-yl]-glutathione (**9a**). NMR data were not obtained since it was difficult to obtain sufficient amounts of this isomer without significant amounts of the major isomer, **9b**. The mass spectral data are presented in Table 2-1.

A single compound with a molecular ion of *m/z* 544 was observed in the GSH-BDA-N^{α}-acetyllysine reaction mixture. This compound eluted at 45.5 min when HPLC Method 1 was employed. This product was identified as *S*-[1-[5-(acetylamino)-5-carboxypentyl]-1*H*-pyrrol-3-yl]-glutathione (**10**). ^{1}H NMR (500 MHz, D_2O): δ 6.80 (s,

1H, H2′), 6.71 (br s, 1H, H5′), 6.11 (br s, 1H, H4′), 4.31-4.26 (m, 1H, Cys α-CH), 4.07-4.01 (m, 1H, H5), 3.85-3.76 (m, 2H, H1), 3.69-3.66 (m, 1H, Glu α-CH), 3.64 (s, 2H, Gly α-CH), 3.08-3.02 (m, 1H, Cys β-CH_a), 2.85-2.77 (m, 1H, Cys β-CH_b), 2.46-2.38 (m, 2H, Glu γ-CH_2), 2.09-2.02 (m, 2H, Glu β-CH_2), 1.88 (s, 3H, $COCH_3$), 1.73-1.61 (m, 3H, H2 and $H4_a$), 1.61-1.51 (m, 1H, $H4_b$), 1.23-1.11 (m, 2H, H3). The mass spectral data are presented in Table 2-1.

Subsequent GSH-BDA-lysine reactions were performed with lower concentrations of reactants: 0.5 or 2 mM L-lysine, 2 mM GSH and 100 μM BDA in a pH 7.4 buffer or RPMI 1640 media with or without 10 mM HEPES, pH 7.3 (total volume of 1 mL). These buffers included 10, 100 or 1000 mM sodium phosphate, Tris-HCl or HEPES. The reaction was incubated at 37 °C for 2 hours and then analyzed using LC-MS Method 1.

Animal Studies. F344 male rats (200-300 g) were purchased from Charles River Laboratories (Kingston, NY). Groups of three rats were treated with 8 mg/kg [$^{12}C_4$]- or [$^{13}C_4$]furan or 40 mg/kg [$^{12}C_4$]furan in 5 mL/kg corn oil by gavage. Control group received only corn oil. Immediately after treatment, rats were transferred to individual metabolism cages. Urine was collected on dry ice for 24 hours and stored at -80 ˚C. The rats were euthanized with CO_2 and tissues were removed. The livers were rinsed twice in ice cold 5 mM sodium phosphate, pH 7.4, containing 0.25 M sucrose and 1 mM desferroximine. The livers were then minced in 30 mL of the same ice cold buffer and homogenized while on ice. The homogenate was transferred in 7.5 mL aliquots to 20 mL centrifuge tubes. Each aliquot was diluted to 18 mL with buffer and centrifuged at 1500

x g for 10 min at 0 °C. The resulting supernatant was further centrifuged at 8500 x g for 10 min at 0 °C. The subsequent supernatant (liver S9) was removed and stored at -80 °C.

Hepatocyte Incubations. Freshly isolated hepatocytes were prepared from Sprague-Dawley or F344 rats according to published methods.[63] The viability of the cells was greater than 85%. Furan's volatility required that the hepatocyte incubations be performed in sealed screw-capped 25 mL Erlenmeyer flasks as previously reported.[4] The cells were suspended at a concentration of 2 x 10^6 cells/mL in RPMI Media 1640, containing 10 mM HEPES, pH 7.3. In some cases, the media was supplemented with 2 mM glutamine or 0.5 mM [4,4,5,5-$^2H_4$]-L-lysine (Cambridge Isotope Laboratories, Inc., Andover, MA). After a 10 min pre-incubation period at 37 °C in an atmosphere of 5% CO_2, the flasks were capped tightly. A solution of furan was added with a syringe through a septum to a final concentration of 100 μM. Controls were performed in the absence of furan or in the presence of 50 μM SKF-525A (Sigma, St. Louis, MO) or 200 μM 1-phenylimidazole. The mixtures were then incubated at 37 °C with gentle shaking. After 4 h, the mixture was centrifuged at 3000 rpm for 5 minutes. The supernatant was removed and stored at -20 °C for LC-MS/MS analysis and the cell pellets were flash frozen and stored at -80° C. Incubations were performed in duplicate and were repeated with different hepatocytes preparations.

LC-MS Analysis of Urine, Hepatocyte Media or *in vitro* Reaction Mixtures. Urine was acidified with TFA to a final concentration of 2%, centrifuged to remove any particulate matter and filtered through a 0.45 μm syringe filter. The hepatocyte medium was analyzed directly. In some cases, the urine was treated with *tris*-

(carboxyethyl)phosphine (Strem Chemicals, Newburyport, MA) to reduce any disulfide bonds.[6,64,65]

LC-MS/MS analyses of urine, hepatocyte extracts or *in vitro* reaction mixtures were conducted with an Agilent (Palo Alto, CA) Zorbax SB-C18 column (5 µm, 150 × 0.5 mm) at a flow rate of 15 µL/min. The column was eluted with the gradient described in Method 1, substituting 10 mM ammonium formate, pH 2.8, for solvent A. In some cases, the gradient described in Method 2 was employed. The HPLC was coupled to an Agilent 1100 series LC/MSD Trap SL mass spectrometer operating in either positive or negative ion mode. Helium was the nebulizing and drying gas (15 psi, 5 L/min) which had a temperature set at 200 °C. Initial analyses were performed with the mass spectrometer set to full scanning mode with a scan range of 100-750 *m*/*z*. Urine from individual animals treated with [$^{12}C_4$]- or [$^{13}C_4$]furan were analyzed separately as well as a 1:1 mixture. The resulting data were searched for compounds that were present in the furan exposed samples and absent in the samples from control rats. The urinary metabolites were confirmed as furan-derived by demonstrating that the mass of the metabolites were shifted by four amu in the urine from [$^{13}C_4$]furan-treated rats relative to that from [$^{12}C_4$]furan-treated rats. The samples were then reanalyzed with the mass spectrometer set in the autoMS^n mode to obtain fragmentation patterns for each of the metabolites.

The entire volume of urine from one furan-treated rat was treated with TFA as described above (total volume = ~4 mL), filtered and fractionated by HPLC. The urinary metabolites were eluted from a Phenomenex (Torrance, CA) Bondclone semi-prep scale column (250 x 10 mm, 10 micron) with 50 mM ammonium formate, pH 2.8. A 10 min

isocratic period was followed by a 40 min linear gradient to 37.5 mM ammonium formate, pH 2.8, containing 12.5% acetonitrile and then a 10 min gradient to water containing 50% acetonitrile (flow rate = 4 mL/min). The UV absorbance was monitored at 254 nm. The fraction containing **5a** was used to obtain HRMS information as well as to perform the derivatization with acidic methanol.

To more accurately determine the ratio of **7a** and **7b** in the hepatocyte extracts or reaction mixtures, LC-MS/MS analyses were conducted on a Nano Acquity UPLC pump (Waters, Milford, MA) coupled to a Finnigan TSQ Quantum Ultra AM mass spectrometer (Thermo Electron, San Jose, CA) operating in positive mode. The mixtures were separated at a flow rate of 12.5 µL/min. The Phenomenex (Torrence, CA) Synergi hydro-RP 80A column (4 µm, 250 × 0.5 mm) was eluted with Method 1 gradient, substituting 10 mM ammonium formate, pH 2.8, for solvent A. Selected reaction monitoring (neutral loss 129) was performed to determine the relative amount of **7a** to **7b** (*m/z* 502 to *m/z* 373) or [$^2H_4$]**7a** to [$^2H_4$]**7b** (*m/z* 506 to *m/z* 377).

Cell extracts. The pelleted hepatocytes were reconstituted in 200 µL of ice cold lysis buffer (50 mM sodium phosphate, pH 7.4, containing 0.25% SDS, 30% glycerol, and 0.5% Triton X-100) with 5 µL/mL cocktail protease inhibitor. The cells were homogenized in microtissue grinders and the resulting solution was stored at -20 °C for Western analysis.

Western Analysis. All proteins concentrations were determined by means of a Bradford assay with BSA standard. Prior to loading on the gel, tissue or cell extracts (50 µg protein, volume range: 10-50 µL) were heated for 10 min at 95 ºC in 62.5 mM Tris-HCl, pH 6.8, containing 1.5% SDS, 7.5% glycerol, 0.01% bromophenol blue in the presence or

absence of 75 mM DTT (dithiothreitol). In some cases, samples were heated in the presence of 50 mM DTT for 10 min at 95 ºC prior to the addition of the solution containing SDS, glycerol, DTT and bromophenol blue buffer (final DTT concentration: 135 mM). DTT was included to remove any protein-GSH mixed disulfide bonds. Protein solutions (50 μg) were loaded on a 10% 1.5mm SDS-PAGE gel and run at 200 Volts until the dye ran off the gel (about 45 minutes). Proteins bands were then electroblotted on nitrocellulose membranes (300 mA, 60 min) with 25 mM Tris-base containing 192 mM glycine and 20% methanol in a Mini-Trans Blot Cell (Bio-Rad, Hercules, CA). The membranes were blocked overnight in phosphate buffered saline containing 5% dry nonfat milk and 0.2% Tween 20 with shaking at 4 ºC. Membranes were then reacted with a 1:1000 dilution of rabbit anti-GSH antibody (Virogen, Watertown, MA) for 1 h at room temperature. After washing the membranes three times for 5 min each with phosphate buffered saline containing 0.2% Tween 20 (PBST), the membranes were incubated for 1 hr with a 1:20,000 dilution of goat anti-rabbit pAb to MSIgG (HRP) secondary antibody (Abcam, Cambridge, MA). The membranes were then washed three times with PBST prior to development with Super Signal West Pico chemiluminescent substrate (Thermo Scientifc, Rockford, IL).

RESULTS

Regioselectivity of reaction of BDA with lysine and N-acetylcysteine/GSH.

BDA was combined with equal molar amounts of L-lysine and *N*-acetyl-L-cysteine or GSH at pH 7.4. HPLC analysis of the reaction mixture indicated the formation of multiple products (Figure 2-1). Mass spectral analysis was employed to determine which peaks were associated with the expected thiol-BDA-lysine cross-links.

Two peaks with the appropriate molecular ion (*m/z* 358) for the expected *N*-acetyl-cysteine-BDA-lysine reaction products were observed in the BDA-lysine-*N*-acetylcysteine reaction mixture in a ratio of 2:1 (n = 5; retention times: 32.8 and 39.9 min; Figure 2-1A). Preparative isolation and characterization by NMR analysis indicated that the peak that elutes at 32.8 min incorporates the lysinyl α-amino group as the pyrrole amino group (*N*-acetyl-*S*-[1-(5-amino-1-carboxypentyl)-1*H*-pyrrol-3-yl]-L-cysteine, **6b**) whereas the compound that elutes at 39.9 min incorporates the ε-amino group as the pyrrole amino group (*N*-acetyl-*S*-[1-(5-amino-5-carboxypentyl)-1*H*-pyrrol-3-yl]-L-cysteine, **6a**).

Similarly, there were two compounds in the GSH-BDA-lysine reaction mixture (retention times of 28.0 and 32.7 min) with the expected molecule ion of *m/z* 502 for the GSH-BDA-lysine reaction products in a ratio of ~1:1 (Figure 2-1B, Table 2-2). Isolation and characterization of the reaction products indicated that the earlier eluting compound is the product resulting from crosslinkage of GSH-BDA with the α-amino group of lysine (*S*-[1-(5-amino-1-carboxypentyl)-1*H*-pyrrol-3-yl]-glutathione, **7b**) and the later eluting compound has lysine crosslinked to GSH-BDA through the ε-amino group (*S*-[1-(5-amino-5-carboxypentyl)-1*H*-pyrrol-3-yl]-glutathione, **7a**). Therefore, independent of the thiol, the α-amino group of lysine is equally or more reactive with thiol-BDA conjugates than the ε-amino group under the conditions of these reactions.

The GSH-BDA-lysine reactions were repeated under more dilute reaction conditions, with a twenty fold excess of GSH and lysine. The ratio of **7b** to **7a** was similar to that observed in the more concentrated solution when the reaction was performed in 1 M sodium phosphate buffer, pH 7.4 (Table 2-2). However, when the

reaction was conducted in RPMI 1640 media, the ratio of **7b** to **7a** dropped to 0.155. These observations suggest that the ε-amino reaction product is favored in the latter case. The buffer concentration plays some role in determining the relative reaction rate at the two amino groups since reducing the phosphate buffer concentration to 6.17 mM reduced the ratio of α to ε reaction products to about 0.3. Similar reactions in pH 7.4 Tris or HEPES buffers generated an α/ε ratio of ~0.3 as well. These ratios were not influenced by the concentration of Tris or HEPES buffer, contrasting with the observation with sodium phosphate buffer. While the pKa of the α-amino group is more than 1 unit lower than that of the ε-amino group (9.2 vs 10.8),[66] preliminary molecular modeling studies indicate that the ε-reaction product is thermodynamically more stable (unpublished results, M.B. Phillips and L.A. Peterson).

Regiochemistry of the urinary metabolites of furan.

Two metabolites, one with a molecular weight 399 (**4a**) and a second with a molecular weight 415 (**5a**) were identified in the urine of furan-treated rats.[26] These metabolites were assigned the following structures: **4a** as *N*-acetyl-*S*-[1-(5-acetylamino-5-carboxypentyl)-1*H*-pyrrol-3-yl]-L-cysteine and **5a** as its sulfoxide. Chemical characterization consisted of co-elution of the metabolite with the corresponding standards and MS analysis. However, the authors did not confirm that *N*-acetylcysteine was linked to the ε-amino group of lysine via BDA; it is possible that the α- and ε-substituted metabolites co-elute with one another under the reported HPLC conditions. Therefore, we prepared both possible regioisomers of the *N*-acetylcysteine-BDA-lysine crosslinks **4a** and **4b** by reacting N^{α}-acetyl-L-lysine or N^{ε}-acetyl-L-lysine, respectively, with equal molar amounts of BDA and *N*-acetyl-L-cysteine according to published

methods.[10] The products were confirmed by NMR and MS analysis. MS analysis of the two isomer demonstrated that they were similar with the exception of three ions in the mass spectrum of **4b** at *m/z* 211, 322 and 253 (Table 2-1, Figure 2-2).

The metabolite with a molecular ion of 400 amu had a similar retention time as standard **4a** (49 min) but not **4b** (45 min, Figure 2-3). There were no significant levels of **4b** detected in the urine from furan-treated rats. In addition, the collision induced mass spectrum of the metabolite was identical to **4a** (Table 2-1, Figure 2-2). The metabolite co-eluted with **4a** in two different HPLC systems (data not shown). Further support for the identity of this furan metabolite was obtained by high resolution mass spectral analysis (Table 2-1). There was also a smaller peak with *m/z* 400 that eluted immediately after **4a** in the urine. This smaller peak is presumably the 2-substituted compound as previously reported.[10]

Oxidation of compounds **4a** and **4b** generated compounds **5a** and **5b**, respectively. NMR analysis of **5a** indicated that the oxidation had occurred on the sulfur atom as demonstrated by the 0.5 ppm downfield shift of the *N*-acetylcysteinyl β-methylene protons of **5a** as compared to those observed in compound **4a**. On the other hand, the methylene protons adjacent to the pyrrole nitrogen had the same chemical shift (3.85 ppm) for both compounds **4a** and **5a**. Furthermore, the mass spectra of **5a** and **5b** have a fragment ion at *m/z* 239, which is consistent with the loss of *N*-acetylcysteine sulfoxide ($M+H^+-177$). The mass spectra of **5a** and **5b** had similar fragment ions but the intensity of these ions was significantly different between the two compounds (Table 2-1, Figure 2-4). The other metabolite (*m/z* 416) co-eluted with **5a** not **5b** (Figure 2-5). There were no detectable levels of **5b** in the urine. High resolution mass spectral analysis of the

metabolite indicates that the exact mass of this metabolite is within 5 ppm of the calculated exact mass for the proposed structure (Table 2-1).

When **5a** was incubated in 3 N methanolic HCl at 50 ºC for 10 min, the major reaction product had a molecular ion at 458 amu, indicating the addition of three methyl groups. Esterification of the *N*-acetylcysteine and the *N*-acetyllysine moieties was expected. The addition of a third methyl group was initially unexpected. ^{1}H NMR analysis of this product confirmed the presence of three singlet methoxy groups at 3.79, 3.75 and 3.67 ppm. The NMR spectrum indicated that one of the pyrrole protons was missing. The two remaining aromatic protons resonated as doublets at 6.28 and 5.29 ppm and were assigned to the pyrrole ring protons C4 and C5, respectively, since a COSY experiment exhibited a cross peak between those two resonances. These data support the formation of two methyl esters and the presence of a third methoxy group at the 2-position of the pyrrole ring. Therefore, the reaction of **5a** in 3 N methanolic HCL is *N*-acetyl-*S*-[1-(5-acetylamino-6-oxo-6-methoxyhexyl)-1*H*-(2-methoxy)pyrrol-3-yl]-L-cysteine methyl ester (**8**, Scheme 2-2). A proposed mechanism for the reaction of methanol with the 2-position of the pyrrole ring is shown in Scheme 2-2. This derivatization reaction was employed to confirm the structure of the urinary metabolite. The semipurified metabolite underwent a similar derivatization reaction, confirming its structure as **5a** (Figure 2-6).

Kellert *et al* reported the presence of **4a** and **5a** in the urine of untreated animals when analyzing the urine by multiple reaction monitoring in negative ion mode (*m/z* 398 and 414, respectively).[26] We also observed the presence of endogenous compounds in the control animals which had the same nominal masses and similar retention times as **4a**

and **5a**. We analyzed the urine from [$^{13}C_4$]furan treated animals to determine if these endogenous compounds had identical retention times to the metabolite derived from furan. We were able to separate the endogenous compounds from the [$^{13}C_4$]metabolites **4a** and **5a** by lengthening the HPLC gradient (Figure 2-7); [$^{12}C_4$]- and [$^{13}C_4$]labeled **4a** have identical retention times when equal amounts of urine from [$^{12}C_4$]- and [$^{13}C_4$]furan-treated animals are mixed prior to LC-MS/MS analysis (data not shown). Therefore, the endogenous compounds are neither **4a** nor **5a** but a different *N*-acetylcysteine conjugate and its sulfoxide with identical nominal masses to **4a** and **5a**. These endogenous chemicals are neither **4b** nor **5b** since their retention times are substantially different from these two compounds (48 min versus 45 min and 33 min versus 30 min, respectively). Since the endogenous compound had the same fragmentation pattern as the furan metabolite **4a** (*m/z* 398 $\rightarrow$ *m/z* 269 and 227), caution will need to be taken when quantitative methods for the analysis of these two metabolites are developed for biomarker studies. The levels of these endogenous compounds were comparable to those of metabolites **4a** and **5a** in the urine of animals treated with 8 mg/kg [$^{13}C_4$]furan (Figure 2-7).

Metabolism of furan in hepatocytes

To explore the initial products of furan metabolism in the target tissue, freshly prepared rat hepatocytes were incubated with 100 μM furan and the medium was analyzed by LC-MS/MS for the presence of metabolites. Several metabolites were observed. Their formation was blocked upon inclusion of the P450 2E1 inhibitor, 1-phenylimidazole, in the incubation mixture. SKF525A did not significantly inhibit the formation of metabolites.

The mono-GSH-BDA reaction product **1**, but not the *bis*-GSH reaction products, was detected (Figure 2-8A). The mass spectrum was consistent with structure **1** (Table 2-1, Figure 2-9). None of the subsequent metabolites of the GSH-BDA reaction products were detected (data not shown).[29] There was evidence for the formation of cysteine-BDA-lysine reaction products since **4a** was detected in these mixtures (Figure 2-8B). As with the urinary metabolites, this metabolite co-eluted with standard **4a** (Figure 2-10) and had the same mass spectrum (Figure 2-2). Metabolite **5a** was not detected. The mass spectral data were also probed for the presence of structurally related metabolites, cysteine-BDA-lysine (*m/z* 316), *N*-acetylcysteine-BDA-lysine (*m/z* 358) and GSH-BDA-lysine (*m/z* 502). No significant ion current was observed at *m/z* 316. However, there was one peak with *m/z* 358 which was not in the controls (Figure 2-8C). This metabolite co-eluted with standard **6a** and had a similar mass spectrum (Figure 2-11). There was no signal consistent with the presence of **6b** in the incubation mixture. Together, these data support the hypothesis that the metabolic reaction had occurred primarily at the ε-amino group of lysine.

There were two major peaks with *m/z* 502 that required the presence of furan, one eluted at 28.2 min (**9b**) and the second eluted at 30.8 min (**7a**, Figure 2-8D). The mass spectra of these two metabolites were dominated by the fragmentation of the glutathione portion of the molecules (Table 2-1). The later eluting metabolite co-eluted with standard **7a** and had an identical MS^2 as the standard (Table 2-1, Figure 2-12). In addition, high resolution MS analysis indicated that the metabolite had the expected exact mass as standard **7a** (Table 2-1). There was a small peak that co-eluted with standard **7b** (Figure

2-8D). Therefore, the major regioisomer formed in the hepatocytes involved the cross link of a GSH-BDA conjugate with the ε-amino group of lysine.

Metabolite **9b** was proposed to be a GSH-BDA reaction product with a different amino acid, glutamine, which has the same nominal mass as lysine. To test this hypothesis, the GSH-BDA-glutamine reaction products were prepared by reacting glutamine with equal molar amounts of BDA and GSH. Two products were observed in a ratio of 14:1. NMR analysis indicated that the major reaction product was GSH-BDA-glutamine where the pyrrole ring involved the α-amino group of lysine (*S*-[1-(4-amino-1-carboxy-4-oxobuty)-1*H*-pyrrol-3-yl]-glutathione, **9b**) and the minor product resulted from reaction with the amide nitrogen (*S*-[1-(4-amino-4-carboxy-1-oxobutyl)-1*H*-pyrrol-3-yl]-glutathione, **9a**) (Scheme 2-3). Metabolite **9b** coeluted with the major reaction product (**9b**) and had an identical mass spectrum (Figure 2-13). Consistently, the exact mass of **9b** is as expected for the proposed structure (Table 2-1). It is possible that there were small amounts of isomer **9a** that had a similar retention time to **7b**. This peak may contain both compounds **7b** and **9a**. The abundance of **7b** relative to this peak is similar to the relative abundance of **9b** and **9a** observed in the reaction of GSH-BDA with glutamine, consistent with the reaction of GSH-BDA with free glutamine in the hepatocytes. Since 2 mM glutamine was present in the medium, it was possible that GSH-BDA was reacting with this glutamine source. When the medium was not supplemented with glutamine, the levels of GSH-BDA-glutamine metabolite were significantly reduced (Figure 2-14).

Another hepatocyte metabolite eluted at 43.0 min with a molecular ion ($M+H^+$) at *m/z* 544 (Figure 2-8E). As with **9b** and **7a**, the mass spectrum of this metabolite was

consistent with the presence of GSH in the structure (Table 2-1). This molecular ion is 42 amu higher than those of **9b** and **7a**, suggesting that it might be an *N*-acetylated version of these metabolites. A standard for *N*-acetylated **7a**, *S*-[1-[5-(acetylamino)-5-carboxypentyl]-1*H*-pyrrol-3-yl]-glutathione (**10**, Scheme 2-3) was generated by reacting N^{α}-acetyl-L-lysine with BDA and GSH. This compound co-eluted with the metabolite (Figure 2-15). Its isomer, *S*-[1-[5-(acetylamino)-1-carboxypentyl]-1*H*-pyrrol-3-yl]-glutathione eluted more than one minute earlier than **10** (data not shown). In addition, high resolution mass spectral analysis demonstrated that the exact molecular weight of the metabolite is within 5.5 ppm of the calculated molecular weight for compound **10**. It is approximately 60 ppm different than that calculated for the *N*-acetylated form of **9b** (544.1708). Together, these data indicate that **10** is a further metabolite of **7a**, and, therefore, likely derived from a degraded GSH-BDA protein adduct.

Evidence for GSH-BDA-protein adducts

As in the chemical reactions, the major isomer for the GSH-BDA-lysine metabolites was **7a**; the ratio of **7b**/**7a** was 0.096 following a 4 h incubation period (Table 2-2). These analyses were performed with media lacking glutamine since **9a** coelutes with **7b**. If the GSH-BDA-lysine metabolite were solely derived from degraded protein adducts, one would expect to see exclusively **7a**. Therefore, it is possible that GSH-BDA is reacting with free lysine within the hepatocyte or in the medium; RPMI medium contains 0.2 mM lysine. To confirm the possibility that GSH-BDA could react with free lysine in the medium, incubations were conducted in which the medium was supplemented with 0.5 mM [4,4,5,5-$^{2}H_4$]-L-lysine. After a 4 h incubation period, the cells were removed and the medium was analyzed by LC-MS/MS with selected reaction

monitoring for the loss of 129. GSH-BDA-lysine products formed with cellular lysine (either free or protein bound) have a molecular ion at *m/z* 502 whereas GSH-BDA-lysine products formed with [4,4,5,5-$^{2}H_4$]-L-lysine have a molecular ion at *m/z* 506. The ratio of [$^{2}H_4$]**7b** to [$^{2}H_4$]**7a** is significantly higher than that observed for the unlabeled metabolites (Table 2-2). To determine the relative reaction with the unlabeled versus labeled lysine, the ratios of [$^{1}H_4$]**7a** to [$^{2}H_4$]**7a** and [$^{1}H_4$]**7b** to [$^{2}H_4$]**7b** were calculated. The ratio of [$^{1}H_4$]**7a**/[$^{2}H_4$]**7a** was 3 (n = 2)whereas the ratio of [$^{1}H_4$]**7b**/[$^{2}H_4$]**7b** was 1.2 (n = 2), indicating that a greater percentage of the ε-substituted regioisomer was formed from unlabeled lysine. If the reaction were completely occurring with free as opposed to protein bound lysine, we would expect the ratio to be the same for both regioisomers. Therefore, it is likely that some of the ε-substituted product is derived from the reaction of GSH-BDA with free lysine and some is derived from degraded protein adducts. Further evidence for this possibility is that the ratio of **7b**/**7a** changes with time (Table 2-2). At the 1 h time point, the ratio of α- to ε-reaction products is closer to that observed in the *in vitro* reactions. By the 4 h time point, there is significantly less of the α-substituted product. These results suggest that at early time points the reaction with free lysine is significant. The relative levels of the ε-reaction product increases as the alkylated proteins are degraded.

These observations suggest that BDA is crosslinking GSH to protein lysinyl residues and the degradation of these modified proteins could be a significant source of furan metabolites. To provide preliminary support for this hypothesis, Western analysis of liver and hepatocyte cell extracts was performed with an anti-GSH antibody to determine if GSH was becoming covalently attached to proteins in furan-exposed cells.

To ensure that the anti-GSH antibody was capable of detecting GSH-BDA-protein adducts, bovine serum albumin was incubated with BDA and GSH and run on a denaturing gel to see if the GSH-BDA-exposed BSA was recognizable by the anti-GSH antibody during Western analysis. The antibody only recognized the protein when it had been exposed to both BDA and GSH; minimal antibody binding was observed in the untreated BSA lanes (data not shown). Proteins from furan treated rat liver S9 and extracts of furan-treated rat hepatocytes were analyzed by Western blot with anti-GSH antibody (Figure 2-16). Antibody recognition required exposure to furan and was inhibited upon inclusion of the P450 2E1 inhibitor, 1-phenylimidazole, in the incubations of furan with hepatocytes. SKF525A had no effect on antibody recognition. The binding was not reversed upon reaction of the extracts with excess DTT prior to loading onto the gel indicating that the antibody was probably recognizing GSH covalently associated with hepatocyte proteins; DTT would reverse any GSH-protein disulfide bonds. These data provide strong preliminary evidence that oxidation of furan results in the crosslinking of GSH to protein residues.

DISCUSSION

Furan's toxicity in hepatocytes is dependent on P450 2E1 catalyzed oxidation of furan.[24] The formation of the hepatocyte metabolites characterized in this report required P450 2E1 catalyzed oxidation since their formation was inhibited by the P450 2E1 selective inhibitor, 1-phenylimidazole, but not by SKF525A which is a general P450 inhibitor but a poor inhibitor of 2E1.[24,67] The initial product of P450 2E1 catalyzed oxidation of furan is BDA (Scheme 2-4).[6] Once formed, BDA is expected to rapidly react nonenzymatically with cellular nucleophiles such as GSH.[6] The chemical structures

of the hepatocyte metabolites indicate that BDA reacts with GSH to form a GSH-BDA reaction product (Scheme 2-4). This product retains two reactive aldehyde groups. Intramolecular reaction with the glutamate amino group will lead to the formation of the mono-GSH-BDA metabolite **1**.[6] Alternatively, GSH-BDA can react with other cellular amines such as lysine or glutamine to form thiol-pyrrole crosslinks like **7a**, **7b** and **9b**. This reaction sequence is supported by model studies with acetylated amino acids which demonstrated that the reaction of BDA with thiols is more rapid than its reaction of amines.[10] Previously, we reported that GSH-BDA also reacts with the glutamate amino group of another molecule of GSH to form *bis*-GSH-BDA reaction products (**11**, Scheme 2-4). It was somewhat surprising that no *bis*-GSH-BDA reaction products were observed as hepatocyte metabolites. We are still investigating the reasons for this but it is likely that other cellular nucleophiles successfully compete with GSH for reaction of GSH-BDA under cellular conditions.

Further metabolic processing of **7a** will lead to the other observed hepatocyte metabolites, *N*-acetylcysteine-BDA-lysine (**6a**), GSH-BDA-*N*-acetyllysine (**10**) and *N*-acetylcysteine-BDA-*N*-acetyllysine (**4a**). The observation of **10** as a hepatocyte metabolite suggests that **7a** undergoes *N*-acetylation in a reaction likely catalyzed by an aminoacylase.[68,69] The mercapturic acid pathway is responsible for the formation of **6a** from **7a**. Either **6a** or **10** are precursors to **4a**. Metabolite **4a** was also detected in the urine of furan treated rats (Figure 2-3).[26] While not observed in hepatocytes, **4a** is oxidized to **5a** *in vivo* (Figure 2-5).[26] The conversion of **4a** to **5a** is likely catalyzed by cytochrome P450 or flavin mono-oxygenase.[70]

Our studies revealed two possible sources for the hepatocyte metabolite, **7a**. One pathway of formation is the reaction of GSH-BDA with unbound lysine. The other is the reaction of GSH-BDA with protein lysine residues with subsequent degradation to **7a**. *In vitro* reactions indicate that GSH-BDA will react preferentially with the ε-amino group of unbound lysine in hepatocyte media (Table 2-2). The ability of metabolically generated GSH-BDA to react with [4,4,5,5-$^{2}H_4$]-L-lysine supplemented in the media indicates that unbound lysine is a target for this reaction. We do not know the extent of uptake of [4,4,5,5-$^{2}H_4$]-L-lysine into the hepatocyte so it is unclear whether [$^{2}H_4$]**7a** and [$^{2}H_4$]**7b** are generated inside or outside the hepatocyte. In any case, there was insufficient time for the labeled compound to be incorporated into proteins so we are confident that the levels of [$^{2}H_4$]**7a** represent reaction of GSH-BDA with free lysine.

There is also evidence suggesting that a portion of **7a** is derived from degraded GSH-BDA-protein adducts (Scheme 2-4). First, the ratio of [$^{1}H_4$]**7a**/[$^{2}H_4$]**7a** is approximately 3 times the ratio of [$^{1}H_4$]**7b**/[$^{2}H_4$]**7b**, indicating that a greater percentage of the ε-substituted regioisomer was formed from unlabeled lysine. This difference indicates that some of the unlabeled **7a** is derived from a source different from unbound lysine. Second, the ratio of **7b**/**7a** decreases with incubation time (Table 2-2). At the 1 h time point, the ratio of α- to ε-reaction products is closer to that observed in the *in vitro* reactions. By the 4 h time point, there is significantly more of the ε-substituted product, **7a**. These results suggest that the reaction with free lysine dominates at early time points, while degradation of GSH-BDA-protein adducts provides a greater source of this metabolite at later time points. In the 24 h urine of furan-treated rats, only the ε-substituted metabolites, **4a** and **5a** are observed. If **4b** and **5b** are present, they were

below the limit of detection. Final support for the formation of GSH-BDA-protein adducts is provided by Western analysis of liver and hepatocyte extracts with an anti-GSH antibody (Figure 2-16). These experiments provide important preliminary evidence that BDA is covalently crosslinking GSH to liver proteins both *in vivo* and in hepatocytes *in vitro*.

The observation that BDA is likely cross-linking GSH to proteins indicates that reaction of BDA with GSH does not completely deactivate BDA as previously suggested.[10] Previous studies indicated that GSH significantly blocked P450 catalyzed protein binding of [^{14}C]furan in microsomes.[60] It was hypothesized that GSH is a good trap for the reactive metabolite because it has both a thiol and an amino group and therefore able to neutralize all the reactive characteristics of BDA.[10] However, the detection of **7a** and **10** as hepatocyte metabolites of furan indicates that the intramolecular reaction to form the mono-GSH reaction product **1** may not be fast enough to protect against alkylation of other cellular nucleophiles. Based on the peak area of **1** relative to the total peak areas of **4a**, **6a**, **7a** and **10** in the LC-MS analyses, it appears that thio-BDA-lysine cross link pathway is the more abundant product in hepatocyte incubations. However, sensitive analytical methods will be required to accurately establish the relative amounts of these metabolic pathways.

GSH-BDA may have a significant lifetime prior to reacting with amino groups in the cell since the levels of GSH-BDA-glutamine reaction products, **9a** and **9b**, could be modified by altering the concentration of glutamine in the hepatocyte medium. The relative ratio of **9a** and **9b** formed in the hepatocytes was similar to that formed in the *in vitro* reaction mixtures indicating that these hepatocyte metabolites are derived from

reaction with free glutamine as opposed to reaction with a glutamine residue in a protein. Similarly, supplementation of the hepatocyte media with labeled lysine led to the formation of labeled **7a** and **7b**. These data suggest that the BDA-GSH reaction product may migrate across membranes to react with nucleophiles distant from the site of formation.

Chemical characterization of the urinary and hepatocyte metabolites of furan suggest that there are at least three different types of protein adducts generated by reactive furan metabolites (Scheme 2-4). First, BDA can react directly with protein lysine residues to generate pyrrolinone adducts. This route is supported by the detection of **3** in the urine of furan treated rats (unpublished results, D. Lu and L.A. Peterson).[26] Second, BDA can react with protein thiol groups to generate a protein thiol-BDA intermediate that can then react with protein lysine groups to form a cysteine-BDA-lysine crosslink within a protein. The third protein adduct is a GSH-BDA-protein lysine crosslink. Our previous model studies with *N*-acetyl-L-lysine and *N*-acetyl-L-cysteine indicated that the pyrrolinone adducts of lysine do not lead to the formation of the thiol-BDA-lysine crosslinks since **3** does not lead to the formation of **4a** when incubated in the presence of N-acetyl-L-cysteine.[10]

The observation that degraded protein adducts are likely abundant *in vivo* metabolites of furan is consistent with a report that approximately 10% of a 8 mg/kg dose of [^{14}C]furan remains covalently associated with liver proteins 24 h post exposure.[7] The structures of the urinary furan metabolites, **3**, **4a** and **5a** indicate that lysine residues in proteins are likely important targets of BDA-mediated alkylation. Identification of the protein targets may provide insights into the mechanisms by which furan induces its

toxicity. It is also possible that the formation of large amounts of alkylated proteins directly triggers cell death through the unfolded protein response pathway, as has been suggested for thiobenzamide.[71]

In summary, the *in vivo* metabolites of furan have provided insights into possible reactive metabolites of furan. Oxidation of furan generates BDA that can then undergo at least three possible protein alkylation reactions (Scheme 2-4). It can either react directly with protein amino groups to form pyrrolinone adducts or it can react with protein cysteinyl residues followed by reaction of the remaining two aldehyde moieties with protein lysine groups. Alternatively, BDA will react with GSH via Michael addition and then proceed to alkylate protein lysinyl groups to form GSH-BDA-protein crosslinks. Future studies will explore the relative contribution of these three protein alkylation pathways to the overall toxic and carcinogenic properties of furan.

Table 2-1. Mass spectral data for the metabolites and standards.

Compound	*m/z*	RT (min)	MS^2 (fragment ions, *m/z*)	HRMS (measured)	HRMS (calculated)
Standard 1	356	28.8	338, 210	356.0894 $(M+H)^+$ [29]	356.0916 $(M+H)^+$
1 from [$^{12}C_4$]furan	356	28.9	338, 210	n.d.	
Standard 4a	400	49.5	382, 364, 336, 295, 271	422.1356 $(M+Na)^+$	422.1362 $(M+Na)^+$
4a from [$^{12}C_4$]furan	400	49.4	382, 364, 336, 295, 271	400.1532 $(M+H)^+$	400.1537 $(M+H)^+$
4a from [$^{13}C_4$]furan	404	49.3	384, 368, 340, 299, 275	n.d.	
Standard 4b	400	45.1	384, 364, 340, 322, 295, 271, 253, 211	n.d.	
Standard 5a	416	31.8	398, 380 339, 321, 269, 241, 239, 234, 223, 182	414.1343 $(M-H)^-$	414.1340 $(M-H)^-$
5a from [$^{12}C_4$]furan	416	31.9	398, 380, 339, 321, 269, 241, 239, 234, 223, 182, 134	416.1480 $(M+H)^+$	416.1486 $(M+H)^+$
5a from [$^{13}C_4$]furan	420	31.6	402, 384, 343, 325, 273, 245, 243, 238, 227, 186, 138	n.d.	
Standard 5b	416	29.6	398, 380, 362, 339, 321, 293, 269, 239, 227, 210, 193, 178	n.d.	
Standard 6a	358	36.6	340, 295,294, 229	356.1282 $(M-H)^-$	356.1286 $(M-H)^-$
6a from [$^{12}C_4$]furan	358	36.5	340, 295,294, 229	n.d.	
Standard 6b	358	30.9	340, 298, 253, 229, 211, 197	n.d.	
Standard 7a	502	28.5	484, 373, 356, 227	502.1954 $(M+H)^+$	502.1966 $(M+H)^+$
7a from [$^{12}C_4$]furan	502	29.1	484, 373, 356, 227	502.1962 $(M+H)^+$	502.1966 $(M+H)^+$
Standard 7b	502	25.0	484, 373, 356, 227	n.d.	
Standard 9a	502	25.1	427, 373, 356, 227	n.d.	
metabolites from [$^{12}C_4$]furan	502	25.1	484, 427, 373, 356, 227	n.d.	
Standard 9b	502	26.2	427, 373, 356, 227	502.1600 $(M+H)^+$	502.1602 $M+H)^+$
9b from [$^{12}C_4$]furan	502	26.1	427, 373, 356, 227	502.1598 $(M+H)^+$	502.1602 $M+H)^+$
Standard 10	544	45.4	469, 415, 398, 269, 241	544.2066	544.2072 $(M+H^+)$
10 from [$^{12}C_4$]furan	544	45.9	469, 415, 398, 269, 241	544.2042	544.2072 $(M+H^+)$

n.d. = not determined

Table 2-2. Ratio of **7b** to **7a** in *in vitro* reactions and media from furan-exposed hepatocytes.

Reaction conditions			α/ε (**7b**/**7a**)[a]
GSH + BDA + lysine in 1 M phosphate buffer	*m/z* 502	n = 5	0.978 ± 0.175
GSH + BDA + lysine in media containing HEPES	*m/z* 502	n = 5	0.155 ± 0.018
Hepatocytes	*m/z* 502	n = 4	0.096 ± 0.008
Hepatocytes with media containing 0.5 mM [4,4,5,5-$^{2}H_4$]-L-lysine	*m/z* 506	n = 2	0.234, 0.237
Hepatocytes time course			
1 h	*m/z* 502	n = 3	0.167 ± .016
2 h	*m/z* 502	n = 3	0.115 ± 0.014
4 h	*m/z* 502	n = 4	0.083 ± 0.021

[a]Relative peak areas were determined by LC-MS or LC-MS/MS selected reaction monitoring as described in Experimental Procedures.

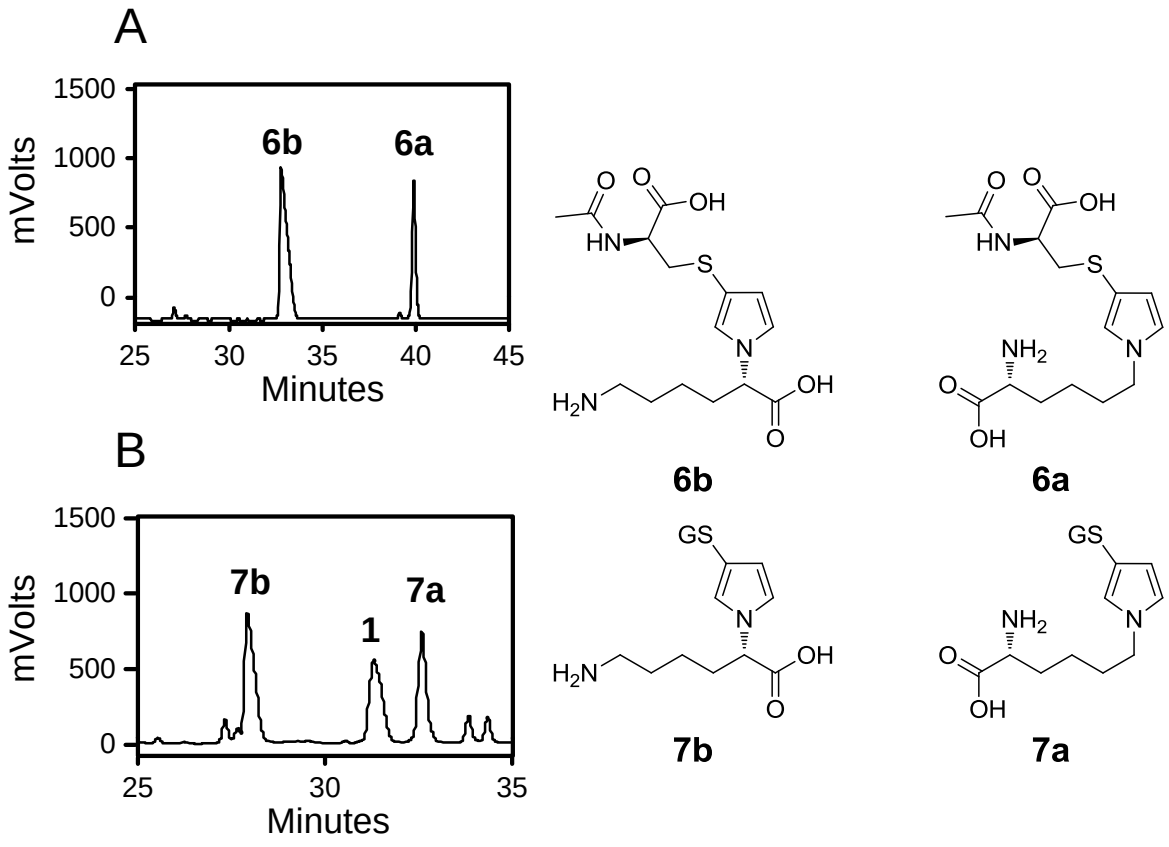

Figure 2-1. HPLC trace of lysine incubation with BDA and *N*-acetylcysteine (A) or GSH (B), monitoring at 254 nm. GS = glutathione.

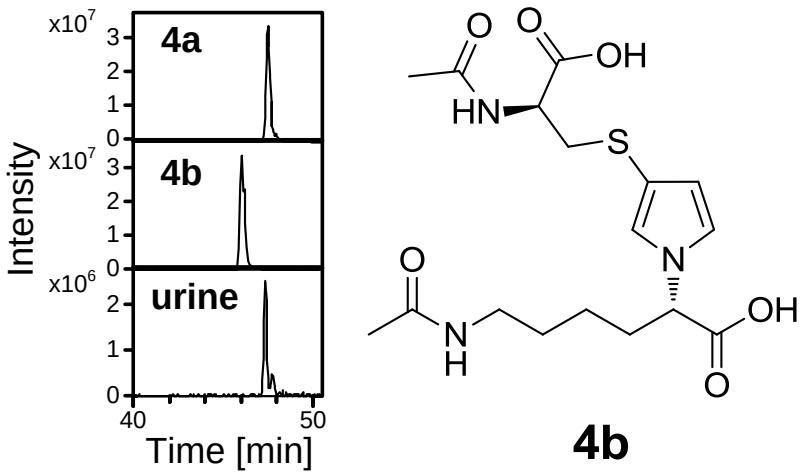

Figure 2-2. Daughter ion mass spectra for the *N*-acetylcysteine-BDA-lysine reaction products, *N*-acetyl-*S*-[1-(5-acetylamino-5-carboxypentyl)-1*H*-pyrrol-3-yl]-L-cysteine (**4a**) and *N*-acetyl-*S*-[1-(5-acetylamino-1-carboxypentyl)-1*H*-pyrrol-3-yl]-L-cysteine (**4b**) as well as those for the urinary and hepatocyte furan metabolites with the same retention time and mass.

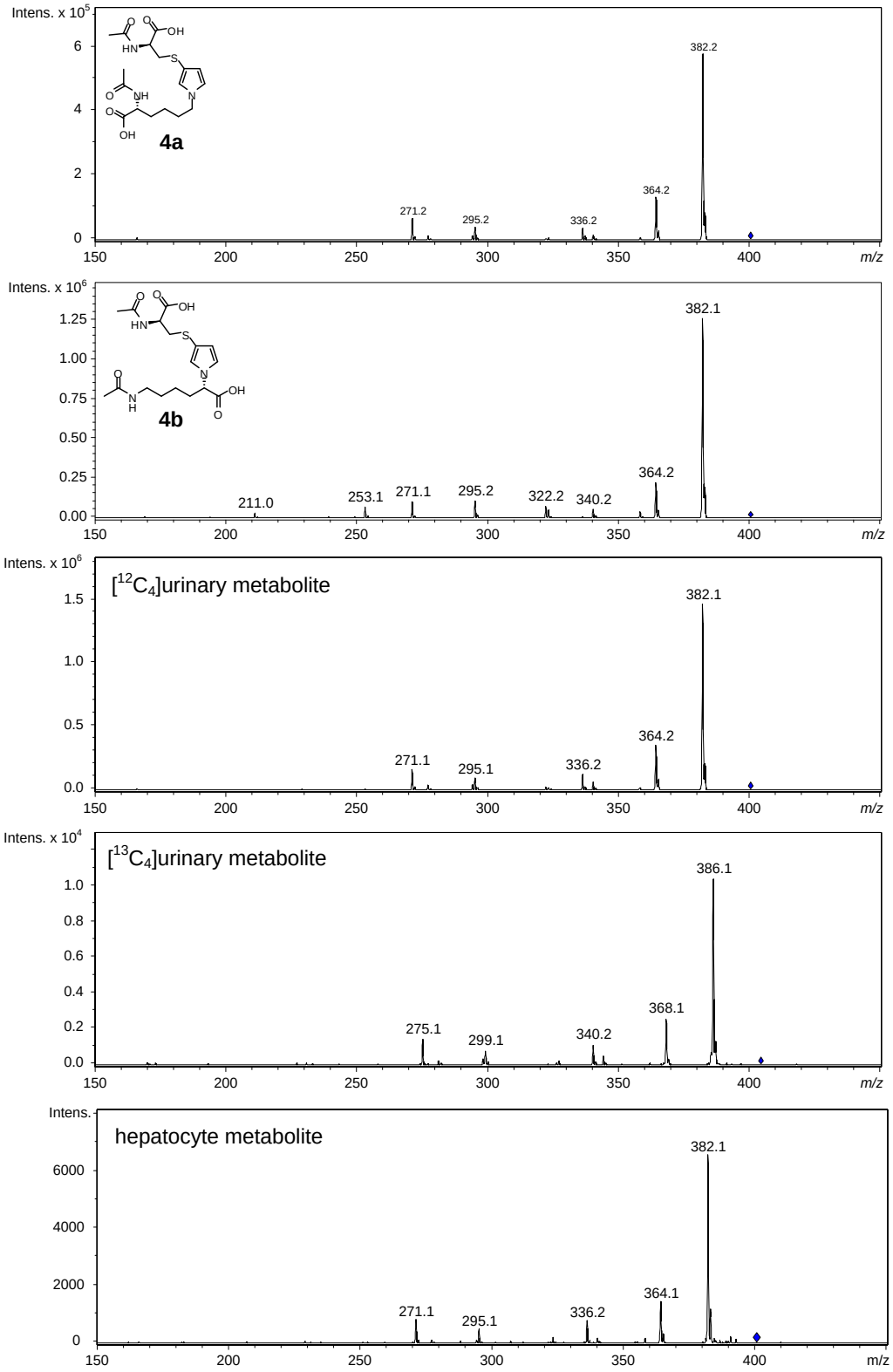

Figure 2-3. Extracted chromatograms at 400 amu for the standards **4a** and **4b** as well as for urine from [$^{12}C_4$]furan-treated rats.

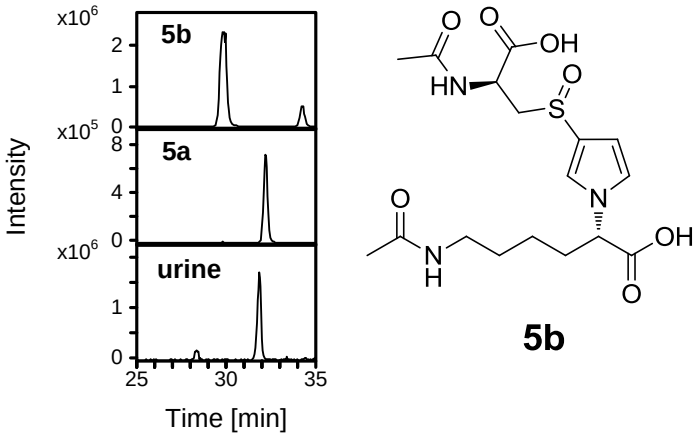

Figure 2-4. Daughter ion mass spectra for the sulfoxides of *N*-acetylcysteine-BDA-lysine reaction products, *N*-acetyl-*S*-[1-(5-acetylamino-5-carboxypentyl)-1*H*-pyrrol-3-yl]-L-cysteine sulfoxide (**5a**) and *N*-acetyl-*S*-[1-(5-acetylamino-1-carboxypentyl)-1*H*-pyrrol-3-yl]-L-cysteine sulfoxide (**5b**) as well as those for the urinary furan metabolite with the same mass and retention time.

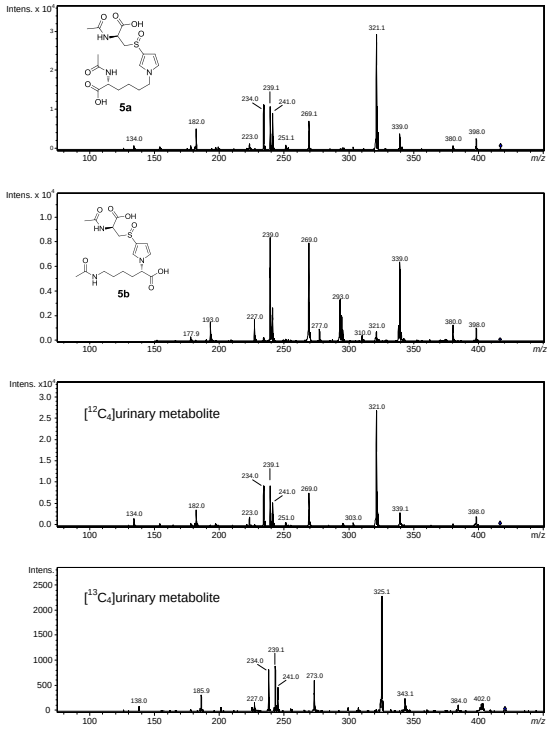

Figure 2-5. Extracted chromatograms at 416 amu for the standards **5a** and **5b** as well as for urine from [$^{12}C_4$]furan-treated rats.

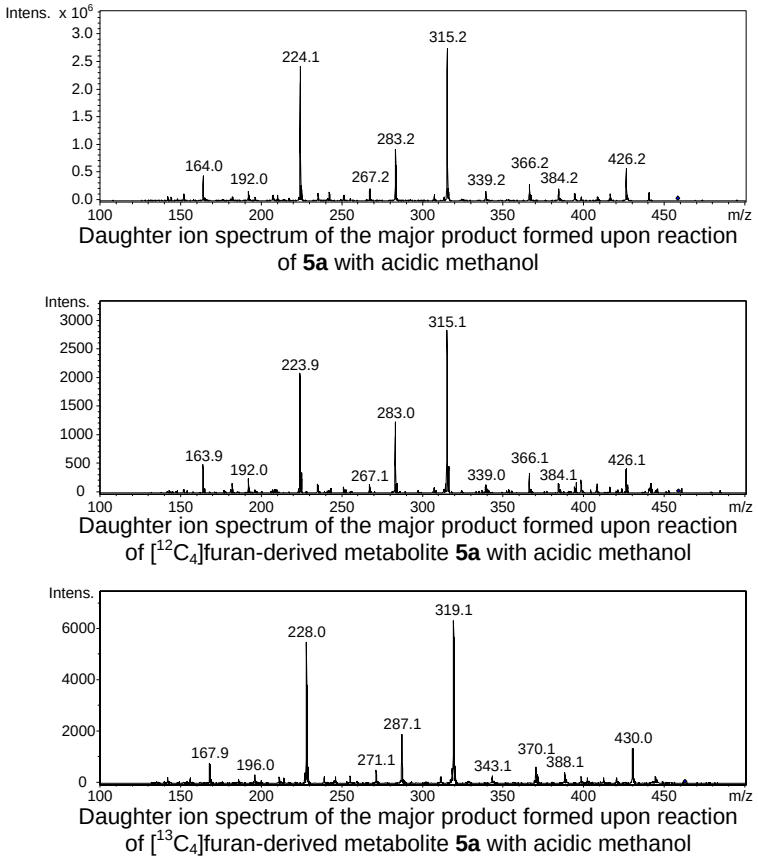

Figure 2-6. Mass chromatograms and mass spectra of the products formed upon incubating *N*-acetyl-*S*-[1-(5-acetylamino-5-carboxypentyl)-1*H*-pyrrol-3-yl]-L-cysteine sulfoxide (**5a**) in methanolic HCl.

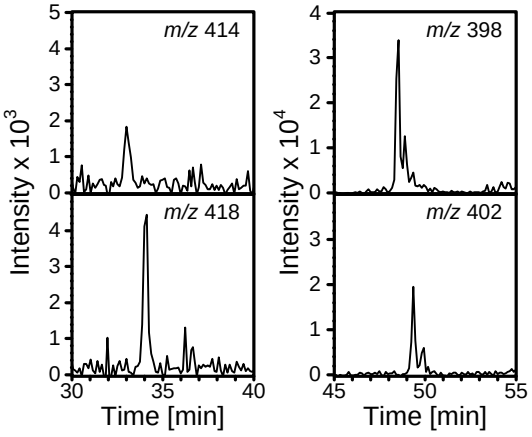

Figure 2-7. Extracted chromatograms at 398/402 and 414/418 amu in urine from [$^{13}C_4$]furan-treated rats (8 mg/kg).

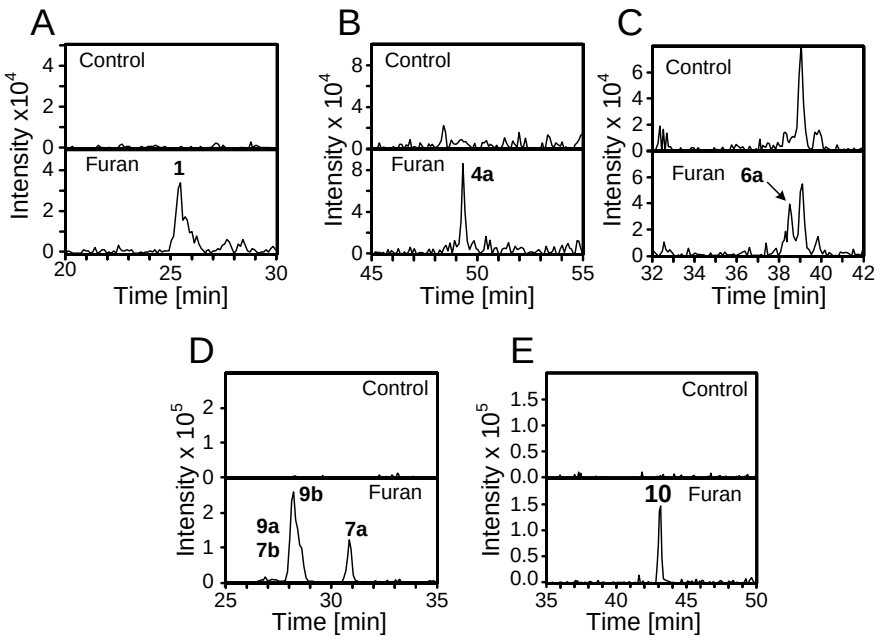

Figure 2-8. Extracted chromatographs for furan metabolites formed in hepatocytes. A) 356 amu; B) 400 amu; C) 358 amu; D) 502 amu and E) 544 amu.

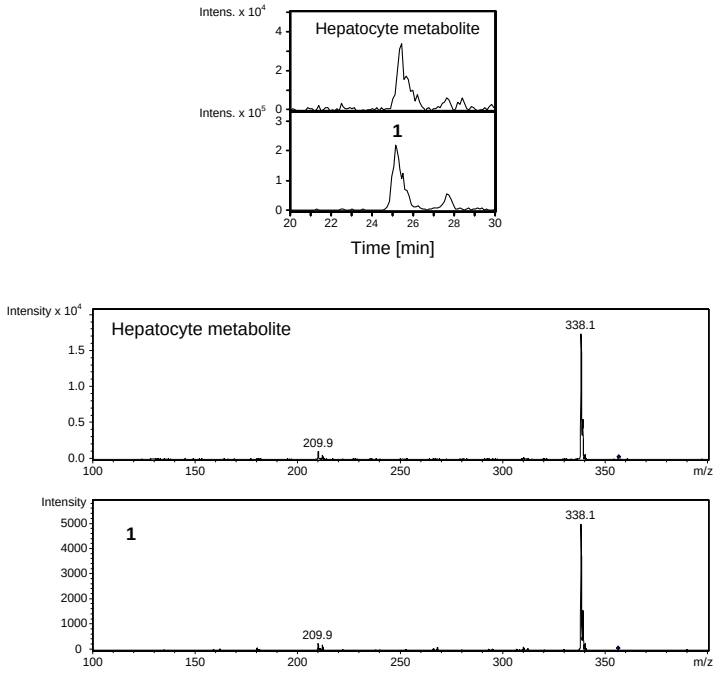

Figure 2-9. Extracted ion current at 356 amu for the medium from furan exposed hepatocytes (top) and a standard solution of the mono-GSH-BDA reaction product **1** (bottom) and the mass spectra corresponding to these LC peaks.

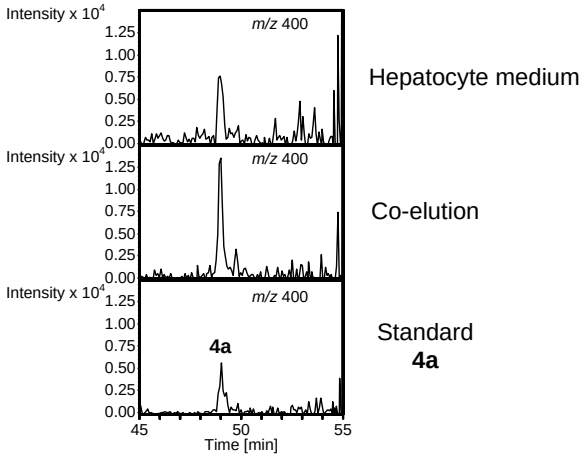

Figure 2-10. Extracted ion current at 400 amu demonstrating co-elution of hepatocyte metabolite with *N*-acetyl-*S*-[1-(5-acetylamino-5-carboxypentyl)-1*H*-pyrrol-3-yl]-L-cysteine (**4a**).

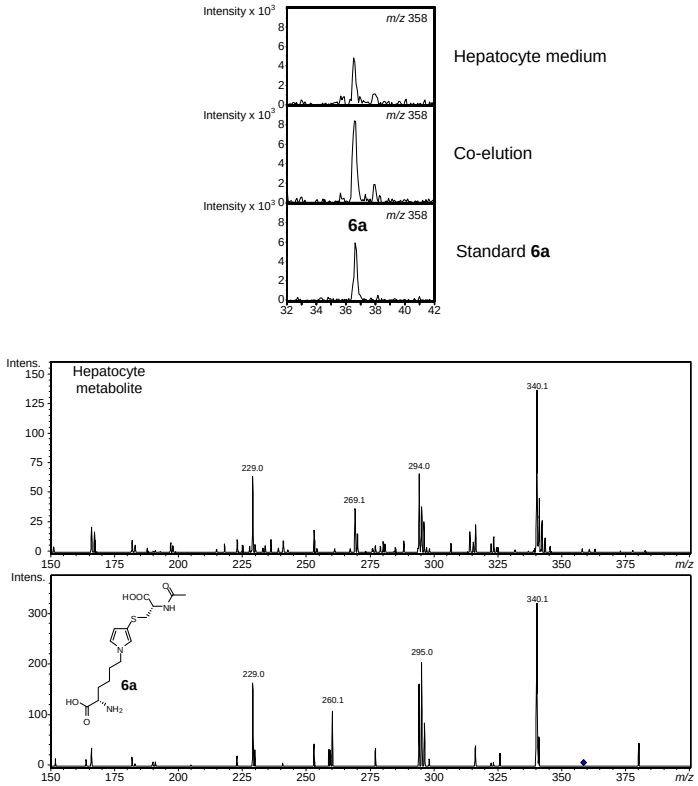

Figure 2-11. Extracted ion current at 358 amu demonstrating co-elution of hepatocyte metabolite with *N*-acetyl-*S*-[1-(5-amino-5-carboxypentyl)-1*H*-pyrrol-3-yl]-L-cysteine (**6a**) as well as the corresponding mass spectra.

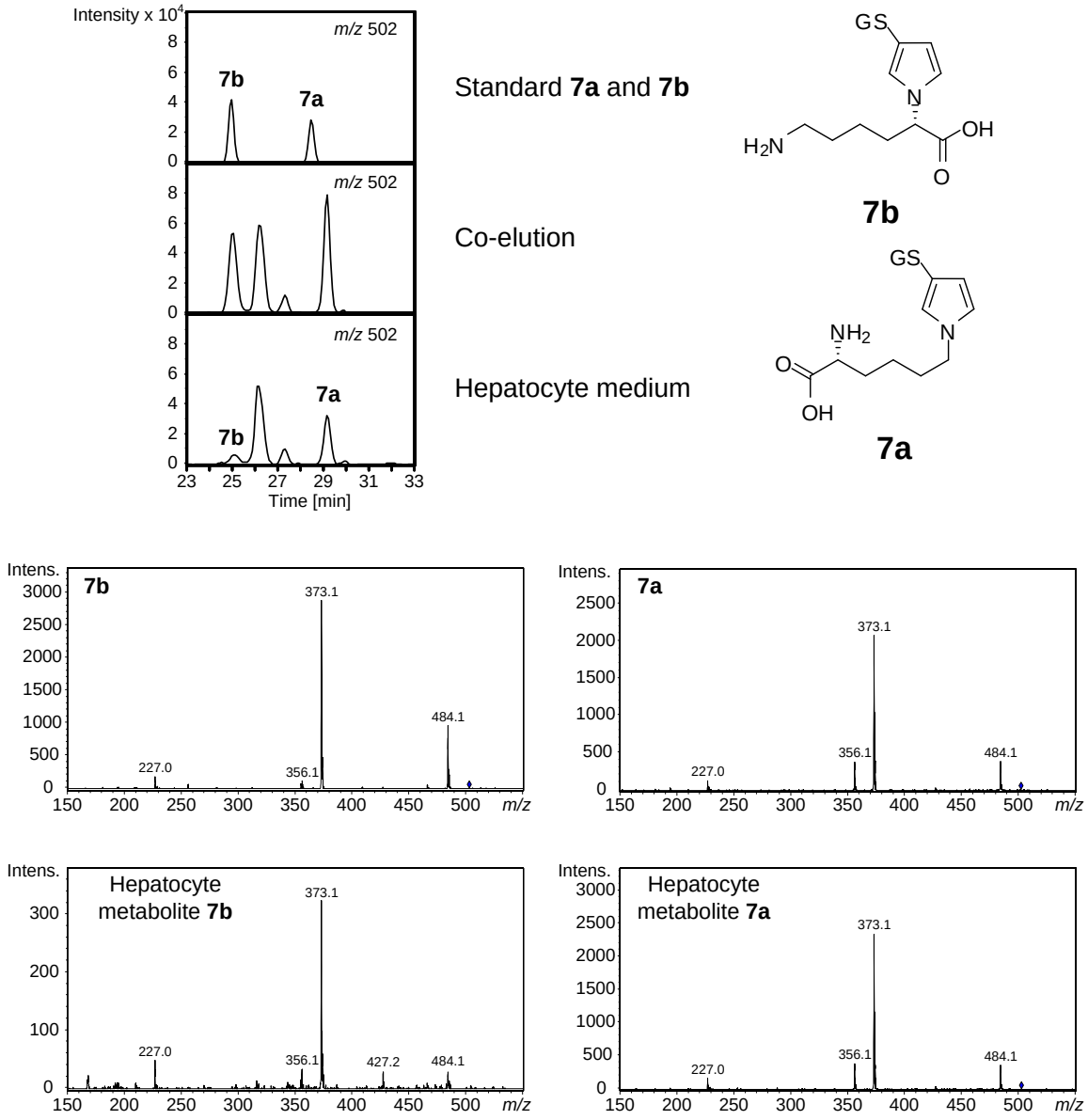

Figure 2-12. Extracted ion current at 502 amu demonstrating co-elution of hepatocyte metabolites with *S*-[1-(5-amino-5-carboxypentyl)-1*H*-pyrrol-3-yl]-glutathione (**7b**) and *S*-[1-(5-amino-1-carboxypentyl)-1*H*-pyrrol-3-yl]-glutathione (**7a**) as well as their corresponding mass spectra.

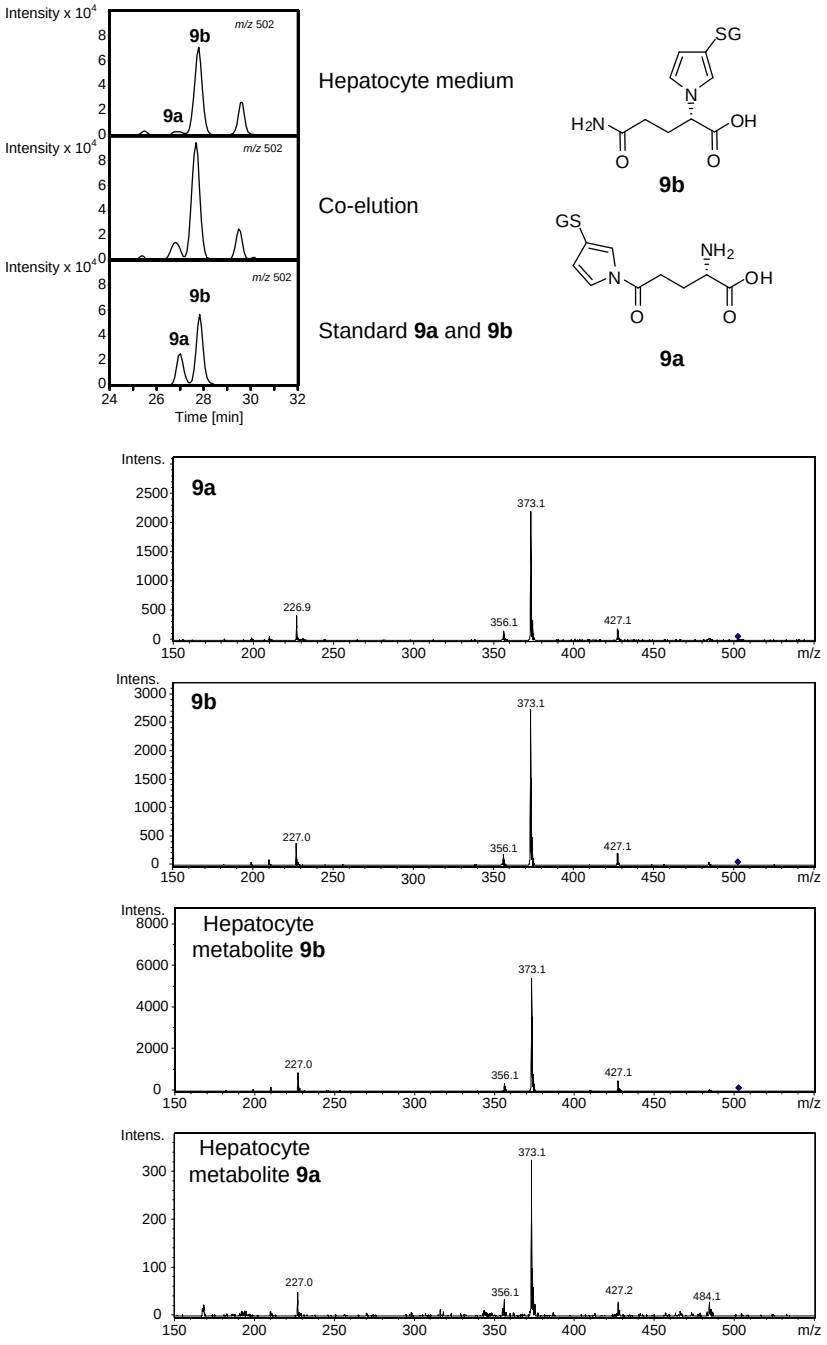

Figure 2-13. Extracted ion current at 502 amu demonstrating co-elution of *S*-[1-(4-amino-1-carboxy-4-oxobuty)-1*H*-pyrrol-3-yl]-glutathione (**9b)** with hepatocyte metabolite **9b** and *S*-[1-(4-amino-4-carboxy-1-oxobutyl)-1H-pyrrol-3-yl]-glutathione (**9a**) with hepatocyte metabolite **9a** as well as their corresponding mass spectra.

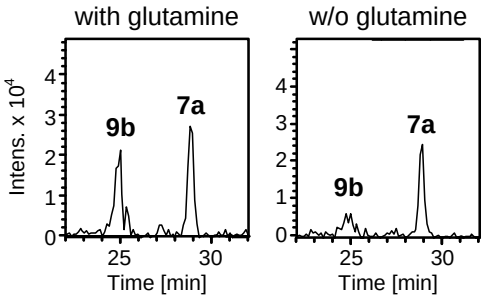

Figure 2-14. Extracted ion current at 502 amu indicating that the levels of glutamine in the hepatocyte medium influence the levels of *S*-[1-(4-amino-1-carboxy-4-oxobuty)-1*H*-pyrrol-3-yl]-glutathione (**9b**) but not *S*-[1-(5-amino-5-carboxypentyl)-1*H*-pyrrol-3-yl]-glutathione (**7a**) in furan exposed hepatocytes.

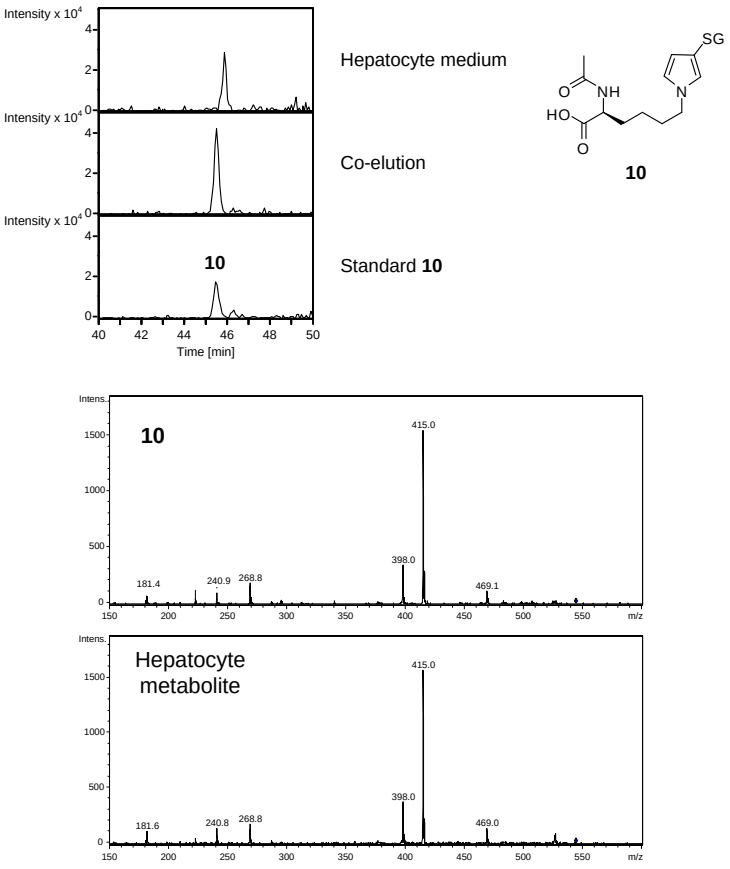

Figure 2-15. Extracted ion current at 544 amu demonstrating co-elution of standard **10** with the hepatocyte metabolite as well as their corresponding mass spectra.

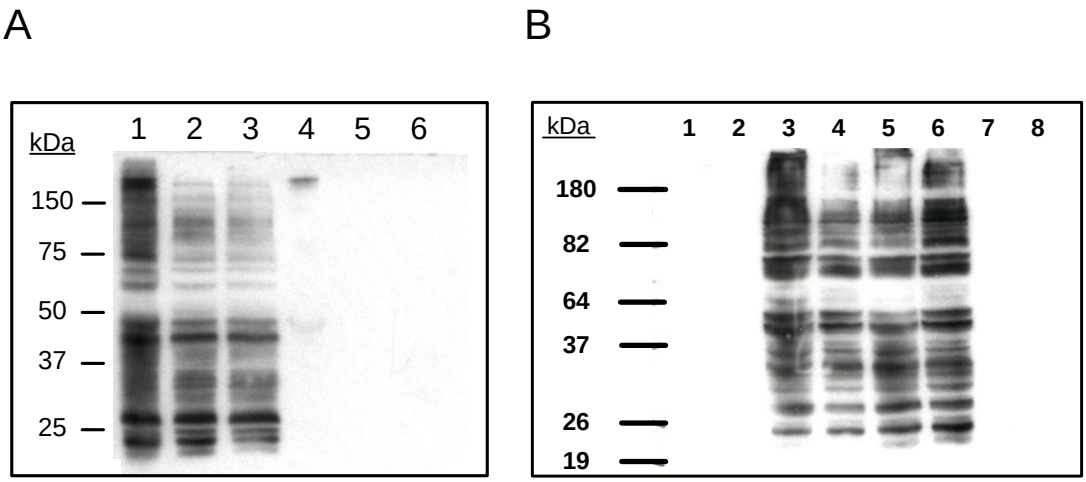

Figure 2-16. Western analysis of A) S9 from rat liver or B) hepatocyte extracts with rabbit anti-GSH antibody. A) Lane 1: liver S9 from furan-treated rats, lane 2: liver S9 from furan-treated rats plus 75 mM DTT; lane 3: liver S9 from furan-treated rats plus 135 mM DTT; lane 4: liver S9 from untreated rats; lane 5, liver S9 from untreated rats plus 75 mM DTT; lane 6: liver S9 from untreated rats plus 135 mM DTT. B) Lane 1: extracts from control hepatocytes; Lane 2: extracts from control hepatocytes plus 75 mM DTT; Lane 3: extracts from furan-treated hepatocytes; Lane 4: extracts from furan-treated hepatocytes plus 75 mM DTT; Lane 5: extracts from SKF525A- and furan-treated hepatocytes; Lane 6: extracts from SKF525A- and furan-treated hepatocytes plus 75 mM DTT; Lane 7: extracts from 1-phenylimidazole- and furan-treated hepatocytes; Lane 8: extracts from 1-phenylimidazole- and furan-treated hepatocytes plus 75 mM DTT.

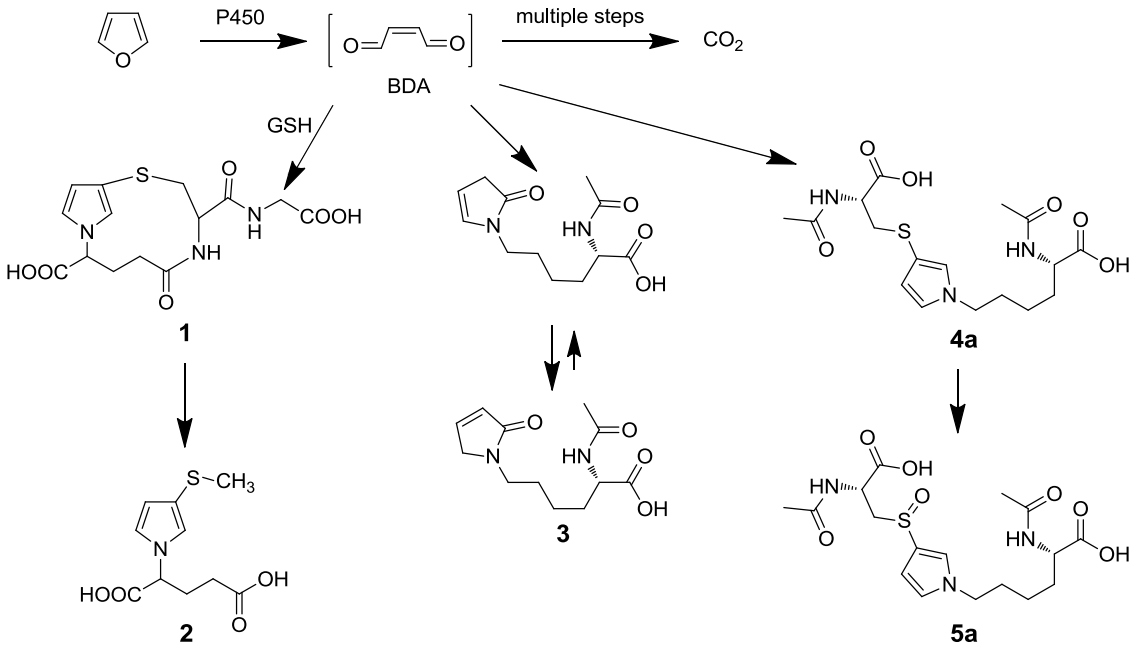

Scheme 2-1. Identified pathways of furan metabolism.

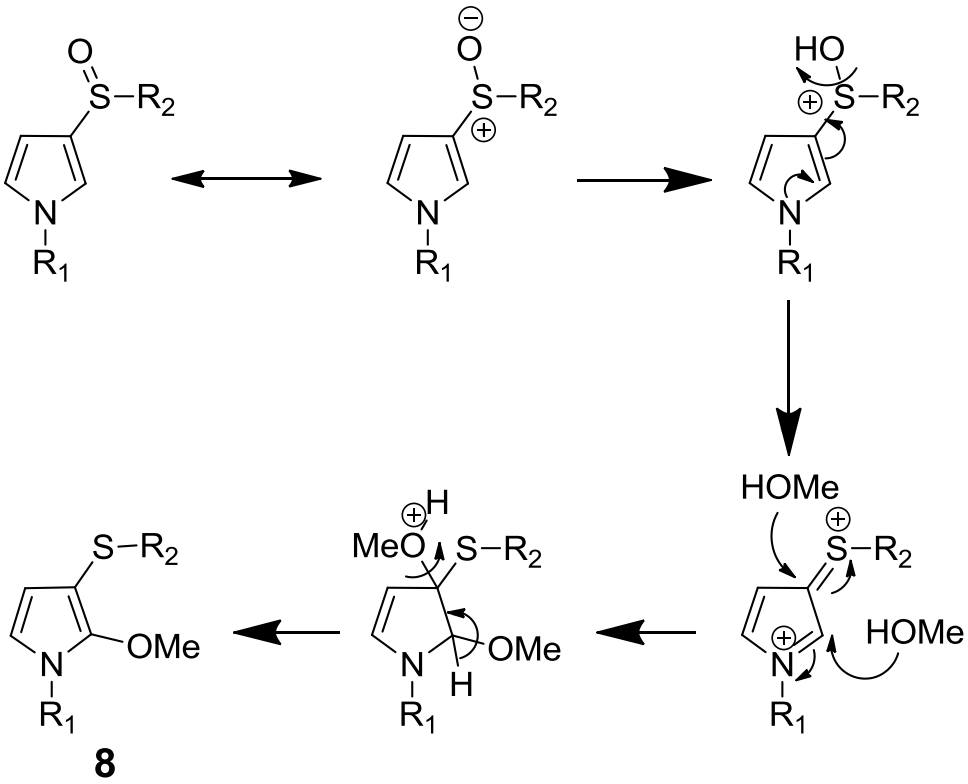

Scheme 2-2. Proposed mechanism for the addition of methanol to the 2-pyrrole position of **5a**.

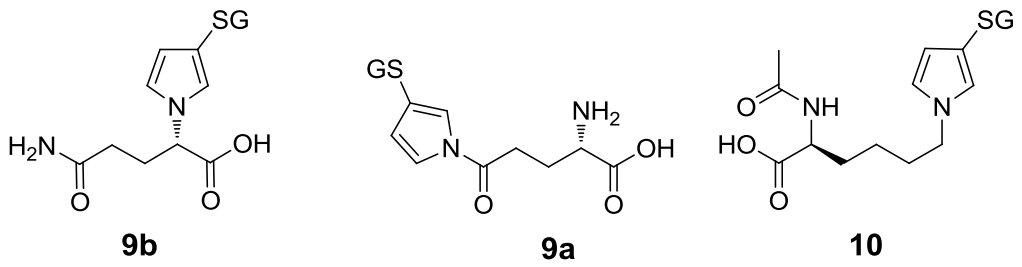

Scheme 2-3. Structure of GSH-BDA-glutamine and GSH-BDA-N^{α}-acetyllysine reaction products. GS = glutathione.

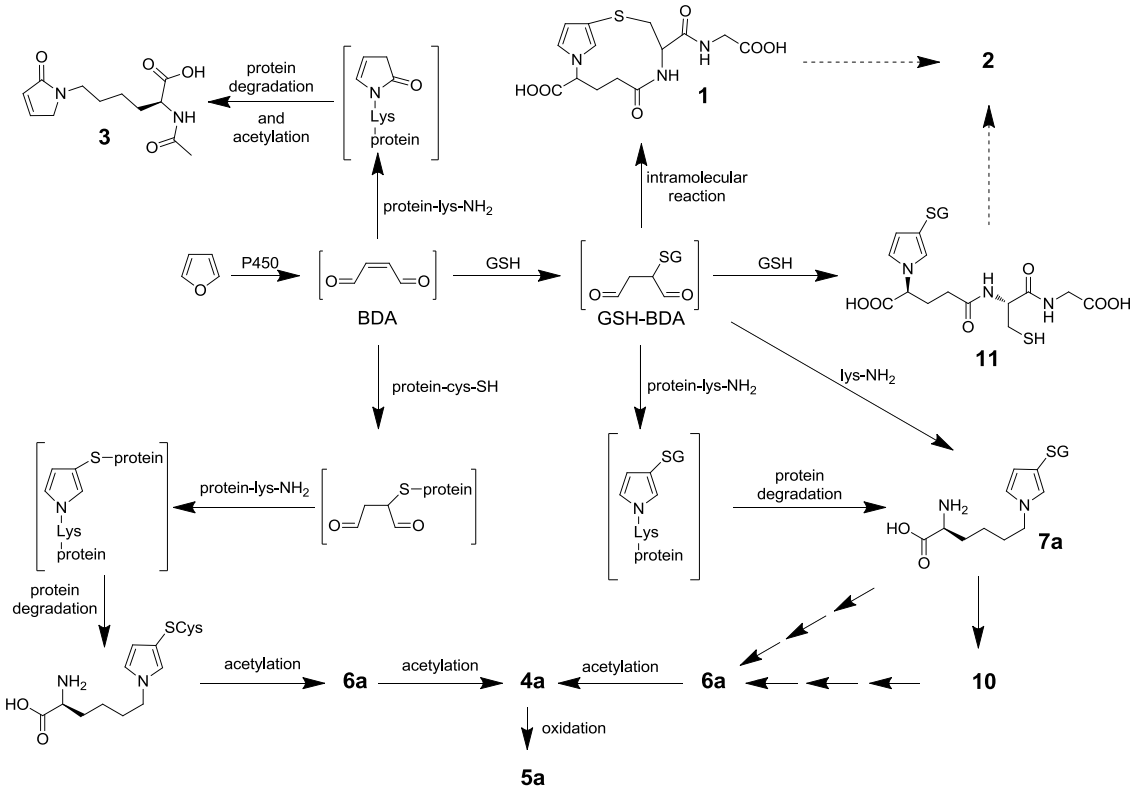

Scheme 2-4. Proposed pathways of furan metabolism.

Chapter 3: Polyamines are traps for reactive intermediates in furan metabolism

Summary – This chapter describes the characterization of polyamine adducts as urinary and hepatocyte metabolites of furan.

Rationale – The structures of many metabolites of furan are still unknown. Characterization of these metabolites is expected to provide insight into the metabolism of furan and its toxicological mechanism. Polyamines play a central role in cell cycle control, apoptosis signaling, and nucleic acid structure, disruption of which has been linked to toxicity and carcinogenic transformation. Since polyamines contain primary amine functional groups, these molecules are probable target for furan's principal reactive intermediate, *cis*-2-butene-1,4-dial, and modification of polyamines may play a role in furan's mechanism of action.

My contribution to this work – I performed the *in vitro* analysis of GSH-BDA-amine cross-link distribution. I also assisted in the preparation and revision of the manuscript**.**

Polyamines are traps for reactive intermediates in furan metabolism

Lisa A. Peterson,[1,2,3] Martin B. Phillips,[3] Ding Lu,[2] and Mathilde M. Sullivan[2]

Division of Environmental Health Sciences, Department of Medicinal Chemistry and Masonic Cancer Center, University of Minnesota, Mayo Mail Code 806, 420 Delaware Street SE, Minneapolis, Minnesota 55455

[1]Division of Environmental Health Sciences

[2]Masonic Cancer Center

[3]Department of Medicinal Chemistry

Reprinted with permission from Peterson, L. A., Phillips, M. B., Lu, D., and Sullivan, M. M. (2011) Polyamines are traps for reactive intermediates in furan metabolism. *Chem. Res. Toxicol. 24*, 1924-1936.

SUMMARY

Furan is toxic and carcinogenic in rodents. Because of the large potential for human exposure, furan is classified as a possible human carcinogen. The detailed mechanism by which furan causes toxicity and cancer is not yet known. Since furan toxicity requires cytochrome P450-catalyzed oxidation of furan, we have characterized the urinary and hepatocyte metabolites of furan to gain insight into the chemical nature of the reactive intermediate. Previous studies in hepatocytes indicated that furan is oxidized to the reactive α,β-unsaturated dialdehyde, *cis*-2-butene-1,4-dial (BDA), which reacts with glutathione (GSH) to form 2-(*S*-glutathionyl)succinaldehyde (GSH-BDA). This intermediate forms pyrrole cross-links with cellular amines such as lysine and glutamine. In this report, we demonstrate that GSH-BDA also forms cross-links with ornithine,

putrescine and spermidine when furan is incubated with rat hepatocytes. The relative levels of these metabolites are not completely explained by hepatocellular levels of the amines or by their reactivity with GSH-BDA. Mercapturic acid derivatives of the spermidine cross-links were detected in the urine of furan-treated rats, indicating that this metabolic pathway occurs in vivo. Their detection in furan-treated hepatocytes and in urine from furan-treated rats indicates that polyamines may play an important role in the toxicity of furan.

INTRODUCTION

Chronic exposure of F344 rats and B6C3F$_1$ mice to furan results in dose-dependent toxicity and carcinogenicity in both species.[1] Furan-treated rats also develop cholangiocarcinomas.[1] Because it is widely distributed in the environment,[2,16] human exposure to furan is likely to be significant. Since there is a large potential for human exposure, furan has been listed by the National Toxicology Program and the International Agency for Research on Cancer as a possible human carcinogen (Group 2B).[2,72] Adequate human risk assessment has been stymied because of the lack of mechanism-based biomarkers.

Furan requires metabolism by cytochrome P450 2E1 to elicit its toxic effects.[4,73] Chemical characterization of the metabolites of furan provides insights into the identity of the reactive intermediates formed as a result of furan metabolism. The initial product of furan oxidation is *cis*-2-butene-1,4-dial (BDA, Scheme 3-1).[6,23] The metabolites characterized to date in urine from furan-exposed rats indicate that BDA reacts with cellular nucleophiles such as glutathione (GSH), cysteine and lysine (Scheme 3-1).[9,26,28,29] The majority of the urinary metabolites are derived from a cysteine-BDA-lysine cross-

link, *S*-[1-(5-amino-5-carboxypentyl)-1*H*-pyrrol-3-yl]-L-cysteine (**1**, Cys-BDA-lysine, Scheme 3-1).[9,26,28] Studies in rat hepatocytes indicate that a major source of metabolite **1** is a GSH-BDA-lysine cross-link, *S*-[1-(5-amino-5-carboxypentyl)-1*H*-pyrrol-3-yl]-glutathione (**2**, GSH-BDA-lysine, Scheme 3-1).[9] This observation suggests that once BDA is formed, it reacts with GSH to form 2-(*S*-glutathionyl)succinaldehyde (GSH-BDA, **3**), which reacts with lysine to form the observed GSH-BDA-lysine cross-link (Scheme 3-1). This cross-link is then further process to the urinary metabolites.

Lysine is not the only target for this cross-linking reaction. Intramolecular cross-linking occurs to form *N*-[4-carboxy-4-(3-mercapto-1*H*-pyrrol-1-yl)-1-oxobutyl]-L-cysteinylglycine cyclic sulfide (mono-GSH-BDA, **4**, Scheme 3-1). Cross-links with glutamine and several other unidentified GSH conjugates were also observed in media from rat hepatocytes exposed to furan.[9] In this report, we provide the chemical identity for five of these unidentified metabolites. They result from the reaction of GSH-BDA with the primary amino groups of ornithine, spermidine and putrescine. These findings led to the characterization of related metabolites in the urine of furan-treated rats. Polyamines are critical for normal cell growth and function.[74] The cellular levels of these compounds are maintained through a tightly regulated network of enzymes involved in their formation and degradation. Imbalance in polyamine pathways is associated with a number of diseases, including cancer.[75-77] The formation of GSH-BDA-polyamine reaction products indicates that polyamines are traps for electrophilic metabolites and suggests pathways, in addition to DNA and protein adduct formation, for furan to exert its toxic effects.

EXPERIMENTAL PROCEDURES

Caution: *BDA is toxic and mutagenic in cell systems. Furan is toxic and carcinogenic in laboratory animals. Both chemicals should be handled with proper safety equipment and precautions*.

Chemicals. [$^{13}C_4$]Furan, BDA, mono-GSH-BDA and GSH-BDA-GSH conjugates were prepared as previously described.[10,29,46,62] The concentration of aqueous solutions of BDA was determined as previously described.[43] Furan was purchased from Acros Organics (Pittsburgh, PA) and distilled before use. Spermine, cadaverine, and putrescine were purchased from MP Biomedicals (Solon, OH). All other reagents were purchased from Aldrich Chemical (Milwaukee, WI) unless stated otherwise. All HPLC solvents were chromatography grade.

Instrumentation. HPLC purifications were carried out on a Shimadzu LC-10AD system coupled to a Shimadzu SCL-10A UV/vis detector. NMR spectra were recorded on 500 or 600 MHz Varian Inova spectrometers or a 700 MHz Bruker Avance spectrometer in the Department of Chemistry or the Department of Biochemistry, Molecular Biology, and Biophysics, University of Minnesota. Chemical shifts are reported in parts per million (ppm) as referenced to the residual solvent peak.

Collision-induced mass spectra of reaction products were obtained on an Agilent 1100 series LC/MSD Trap SL mass spectrometer operating in positive ion mode. Each compound was dissolved in 10 mM ammonium formate, pH 2.8, and directly infused into the ion source. Helium was the nebulizing and drying gas (15 psi, 5 L/min) which had a temperature set at 200 °C. High resolution mass spectral data for the synthetic standards were obtained on a Bruker BioTOF II mass spectrometer in the Department of Chemistry,

University of Minnesota or a Thermo Ultra AM Triple Quadrupole mass spectrometer in the Masonic Cancer Center, University of Minnesota.

For most of the HPLC and LC-MS analyses, the column was eluted with the following gradient: 10 min at 100% A; 26 min gradient to 75% A, 25% B; 10 min gradient to 50% A, 50% B; 4 min gradient to 100% B where solvent A was 10 or 50 mM ammonium formate, pH 2.8 and solvent B was 50% acetonitrile in water. This gradient will subsequently be referenced as HPLC method 1.

Reactions between GSH, BDA, and Amines. GSH (21 mg, 68 μmol) and L-ornithine hydrochloride (11 mg, 68 μmol), putrescine (6.0 mg, 68 μmol), spermidine (9.8 mg, 68 μmol), spermine (14 mg, 68 μmol) or cadaverine (6.9 mg, 68 μmol) were added to a solution of BDA (68 μmol) in 50 mM or 1 M sodium phosphate, pH 7.4 (total volume: 2 mL). After 2 h at 37 °C, the products were purified on a semipreparative Phenomenex (Torrence, CA) Synergi 4μ Hydro-RP column (250 × 10 mm, 4 μm) employing HPLC method 1 (solvent A was 50 mM ammonium formate, pH 2.8) with a flow rate of 4 mL/min. The eluting peaks were collected and concentrated under reduced pressure. The buffer salts were removed by HPLC purification as described for each compound.

GSH-BDA-Ornithine. When the reaction was performed with ornithine, the resulting reaction mixture was complex. However, there were two prominent UV-absorbing products in a ratio of 5:7 whose mass spectra had a molecular ion at *m/z* 488. This mass is consistent with the formation of a cross-link between ornithine and GSH via BDA. Mass spectral analysis indicated that the other peaks were either GSH-BDA reaction products (*m/z* 356, GSH-BDA [$M+H^+$]) or further BDA or GSH-BDA reaction products of GSH-BDA-ornithine (*m/z* 554, GSH-2BDA-ornithine [$M+H^+$] or *m/z* 422,

2GSH-2BDA-ornithine $[M+2H]^{2+}$). The two GSH-BDA-ornithine products eluted at 22.8 min and 27.7 min when HPLC method 1 was employed (solvent A was 50 mM ammonium formate, pH 2.8). Following preparative isolation by HPLC, they were desalted on a semipreparative Synergi 4μ Hydro-RP column with the following gradient (4 mL/min): 5 min at 100% A; 20 min gradient to 85% A, 15% B; 5 min gradient to 70% A, 30% B where solvent A was 0.1% v/v formic acid and solvent B was 50 % acetonitrile in water. The compound that eluted at 22.8 min was identified as *S*-[1-(4-amino-1-carboxybutyl)-1*H*-pyrrol-3-yl]-glutathione (GSH-BDA-N^{α}-ornithine). ^{1}H NMR (500 MHz, D_2O): δ 6.88 (s, 1H, H2'), 6.71 (s, 1H, H5'), 6.19 (s, 1H, H4'), 4.45 (dd, 1H, H1), 4.25 (dd, 1H, Cys α-CH), 3.70 (m, 1H, Glu α-CH), 3.64 (s, 2H, Gly α-CH_2), 3.12 (dd, 1H, Cys β-CH_a), 2.92 (m, 2H, H4), 2.80 (dd, 1H, Cys β-CH_b), 2.47 (m, 2H, Glu γ-CH_2), 2.13–2.08 (m, 3H, Glu β-CH_2, $H2_a$), 1.96 (m, 1H, $H2_b$), 1.57 (m, 1H, $H3_a$), 1.41 (m, 1H, $H3_b$). MS data are displayed in Table 3-1. The compound that eluted at 27.7 min was characterized as *S*-[1-(4-amino-4-carboxybutyl)-1*H*-pyrrol-3-yl]-glutathione (GSH-BDA-N^{δ}-ornithine). ^{1}H NMR (500 MHz, D_2O): δ 6.77 (s, 1H, H5'), 6.16 (d, 1H, H4'), 4.29 (m, 1H Cys α-CH), 3.90 (m, H4), 3.80 (s, 2H, Gly α-CH_2), 3.74 (m, 1H, Glu α-CH), 3.69 (m, 1H, H1), 3.09 (dd, 1H, Cys β-CH_a), 2.83 (dd, 1H, Cys β-CH_b), 2.45 (m, 2H, Glu γ-CH_2), 2.09 (m, 2H, Glu β-CH_2), 1.80 (m, 1H, $H3_a$), 1.72–1.70 (m, 3H, $H3_b$ and H2). MS data are displayed in Table 3-1.

GSH-BDA-Spermidine. The GSH-BDA-spermidine reaction mixture contained multiple products. Two UV-absorbing products had the expected molecular ions at *m*/*z* 501. These products, which eluted at 24.5 and 28.1 min, were present in a ratio of 4:1 (HPLC Method 1, solvent A was 50 mM ammonium formate, pH 2.8). Based on mass

spectral analysis, the other peaks were either GSH-BDA reaction products (m/z 356, GSH-BDA [M+H^+]) or further reaction products of GSH-BDA-spermidine with additional molecules of BDA (*m/z* 567, GSH-2BDA-spermidine [M+H^+] or *m/z* 633, GSH-3BDA-spermine [M+H^+]). The GSH-BDA-spermidine reaction products were purified by semipreparative HPLC (HPLC method 1, 50 mM ammonium formate, pH 2.8) and the collected products were desalted for NMR analysis on a semipreparative Synergi 4µ Hydro-RP column with the following gradient (4 mL/min). 5 min at 100% A; 15 min gradient to 85% A, 15% B; 5 min gradient to 70% A, 30% B where solvent A was 0.1% v/v formic acid and solvent B was 50 % acetonitrile in water. The major isomer that eluted at 24.5 min was identified as *N*-(3-(3-(*S*-glutathionyl)-1*H*-pyrrol-1-yl)propyl)butane-1,4-diamine (GSH-BDA-N^1-spermidine). ^{1}H NMR (500 MHz, D_2O): 6.68 (s, 1H, H5'), 6.10 (s, 1H, H4'), 4.17 (dd, 1H, Cys α-CH), 3.88 (t, 2H, H1), 3.63 (t, 1H, Glu α-CH), 3.54 (s, 2H, Gly α-CH_2), 3.01 (dd, 1H, Cys β-CH_a), 2.93–2.83 (m, 4H, H4 and H7), 2.81–2.70 (m, 3H, H3, Cys β-CH_b), 2.38 (m, 2H, Glu γ-CH_2), 2.02–1.93 (m, 4H, Glu β-CH_2, H2), 1.56 (m, 4H, H5 and H6). MS data are displayed in Table 3-1.

The minor isomer that eluted at 28.1 min was identified as *N*-(4-(3-(*S*-glutathionyl)-1*H*-pyrrol-1-yl)butyl)propane-1,3-diamine (GSH-BDA-N^8-spermidine). ^{1}H NMR (500MHz, D_2O): δ 6.67 (s, 1H, H5'), 6.08 (s, 1H, H4'), 4.14 (dd, 1H, Cys α-CH), 3.80 (t, 2H, H1), 3.63 (t, 1H, Glu α-CH), 3.58 (s, 2H, Gly α-CH_2), 3.00 (dd, 1H, Cys β-CH_a), 2.96–2.88 (m, 4H, H5 and H7), 2.83 (t, 2H, H4), 2.71 (dd, 1H, Cys β-CH_b), 2.38 (m, 2H, Glu γ-CH_2), 2.01 (q, 2H, Glu β-CH_2), 1.88 (m, 2H, H6), 1.66 (m, 2H, H2), 1.42 (m, 2H, H3). MS data are displayed in Table 3-1.

GSH-BDA-Cadaverine. A single UV-absorbing compound with a molecular ion of *m*/*z* 458 was observed in the GSH-BDA-cadaverine reaction mixture. This compound eluted at 35.2 min when HPLC method 1 was employed (solvent A was 50 mM ammonium formate, pH 2.8). The HPLC purified product was desalted on a semipreparative Synergi 4µ Hydro-RP column with the following gradient (4 mL/min): 5 min at 100% A; 10 min gradient to 75% A, 25% B; 5 min gradient to 25% A, 75% B where solvent A was 0.1% v/v formic acid/water and solvent B was 50% acetonitrile in water. The product was identified as *S*-(1-(5-aminopentyl)-1*H*-pyrrol-3-yl)glutathione (GSH-BDA-cadaverine). ^{1}H NMR (500 MHz, DMSO-d_6): δ 6.84 (s, 1H, H2'), 6.77 (s, 1H, H5'), 6.07 (s, 1H, H4'), 4.24 (dd, 1H, Cys α-CH), 3.84 (m, 2H, H1), 3.55 (m, 2H, Gly α-CH_2), 3.45 (m, 1H, Glu α–CH), 2.95 (dd, 1H, Cys β-CH_a), 2.75 (t, 2H, H5), 2.63 (dd, 1H, Cys β-CH_b), 2.35 (m, 2H, Glu γ-CH_2), 1.97 (m, 2H, Glu β-CH_2), 1.63 (m, 2H, H2), 1.54 (m, 2H, H4), 1.20 (m, 2H, H3). MS data are displayed in Table 3-1.

GSH-BDA-Putrescine. In the reaction mixture of GSH-BDA-putrescine, one UV absorbing compound was observed with the expected molecular ion of *m*/*z* 444. This compound eluted at 30.5 min when HPLC method 1 was employed (solvent A was 50 mM ammonium formate, pH 2.8). Fractions containing this compound were desalted on a semipreparative Synergi 4µ Hydro-RP column with the following gradient (4 mL/min): 5 min at 100% A; 10 min gradient to 75% A, 25% B; 5 min gradient to 25% A, 75% B where solvent A was 0.1% v/v formic acid/water and solvent B was 50% acetonitrile in water. It was identified as *S*-(1-(4-aminobutyl)-1*H*-pyrrol-3-yl)glutathione (GSH-BDA-putrescine). ^{1}H NMR (500 MHz, D_2O): δ 6.76 (m, 1H, H2'), 6.68 (m, 1H, H5'), 6.07 (m, 1H, H4'), 4.18 (dd, 1H, Cys α-CH), 3.80 (t, 2H, H1), 3.62 (t, 1H, Glu α-CH), 3.57 (m,

2H, Gly α-CH_2), 3.01 (dd, 1H, Cys β-CH_a), 2.77 (m, 2H, H4), 2.73 (dd, 1H, Cys β-CH_b), 2.37 (m, 2H, Glu γ-CH_2), 2.01 (m, 2H, Glu β-CH_2), 1.66 (m, 2H, H2), 1.42 (m, 2H, H3). MS data are displayed in Table 3-1.

GSH-BDA-Spermine. One UV-absorbing compound with the expected molecular ion of *m*/*z* 558 was observed in the reaction mixture containing GSH, BDA, and spermine. This compound eluted at 27.8 min when HPLC method 1 was employed (solvent A was 50 mM ammonium formate, pH 2.8). Fractions containing this reaction product were desalted with HPLC method 1. It was identified as *N*-(3-((*S*-glutathionyl)-1*H*-pyrrol-1-yl)propyl)butane-1,4-diamine (GSH-BDA-spermine). ^{1}H NMR (500 MHz, D_2O): δ 6.75 (s, 1H, H2'), 6.67 (m, 1H, H5'), 6.09 (m, 1H, H4'), 4.14 (dd, 1H, Cys α-CH), 3.87 (t, 2H, H1), 3.63 (t, 1H, Glu α–CH), 3.57 (d, 2H, Gly α–CH_2), 3.01 (m, 1H, Cys β–CH_a), 2.98–2.82 (m, 8H, H4, H7, H8, H10), 2.77–2.68 (m, 3H, Cys β-CH_b, H3), 2.38 (m, 2H, Glu γ-CH_2), 2.05–1.86 (m, 6H, Glu β-CH_2, H2, H9), 1.61–1.49 (m, 4H, H5, H6). MS data are displayed in Table 3-1.

Reaction between NAC, BDA, and L-ornithine. *N*-Acetyl-L-cysteine (NAC) (8 mg, 50 μmol) and BDA (50 μmol) were incubated in 1 mL of 1 M sodium phosphate, pH 7.4, at 37 ºC for 30 min before adding L-ornithine monohydrochloride (8 mg, 50 μmol). The reaction was stirred for 15 hours. LC-MS analysis of the reaction mixture with HPLC method 1 demonstrated two major peaks (*m/z* 344) eluting at 37.0 min and 50.3 min. MS data are displayed in Table 3-1.

Reaction between NAC, BDA, and spermidine. NAC (45 mg, 270 μmol) and BDA (135 μmol) were incubated in 3 mL of 1 M sodium phosphate, pH 7.4, at 37 ºC for 25 min before adding spermidine (39 mg, 270 μmol). The reaction was stirred for 15

hours. HPLC analysis of the reaction mixture with HPLC method 1 demonstrated two major UV-absorbing peaks eluting at 32.0 min and 37.1 min in a ratio of 6:1. The two diastereomers (*m/z* 357) were purified by semipreparative HPLC. The organic solvent was removed under reduced pressure and the buffer salt was removed by solid phase extraction using Strata-X cartridges.

The first compound that eluted at 32.0 min was identified as *N*-acetyl-*S*-[1-(3-((4-aminobutyl)amino)propyl)-1*H*-pyrrol-3-yl]-L-cysteine (NAC-BDA-N^1-spermidine). ^{1}H NMR (500 MHz, D_2O): δ 6.75 (s, 1H, H2'), 6.67 (t, 1H, *J*=2.5 Hz, H5'), 6.09 (t, 1H, *J*=2.5 Hz, H4'), 4.03 (dd, 1H, *J*=4.0, 9.5, Cys α-CH), 3.86 (dd, 2H, *J*=5.0, 6.5 Hz, H1), 3.03-3.00 (m, 1H, Cys β-CH_a), 2.89-2.82 (m, 4H, H4 and H7), 2.77 (t, 2H, *J*=7.5 Hz, H3), 2.72-2.67 (m, 1H, Cys β-CH_b), 2.00-1.96 (m, 2H, H2), 1.86 (s, 3H, Ac), 1.58-1.52 (m, 4H, H5 and H6). MS data are displayed in Table 3-1.

The compound that eluted at 37.1 min was identified as *N*-acetyl-*S*-[1-(4-((3-aminobutyl)amino)propyl)-1*H*-pyrrol-3-yl]-L-cysteine (NAC-BDA-N^8-spermidine). ^{1}H NMR (700 MHz, D_2O): δ 6.83 (s, 1H, H2'), 6.75 (s, 1H, H5'), 6.16 (s, 1H, H4'), 4.12-4.08 (m, 1H, Cys α-CH), 3.88-3.84 (m, 2H, H1), 3.11-3.08 (m, 1H, Cys β-CH_a), 2.99-2.93 (m, 4H, H5 and H7), 2.88-2.85 (m, 2H, H4), 2.78-2.74 (m, 1H, Cys β-CH_b), 1.98-1.93 (m, 2H, H6), 1.96 (s, 3H, Ac), 1.75-1.65 (m, 2H, H2), 1.52-1.46 (m, 2H, H3). MS data are displayed in Table 3-1.

General procedure for the synthesis of sulfoxide standards. *m*-Chloroperbenzoic acid (mCPBA) (3 μmol) was added to a stirred solution of the corresponding sulfide (3 μmol) in methanol-dichloromethane (1:1) at -78 °C (total volume: 1 mL). The reaction was stirred for 1 h before it was allowed to warm up to

room temperature. The solvent was removed under a stream of nitrogen. The crude product was dissolved in water and purified by semipreparative HPLC method 1 (solvent A was 50 mM ammonium formate, pH 2.8). The organic solvent was removed under reduced pressure, and buffer salts were removed by solid phase extraction using Strata-X cartridges. The identities of products were established by MS and NMR analysis.

N-*Acetyl*-S-*[1-(3-(4-aminobutyl)aminopropyl)-1*H-*pyrrol-3-yl]*-L-*cysteine sulfoxide.* NAC-BDA-N^1-spermidine was oxidized with mCPBA to generate *N*-acetyl-*S*-[1-(3-(4-aminobutyl)aminopropyl)-1*H*-pyrrol-3-yl]-L-cysteine sulfoxide. This product eluted at 3.7 min when HPLC method 1 was employed (solvent A was 50 mM ammonium formate). ^{1}H NMR analysis showed the presence of two diastereomers in a 6:5 ratio. MS data are displayed in Table 3-1.

Major isomer: ^{1}H NMR (700 MHz, DMSO-d_6): δ 7.88 (d, 1H, *J*=8.2 Hz, NH), 7.30 (s, 1H, H2'), 6.95 (s, 1H, H5'), 6.39 (s, 1H, H4'), 4.04-4.01 (m, 2H, H1), 3.79-3.76 (m, 1H, Cys α-CH), 3.30 (dd, 1H, *J*=3.1, 12.2 Hz, Cys β-CH_a), 3.07 (t, 1H, *J*=10.6 Hz, Cys β-CH_b), 2.74-2.72 (m, 2H, H4), 2.57-2.55 (m, 2H, H7), 2.41-2.38 (m, 2H, H3), 1.91-1.88 (m, 2H, H), 1.79 (s, 3H, -C(O)-CH_3), 1.54-1.52 (m, 2H, H5), 1.46-1.44 (m, 2H, H6).

Minor isomer: ^{1}H NMR (700 MHz, DMSO-d_6): δ 7.74 (d, 1H, J=7.7 Hz, NH), 7.30 (s, 1H, H2'), 6.92 (s, 1H, H5'), 6.36 (s, 1H, H4'), 4.20-4.17 (m, 1H, Cys α-CH), 4.04-4.01 (m, 2H, H1), 3.37-3.35 (m, 1H, Cys β-CH_a), 2.97-2.94 (m, 1H, Cys β-CH_b), 2.74-2.72 (m, 2H, H4), 2.57-2.55 (m, 2H, H7), 2.41-2.38 (m, 2H, H3), 1.91-1.88 (m, 2H, H), 1.83 (s, 3H, -C(O)-CH_3), 1.54-1.52 (m, 2H, H5), 1.46-1.44 (m, 2H, H6).

N-*Acetyl*-S-*[1-(4-(3-aminobutyl)aminopropyl)-1*H-*pyrrol-3-yl]*-L-*cysteine sulfoxide*. NAC-BDA-N^8-spermidine was oxidized with mCPBA to generate *N*-acetyl-*S*-

[1-(4-(3-aminobutyl)aminopropyl)-1*H*-pyrrol-3-yl]-L-cysteine sulfoxide. This product eluted at 3.5 min when HPLC method 1 was employed. ^{1}H NMR analysis showed the presence of two diastereomers in a 6:5 ratio. MS data are displayed in Table 3-1.

Major isomer: ^{1}H NMR (700 MHz, DMSO-d_6): δ 7.86 (d, 1H, *J*=8.1 Hz, NH), 7.42 (s, 1H, H2'), 6.94 (s, 1H, H5'), 6.35 (s, 1H, H4'), 4.18-4.16 (m, 1H, Cys α-CH), 4.06-3.96 (m, 2H), 3.59-3.57 (m, 1H, Cys β-CH_a), 3.27-3.24 (m, 1H, Cys β-CH_b), 2.86-2.70 (m, 4H), 2.62-2.60 (m, 2H), 1.81 (s, 3H, -C(O)-CH_3), 1.81-1.69 (m, 4H), 1.36-1.30 (m, 1H), 1.27-1.21 (m, 1H).

Minor isomer: ^{1}H NMR (700 MHz, DMSO-d_6): δ 8.05 (d, 1H, *J*=8.2 Hz, NH), 7.29 (s, 1H, H2'), 6.96 (s, 1H, H5'), 6.40 (s, 1H, H4'), 4.06-3.96 (m, 2H), 3.72-3.70 (m, 1H, Cys α-CH), 3.23-3.15 (m, 1H, Cys β-CH_a), 3.08-3.05 (m, 1H, Cys β-CH_b), 2.86-2.70 (m, 4H), 2.62-2.60 (m, 2H), 1.83 (s, 3H, -C(O)-CH_3), 1.81-1.69 (m, 4H), 1.36-1.30 (m, 1H), 1.27-1.21 (m, 1H).

Hepatocyte Incubations. Freshly isolated hepatocytes were prepared from F344 rats according to published methods.[63] The viability of the cells was greater than 85% as judged by trypan blue exclusion. The hepatocyte incubations were performed in sealed screw-capped 25 mL Erlenmeyer flasks to prevent furan evaporation as previously reported.[4] The cells were suspended at a concentration of 2 million cells/mL in RPMI 1640 media, containing 10 mM HEPES, pH 7.4. After a 10 min preincubation period at 37 °C in an atmosphere of 5% CO_2, the flasks were capped tightly and a solution of furan was added with a syringe through a septum to a final concentration of 100 μM. Controls were performed in the absence of furan or in the presence of 200 μM 1-phenylimidazole (an inhibitor of CYP2E1). The mixtures were then incubated at 37 °C with gentle

shaking. After 4 h, the mixture was centrifuged at 3000 rpm for 5 min. The supernatant was removed and stored at -20 °C for LC/MS/MS analysis. Incubations were performed in duplicate and were repeated with different hepatocyte preparations. The supernatants from the incubations were directly analyzed by LC/MS for metabolites.

Animal Studies. F344 male rats (200-300 g) were purchased from Charles River Laboratories (Kingston, NY). Groups of three rats were treated with 8 mg/kg [$^{12}C_4$]- or [$^{13}C_4$]furan in 5 mL/kg corn oil by gavage. The control group received only corn oil. Immediately after treatment, rats were transferred to individual metabolism cages. Urine was collected on dry ice for 24 hours and stored at -80 ˚C. Prior to MS analysis, it was acidified with TFA to a final concentration of 2% (v/v), centrifuged to remove any particulate matter, and filtered through a 0.45 μm syringe filter.

LC/MS Analysis of Metabolites. LC/MS/MS analyses of supernatants from hepatocyte incubations, in vitro reaction mixtures, or urine were conducted with a Phenomenex (Torrence, CA) Synergi Hydro-RP 80Å column (250 mm x 0.5 mm, 4 μm) at a flow rate of 12.5 μL/min. The column was eluted with HPLC method 1 (solvent A was 10 mM ammonium formate, pH 2.8). The HPLC was coupled to an Agilent 1100 series LC/MSD Trap SL mass spectrometer operating in positive ion mode. Helium was the nebulizing and drying gas (15 psi, 5 L/min), and had a temperature set at 200 °C. Initial analyses were performed with the mass spectrometer set to full scanning mode with a scan range of 75-750 *m*/*z*. The resulting data were mined for compounds that were present in the furan-exposed samples and absent in the control samples. The samples were then reanalyzed with the mass spectrometer set in the auto-MS^2 mode to obtain fragmentation patterns for each of the metabolites.

For a more sensitive scan of the hepatocyte supernatants and synthetic standards, LC/MS/MS analyses were conducted on a nanoACQUITY UPLC pump (Waters, Milford, MA) coupled to a Finnigan TSQ Quantum Ultra AM mass spectrometer (Thermo Electron, San Jose, CA) operating in positive mode. The compounds were separated on a Phenomenex Synergi Hydro-RP 80Å column (250 mm × 0.5 mm, 4 μm) at a flow rate of 10 μL/min. The column was eluted with the following gradient: 10 min at 100% A; 15 min gradient to 75% A, 25% B; 5 min gradient to 50% A, 50% B; 5 min gradient to 100% B, where solvent A was 10 mM ammonium formate, pH 2.8, and solvent B was 50% acetonitrile in water. Selected reaction monitoring (neutral loss 129) was used to target for specific GSH-BDA-amine cross-links.

To detect metabolites with unknown parent masses but known structure (NAC and NAC sulfoxide conjugates), LC/MS/MS analyses were conducted on a nanoACQUITY UPLC pump (Waters, Milford, MA) coupled to a Finnigan TSQ Quantum Ultra AM mass spectrometer (Thermo Electron, San Jose, CA) operating in positive ion mode. The compounds were separated at a flow rate of 10 μL/min on a Phenomenex Synergi Hydro-RP 80Å column (250 mm × 0.5 mm, 4 μm) with HPLC method 1 (solvent A was 10 mM ammonium formate, pH 2.8). The mass spectrometer was operated in constant neutral loss (CNL) mode with a scan range (parent mass) of 300-450 *m/z*. A neutral loss of 129 was used for NAC conjugates, while a neutral loss of 177 was used for the NAC sulfoxide conjugates.[9,26]

High resolution mass spectral data for the metabolites were obtained on a Thermo Ultra AM Triple Quadrupole mass spectrometer. The compounds were separated on a Phenomenex Synergi Hydro-RP 80Å column (250 mm × 0.5 mm, 4 μm) using a flow rate

of 10 μL/min. The column was eluted with HPLC method 1 where solvent A was 0.1% (v/v) phosphoric acid in water and solvent B was 1% (v/v) phosphoric acid in water containing 50% acetonitrile. Selected reaction monitoring (SRM) experiments were performed using the same instrumentation, but the column was eluted with HPLC Method 1 (solvent A was 10 mM ammonium formate, pH 2.8) with a flow rate of 15 μL/min. Argon was used as the collision gas with a collision energy set at 15 eV.

In vitro relative reactivity experiments. GSH (1.5 mg, 5 μmol) and an equimolar mixture of putrescine, cadaverine, L-ornithine, spermine, spermidine, and L-lysine (100 nmol each) were combined in a 1.5 mL amber vial with either sodium phosphate buffer (150 mM, pH 7.4) or hepatocyte medium (total volume: 1 mL). The reaction was initiated upon addition of BDA (100 nmol). After 90 min at 37 °C, the reaction mixture was analyzed by LC/MS (flow rate 12 μL/min) using HPLC method 1 (solvent A was 10 mM ammonium formate, pH 2.8) to determine the relative levels of the GSH-BDA-amine reaction products.

The data were corrected for differences in ionization. This was determined as follows: Equimolar amounts of GSH, BDA, and an amine (putrescine, cadaverine, L-ornithine, spermine, spermidine, or L-lysine) were combined in 150 mM sodium phosphate buffer, pH 7.4. The GSH-BDA-amine reaction products were isolated by HPLC and desalted as described above. The identity of products was established by MS analysis. Assuming that the molar extinction coefficient of each product was similar, the GSH-BDA-amine fractions were combined into an equimolar mixture of each product. This generated an HPLC trace that contained equal peak areas for all the GSH-BDA-amine products using analytical HPLC Method 1. The mixture was diluted 1:10 into

three different solutions: water, hepatocyte media, or 150 mM sodium phosphate buffer (pH 7.4). These diluted solutions were analyzed by LC/MS using HPLC Method 1 (flow rate 12 μL/min). The ratio of the area of each peak to the sum of all peaks was calculated. This ratio was divided by 1/9 (≈11.1%), which is the expected ratio if each of the nine isomers gave an identical response. The resulting fraction is the correction factor listed in Table 3-2.

RESULTS

Hepatocyte metabolites. Previously, we reported that freshly isolated hepatocytes convert furan to several metabolites, including GSH-BDA cross-links to the α- and ε-amino groups of lysine and a GSH-BDA cross-link to glutamine (*S*-[1-(4-amino-1-carboxy-4-oxobuty)-1*H*-pyrrol-3-yl]-glutathione, GSH-BDA-glutamine, (**5**, Scheme 3-2).[9] Constant neutral loss (CNL) analysis of the LC-MS/MS data of hepatocyte supernatants indicated the presence of several additional glutathione reaction products (Figure 3-1). The formation of these metabolites required furan and was blocked upon inclusion of 1-phenylimidazole, a selective cytochrome P450 2E1 inhibitor.[78] Our hypothesis was that these metabolites were GSH-BDA cross-links with cellular amines similar to GSH-BDA-lysine or GSH-BDA-glutamine.

The metabolite with the largest area had a molecular ion at *m/z* 488 (Figure 3-1). Extraction of the ion current at 488 m/z indicated the presence of two metabolites (Figure 3-2a). This nominal mass of these metabolites is 14 amu less than the GSH-BDA-lysine and GSH-BDA-glutamine cross-links. Two amino acids with the appropriate molecular weight are asparagine and ornithine. Reaction of asparagine with BDA in the presence of GSH generated the formation of one major and one minor reaction product with

molecular ions of *m/z* 488. The major isomer was likely the cross-link with the α-amino group as was observed with glutamine (**6**, Scheme 3-2).[9] Preliminary studies indicated that the hepatocyte metabolites did not co-elute with these reaction products (data not shown) so we did not chemically characterize these products.

Ornithine also reacts with BDA in the presence of GSH to form two reaction products with molecular ions at *m/z* 488. These compounds co-eluted with the hepatocyte metabolites (Figure 3-2a). Preparative scale isolation and chemical characterization of the GSH-BDA-ornithine reaction products indicated that the first eluting product results from pyrrole formation with the α-amino group (*S*-[1-(4-amino-1-carboxybutyl)-1*H*-pyrrol-3-yl]-glutathione, GSH-BDA-N^{α}-ornithine, **7a**, Scheme 3-2) and the second eluting product has the cross-link occurring on the δ-amino group (*S*-[1-(4-amino-4-carboxybutyl)-1*H*-pyrrol-3-yl]-glutathione, GSH-BDA-N^{δ}-ornithine, **7b**) (Figure 3-3). These standards had the same exact mass and MS^2 fragmentation pattern as the metabolites (Table 3-1, Figure 3-2b).

Another metabolites detected in the CNL 129 mass chromatogram had molecular ion at *m/z* 501 (Figure 3-1). Extraction of *m/z* 501 indicated the presence of two metabolites with this mass (Figure 3-4a). This mass is consistent with the formation of GSH-BDA cross-links with spermidine which has a nominal mass of 145 Da. Reaction of BDA with spermidine and GSH generated two GSH-BDA-spermidine products with molecular ions of *m/z* 501 that co-eluted with the hepatocyte metabolites (Figure 3-4a). COSY NMR analysis of the chemical reaction products indicated that the first eluting product resulted from the cross-link being formed with the primary amine attached to the three-carbon chain (*N*-(3-(3-(*S*-glutathionyl)-1*H*-pyrrol-1-yl)propyl)butane-1,4-diamine,

GSH-BDA-N^1-spermidine, **8a**, Scheme 3-2) and the later eluting product resulted from cross-link formation with the primary amino group attached to the four-carbon chain (*N*-(4-(3-(*S*-glutathionyl)-1*H*-pyrrol-1-yl)butyl)propane-1,3-diamine, GSH-BDA-N^8-spermidine, **8b**, Scheme 3-2) (Figure 3-5). The MS^2 fragmentation and exact mass of the metabolites matched those of the synthetic standards (Table 3-1, Figure 3-4b).

After observing that GSH-BDA reacts with spermidine to form cross-links, we prepared the synthetic standards for the GSH-BDA cross-links to the other polyamines, putrescine, spermine and cadavarine. Reaction of GSH-BDA with putrescine generates a single cross-link with a molecular ion of *m/z* 444 (Table 3-1, Figure 3-6). NMR analysis confirmed the structure as *S*-(1-(4-aminobutyl)-1*H*-pyrrol-3-yl)glutathione (GSH-BDA-putrescine, **9**, Scheme 3-2). This metabolite was not observed when the hepatocyte medium was analyzed by LC/MS/MS on the ion trap mass spectrometer. However, when the hepatocyte medium was analyzed by selected reaction monitoring (SRM) for the transition of *m/z* 444 → *m/z* 315 (neutral loss of 129) on a triple quadrupole mass spectrometer, a peak with a similar retention time to the synthetic standard was observed (Figure 3-7). Subsequently, we demonstrated that this metabolite co-eluted with the synthetic standard (Figure 3-7).

GSH-BDA reacts with spermine or cadaverine to form single reaction products with molecular ions at *m/z* 558 and 458, respectively (Table 3-1). NMR analysis confirmed the structures as *N*-(3-((*S*-glutathionyl)-1*H*-pyrrol-1-yl)propyl)butane-1,4-diamine (GSH-BDA-spermine, **10**) and *S*-(1-(5-aminopentyl)-1*H*-pyrrol-3-yl)glutathione (GSH-BDA-cadaverine, **11**, Scheme 3-2). Neither compound was observed in the

hepatocyte medium even when SRM analysis on a triple quad mass spectrometer was performed (**10**: *m/z* 558 → *m/z* 429 or **11**: *m/z* 458 → *m/z* 329; data not shown).

Urinary Metabolites. Since GSH-BDA cross-links to ornithine, spermidine and putrescine were observed as rat hepatocyte metabolites of furan, we investigated whether the *N*-acetyl-L-cysteine (NAC) derivatives of these compounds were present in the urine from furan-treated rats. The mercapturates were targeted since the major metabolites detected in the urine thus far had been NAC-BDA-lysine metabolites.[9,28] We focused on the ornithine and spermidine cross-links since they were the most abundant hepatocyte metabolites. Standards for the NAC-BDA-amine cross-links were prepared by combining the amine with BDA in the presence of NAC.

Two ornithine reaction products (*m/z* 344) were formed when NAC, BDA and ornithine were combined, eluting at 37 and 50 minutes (Table 3-1). In the urine of furan-treated rats, there were no peaks unique to furan exposure with this mass, even when analyzed by SRM (*m/z* 344 → *m/z* 197 and *m/z* 344 → *m/z* 215; data not shown).

When BDA was combined with spermidine and NAC, two major UV-absorbing peaks were observed in the HPLC trace, eluting at 32.0 min and 37.1 min in a ratio of 6:1. Mass spectral analysis demonstrated that they had the expected molecular ion (*m/z* 357) for the NAC-BDA-spermidine cross-links (Table 3-1). Preparative isolation and characterization by NMR analysis indicated that the peak that elutes at 32.0 min is the spermidine-N^1 cross-link (*N*-acetyl-*S*-[1-(3-((4-aminobutyl)amino)propyl)-1*H*-pyrrol-3-yl]-L-cysteine, NAC-BDA-N^1-spermidine, **12a**), whereas the compound that elutes at 37.1 min is the spermidine-N^8 cross-link (*N*-acetyl-*S*-[1-(4-((3-

aminobutyl)amino)propyl)-1*H*-pyrrol-3-yl]-L-cysteine, NAC-BDA-N^8-spermidine, **12b**) (Scheme 3-3).

There were metabolites in the urine of furan-treated rats with retention times and molecular ions as well as fragmentation patterns identical to the synthetic standards (Figure 3-8, Table 3-1). These compounds were not present in the urine of vehicle-treated controls. The mass of the NAC-BDA-spermidine metabolites were increased by 4 mass units in the urine from [$^{13}C_4$]furan-treated rats (Figure 3-8, Table 3-1). Their identity was further verified by co-elution with the synthetic standards (Figure 3-9) and by high resolution mass spectral analysis (Table 3-1).

Since we had observed sulfoxide derivatives of the NAC-BDA-lysine metabolites in urine from furan-treated rats,[9,28] we investigated the possibility that the NAC-BDA-spermidine cross-links also underwent oxidation to their corresponding sulfoxides. Standards for these metabolites were prepared by oxidizing each of the NAC-BDA-spermidine cross-links with *m*-chloroperbenzoic acid (mCPBA). The products of the oxidation had the expected molecular ion at *m/z* 373. NMR analysis of the products was performed to confirm that the oxidation had occurred on the sulfur atom. This analysis indicated that each peak was a mixture of two diastereomers in a 6:5 ratio major:minor (based on the orientation of the sulfoxide oxygen). The sulfoxides for NAC-BDA-N^1-spermidine eluted at 3.7 min (*N*-acetyl-*S*-[1-(3-(4-aminobutylamino)propyl)-1*H*-pyrrol-3-yl]-L-cysteine sulfoxide), whereas the sulfoxides for NAC-BDA-N^8-spermidine eluted at 3.5 min (*N*-acetyl-*S*-[1-(4-(3-aminobutylamino)propyl)-1*H*-pyrrol-3-yl]-L-cysteine sulfoxide). Given that these compounds eluted very early and there were co-eluting

peaks with the same mass, it was difficult to judge whether these compounds were formed in vivo.

To look for evidence for the possible presence of NAC-BDA-putrescine or further metabolites of NAC-BDA-ornithine or NAC-BDA-spermidine, urine from furan- and vehicle-treated rats were analyzed by CNL scanning using a triple quadrupole mass spectrometer. Both CNL 129 (for the NAC conjugates) and CNL 177 (for NAC sulfoxides) were performed.[9] No evidence for these metabolites was obtained (data not shown).

Relative Formation of GSH-BDA-Amines. In rat hepatocytes, the relative abundance of GSH-BDA-amine reaction products was GSH-BDA-N^{δ}-ornithine > GSH-BDA-N^{α}-ornithine ≥ GSH-BDA-N^{ϵ}-lysine and its acetylated counterpart ≥ GSH-BDA-N^{1}-spermidine > GSH-BDA-N^{8}-spermidine > GSH-BDA-N^{α}-lysine > GSH-BDA-putrescine. Neither GSH-BDA-spermine nor GSH-BDA-cadaverine was observed. To determine the relative reactivity of GSH-BDA with these various amines, 5 mM GSH was reacted with 100 μM BDA and an equimolar mixture of the amines (100 μM each putrescine, cadaverine, spermine, spermidine, ornithine, and lysine) in either 150 mM sodium phosphate buffer (pH 7.4) or in hepatocyte medium (RPMI 1640 media, containing 10 mM HEPES, pH 7.4). The reaction was allowed to proceed for 90 min at 37 °C before analysis by LC/MS using an ion trap mass spectrometer as a detector (Figure 3-10). The peak areas were corrected for ionization efficiency (Table 3-2). The results of these experiments are summarized in Figure 3-11. The expected products are shown in Scheme 3-2. In addition to GSH-BDA cross-links to putrescine, cadaverine,

spermine, spermidine, ornithine, and lysine, intramolecular and intermolecular cross-links to GSH were also formed (mono-GSH-BDA, **4,** and GSH-BDA-GSH, **13**; Scheme 3-2).

The relative amount of each reaction product formed was dependent on the nature of the buffer. In 150 mM sodium phosphate, pH 7.4, the most abundant product was GSH-BDA-GSH. The relative abundance of the amino acid and polyamine reaction products was GSH-BDA-spermine > GSH-BDA-N^1-spermidine ≥ GSH-BDA-putrescine ≥ GSH-BDA-N^{δ}-ornithine ≥ GSH-BDA-cadaverine > GSH-BDA-N^8-spermidine > GSH-BDA-N^{ε}-lysine > GSH-BDA-N^{α}-lysine >>> GSH-BDA-N^{α}-ornithine (not detected). In hepatocyte medium, the most abundant product was GSH-BDA-spermine. Only low levels of GSH-BDA-GSH were formed in this reaction buffer. The order of reaction was GSH-BDA-spermine > GSH-BDA-N^1-spermidine > GSH-BDA-putrescine > GSH-BDA-N^8-spermidine > GSH-BDA-cadaverine > GSH-BDA-N^{ε}-lysine > GSH-BDA-N^{δ}-ornithine > GSH-BDA-N^{α}-lysine >>> GSH-BDA-N^{α}-ornithine (not detected). Upon summing together the regioisomers formed from each amine, the relative order of reactivity was spermine > spermidine > putrescine ≥ ornithine ≈ lysine ≈ cadaverine in both reaction solvents.

The overall yield of the reaction products was lower when the reaction was performed in hepatocyte medium (Figure 3-10). The medium contains many chemicals that are likely to compete with the amines (including the amino group of GSH) for reaction with BDA or GSH-BDA, reducing the overall yield of cross-links. A major reaction product was observed in the hepatocyte media reaction that was not present in the buffer reaction mixture. This compound eluted at 33.9 min and had a molecular ion at *m/z* 477. This compound was formed in the absence of the amine mixture but required

BDA, GSH and the media. The formation of this compound likely competes with production of the GSH-BDA-amine cross-links. The chemical structure of this compound was not determined. The daughter ion mass spectrum indicated that it was a reaction product containing GSH since it contained ions resulting from neutral losses characteristic of GSH (NL 75 and 129). This compound is not likely a GSH-BDA-amine cross-link since there are no amines present in the hepatocyte medium that would generate a GSH-BDA-amine cross-link with the correct mass. Additionally, the MS^2 spectrum of the unknown contained an ion indicating the neutral loss of GSH (neutral loss of 307). This fragmentation is not observed in any of the GSH-BDA-amine cross-links characterized to date.

Further evidence that the presence of additional nucleophiles affects the product distribution was provided by comparing the regioselectivity of the reaction of GSH-BDA with ornithine, lysine and spermidine (Table 3-3) between the different reaction settings. In the in vitro reaction with the amine mixture, the GSH-BDA-N^{α}-ornithine cross-link was not detected. However, both the α- and δ-ornithine reaction products were observed when ornithine was reacted with GSH and BDA alone, with the reaction preferentially occurring with the δ amino group. The nature of the reaction buffer did not influence the relative product formation for this amino acid. There was a slight effect of reaction medium on the relative reactivity of the N^{α}- and N^{ε}-amino groups of lysine. The preference of reaction with the N^{ε}-amino group has been previously reported.[9] There was also significant regioselectivity in the reaction of BDA-GSH with the two amino groups of spermidine with the reaction preferentially occurring on the N^1 nitrogen atom. For this

amine, the reaction medium significantly influences the relative reactivity of the two amino groups.

DISCUSSION

Previously we demonstrated that a significant route of furan metabolism involves the oxidation of furan to BDA, followed by reaction of BDA with GSH to form a GSH-BDA reaction product that can cross-link with amines like lysine and glutamine.[9,28] In this report, we characterized GSH-BDA-ornithine, GSH-BDA-spermidine and GSH-BDA-putrescine as hepatocyte metabolites of furan. These compounds indicate that any endogenous amine could be a target for alkylation by GSH-BDA. More importantly, they indicate that polyamines may play an important role in the toxicity of furan.

To our knowledge, this is the first identification of xenobiotic-polyamine adducts in a cell- or animal-based system. The formation of these products suggests that polyamines serve as traps for electrophiles, detoxifying the reactive aldehydes formed during furan metabolism and preventing them from modifying proteins or other critical targets. This protection is expected to dominate at lower furan exposures, where the concentrations of GSH-BDA are insufficient to result in significant depletion of polyamines. Polyamines are known to protect against oxidative damage, radiation damage and alkylation damage by a variety of mechanisms.[79-86] Mechanisms for protection include direct scavenging of the reactive molecule, induction of conformational changes in DNA, physical blocking of DNA from interactions with the reactive intermediate, or a combination of all four. Until this report, the products of these scavenging reactions have only been chemically characterized in vitro.[79,82,86]

These products could also represent adverse effects for furan-exposed cells since polyamines play a vital role in cellular homeostasis. They are essential for a wide variety of cellular functions including cell growth and differentiation.[87-89] Therefore at high furan exposure, one might envision that the formation of GSH-BDA-polyamine adducts might significantly alter the balance of polyamines in the liver. Changes in the polyamine pools have major influence on cellular physiology; consequently their levels are tightly regulated through altered expression of the enzymes involved in their synthesis and degradation.[88] Increased polyamine levels are associated with increased cell proliferation, decreased apoptosis and increased expression of oncogenic genes.[75] An exception to this is that extremely high levels of polyamines leads to apoptosis.[75] Alternatively, decreased polyamine levels are associated with decreased cell growth and apoptosis.[77,85,90,91] Therefore, if furan disrupts these polyamine pools via the formation of GSH-BDA-polyamine metabolites, these changes could play an important role in the overall toxicological effects of furan.

It is also possible that the products of these reactions, GSH-BDA-polyamine, are themselves toxic. Polyamine analogs have been explored for their potential as antitumor agents.[92] A number of these compounds are cytotoxic at submicromolar concentrations, so it is possible that the analogs we are detecting as a result of furan metabolism may have toxic properties. Taken together, it is possible that the modification of polyamines by reactive intermediates in furan metabolism could play an important role in furan-derived toxicity by disturbing the polyamine pools, triggering compensatory changes in enzyme levels to replace modified polyamines, and/or altering the biological activity of

polyamines as a result of chemical modification of the terminal amino group. These possibilities are currently being explored.

A critical step in understanding the potential importance of these metabolites to the toxicity of furan is defining patterns of reactivity of GSH-BDA in various biologically relevant contexts. The relative amount of product formed in hepatocytes is GSH-BDA-ornithine > GSH-BDA-lysine > GSH-BDA-spermidine > > GSH-BDA-putrescine. GSH-BDA-spermine and GSH-BDA-cadaverine were not observed. The only GSH reaction product was mono-GSH-BDA, not GSH-BDA-GSH. Our chemical studies indicate that there are multiple factors that influencing the cross-link product distribution in the isolated hepatocytes. They include the relative concentration of the amines in hepatocytes, the relative reactivity of the amino groups, and the presence of competing nucleophiles. Biochemical stability of the resulting products will also affect the amounts detected.

As shown in Table 3-4, the absence of GSH-BDA-cadaverine can be explained by the extremely low hepatocellular cadaverine concentrations.[93] Similarly, the relatively low levels of GSH-BDA-putrescine are likely explained by the low amounts of putrescine present in hepatocytes.[94] However, amine hepatocellular concentrations do not explain the relative levels of GSH-BDA-lysine, GSH-BDA-ornithine, GSH-BDA-spermidine, GSH-BDA-spermine and GSH-BDA-GSH. Given the reported hepatocellular levels of these amines (Table 3-4),[94-97] one would predict that the relative hepatocellular levels of these conjugates should be GSH-BDA-GSH > GSH-BDA-spermine ≈ GSH-BDA-spermidine > GSH-BDA-lysine ≥ GSH-BDA-ornithine. Since the relative distribution of

these metabolites is very different than this, factors other than relative concentration of the amines must play a role in the relative product distribution observed in hepatocytes.

One contributor to the product distribution could be the relative reactivity of the various biological amines. Our chemical studies indicated that relative reactivity was spermine > spermidine > putrescine ≥ ornithine ≈ lysine ≈ cadaverine in both reaction solvents. Additionally, the reaction of GSH-BDA at the terminal amino group of ornithine and lysine was favored over the corresponding α-amino group. These observations are consistent with previous studies which demonstrated that α,β-unsaturated aldehydes react with spermine > spermidine > putrescine ≥ N^{ε}-lysine > N^{α}-amine of amino acids.[86,98]

Another factor influencing product distribution could be the pK_a of the individual amino groups since the protonation state of a primary amine is an important factor determining its nucleophilicity.[99] While the relative reactivity of the amines with GSH-BDA **3** does not strictly correlate to their pK_a values (Table 3-4), relative pK_a values can be used to justify reactivity when looking at structurally related pairs. For example, putrescine has a pK_a of 9.63 versus cadaverine with a pK_a of 10.05 (Table 3-4). Therefore, a greater fraction of putrescine will be unprotonated and available for nucleophilic attack, justifying its greater extent of product formation in comparison with that of cadaverine in our model reactions. In contrast, the lower pK_a values of the α-amino groups do not lead to greater reaction at this position compared to that of the side-chain amines for the reasons discussed above. Therefore, the utility of the analysis based on pK_a is limited to the consideration of structurally related molecules. The stability of the reaction intermediates may also influence product distribution.

The regiochemistry of the reaction of GSH-BDA with ornithine, spermidine and lysine in hepatocytes reflects the relative reactivity of the amino groups observed in our chemical reactions (Table 3-3). In hepatocytes, the reaction of GSH-BDA was more skewed to the ε-amino group of lysine than in the in vitro reactions. As previously reported, there are two possible sources of GSH-BDA-lysine: one is the reaction of GSH-BDA with free lysine and the other is the degradation and processing of GSH-BDA-lysine protein adducts.[9] The latter adduct will only lead to GSH-BDA-N^{ε}-lysine since the α-amino group is involved in peptide bonds, explaining the observed α/ε ratio observed in hepatocytes.[9]

However, the relative levels of GSH-BDA-lysine, GSH-BDA-ornithine, GSH-BDA-spermidine, GSH-BDA-spermine and GSH-BDA-GSH in hepatocytes cannot be explained by differences in chemical reactivity of the amines with GSH-BDA. Another factor that could contribute to the hepatocyte product distribution is the chemical make up of the reaction site, as indicated by the different results obtained in sodium phosphate buffer versus hepatocyte medium. The presence of competing nucleophiles reduced the formation of GSH-BDA-GSH in hepatocyte medium (Figure 3-11). This reduction was accompanied by the abundant formation of a medium component-derived reaction product (*m/z* 477). Therefore, it is likely that GSH-BDA-GSH is not observed in furan-exposed hepatocytes because there are many nucleophiles that can compete with GSH for reaction with GSH-BDA in the cell. A similar argument can be made for the difference in regioselectivity in the formation of GSH-BDA-spermidine regioisomers. The presence of additional nucleophiles will compete with the amines so that GSH-BDA will combine with the most reactive ones. This hypothesis also explains the enhanced regioselectivity

of the reaction of GSH-BDA with spermidine in the hepatocyte medium versus sodium phosphate and with ornithine when multiple amines are present (Table 3-3). However, it does not provide insight into the absence of GSH-BDA-spermine and the relative amounts of GSH-BDA-spermidine, GSH-BDA-ornithine and GSH-BDA-lysine detected in rat hepatocytes.

Since the chemical reactions indicate that spermine and spermidine are very reactive with GSH-BDA, it is surprising that GSH-BDA-spermine was not detected and that the levels of GSH-BDA-spermidine are lower than those observed for GSH-BDA-lysine and GSH-BDA-ornithine. It is possible that spermine and spermidine may not be readily available for reaction with GSH-BDA since their free concentration is substantially lower than the total cellular polyamine concentration.[88] A likely possibility is that GSH-BDA-spermine is formed but rapidly degraded to GSH-BDA-spermidine by enzymes in the cell, such as amine oxidases.[88,100] A similar mechanism could explain the lower than expected amounts of GSH-BDA-spermidine. These degradation reactions produce hydrogen peroxide and aldehydes known to be toxic to cells.[77] The metabolism of these conjugates could be responsible for the oxidative stress observed in liver following furan treatment.[52] We observed that GSH-BDA-spermidine was unstable in the hepatocyte incubations with the N^1-isomer more unstable than the N^8-isomer (data not shown). This instability was not observed in the absence of cells. The biological fate of these metabolites requires investigation.

The only downstream metabolite of these newly characterized GSH-BDA-amine products that was detected in urine of furan-treated rats was NAC-BDA-spermidine. The lack of detection of NAC-BDA-putrescine in the urine of furan-treated rats is not

surprising since only low levels of this metabolite were detected in hepatocytes. Given the large abundance of GSH-BDA-ornithine in furan-treated rat hepatocytes, it is surprising that there were no detectable levels of NAC-BDA-ornithine in rat urine following furan exposure. Further studies will be necessary to determine if GSH-BDA-ornithine is formed in vivo and, if so, what its fate is.

The levels of NAC-BDA-spermidine appear to be much lower than NAC-BDA-lysine and related metabolites based on MS analysis. While this observation could result from large differences in ionization efficiency of the two metabolites in the mass spectrometer, a more likely possibility is that CYS-BDA-lysine cross-links dominate in vivo since a major source of this cross-link is likely to be BDA-derived protein adducts.[9] Thirteen percent of an 8 mg/kg dose of furan becomes bound to proteins,[7] therefore the degradation products of these adducts are expected to dominate in the urine and feces of furan-treated rodents.[9,26,27] Future studies will focus on the development of analytical methods to quantify each of the metabolites detected in the urine of furan-treated rats to get a better sense of the overall mass balance of the various pathways.

In summary, GSH-BDA-amine cross-links to ornithine, putrescine and spermidine were detected following exposure of rat hepatocytes to furan. Degradation products of the GSH-BDA-spermidine products were detected in low levels in urine of furan-treated rats. The high reactivity of GSH-BDA with spermine and spermidine suggest that the formation of these conjugates could represent detoxification pathways at low furan exposures. At higher exposure levels, these reactions may cause imbalances in polyamine metabolism through a variety of mechanisms. Imbalances in polyamine

metabolism have been linked to cancer and cell death.[77] These furan metabolites may be important clues into the mechanisms by which furan causes its harmful effects.

Table 3-1. Mass spectral data for the metabolites and standards.

Compound	*m/z*	RT[b](min)	MS^2 (fragment ions, *m/z*)	HRMS measured[a]	HRMS calculated
GSH-BDA-N^{α}-ornithine standard **7a**	488	24.4	470, 452, 359, 341	488.1806	488.1810
Hepatocyte metabolite	488	24.4	470, 452, 359, 341	488.1813	488.1810
GSH-BDA-N^{δ}-ornithine standard **7b**	488	31.8	470, 359, 342, 227, 213	488.1815	488.1810
Hepatocyte metabolite	488	31.9	470, 359, 342, 227, 213	488.1825	488.1810
GSH-BDA- N^{1}-spermidine standard **8a**	501	23.7	483, 372, 355, 301,227	501.2489	501.2490
Hepatocyte metabolite	501	23	483, 372, 355, 301, 227	n.d.[c]	501.2490
GSH-BDA-N^{8}-spermidine standard **8b**	501	28.4	483, 372, 228	501.2491	501.2490
Hepatocyte metabolite	501	28.5	483, 372, 228	n.d.	501.2490
GSH-BDA-putrescine **9**	444	34.4	426, 315	444.1890	444.1911
Hepatocyte metabolite	444	34.4	n.d.	n.d.	444.1911
GSH-BDA-cadaverine standard **11**	458	41.6	440, 329	458.2051	458.2068
GSH-BDA-spermine standard **10**	558	19.6	540, 429, 355, 285	558.3085	558.3068
NAC-BDA-N^{α}-ornithine standard	344	37.2	326, 308, 266, 221, 197	n.d.	344.1275
NAC-BDA-N^{δ}-ornithine standard	344	50.5	326, 308, 280, 215	n.d.	344.1275
NAC-BDA-N^{1}-spermidine standard **12a**	357	32.2	340, 322, 286, 268, 250, 211, 140	357.1939	357.1955
[$^{12}C_4$]Urinary metabolite	357	35.4	340, 322, 286, 268, 250, 211, 140	357.1948	357.1955
[$^{13}C_4$]Urinary metabolite	361	35.4	344, 326, 290, 272, 254, 215, 144		
NAC-BDA-N^{8}-spermidine standard **12b**	357	37.1	340, 300, 228	357.1958	357.1955
[$^{12}C_4$]Urinary metabolite	357	38.9	340, 300, 228	n.d.	357.1955
[$^{13}C_4$]Urinary metabolite	361	38.9	344, 304, 232		
NAC-BDA-N^{1}-spermidine sulfoxide standard	373	7.8	373, 244, 226, 155, 122	373.1913	373.1904
NAC-BDA-N^{8}-spermidine sulfoxide standard	373	8.2	373, 244, 226, 193, 176	373.1922	373.1904

[a][$M+H^+$] (*m/z*), [b]RT = retention time; [c]n.d. = not determined. Data was acquired using HPLC Method 1 with 10 mM ammonium formate, pH 2.8.

Table 3-2. Ion-suppression correction factors for LC/MS analyses.

Amine	Water	Buffer	Media
GSH-BDA-putrescine	0.92	0.82	0.86
GSH-BDA-cadaverine	0.67	0.59	0.63
GSH-BDA-N^{α}-ornithine	1.62	9.17	1.91
GSH-BDA-N^{δ}-ornithine	1.09	1.03	1.02
GSH-BDA-spermine	2.09	2.70	2.61
GSH-BDA-N^{1}-spermidine	0.83	0.85	0.87
GSH-BDA-N^{8}-spermidine	0.93	0.83	0.92
GSH-BDA-N^{α}-lysine	1.09	1.06	1.04
GSH-BDA-N^{ε}-lysine	0.83	0.76	0.86

Table 3-3. Regioselectivity of the reaction between GSH-BDA and ornithine, lysine or spermidine

	Amine mixture[a]		Individual amines[b]		
Amine	Buffer	Media	Buffer	Media	Hepatocytes
N^{α}/N^{δ} ornithine (**7a**/**7b**)	0	0	0.47	0.55	0.51 ± 0.17
N^{1}/N^{8} spermidine (**8a**/**8b**)	2.5 ± 0.3	6.9 ± 0.6	2.6	7.8	5.5 ± 1.8
$N^{\alpha}/N^{\varepsilon}$ lysine (**2b**/**2a**)	0.45 ± 0.05	0.26 ± 0.06	0.57	0.37	0.083 ± 0.021[c]

[a]GSH (5 mM) was combined with 100 μM BDA and an equimolar mixture of amines (100 μM each putrescine, cadaverine, spermine, spermidine, ornithine, and lysine) in either 150 mM sodium phosphate, pH 7.4 (buffer) or RPMI 1640 media, containing 10 mM HEPES, pH 7.4 (media). The reaction mixture was analyzed by LC-MS and the resultant peak areas were corrected for the ionization efficiency of each reaction product (Table 3-2) prior to calculating the ratio of the two possible regioisomers.
[b]GSH (5 mM) was combined with 100 μM BDA and 100 μM ornithine, lysine or spermidine in either 150 mM sodium phosphate, pH 7.4 (buffer) or RPMI 1640 media, containing 10 mM HEPES, pH 7.4 (media). The reaction mixtures were analyzed as described above.
[c]Previously published.[9]

Table 3-4. Cellular amines pK_as and their concentrations in hepatocytes.

Amine	pK_a of amine	reference	Conc. (nmol/g)	reference
Ornithine	N^{α}: 8.69; N^{δ}:10.76	{}	230-370	95,101,102
Lysine	N^{α}: 9.06; N^{ε}:10.54	103	200-730	96,101,102
Putrescine	9.63; 10.80	103	18-57	93,94,104,105
Cadaverine	10.05; 10.93	103	2.6-7.9	93,106
Spermine	10.1; 10.9	107	618-1591	94,104,105
Spermidine	N^{1}: 10.9; N^{8}: 9.9	107	646-2205	93,94,104,105
GSH	8.75	103	5000-7000	108,109

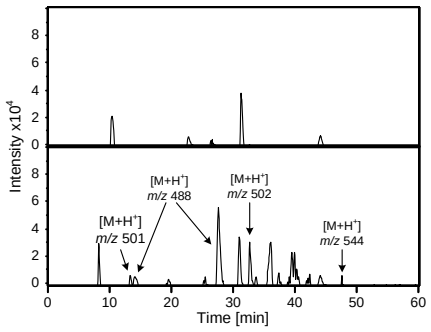

Figure 3-1. Mass chromatogram generated upon extraction of the CNL 129 ion current from LC/MS/MS analysis of 100 µM furan-treated rat hepatocytes (HPLC method 1 with 10 mM ammonium formate, pH 2.8) obtained on an Agilent ion trap mass spectrometer. Previously characterized metabolites are *m/z* 502 (GSH-BDA-lysine) and *m/z* 544 (GSH-BDA-N^{α}-acetyl-lysine).[9] Unknowns are: *m/z* 488 and *m/z* 501.

A.

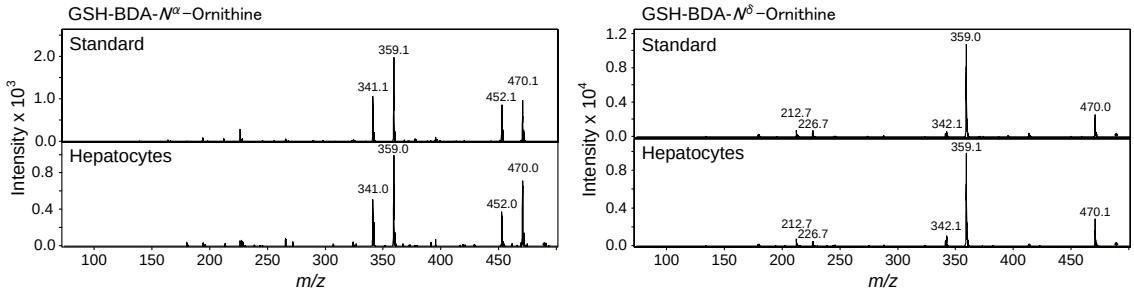

B.

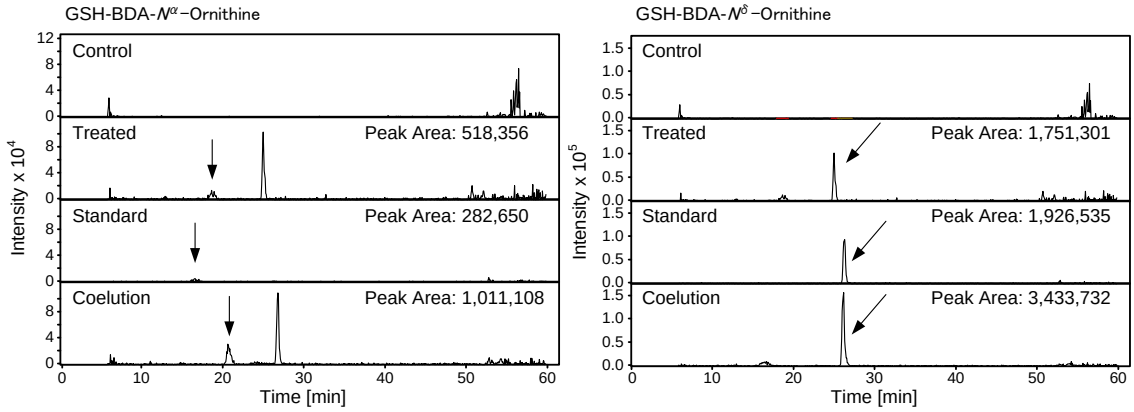

Figure 3-2. A. Mass spectra of GSH-BDA-N^{α}-ornithine and GSH-BDA-N^{δ}-ornithine. B. LC/MS chromatograms demonstrating co-elution of the synthetic GSH-BDA-ornithine isomers with the hepatocyte metabolites of furan. The mixtures were eluted from the HPLC column with the following gradient: after ten minutes in 10 mM ammonium formate, pH 2.8, a 16 minute linear gradient was run to 10 mM ammonium formate, pH 2.8, containing 12.5% acetonitrile followed by a 10 minute linear gradient to 25% acetonitrile.

A **B**

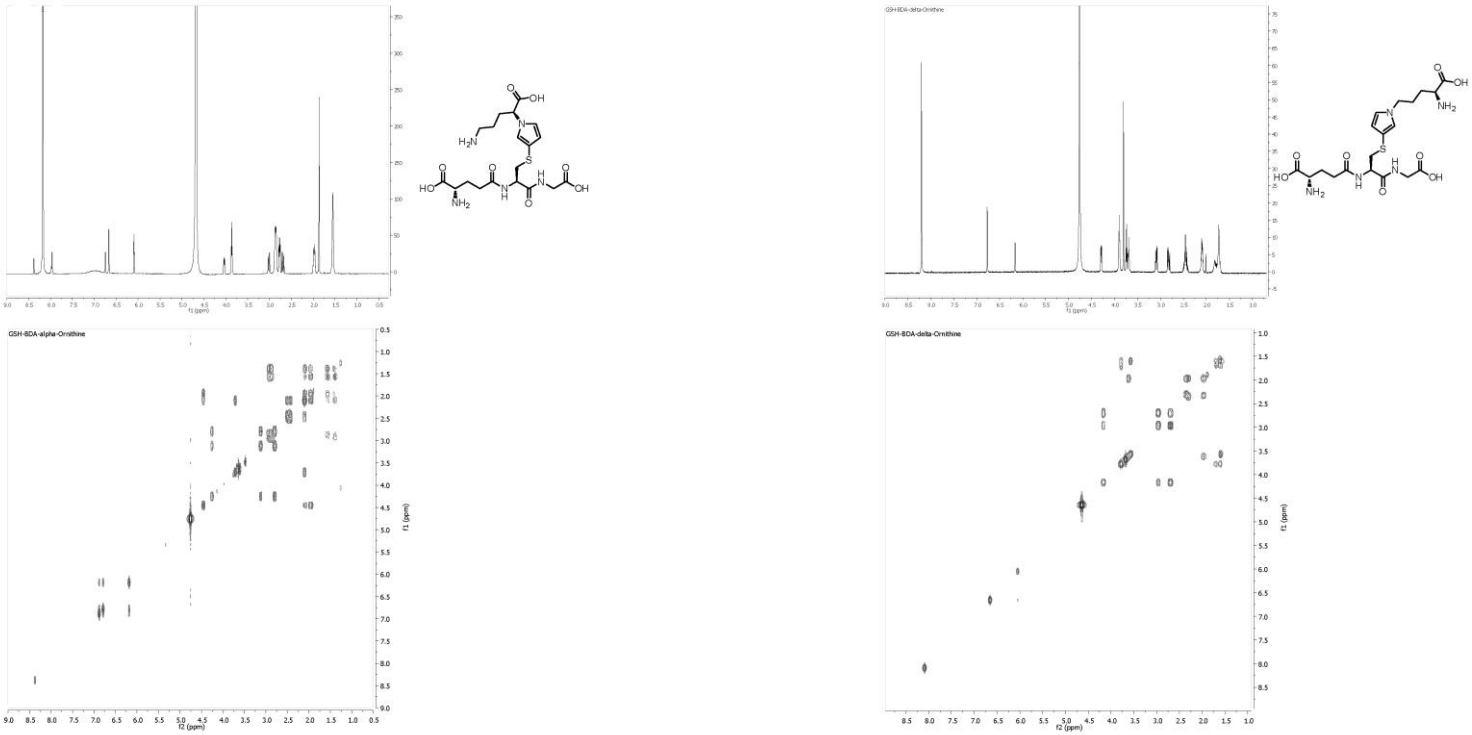

Figure 3-3. COSY NMR spectra for A) GSH-BDA-N^{α}-ornithine and B) GSH-BDA-N^{δ}-ornithine. The C2 proton of the pyridine ring in both compounds exchanged rapidly with D_2O.

A.

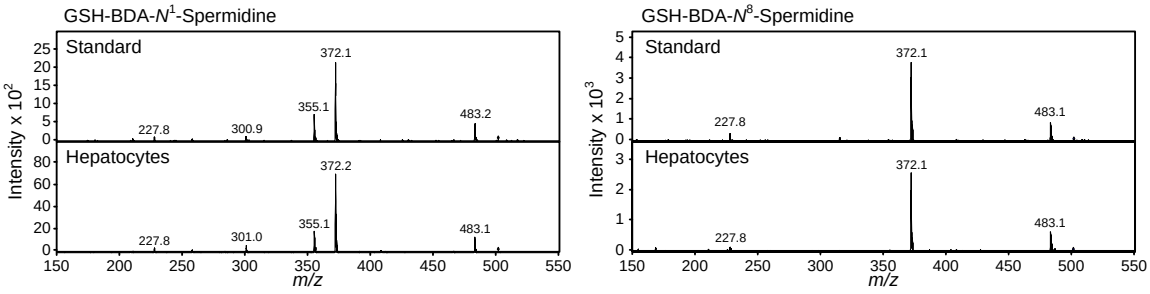

B.

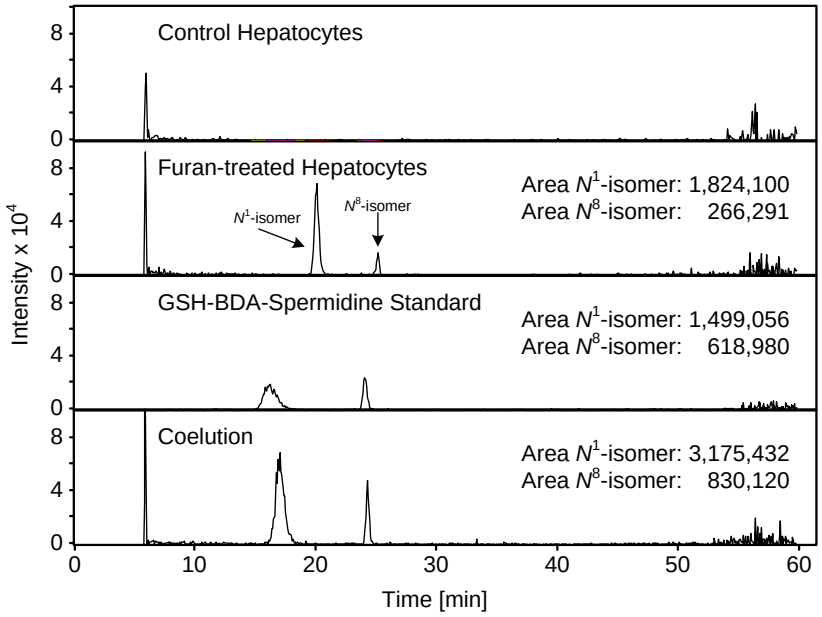

Figure 3-4. A. Mass spectra of GSH-BDA-N^1-spermidine and GSH-BDA-N^8-spermidine. B. LC/MS chromatograms demonstrating co-elution of the synthetic GSH-BDA-spermidine isomers with the hepatocyte metabolites of furan. The mixtures were eluted from the HPLC column with the following gradient: after ten minutes in 10 mM ammonium formate, pH 2.8, a 16 minute linear gradient was run to 10 mM ammonium formate, pH 2.8, containing 12.5% acetonitrile followed by a 10 minute linear gradient to 25% acetonitrile.

A

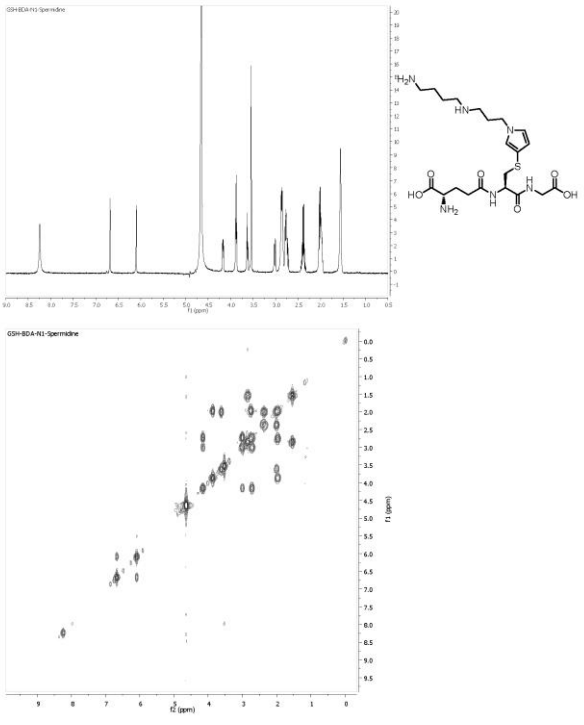

B

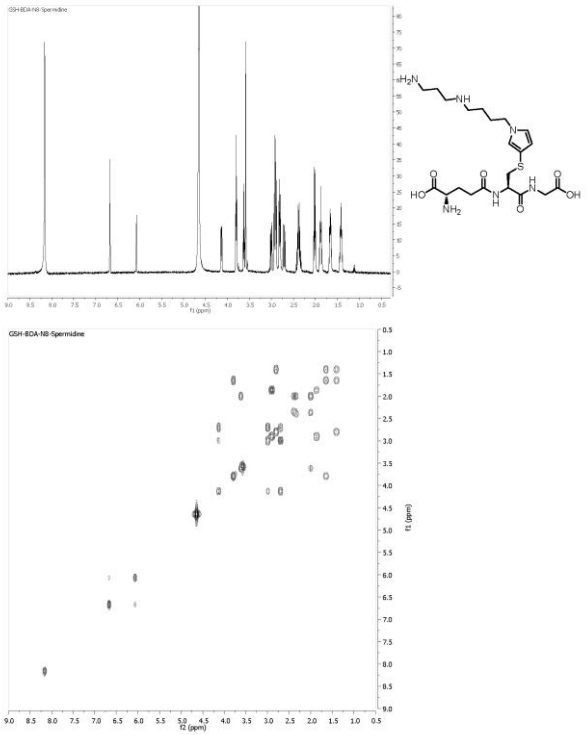

Figure 3-5. COSY NMR of A) GSH-BDA-N^1-spermidine and B) GSH-BDA-N^8-spermidine. The C2 proton of the pyridine ring in both compounds exchanged rapidly with D_2O.

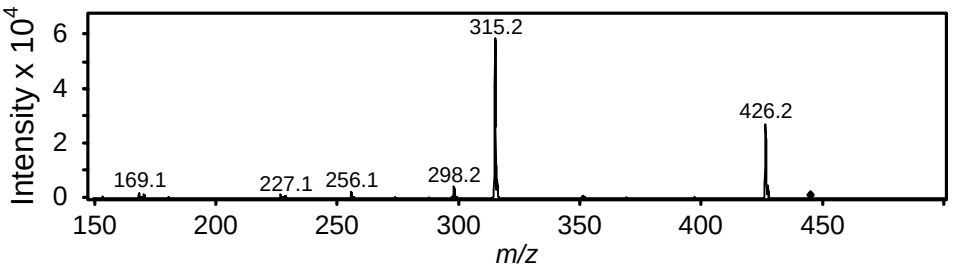

Figure 3-6. Mass spectrum of synthetic GSH-BDA-putrescine.

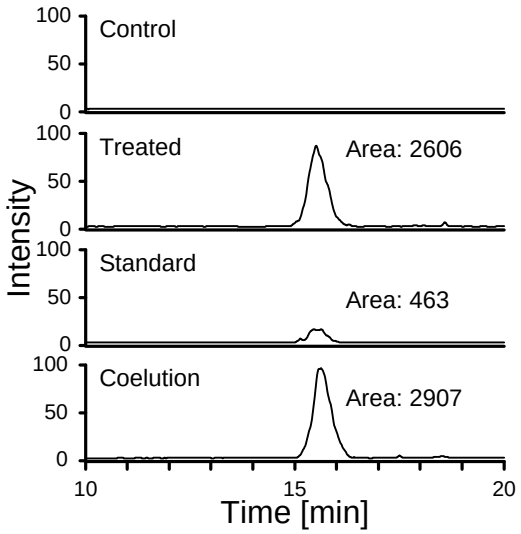

Figure 3-7. LC/ESI-MS/MS analysis of media from furan- and control-treated hepatocytes for GSH-BDA-putrescine in the absence and presence of synthetic standard. The traces were generated by monitoring for the neutral loss of 129 from the molecular ion (*m/z* 444 → *m/z* 315).

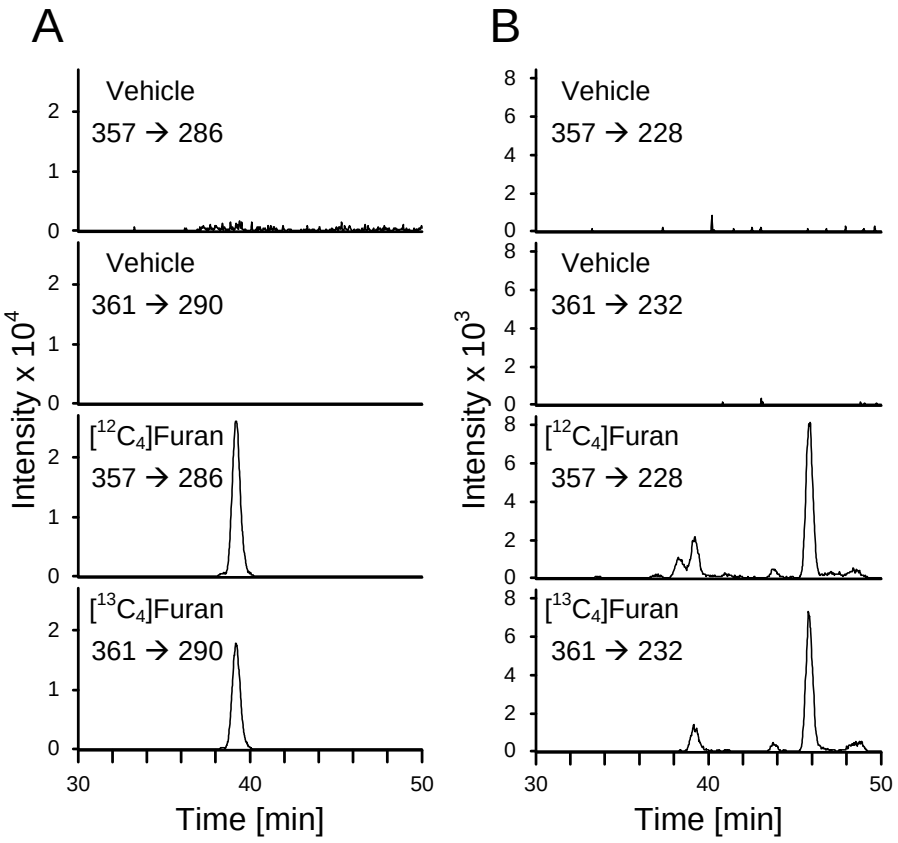

Figure 3-8. LC/ESI-MS/MS analysis of rat urine for NAC-BDA-spermidine cross-links. Animals were treated with either corn oil alone or corn oil containing [$^{12}C_4$]- or [$^{13}C_4$]furan. A. The traces were generated by monitoring for the neutral loss of 71 from the molecular ion ([$^{12}C_4$]: *m/z* 357 → *m/z* 286; [$^{13}C_4$]: *m/z* 361 → *m/z* 290). B. The traces were generated by monitoring for the neutral loss of 129 from the molecular ion ([$^{12}C_4$]: *m/z* 357 → *m/z* 228; [$^{13}C_4$]: *m/z* 361 → *m/z* 232).

A.

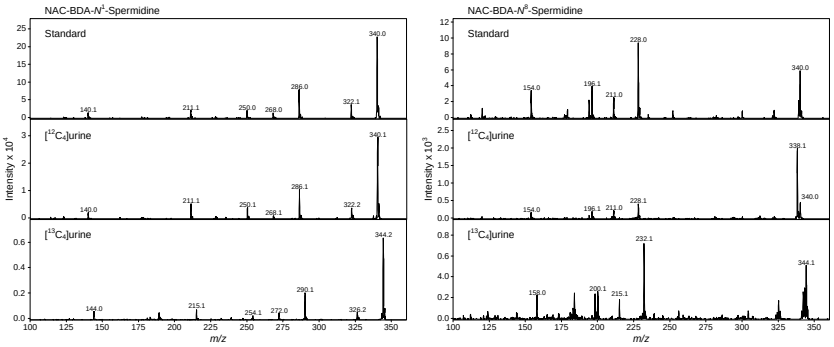

B.

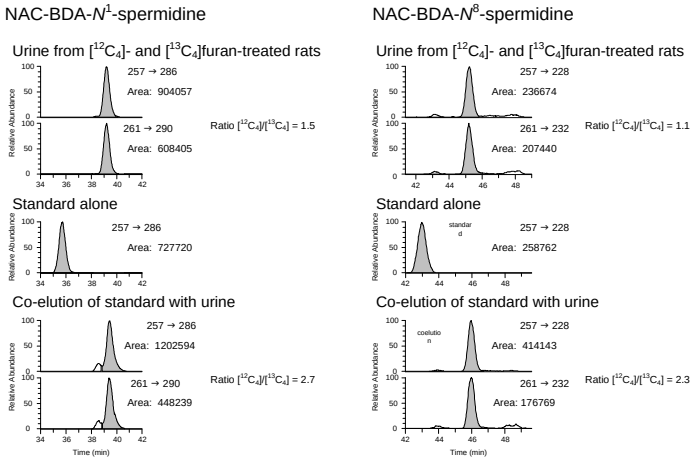

Figure 3-9. A. Mass spectrum for the NAC-BDA-spermidine standards and metabolites observed in urine from [$^{12}C_4$]- and [$^{13}C_4$]furan-treated rats. The fragment at *m/z* 338 in the mass spectrum for the urinary metabolite, [$^{12}C_4$]NAC-BDA-N^8-spermidine, is from a co-eluting peak that also has a molecular ion at *m/z* 357. B. LC/MS chromatograms obtained with a mixture of urine from [$^{12}C_4$]- and [$^{13}C_4$]furan-treated rats demonstrating co-elution of these metabolites with the synthetic standards of the NAC-BDA-spermidine isomers. HPLC method 1 was employed using 10 mM ammonium formate, pH 2.8.

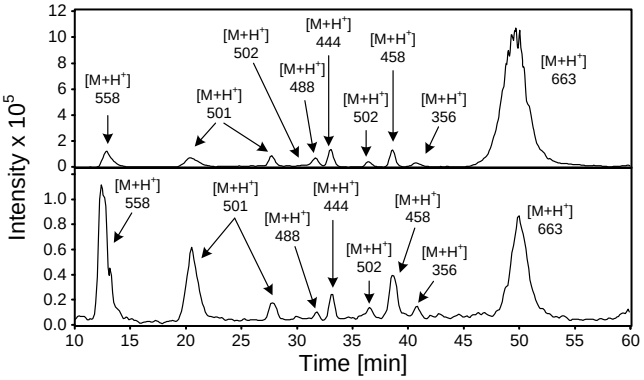

Figure 3-10. Representative mass chromatograms of solutions of 5 mM GSH, 100 μM BDA and an equimolar mixture of the amines (100 μM each putrescine, cadaverine, spermine, spermidine, ornithine, and lysine) in either 150 mM sodium phosphate, pH 7.4, (top) in hepatocyte media (RPMI 1640 media containing 10 mM HEPES, pH 7.4, bottom).

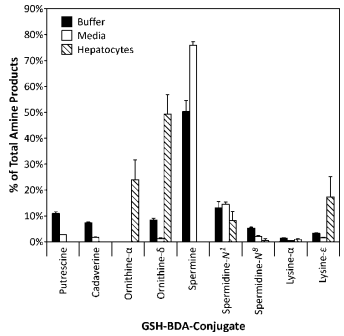

Figure 3-11. Relative distribution of GSH-BDA-amine products in sodium phosphate, pH 7.4, hepatocyte media, and media from furan-treated rat hepatocytes as determined by LC-MS analysis. The amount of GSH-BDA-N^{α}-lysine (**2b**) in furan treated-hepatocytes was calculated from the relative amount of **2b**/**2a** analysis using SRM monitoring.[9] *Includes N^{α}-acetyl-L-lysine derivative of GSH-BDA-lysine.

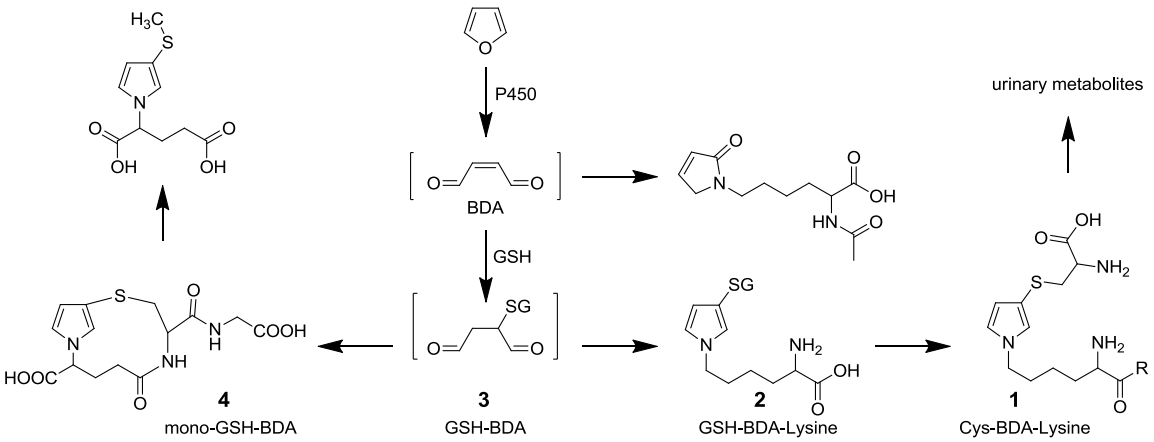

Scheme 3-1. Major pathways of furan biotransformation in rats.

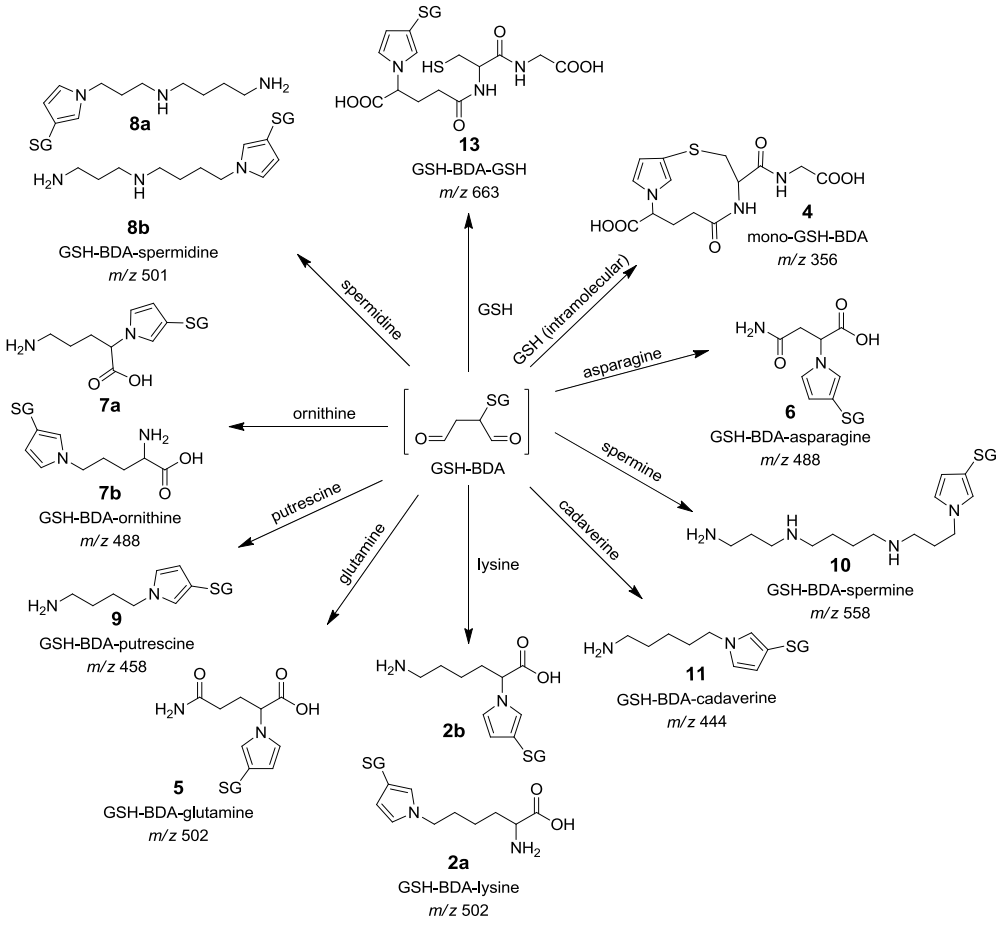

Scheme 3-2. The reaction products formed when GSH-BDA is reacted with a variety of cellular amines.

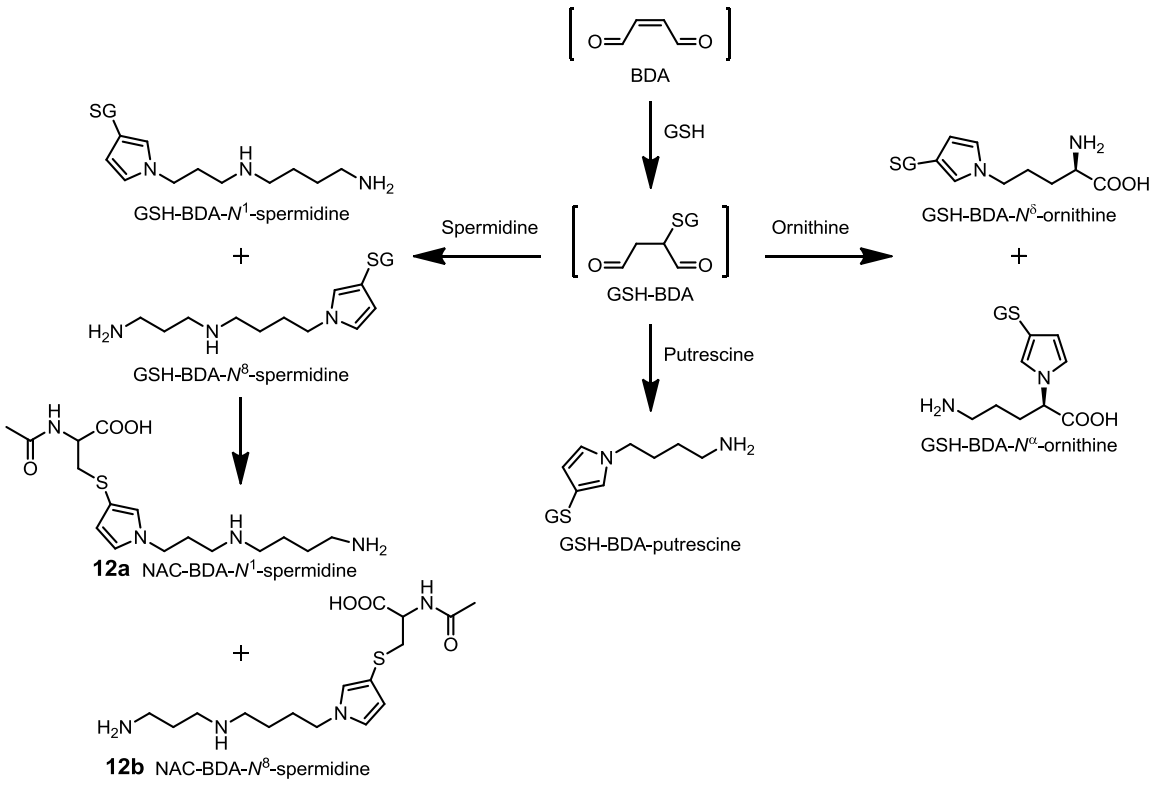

Scheme 3-3. Proposed pathways of furan metabolism. GSH: L-Glutathione; NAC: *N*-Acetyl-L-cysteine.

Chapter 4: Kinetic and Dynamic Analysis of *cis*-2-Butene-1,4-dial, a Reactive Intermediate of Furan

Martin B. Phillips and Lisa A. Peterson

SUMMARY GRAPHIC

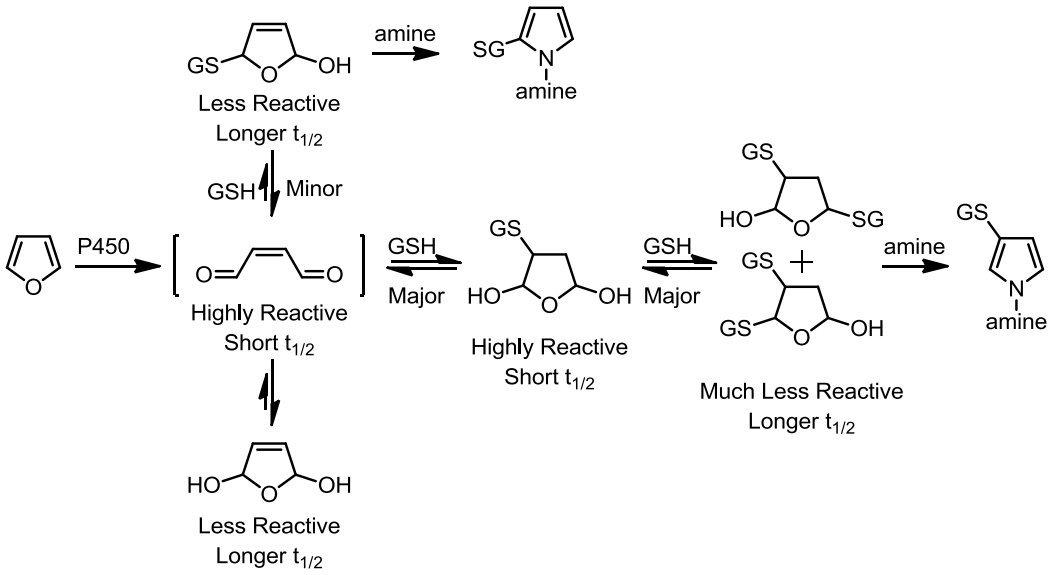

INTRODUCTION

Furan (Scheme 4-1, **1**) is a widespread environmental contaminant.[2] It is known to be toxic and carcinogenic in both F344/N rats and B6C3F$_1$ mice.[1,2] The target organ in these species is the liver, although the adrenal gland is also affected in mice.[1] Humans are exposed to furan via ingestion and inhalation, as furan is present at elevated levels in heat-treated foods and – being a product of incomplete combustion – is a component of cigarette smoke, car exhaust, and wood smoke.[2,56]

Biotransformation is necessary for furan's toxic effects.[4,24,73] Furan is oxidized by cytochrome P450 in the liver of rodents, primarily by the CYP2E1 isoform.[4,23] The

product of oxidation is the α,β-unsaturated dialdehyde, *cis*-2-butene-1,4-dial (BDA, **2**).[23] In aqueous solutions BDA exists as its cyclic hydrate **3**.[23] BDA is one of furan's protein-reactive metabolites. It reacts with amino groups to form pyrrolidinone adducts.[10] Reaction with thiols generates an unstable product which readily forms a thiol-BDA-amine pyrrole cross-link in the presence of amines.[10,23,43,44] The urinary metabolites are derived from BDA reacting with cellular nucleophiles.[9,28] The BDA-lysine reaction product **4** is one of these metabolites (Scheme 4-1). The majority of the urinary metabolites are derived from cysteine-BDA-lysine pyrrole cross-links.[9,26,28] Studies in hepatocytes indicate that GSH is the most likely source of cysteine in these cross-links.[9,28,110] Therefore, the reaction of GSH with BDA to form 2-(*S*-glutathionyl)succinaldehyde (GSH-BDA, **5**, Scheme 4-1) appears to be a major pathway in vivo. The relative amounts of **4** and downstream metabolites of **5** indicate that the formation of **5** is the dominant pathway in liver cells. Data obtained in hepatocytes suggests that **5** has sufficient stability to exit hepatocytes and alkylate nucleophiles at sites distant to its formation.[9]

The available experimental data indicate that there are two reactive intermediates of furan, BDA **2** and GSH-BDA **5**. In our system GSH-BDA goes on to react with a second molecule of GSH to form *bis*-3-GSH (**6**) as the major product. The goal of this study was to determine the relative lifetimes of **2** and **5**. Our hypothesis was that **2** has a shorter half-life than **5** because of the nature of the conjugated dialdehyde, with **5** losing the α,β-unsaturation. We also predicted that hydration of both compounds would extend their lifetime. The concentration of the reactive form of BDA (the unmasked aldehyde)

was then predicted to be a major limiting factor in the reaction. GSH-BDA **5** is also predicted to readily form a hydrate. GSH-BDA may exist in multiple forms, depending on the initial site of addition, hydration status, and substitution of hydroxyls in the hydrate for additional equivalents of GSH (theoretically up to five equivalents of GSH for every BDA).

The identification of GSH-BDA as a key reactive intermediate of furan is a major step forward in the understanding of the complexities of furan metabolism and, by extension, its toxicity. Almost every furan metabolite characterized to date must go through a GSH-BDA intermediate.[6,9,26,28,29,110] The formation of **3** and other stable intermediates opens up the potential for systemic distribution of reactive metabolites of furan. This may lead to damage far from the site of furan oxidation in the active site of liver P450s, such as the damage to cholangiocytes seen in vivo that led to biliary hyperproliferation and cholangiocarcinomas in rats.[1]

EXPERIMENTAL PROCEDURES

Caution: *BDA is toxic and mutagenic in cell systems. Furan is toxic and carcinogenic in laboratory animals. Both chemicals should be handled with proper safety equipment and precautions*.

Chemicals. Aqueous solutions of BDA hydrate were synthesized from the hydrolysis of 2,5-diacetoxy-2,5-dihydrofuran and quantified as previously described.[43,46] Deuterium oxide (D_2O) (99.9% D) was purchased from Cambridge Isotope Laboratories, Inc (Andover, MA). Semicarbazide monohydrochloride was purchased from Acros Organics (Pittsburgh, PA). Sodium phosphate monobasic dihydrate was purchased from

Fluka Analytical (St. Louis, MO). Spermine, cadaverine, and putrescine were purchased from MP Biomedicals (Solon, OH). All other reagents were purchased from Sigma-Aldrich (St. Louis, MO). All HPLC solvents were chromatography grade.

Instrumentation. HPLC purifications were carried out on a Shimadzu LC-10AD system coupled to a Shimadzu SCL-10A UV/vis detector. NMR spectra were recorded on a 500 MHz Varian Inova spectrometer in the Department of Chemistry or on either a 700 MHz Bruker Avance II spectrometer or a 850 MHz Bruker Ascend spectrometer equipped with proton-enhanced cryoprobes in the Department of Biochemistry, Molecular Biology, and Biophysics, University of Minnesota. Chemical shifts are reported in parts per million (ppm) as referenced to the residual solvent peak.

LC/MS/MS analyses were performed using an Agilent 1100 series LC/MSD Trap SL mass spectrometer operating in positive ion mode as the detector. Helium was the nebulizing and drying gas (15 psi, 5 L/min) which had a temperature set at 200 °C. The mass spectrometer is located in the Analytical Biochemistry core facility of the Masonic Cancer Center, University of Minnesota.

For most of the HPLC and LC/MS analyses, the column was eluted with the following gradient: 10 min at 100% A; 26 min linear gradient to 75% A, 25% B; 10 min linear gradient to 50% A, 50% B; 4 min linear gradient to 100% B where solvent A was 10 or 50 mM ammonium formate, pH 2.8 and solvent B was 50% (v/v) acetonitrile in water. This gradient will subsequently be referenced as HPLC method 1.

Time Course of Cross-Link Formation. Reactions of BDA hydrate with GSH and a number of primary-amine containing reaction partners were performed in

quadruplicate as previously described.[110] Briefly, 5 mM GSH was combined with an equimolar mixture of putrescine, cadaverine, L-ornithine, spermine, spermidine, and L-lysine (0.1 μM each) in a glass vial with either 150 mM sodium phosphate, pH 7.4, or RPMI media containing 10 mM HEPES, pH 7.4 (total volume: 1.1 mL). The reaction was initiated upon addition of BDA hydrate (0.1 μM). After a variable amount of time (0-255 min) at 37 °C, the reaction mixture was analyzed by HPLC/UV (Synergi 4 μm Hydro-RP 80 Å 250 x 4.60 mm column, flow rate 1 mL/min) using HPLC method 1 (solvent A was 50 mM ammonium formate buffer, pH 2.8). Product formation was monitored at 248 nm (λ_{max} of the *bis*-3-GSH product **6**).

BDA Consumption by Semicarbazide Trapping Coupled with HPLC/UV Analysis. BDA hydrate (0.1 mM) was added to a solution of 5 mM GSH in 150 mM sodium phosphate, pH 7.4 containing 10% (v/v) D_2O at 37 °C (total volume: 500 μL). For some reactions, an equimolar mixture of putrescine, cadaverine, L-ornithine, spermine, spermidine, and L-lysine was also added as in the product formation assay (0.1 mM each). At various time points (0-30 min), the reaction was quenched by the addition of semicarbazide monohydrochloride (1.4 mg, 13 μmol) which converted any unreacted BDA to the *cis*- and *trans*-*bis*-semicarbazones.[43] A similar experiment was performed with 5 mM BDA hydrate and 100 mM GSH in 80 mM sodium phosphate, pH 7.4, containing 10% v/v D_2O. This latter reaction was quenched with 200 μmol semicarbazide (22 mg) (total volume: 200 μL). Thirty minutes following the addition of semicarbazide, the reaction mixture was separated on a Bondclone 10 μm C18 column (300 x 3.90 mm) which was isocratically eluted with 5.5% (v/v) acetonitrile in water

(flow rate 1 mL/min). UV detection was at 311 nm.[23] The *cis*- and *trans*-*bis*-semicarbazones eluted at 10.4 and 19.4 min, respectively. These studies were performed two or more times. Controls were performed in the absence of GSH.

GSH-BDA Trapping Studies. BDA hydrate (0.1 mM) was added to a 5 mM solution of GSH in 150 mM sodium phosphate, pH 7.4 (total volume 1 mL). The reaction was quenched with 1 N NaOH (500 μL). Some reactions were reduced with $NaBH_4$ (20 μL of 1 M $NaBH_4$ in 10 M NaOH). Following quenching and/or reduction, 1 N HCl (500 or 700 μL) was added before analysis by LC/MS using HPLC method 1 (solvent A was 10 mM ammonium formate buffer, pH 2.8). A GSH-free control, BDA-free control, NaOH-free control, and HCl-free control were run. Analysis was on a Synergi 4 μm Hydro-RP 80 Å 250 x 0.50 mm column, flow rate 12 μL/min.

Synthesis of *N*-[4-carboxy-4(*S*)-(2-oxo-2,5-dihydro-1*H*-pyrrol-1-yl)-1-oxobutyl]-L-cysteinylglycine. GSH (41 mg, 130 μmol) was dissolved in 750 μL sodium phosphate (150 mM, pH 7.4). Sodium hydroxide (1 N, 0.5 mmol) was added, followed by BDA hydrate (5.7 mg, 68 μmol). After 30 min, HCl (1 N, 0.5 mmol) was added to neutralize the reaction. The products were initially purified by HPLC/UV (Synergi 4 μm Hydro-RP 80 Å 250 x 10.0 mm column, flow rate 4 mL/min) using the following gradient: 15 min hold at 100% A, followed by a 5 min linear gradient to 0% A, 100% B. Solvent A was 100 mM ammonium acetate buffer, pH 6.8, solvent B was 50 % (v/v) acetonitrile in water with detection at 254 nm. Two products were observed with retention times of 9.7 and 10.9 min. The collected fractions were desalted by HPLC

using the following gradient: 4 min hold at 100% A, followed by a 5 min linear gradient to 0% A, 100% B. Solvent A was water, solvent B was 50% (v/v) acetonitrile in water.

The two products were dried *in vacuo* and then dissolved in 700 μL D_2O for NMR analysis. Peak 1 was *N*-[4-carboxy-4(*S*)-(2-oxo-2,5-dihydro-1*H*-pyrrol-1-yl)-1-oxobutyl]-L-cysteinylglycine (GSH-pyrrolinone): ^{1}H NMR (500 MHz, D_2O) δ 7.43 – 7.31 (ddd, *J* = 5.9, 4.2, 1.9 Hz, 1H, 4H), 6.23 – 6.06 (m, 1H, 3H), 4.58 – 4.50 (t, *J* = 6.0 Hz, 1H, Cys α-CH), 4.50 – 4.42 (dd, *J* = 11.3, 3.5 Hz, 1H, Glu α-CH) 4.28 – 4.02 (m, 1H, 5H), 3.78 – 3.72 (s, 2H, Gly α-CH_2), 3.06 – 2.78 (m, 2H, Cys β-CH_2), 2.43 – 2.19 (m, 2H, Glu γ-CH_2), 2.17 – 2.03 (m, 2H, Glu β-CH_2). ESI^+-MS/MS [$M+H^+$] (m/z) (rel intensity): 356 (5.6), 338 (4.6), 299 (100), 271 (15.4).

NMR analysis of Peak 2 indicated the presence of three species: GSH-pyrrolinone along with *N*-[4-carboxy-4-(3-mercapto-1*H*-pyrrol-1-yl)-1-oxobutyl]-L-cysteinylglycinecyclic sulfide (*mono*-3-GSH, **7**, Scheme 4-2).[6] ESI^+-MS/MS [$M+H^+$] (m/z) (rel intensity): 356 (6.7), 338 (4.1), 299 (100), 271 (13.8). An unknown compound was also detected with a structure similar to GSH-pyrrolinone. The sample was reanalyzed by LC-MS/MS in order to learn more about the unknown compound.

The NMR samples were diluted (1:100 for peak 1, 1:10 for peak 2) and were reanalyzed by LC/MS/MS using the following gradient: 15 min linear gradient from 100% A to 75% A, 25% B, followed by a 2 min hold at 75% A, 25% B, followed by a 5 min linear gradient to 100% B. Solvent A was 10 mM ammonium formate, pH 2.8 and solvent B was 50% (v/v) acetonitrile in water. The crude reaction mixture was also analyzed undiluted by this method for comparison. Peak 1 had a retention time of 20.3

min, a parent mass of 374 *m/z* [M+H^+], and fragmentation identical to the standard (Figure 4-1). Peak 2 showed a peak at 20.5 min, a parent mass of 374 *m/z* [M+H^+], and fragmentation identical to the standard. Additionally, there was a new peak at 18.9 min with a parent mass of 373 *m/z* [M+H^+] and fragmentation different than the standards (Figure 4-2). ESI^+-MS/MS [M+H^+] (m/z) (rel intensity): 244 (100), 227 (48.9), 298 (4.0), 355 (1.5). This new compound was the major component of Peak 2 and was not present to any significant extent in Peak 1 or in the crude reaction mixture, suggesting that it is a rearrangement product. Both samples contained **7** that separated from the 374 peak when reinjected. The **7** peak eluted at 26.9 min in both samples and had 338 at its principal fragment (loss of water).

Time Course of the Reaction of GSH with BDA by NMR Analysis. An NMR tube containing GSH (5, 50, or 100 mM final concentration) in 80-128 mM sodium phosphate, pH 7.4 containing 10% D_2O was brought to 37 °C using an equilibration time of ≥10 min. The volume of sodium phosphate buffer was chosen (375-595 μL) so that the final volume of the reaction mixture after BDA hydrate addition was 700 μL. 3D gradient shimming was performed on the sample and the 90° pulse width and transmitter offset were optimized using a pre-programmed calibration procedure. The relaxation time (T_1) of GSH was experimentally determined to be ≤0.3 s. The acquisition time was set at 5 s with an additional delay of 0.1 or 1 s, giving a total recycle time of 5.1 or 6 s, which is >17*T_1. Since 5*T_1 is sufficient relaxation time to recover >99% of the signal, the integration was assumed to be quantitative. The sample was removed from the probe and BDA hydrate (0.1 or 5 mM final concentration) was added. A concentrated stock

solution of BDA hydrate was used so that the added volume was very small (<15 μL). The exact time of BDA hydrate addition was recorded. The solution was pipetted back into the NMR tube and placed back in the probe. Another round of gradient shimming was performed: 1D for time course studies and 3D for structural studies. For time course studies, 1D-^{1}H scans with water suppression were recorded in ~1 min intervals for 60 min. Time course studies were performed two times with the following exceptions. The 5 mM GSH/0.1 mM BDA hydrate studies were performed in triplicate, and the 100 mM GSH/5 mM BDA hydrate studies were performed in quadruplicate.

These experiments were repeated at low temperature (15 °C or 18 °C) for structural studies. The lower temperature retarded the reaction so that a series of absolute-value 2D-COSYs, phase-sensitive 2D-NOESYs, and selective excitation 1D-TOCSYs could be acquired with good resolution. The chemical shifts of unreacted GSH, as well as the ranges of the GSH-derived protons in the intermediates are included in Table 4-1.

Assignment and Integration of NMR Resonances

The time course of reactant consumption, intermediate generation and consumption, and final product generation were determined by integrating the appropriate signals as described below. The boundaries of integration were initially set using the 100 mM GSH + 5 mM BDA reaction. See Schemes 4-1 and 4-2 for structures. For **3** (the BDA hydrate), the *cis*- and *trans*-vinylic protons co-resonated with **8** (H4), so this signal (6.20-6.14 ppm) was summed with the *cis*-methine protons (5.91-5.85 ppm) and the interfering area from **8** was subtracted out using the well-separated H3 peak

(6.70-6.66 ppm). The result was divided by 4 to account for the four protons of BDA per molecule. The other signals were: **6** (H2: 6.96-6.90 ppm), **9** (H3: 6.48-6.42 ppm), **7** (H4: 6.37-6.32 ppm), **8** (H3: 6.70-6.66 ppm), and Int 1A (H3: 6.00-5.95 ppm). The H3 signals for Int 1B and Int 1C co-resonated with the H2 signal for Int 1A at 6.11-6.05 ppm, so this peak was integrated and the Int 1A signal was removed by subtracting the area of its H3 peak (6.00-5.95 ppm). The Int 2 region corresponding to the H2 and H5 signals was integrated as a whole (5.68-5.03 ppm) and divided by two. The structures of Int 1 and Int 2 are shown in Scheme 4-3. The area of the acetate peak (2.08-2.00 ppm) leftover from the hydrolysis of 2,5-diacetoxy-2,5-dihydrofuran was used to calculate the concentration of each reaction component since this area is directly proportional to the concentration of BDA hydrate and does not change as it is not a participant in any reactions.

Additional products were added for the 50 mM GSH + 5 mM BDA reaction: **10**, (6.64-6.61 ppm), and Int 2C-vi (5.69-5.64 ppm). Two more chemical species were added for the 5 mM GSH + 5 mM BDA reaction: **11** (H2: 6.88-6.84 ppm) and (**12**, 9.57-9.49 ppm). For the 5 mM GSH + 0.1 mM BDA condition there was no **8** to interfere with the BDA resonances so the signals (*cis*- and *trans*-vinylic protons at 6.19-6.05 ppm and the *trans*-methine protons at 5.89-5.79 ppm) were summed together and divided by four.

Boundaries of integration were customized for each condition tested. Customization was necessary since the distribution of products and their exact chemical shifts varied between conditions (but not in a significant way between experiments under the same conditions). Spectra were manually phased and baseline corrected using a linear baseline correction algorithm in the TopSpin software. The concentrations were

calculated on a scan-by-scan basis by relating the $C\underline{H}_3COO^-$ signal to the known concentration of acetate in the reaction mixture.

Time Course of the Reaction of *N*-acetyl-L-lysine (NAL) with BDA by NMR Analysis. BDA (5 mM) was reacted with NAL (100 mM) in X mM sodium phosphate, pH 7.4, containing 10% D_2O at 37 °C as described above. Boundaries of integration for the NAL-BDA reactions were set as follows: BDA (*cis*-methine protons: 5.97-5.78 ppm), **13** (Scheme 4-2, H5: 6.67-6.49 ppm summed with H4: 5.61-5.45 ppm and divided by two), **4** (Scheme 4-1, 4H: 7.34-7.29 ppm), and acetate (1.93-1.86 ppm). Because one of the peaks of **4** has the same chemical shift as the *cis* and *trans* combined peak of BDA hydrate (**3**), only the *cis*-methine peak was used. Background subtraction was performed on the *cis*-methine peak by subtracting the average of the last 20 scans from the peak area at each time point.

Reaction of *N*-acetyl-L-cysteine (NAC) with BDA by NMR Analysis. BDA (5 mM) was reacted with 5 or 100 mM NAC in X mM sodium phosphate, pH 7.4, containing 10% D_2O at 15 °C or 18 °C.

Mathematical Analysis. NMR data of the NAL + BDA reaction (BDA consumption only) was fit to a mathematical model of a pseudo-first order reaction using nonlinear regression in Matlab (v7.10.0 R2010a).[111] Equation: $y = ae^{-bx}$.

RESULTS

Our studies of the reaction of BDA with amines in the presence of GSH indicated that the initial reaction involved GSH and BDA, and that the addition of the amine took place after this step. Mass spectrometric analysis of hepatocyte supernatants using a

constant neutral loss (CNL) 129 method to detect GSH conjugates showed that they include many chemically distinct metabolites.[110] The GSH substitution is conserved across a number of metabolites, while the amines vary, providing indirect evidence that the first step (GSH-conjugation) is conserved, and the second step varies depending on the amines present. When we characterized the distribution of GSH-BDA-amine cross-links,[110] we needed to know how long we needed to wait before this distribution stopped changing. Our hypothesis at the time was that BDA would react almost instantaneously. While the relative contribution of each cross-link changed negligibly over time, the data indicated that at least 15 minutes were necessary to reach maximal cross-link levels at 37 °C and pH 7.4. This was much longer than we had initially predicted.

Because of the greater technical challenges in developing a quantitative mass spectrometry assay, an HPLC-UV method was used to track the time course of cross-link formation in vitro. The results of this HPLC time course are shown in Figure 4-3. The concentrations chosen were: 5 mM GSH (hepatocellular concentration),[108] 0.1 mM each amine, and 0.1 mM BDA hydrate. The amines used in the analysis were L-lysine, L-ornithine, spermine, spermidine, putrescine, and cadaverine. Product peaks that were well-separated from neighboring peaks were used to determine kinetic rate constants. The peaks chosen were *bis*-3-GSH (**6**), *bis*-2-GSH (**9**), GSH-BDA-spermine (**14**), GSH-BDA-N^1-spermidine (**15**), and GSH-BDA-α-ornithine (**16**) (Scheme 4-4). Figure 4-3 shows that it takes ~30 min for the reaction to reach completion.

Since product formation tells only half the story of a reaction, BDA consumption was monitored by trapping BDA as its *bis*-semicarbazone (Scheme 4-5).[23] The levels of

the semicarbazones were determined by HPLC with UV detection monitoring at 311 nm. The reaction was performed in the presence of the six amines as described above. The results of the reactant kinetics study are shown in Table 4-2. This table shows that 99% of BDA has reacted by 3 min. This is about one-tenth the time it takes for product formation. The necessity of trapping before UV detection complicated the kinetic analysis. For instance, the amount of BDA-*bis*-semicarbazone detected differed greatly at 0 min reaction time depending on whether GSH were present or absent, even though the trapping agent was added before BDA hydrate (Table 4-2). This may be a result of competition between semicarbazide and GSH for reaction with BDA. This competition is inefficient even when semicarbazide is present at 10-fold excess when compared to GSH and 200-fold excess when compared to BDA.

The gap between reactant consumption and product formation indicated that there is an intermediate, most likely GSH-BDA. This intermediate was not expected to have any significant UV absorbance, and could not be detected by mass spectrometry. Trapping the intermediate was seen as a way to potentially form a new compound that would absorb UV light and/or be stable enough for chromatographic separation and detection. Sodium borohydride was the first trapping agent tested. It was expected that this would reduce the dialdehyde to the corresponding diol or possibly a substituted furanyl ring (Scheme 4-6). Because $NaBH_4$ is unstable under acidic or neutral conditions, it was dissolved in 10 N sodium hydroxide and the solution was neutralized after the reaction was complete to make it compatible with separation on HPLC. Reduction of GSH-BDA to the diol would give a molecular weight of 396 *m/z*, while the

substituted furanyl ring would give 374 *m/z*. Two major peaks were seen by LC/MS with a molecular ion at 374 *m/z* (Figure 4-1A) and fragmentation spectra dominated by a loss of 75 indicative of a GSH cross-link (Figure 4-1B). However, when control reactions were performed it was determined that $NaBH_4$ was not required to generate the product; rather, it only depended on NaOH treatment followed by neutralization with HCl (Figure 4-4). To determine the structure of the 374 *m/z* trapping products, the two peaks were purified by HPLC and analyzed by NMR. The proton spectra showed that the earlier-eluting peak was primarily the GSH-pyrrolinone, while the later-eluting peak contained the GSH-pyrrolinone, an unknown related structure, and a significant level of the *mono*-GSH product. The signals at δ 7.38, 6.16, and 4.17 ppm were similar to the pyrrolinone structure seen as the major product in the reaction between N^{α}-acetyl-L-lysine and BDA (L-2-(acetylamino)-6-(2,5-dihydro-2-oxo-1*H*-pyrrol-1-yl)-1-hexanoic acid). Reinjection of the peaks confirmed these assignments (Figure 4-1C and 4-1F) but also showed that the unknown component of the second peak had a parent mass of 373 *m/z* (Figure 4-2C). This peak was absent from the crude reaction mixture and from the first peak (Figure 4-2A & 4-2B), suggesting that it is a rearrangement product of the GSH-pyrrolinone. Preliminary studies applying this trapping protocol to in vitro reactions with monitoring by LC-MS showed that the level of trappable intermediate did decrease over time until maximal product formation. Because of the lack of an isotopically-labeled standard for quantitation this approach was discontinued in favor of NMR experiments.

NMR is a method that can be used to detect unstable intermediates that do not have strong UV absorbances. Given the time course of BDA consumption/product

generation it was hypothesized that this method might allow for the detection and characterization of the GSH-BDA intermediate. It would also allow us to determine the kinetic rate constants for BDA disappearance and product formation. The choice of NMR for chemical kinetics offers several advantages over other techniques. Most importantly, when pulse sequence parameters are set appropriately, NMR is inherently quantitative, even when considering structurally dissimilar molecules that might have different UV/vis absorption spectra or MS ionization efficiencies. Additionally, it allows the *in situ* characterization of the structures of reactive intermediates. Finally, it requires minimal adaptation – no trapping agents complicating the kinetic analysis, no separation (and possible rearrangement) on HPLC, and precise temperature control via the probe heating/cooling unit.

Representative spectra from the NMR kinetics study are shown in Figure 4-5. To facilitate detection, initial studies were performed with 100 mM GSH and 5 mM BDA hydrate. The reaction was followed at 37 °C using a nearly identical methodology to the previous experiments, where the starting materials were pre-warmed and the reaction was initiated with the addition of BDA hydrate, followed by carefully-timed collection of the kinetics data. The resonances seen in the experiment can be divided into three broad groups: reactants, intermediates, and products. These have been labeled with a letter (R, I, or P) followed by a number for each resonance. The groups were initially assigned by their concentration vs. time profiles (reactants decreasing only, intermediates increasing then decreasing, products increasing only). Structural studies were used to determine structure and as a guide to place each chemical species in the overall reaction scheme.

Two major types of intermediates were seen in the NMR study. The first major type, Type I, have proton signals (6.04-5.75 ppm) in between those of the reactant, BDA hydrate: 6.24-6.14 ppm and 5.91-5.85 ppm (Table 4-3). The temperature at which the chemical shifts were recorded is noted since the shift of HDO, the reference peak, is highly temperature dependent.[112] Three isomers were seen, in a ratio of 1:1:4, suggesting a diastereotopic pair and third isomer. The range of chemical shifts suggested that the allylic system was retained for these intermediates, and so 1,2-addition was expected.

The Type I intermediates were tentatively assigned the structures given in Scheme 4-3, with the measured shifts given in Table 4-3. 1D-TOCSY and 2D-COSY experiments confirmed that these atoms were attached only to others in the same chemical shift range. This is consistent with the hydrated allylic system, where each proton is in a similar chemical environment. The coupling patterns of these protons is similar to the BDA hydrate starting material.[23]

The Type II intermediates were identified by their resonances between 5.0 and 5.6 ppm (i.e. between the HDO and BDA hydrate peaks) (Table 4c & 4d). Based on the analysis of the 2D-COSY data, the compounds with resonances in this region were classified as straight-chain structures with thiol substitution at the 2-position and no double bond (Int 2A) or as 2,5-dihydroxytetrahydrofuran rings with the protons at the 2- and 5-positions in a *trans* relationship (Int 2B) or a *cis* relationship (Int 2C) (Scheme 4-3). The protons attached to the 2- and 5-positions (adjacent to the furanyl oxygen and geminal to electronegative hydroxyl groups) were the most deshielded, giving chemical shifts downfield of the HDO peak. They were connected to the protons attached to

saturated carbons at positions 3 and 4, but not to one another. Therefore, the assignments are consistent with the structures given in Scheme 4-3.

The structural assignments of the intermediates were confirmed using a variety of techniques. 1D-TOCSY experiments were performed where the selection frequency was iteratively scanned through the region downfield of the residual water peak. These experiments allow the detection of all the protons in the same spin system as the irradiated proton. The magnetization was seen to transfer from peaks in the 5-6 ppm range to peaks in the 1.5-3.5 ppm range and then back to protons in the 5-6 ppm range. 2D-COSY experiments confirmed these findings with no off-diagonal peaks directly connecting the protons in the 5-6 ppm range, proving that the connection was long-range. This is consistent with a tetrahydrofuran ring, where the protons at the 2- and 5-positions have a higher chemical shift than the fully saturated carbons at the 3- and 4-positions.

The point of connection between the GSH- and BDA-derived portions of the intermediates was still undetermined, i.e. *N*-linked or *S*-linked conjugates. Model reactions were performed to establish the connectivity of the intermediates and as confirmation of the NMR assignments in the GSH + BDA reaction. N^{α}-Acetyl-L-lysine (NAL) has only one primary amino group, while *N*-acetyl-L-cysteine (NAC) has only a sulfhydryl group. These compounds were used as model nucleophiles in additional NMR experiments.

NAL (100 mM) or NAC (5, 50, or 100 mM) was combined with 5 mM BDA and followed by NMR as described above for the GSH-BDA reaction mixtures. Data collection was otherwise identical to the GSH + BDA reactions. In the NAL-BDA

reactions, we observed the formation of L-2-(acetylamino)-6-(2,3-dihydro-2-oxo-1*H*-pyrrol-1-yl)-1-hexanoic acid (4-5 NALpy, **13**), which rearranged to L-2-(acetylamino)-6-(2,5-dihydro-2-oxo-1*H*-pyrrol-1-yl)-1-hexanoic acid (3-4 NALpy, **4**) over time.[10] No intermediates in this process were observed. The structures of the NAL-BDA products indicate that primary amines combine with BDA in a 1,2-direct addition reaction.

Reaction intermediates similar to the Type I and II intermediates formed in the GSH reaction were seen only in the NAC reaction mixtures (Figure 4-6). The Type I intermediates were found to be very similar to those seen in the GSH-BDA reactions; their chemical shifts are listed in Table 4-3. The connectivity seen in the COSY spectra of the Type II intermediates in the GSH-BDA and NAC-BDA reactions, by comparison, suggest that the thiol is reacting with BDA in a 1,4-conjugate addition reaction. The relative integration of the Type I and Type II signals show that 1,4-conjugate addition is preferred.

For Int 1A, the chemical shifts of the H1 and H4 protons are lower for NAC vs. GSH, while the chemical shifts of the H2 and H3 protons are higher (Tables 4-4 & 4-5). For Int 1B and Int 1C, the chemical shifts of H2, H3, and H4 are lower for NAC vs. GSH, while the chemical shift for H5 is about the same.

The fact that the effect of NAC substitution on Int 1A vs. Int 1B & Int 1C is maintained is additional evidence that Int 1B & Int 1C are structurally related to one another, and distinct from Int 1A. For Int 1B & Int 1C, the H3 and H4 protons are about the same while the H2 and H5 protons are more distinct from one another. This is evidence that they could be *cis*- vs. *trans*-isomers of one another. For BDA cyclic

hydrate, the *cis*-methine proton has a lower chemical shift than the *trans*-methine proton.[23] Based on this, Int 1B can be assigned as the *trans*-isomer and Int 1C can be assigned as the *cis*-isomer. It is likely all three isomers are formed from a single equivalent each of BDA and NAC. If there were multiple thiol substitutions we would expect to see more than three isomers, since the singly-substituted isomers would be precursors to the multiply-substituted ones and would still be detectable.

The NAC-BDA Type II structures can clearly be divided into two groups, one with an open chain structure (Int 2A, Table 4-4) and two types of ring structures where the substituents at the 2 and 5 positions are *trans* to each other (Int 2B) and where they are *cis* to each other (Int 2C) (Table 4-4). This grouping can be made because the cyclic structures show a large diastereotopic coupling, while the open structure does not.

When comparing cyclic structures, one way these differ is in the magnitude of diastereotopic coupling. The Int 2B structures have a larger ppm difference between diastereotopic protons – from 0.82 to 1.08 ppm – while the Int 2C structures have a smaller ppm difference – from 0.11 to 0.23 ppm (Table 4-4). The diastereotopic protons at H4 have two close neighbors – the NAC at H3 and the hydroxyl or additional equivalent of NAC at H5. When these substituents are on the same face of the ring, the two protons are in very different environments – one is experiencing the effect of both substituents very strongly, while the other feels them very weakly. This effect is due to hyperconjugation of the C-S bond from the NAC substitutent at C3 and the C-O bond from the hydroxyl substituent at C5 with the corresponding σ-bonds with one of the 4-methylene protons but not the other.[113] When the substituents are on opposite faces of

the ring, each proton in the diastereotopic pair experiences the effect of one substitutent strongly and the other weakly, so there is less difference in their chemical shifts compared to when they are *cis*. Similar patterns have been seen with D-penturonic acids.[114] Int 2B-i is most like Int 2B-ii based on the larger spread between the diastereotopic protons. These isomers will have the substituents on opposite faces of the ring. Int 2C-i is most like Int 2C-ii based on the smaller difference. These isomers will have the substituents on the same face of the ring.

Int 2B-i and Int 2C-i are seen in the 1:1 (equimolar) NAC:BDA reaction, while Int 2B-ii and Int 2C-ii are seen in the 20:1 (excess) NAC:BDA reaction. Multiple additions of NAC are more likely when NAC is in excess. Because of the aqueous environment, the various intermediates are detected in their hydrated forms as opposed to the free aldehyde form. Many of these hydrates can undergo substitution reactions where additional equivalents of thiol replace the hydroxyl groups in the hydrates. To predict the effect of these substitutions on the chemical shifts of the intermediates, a series of 2-substituted 1,3-dioxolanes, -dithiolanes, and –oxothiolanes were compared (Scheme 4-7). Each of these contains a methine carbon bonded to a hydrogen, an R-group, and two electronegative atoms (two oxygens, two sulfurs, or one oxygen and one sulfur). By looking at the trend in the methine hydrogen as the R-group and combination of *O* and *S* atoms are varied, the effects of these substitutions on the chemical shift may be deduced.

For 2-propyl and 2-pentyl substitutions, the methine proton had the highest chemical shift for the dioxolanes (5.18 ppm[115] & 5.74 ppm[116]), the lowest chemical shift for the dithiolanes (4.4 ppm[117] & 4.5 ppm[118]), and an intermediate chemical shift for the

oxothiolanes (4.72 ppm & 4.55 ppm[119]). This follows the pattern expected from looking at the electronegativities of *O* and *S* atoms – two oxygens in dioxolanes have the greatest deshielding effect, while two sulfurs in dithiolanes have the least deshielding effect, with one oxygen and one sulfur in an intermediate position.[120,121]

Two five-membered heterocyclic substitutions 2-(furan-2-yl) and 2-(thiophen-2-yl) were also considered. The pattern of methine protons changes for these two substitutions. For the furanyl ring, the oxothiolane gives the highest methine shift at 6.02 ppm.[119] The dioxolane gives an intermediate chemical shift (5.92 ppm[122]), with the dithiolane as usual giving the lowest shift (5.6 ppm[123]). The thiophenyl ring has the dioxolane in its usual place with the highest methine shift at 6.11 ppm, but now the oxothiolane gives the lowest shift at 5.31 ppm and the dithiolane with the intermediate shift at 5.92 ppm.[124]

Overall, the range of shifts for the methine proton of 2-substituted dioxolanes is 5.18 (2-propyl) to 6.11 ppm (2-(thiophen-2-yl)), the range of 2-substituted dithiolanes is 4.4 (2-propyl) to 5.92 ppm (2-(thiophen-2-yl)), and the range of oxothiolanes is 4.55 (2-pentyl) to 6.02 (2-(furan-2-yl)).[115,119,124] In general, the dioxolanes had the highest methine shifts, the dithiolanes had the lowest, and the oxothiolanes had intermediate shifts, although there were exceptions. This trend seemed to hold more for the 2-alkyl substituted compounds than the 2-aryl substituted compounds. Both NAC and GSH have alkyl chains at the point of connection through the thioether linkage, so increasing the level of thiol substitution should cause the neighboring proton signals to shift upfield.

The Int 2A isomers (Table 4-4) also can have multiple NAC substitutions. When NAC is present in excess, the additional NAC substitution is likely to be located at the 2-position, since the greatest changes in chemical shifts are at the H2 and H3 positions while the H5 positions are relatively unchanged. Int 2A-i is almost identical to product Int 2C-i except H1 and H2 are more deshielded, so the double-hydroxyl at the 1-position is likely. Int 2A-i, being open chain, also does not show diastereotopic coupling like Int 2C-i does. Int 2A-iv is almost identical to Int 2B-i except for the coupling of the diastereotopic protons. Since with Int 2A-i, the double hydroxyl leads to deshielding of the H1 and H2 protons, Int 2A-iv likely has an NAC substitution at this position. Int 2A-iii is similar to Int 2C-i, except the H1 of Int 2A-iii has a higher chemical shift than the H2 of Int 2C-i, and the H4 of Int 2A-ii has a lower chemical shift than the H5 of Int 2C-i. Int 2A-ii probably has an NAC substitution at H4, lowering the chemical shift, and is double-hydroxyl substituted at H1, leading to a higher chemical shift. Int 2A-ii is much like Int 2C-ii, except that the H2 proton of Int 2A-ii has a lower chemical shift than the H3 proton of Int 2C-ii. This can be explained by loss of the rigidity provided by the ring structure. Int 2A-ii is therefore likely to be substituted with NAC at the 1-position. Comparing 2A-ii with 2A-iii, the former has the higher H4 shift, so it probably has a double hydroxyl substitution at the H4 position, while the latter has an NAC substitution.

GSH-BDA Int 2B-ii probably has a similar structure to NAC-BDA Int 2B-ii (Table 4-4 & 4-5). GSH-BDA Int 2C-ii probably has a similar structure to NAC-BDA Int 2C-ii. The chemical shift differences between these products are on the order of ± 0.03 ppm. GSH-BDA Int 2C-v is similar to Int 2C-ii except it probably has an amine-

substitution at the 2 position, and the difference in the diastereotopic protons of 0.99 makes it likely that the -OH and -SG substituents at postions 5 and 3 (respectively) are on the same side of the ring. The amine substitution is responsible for the drop in chemical shift of the H2 proton down to 4.48 ppm, much lower than any of the others.

GSH-BDA Int 2B-iii and Int 2C-iii are the same, except Int 2B-iii has the substituents at the 3- and 5-positions on the same side of the ring, and Int 2C-iii has them on the opposite sides. This is indicated by the large diastereotopic coupling at H4 for Int 2B-iii (0.78 ppm) as compared to the small one for Int 2C-iii (0.08 ppm). They are likely GSH-substituted at the 5-position, since they have lower chemical shifts than the other H5 protons for the –i and –ii isomers.

When the hydroxyl group at the 2-position (as in Int 2B-i, Int 2C-i, Int 2B-iii, and Int 2C-iii) are switched out for additional equivalents of GSH (as in the –ii and –iv isomers) the H2 proton resonance shifts upfield (Table 4-5). Only Int 2C-v has an H2 chemical shift down at 4.48 ppm, suggesting an *N*-linked GSH at the 2-position for this isomer. A similar trend is seen for the 5-position. Int 2B-i, Int 2C-i, Int 2B-ii, and Int 2C-ii all have hydroxyl substitutions, while these have been switched out for additional equivalents of GSH for the –iii and –iv isomers shifting the H5 resonance upfield.

Unlike the NAC-BDA reactions, the GSH-BDA reactions have open chain products that are detectable under the 1:1 condition. These open chain products are detectable only at the 20:1 condition in the NAC-BDA reactions. In the 1:1 GSH:BDA condition, the three open chain products are part of a series. Int 2A-i has two hydroxyls at H1 (highest shift – 5.47 ppm), Int 2C-i has one hydroxyl and one GSH (intermediate

shift – 5.38 ppm), and Int 2A-v has two GSH at H1 (lowest shift – 5.13 ppm) (Table 4-5). They all have almost the same shifts at H4 (range 5.41-5.48 ppm) so there is no substitution on that end.

The same series occurs at the 10:1 GSH:BDA condition, except the H4 proton now has a shift of 5.33-3.35 ppm, so there is one GSH substitution on that end. At the 1-position, Int 2A-iii has two hydroxyls (highest H2 shift – 3.42 ppm), Int 2A-iv has one GSH substitution (intermediate H2 shift – 3.28 ppm), and Int 1A-vi has two GSH substitutions (lowest H2 shift – 3.09 ppm).

The NMR time course data was used for a detailed kinetic analysis (Figure 4-7). Additional studies were performed where the concentration of GSH was dropped from 100 mM to 50 mM and finally to 5 mM, holding the BDA hydrate concentration at 5 mM. Since the ^{1}H-enhance cryoprobe offered such a large S/N enhancement, the conditions were extended to include 5 mM GSH and 0.1 mM BDA hydrate.

The concentration vs. time profiles for each GSH:BDA reaction are plotted in Figure 4-7. The 100 mM GSH + 5 mM BDA (20:1) reaction is shown in Figure 4-7a. Table 4-6 contains a qualitative measure of the relative time scales of the different reaction steps. For the intermediates, which are formed but then disappear over time, the relevant measure is the time when the maximum concentration is reached (grey cells). Type I intermediates were only detected in the 100 mM GSH + 5 mM BDA condition. It is likely that the concentration of these intermediates reached their maximum level before the first time point could be collected; they decayed rapidly in parallel with the BDA cyclic hydrate (**3**). Both BDA hydrate and Int 1 were undetectable by ~20 min.

There were a variety of Type II intermediates that were detected, which is consistent with the large number of isomers seen in the structural studies (discussed above). In general, as the GSH:BDA ratio increased the number of GSH equivalents per intermediate increased. The time of maximum concentration of the Type II intermediates taken as a class varied by a factor of ~3x between the different conditions. The longest time to peak concentration was in the 100 mM GSH + 5 mM BDA reaction at 17 ± 2 min, while the shortest was in the 5 mM GSH + 0.1 mM BDA reaction at 7 ± 1 min. Some isomers in the other conditions were shorter lived (Int 2B-i peaked by the first scan in the 50 mM GSH + 5 mM BDA reaction) but there were other, longer lived isomers present as well.

Another species that can be classified as an intermediate based on its concentration vs. time profile is (*E*)-4,4-dihydroxybut-2-enal (*trans*-BDA, **12**). It reached detectable levels only in the 5 mM GSH + 5 mM BDA reaction, peaking at 13 ± 4 min. This compound had a proton resonance at 9.57-9.49 ppm that is distinctive for an aldehydic proton. The chemical shifts of this compound matched those of a *trans*-BDA (data not shown).

For the products in the GSH-BDA reaction, the relevant measure is the time to completion, taken here as 95% of the maximum level for convenience. As the peak time of the longest-lived Type II intermediate got longer, so did the length of time until reaction completion. In the 100 mM GSH + 5 mM BDA reaction, the longest-lived Int 2 peaked at 17 ± 2 min and the reaction was complete at ~60 min. In the 50 mM GSH + 5 mM BDA reaction, the longest-lived Int 2 peaked at 8 min and the reaction was complete

earlier, at ~30 min. In the 5 mM GSH + 5 mM BDA reaction, the longest-lived Int 2 peaked at 13 ± 4 min and the time to completion was ~60 min, similar to the 100 mM + 5 mM reaction. In the 5 mM GSH + 0.1 mM BDA reaction, the longest-lived Int 2 peaked at 7 ± 1 min and the time to completion was reduced to ~25 min. Therefore, the time until peak Int 2 concentration is strongly correlated to the time to reaction completion, which makes sense if the intermediates are direct precursors to the products.

The oxazolidinone (**10**) and dimer-3-GSH (**11**) products are formed much more quickly than the *bis*- and *mono*-GSH products. The structure of **10** is analogous to one formed during the microsomal incubation of ipomeanine.[125] Whether this effect is due to an equilibrium effect or a kinetic effect cannot be determined from the data. The other major products all form on virtually identical timescales, suggesting different reaction pathways for **10** and **11** compared to the others.

Table 4-7 shows the percentage contribution of each product at the final time point (~80 min). In the 100 mM GSH + 5 mM BDA reaction the *bis*-3-GSH product (**6**) dominates with 77%. The concentrations of **7**, **8**, **9**, and **11** are approximately equal. In Figure 4-7 it is shown that the final concentration of **6** is just under 3 mM, with most of the remaining 2 mM of mass in the form of the Type II intermediates. Table 4-7 shows that **6** is the major product in every condition where GSH is in excess. The situation changes, however, with the 1:1 GSH:BDA condition. In this case, **11** becomes the major product and neither **6** nor **9** are detected at all. This is hypothesized to be a result of the limiting amount of GSH, since **6** and **9** require 2 equivalents of GSH for every equivalent of BDA, while **11** has a similar structure but the ratio is 1:1 equivalents. The formation

of **11** was undetectable in any of the reactions where GSH was in excess as previously reported.[23]

It was of interest to determine if the lack of any significant formation of a GSH-pyrrolinone was due to kinetic effects or if it were due to some other factor. An NMR time course was performed with NAL in place of GSH. The 4-5 pyrrolinone isomer (4-5 NALpy, **13**) is formed first, which isomerizes to the conjugated 3-4 pyrrolinone (3-4 NALpy, **4**). The half-life of BDA hydrate in the 100 mM NAL + 5 mM BDA reaction was determined to be 3.1 ± 0.2 min (Figure 4-8).

The initial HPLC product formation assay and BDA consumption assay that showed a difference between the kinetics of reactant consumption and product formation were performed with 5 mM GSH, 0.1 mM BDA hydrate, and 0.1 mM each of six different amines (Table 4-2). To test the influence of the amine mixture, the BDA consumption assay was performed in the absence of the six amines (Table 4-8). The results were virtually identical in the presence and absence of the amine mixture with the absolute difference at any timepoint ≤0.2% of the control peak area. To compare the HPLC data with the NMR data obtained at higher concentrations of both GSH and BDA hydrate, the assay was repeated with 100 mM GSH, 5 mM BDA, and 10% (v/v) D_2O (Table 4-8). The reaction was slowed down significantly, with 20 min elapsing before 99% of the BDA was consumed vs. 3 min at the lower concentration.

DISCUSSION

It has long been established that the initial step in furan bioactivation is oxidation by P450 to form BDA.[23] The purpose of this investigation was to better understand the

structures of the intermediates that exist between BDA and the detectable end metabolites. Because of the intimate relationship between structure and the chemical and toxicological properties of molecules, the characterization of these intermediates should provide insight into the toxicological mechanism of furan in living systems. Kinetics experiments are invaluable tools to probe the chemical properties of components of a reaction network. The rate at which chemical reactions occur is inextricably connected to the effect that a substance has on its surroundings.

The first experiment was a product formation assay by HPLC/UV (Figure 4-3). Products reached maximum levels by ~30 min, however they are only one third of a chemical reaction, with intermediates and reactants forming the remainder. The next experiment focused on the reactant: BDA.

The consumption of BDA can be measured by semicarbazide trapping. The resulting *bis*-semicarbazone can be detected by UV. The same reaction studied in the product formation assay was repeated for the BDA consumption study and it was found 99% of the BDA was gone by 3 min (Table 4-2). The mismatch between the time scales of BDA consumption and product formation were evidence that intermediates play a significant role in the reaction network.

Because these intermediates were not detected by the reactant or product assays used previously, it was thought that a new trapping protocol could be developed based on the presumed chemical structure of the intermediate (GSH-BDA, **5**). The reaction was treated with $NaBH_4$ in an attempt to reduce the dialdehyde of **5** to form the corresponding diol or perhaps a related structure (Scheme 4-6). Unexpectedly it was discovered that the

base the $NaBH_4$ was dissolved in for stability was able to trap an intermediate in the form of the GSH pyrrolinone. Because of the necessity for a trapping step as well as detection by MS, this approach was found to be unsuitable for quantitative kinetics experiments. An NMR assay was hypothesized to be an excellent solution since it a) is quantitative (given the appropriate parameters), b) is fast (time points can be taken close together) c) is sensitive (when using a cryoprobe on a high-field instrument), d) can be used to monitor the reaction *in situ* (no chromatography), and e) can be used to detect reactants, intermediates, and products simultaneously.

Scheme 4-8 shows one possible reaction scheme that is consistent with the results of our work. The reaction starts when BDA hydrate converts into the activated aldehyde form, which allows it to react with GSH. It became immediately apparent upon inspection of the concentration vs. time profiles of the 100 mM GSH + 5 mM BDA reaction (Figure 4-7A) that there were two types of intermediates. This fit well with the knowledge that both 2- and 3-substituted reaction products (ex. **9** and **6**) have been characterized as a result of either 1,2-direct or 1,4-conjugate addition to BDA.[10] The Type I intermediates come from direct addition and are both formed very quickly and decay rapidly. They are not detected at all except at the highest concentration of GSH. The Int 1 end-product, *bis*-2-GSH, is found at all the reaction conditions except for where [BDA] = 0.1 mM, so we propose that Int 1 is formed but reacts quickly (before the first timepoint can be acquired) and is below the limit of detection for the remainder of the time course. Mass balance indicates that the formation of Int 1 must be reversible, since

if it is not, then all of the mass of Int 1 should eventually be converted to *bis*-2-GSH and this is not the case.

The Type II intermediates accumulate to detectable levels in all of the GSH + BDA reactions. These intermediates include open chain structures and cyclic structures consisting of a THF ring with GSH attached at the 3-position. The assignment of this structure is based on the chemical shifts and the connectivity seen by NMR.

The initial step in the reaction is not second order. On the contrary, BDA reacts more slowly when the concentration of GSH is increased (Table 4-8, Figure 4-7). If the rate limiting step were [GSH + BDA → Intermediates] then the rate should double if the concentration of GSH is doubled, but this does not occur. This is evidence that the rate limiting step is some sort of activation of BDA hydrate. Dehydration to produce the unmasked aldehyde fits this pattern (Scheme 4-8). A different possibility is that GSH can act as a base to abstract a proton at the 4-position of Int 2 to regenerate the starting materials (not shown). This is not the same as reversibility. It accomplishes the same result as if the reaction were reversible, namely regeneration of the starting materials, but the key difference is that the rate of regenerating the starting materials would increase with increasing [GSH] whereas in a reversible reaction it increases as the concentration of the intermediates increase.

From these data it can be concluded that the reaction of BDA hydrate will not be instantaneous even given the large excess of GSH in the cytosol (~5 mM)[108] compared to BDA. The ability to form a hydrate limits the reactivity of BDA formed by oxidation of

furan and extends its half-life past what might be expected of an α,β-unsaturated dialdehyde.

When comparing the time needed to form peak intermediate concentration and the time until product formation is complete (Table 4-6), it is clear that the intermediates have a significant lifetime. These intermediates could therefore exist long enough to modify proteins or other cellular nucleophiles at sites distant from where the intermediate is formed. The GSH conjugates of structurally similar electrophiles, such as 4-hydroxy-2-nonenal (HNE), are exported from the cell via membrane transporters such as RLIP76.[11] GSH-BDA intermediates retaining their ability to modify nucleophiles could be exported by the same system to the bile canaliculi, which would be consistent with furan's adverse effects on cholangiocytes that lead to cholangiocarcinomas in rats.

Reaction kinetics have an important effect on toxicology. The lifetimes and structures of various intermediates determine how they are distributed, whether the toxic and carcinogenic effects of different metabolites are limited to the site of bioactivation or if systemic distribution is a possibility. BDA hydrate and the two intermediates are less reactive than BDA, and moderate the speed with which it forms various metabolites.

BDA hydrate and the GSH-BDA intermediates have half-lives that could allow these metabolic intermediates to distribute to cells distant from the hepatocytes where they are formed. The movement of these stabilized intermediates throughout the animal could explain the cholangiocarcinomas in F344/N rats treated with furan, as well as with the development of adrenal tumors in mice documented in the 1993 NTP report on furan.[1] The ability of these intermediates to cross cell membranes is also consistent with

experiments performed in our laboratory in which GSH-BDA-amine cross-links were formed with components of the media (such as $^{2}H_4$-labeled lysine). These media components were hydrophilic and had limited time to be transported into the cell, so it is more likely that a reactive intermediate was transported out of it.

Int 1 and Int 2 discussed in this report (Scheme 4-3), are likely key intermediates in the formation of the observed metabolites detected in hepatocyte cell culture and in the urine of furan-treated animals. The detection of these intermediates better explains the time course of metabolite formation and the chemical structure of metabolites than does BDA, and should be considered central to the process of furan metabolism.

Table 4-1. Chemical shift ranges of the GSH backbone at 15 °C (700 MHz, D_2O).

		δ Range (ppm)	
Assignment	GSH	GSH (multiplicity)	GSH-BDA
Cys Amide-NH	8.33	d, *J* = 7.5 Hz	8.51-8.28
Gly Amide-NH	8.23	t, *J* = 6.2 Hz	8.28-8.04
Cys α-CH	4.34	td, *J* = 7.3, 5.3 Hz	4.38-3.99
Gly α-CH_2	3.62	d, *J* = 6.0 Hz	3.82-3.60
Glu α-CH	3.55	t, *J* = 6.7 Hz	3.58-3.51
Cys β-CH_a	2.72	dd, *J* = 14.2, 5.3 Hz	2.97-2.66
Cys β-CH_b	2.72	dd, *J* = 14.2, 7.0 Hz	
Glu γ-CH_2	2.31	m	2.44-2.09
Glu β-CH_a	1.94	dd, *J* = 6.8, 2.3 Hz	2.07-1.85
Glu β-CH_b	1.91	dd, *J* = 7.0, 2.6 Hz	

Table 4-2. Consumption of BDA as measured by *bis*-semicarbazone trapping for the 5 mM GSH + 0.1 mM BDA reaction with amines.

GSH	Time (min)	*bis*-semicarbazone
-	0	100%, 100% (basis)
+	0	15.2%, 15.0%
+	1	5.5%, 5.3%
+	2	2.4%, 1.7%
+	3	0.9%, 0.7%
+	4	0.3%, 0.3%
+	5	0.1%, 0.1%

BDA hydrate (0.1 mM) was added to a solution of 5 mM GSH and 0.1 mM each putrescine, cadaverine, L-ornithine, spermine, spermidine, and L-lysine in 150 mM sodium phosphate, pH 7.4 containing 10% (v/v) D_2O at 37 °C. The reaction was quenched by the addition of semicarbazide monohydrochloride (1.4 mg, 13 μmol) and analyzed by HPLC-UV with detection at 311 nm. Averaged results for $N = 2$.

Table 4-3. Chemical shift assignments for Int 1 structures in NAC-BDA and GSH-BDA reactions.

Structure	Name	Temp.	δ H1	δ H2	δ H3	δ H4
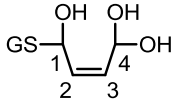	GSH Int 1A	15 °C	5.94	5.83	5.75	5.90
		37 °C	n.d.	6..07	5.97	6.12
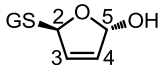	GSH Int 1B	15 °C	6.04	5.95	5.86	5.96
		37 °C	6.25	n.d.	6.09	n.d.
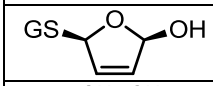	GSH Int 1C	15 °C	6.00	5.93	5.86	5.98
		37 °C	6.21	n.d.	6.08	n.d.
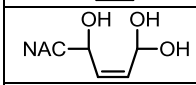	NAC Int 1A	15 °C	5.94	5.81	5.74	5.87
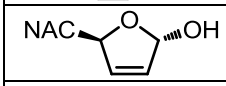	NAC Int 1B	15 °C	6.02	5.91	5.85	5.96
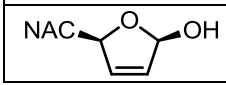	NAC Int 1C	15 °C	5.98	5.89	5.83	5.97

Table 4-4. Chemical shift assignments for Int 2 structures in NAC-BDA reactions.						
Int 2A Structures	Name	Temp.	δ H1	δ H2	δ H3	δ H4
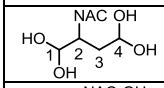	NAC Int 2A-i	15 °C	5.51	3.63	2.01	5.41
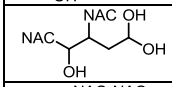	NAC Int 2A-ii	15 °C	5.34	3.35	2.15	5.32
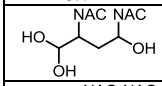	NAC Int 2A-iii	15 °C	5.25	3.18	2.53	5.10
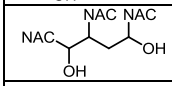	NAC Int 2A-iv	15 °C	5.18	3.22	2.17	5.25
Int 2B & 2C Structures	Name	Temp.	δ H2	δ H3	δ H4	δ H5
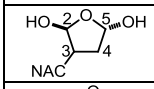	NAC Int 2B-i	15 °C	5.16	3.14	2.39, 1.57	5.29
		15 °C	5.23	3.00	2.50, 1.54	5.41
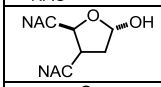	NAC Int 2B-ii	15 °C	5.17	3.02	2.67, 1.59	5.24
		15 °C	5.08	3.10	2.51, 1.54	5.40
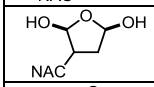	NAC Int 2C-i	15 °C	5.12	3.18	2.09, 1.91	5.34
		15 °C	5.31	3.34	1.99, 1.88	5.39
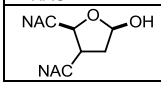	NAC Int 2C-ii	15 °C	4.92	3.28	2.16, 1.93	5.38
		15 °C	4.99	3.31	2.14, 1.92	5.40

Table 4-5. Chemical shift assignments for Int 2 structures in GSH-BDA reactions.						
Int 2A Structures	Name	Temp.	δ H1	δ H2	δ H3	δ H4
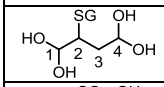	GSH Int 2A-i	18 °C	5.47	3.42	1.96	5.45
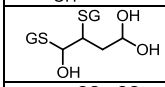	GSH Int 2A-ii	18 °C	5.38	3.35	2.15	5.35
		37 °C	5.57	3.56	2.36	5.54
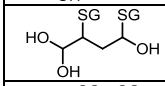	GSH Int 2A-iii	18 °C	5.41	3.42	2.18	5.33
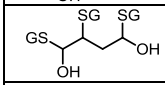	GSH Int 2A-iv	18 °C	5.28	3.28	2.27	5.35
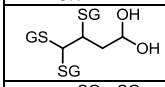	GSH Int 2A-v	18 °C	5.13	2.94	2.57	5.48
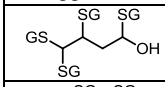	GSH Int 2A-vi	18 °C	n.d.	3.09	1.65	5.35
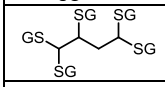	GSH Int 2A-vii	18 °C	5.11	3.54	2.50	4.90
		37 °C	5.25-5.20	n.d.	n.d.	n.d.
Int 2B & 2C Structures	Name	Temp.	δ H2	δ H3	δ H4	δ H5
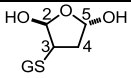	GSH Int 2B-i	18 °C	5.48	3.47	2.37,1.90	5.45
		37 °C	5.64	3.79	2.19	4.58
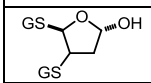	GSH Int 2B-ii	15 °C	5.10	3.10	2.55, 1.55	5.41
		37 °C	5.27	3.30	2.75, 1.78	5.61
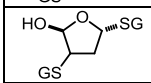	GSH Int 2B-iii	15 °C	5.28	3.19	2.54, 1.66	5.13
		37 °C	5.45	3.40	2.77, 1.89	5.33
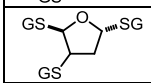	GSH Int 2B-iv	15 °C	5.18	3.02	2.69, 1.61	5.26
		37 °C	5.41	3.25	2.91, 1.82	5.48
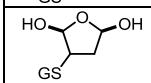	GSH Int 2C-i	18 °C	5.38	3.42	n.d., 1.96	5.41
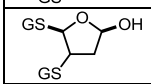	GSH Int 2C-ii	15 °C	4.98	3.28	2.15, 1.90	5.40
		18 °C	5.05	3.35	2.22, 1.96	n.d.
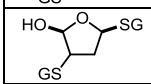	GSH Int 2C-iii	15 °C	5.22	3.20	2.20, 2.12	5.26
		37 °C	5.47	3.91	2.37, n.d.	5.46
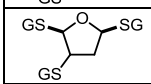	GSH Int 2C-iv	18 °C	5.19	3.69	2.15, 1.82	5.18
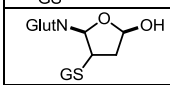	GSH Int 2C-v	15 °C	4.48	2.98	2.51, 1.52	5.40
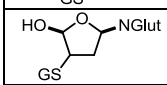	GSH Int 2C-vi	18 °C	5.52	3.43	2.43,2.11	4.20
		37 °C	5.67	n.d.	n.d.	n.d.

Table 4-6. Characteristic time scales for reaction of intermediates and products in the GSH + BDA conditions.

[GSH] (mM)	100	50	5	5
[BDA] (mM)	5	5	5	0.1
Number of replicates	4	2	2	3
Int 1	First Scan	-	-	-
Int 2A (-i, -ii, -iii, -iv)	-	-	-*	-
Int 2A-vi	-	First Scan	-	-
Int 2A-vii	-	-	10 (8, 11)	-
Int 2B-i	n.d.	First Scan	6 (5,8)	-
Int 2C-i	-	-	5 (5,6)	-
Int 2B & 2C (except -i)	17 ± 2	-	-	7 ± 1
Int 2C-vi	-	8 (7, 9)	First Scan	-
trans-BDA (**12**)	-	-	13 ± 4	-
bis-3-GSH (**6**)	65 ± 4	19 ± 1	-	32 ± 10
mono-3-GSH (**7**)	58 ± 5	36 ± 2	62 ± 2	-
mono-2-GSH (**8**)	62 ± 5	34 ± 4	63 ± 4	-
bis-2-GSH (**9**)	59 ± 5	24 ± 5	-	21 ± 16
oxazolidinone (**10**)	10 ± 1	5 (4, 7)	28 ± 5	-
dimer-3-GSH (**11**)	-	-	28 ± 5	-

n.d.: not determined because of a co-resonating peak

- : not detected

-* : only detected when the reaction was slowed down by lowering the temperature

x: detected (product)

First Scan: maximum concentration at the first scan

Number (intermediates): time until maximum concentration

Number (products): time to 95% completion

Times are given in minutes and are ± SD (or each datum is listed for N=2). For some compounds (ex. **6**) there were multiple resonances monitored per compound so a SD was calculated even though the experiment may have only been run in duplicate.

Table 4-7. Percent contribution of each reaction product to total products at the final time point as measured by NMR for the GSH + BDA reactions.

[GSH] (mM)	100	50	5	5
[BDA] (mM)	5	5	5	0.1
N	4	2	2	3
bis-3-GSH (**6**)	77% ± 1%	66.7%, 66.8%	-	76% ± 5%
mono-3-GSH (**7**)	8.0% ± 0.6%	11.8%, 12.0%	27.3%, 26.6%	-
mono-2-GSH (**8**)	6.3% ± 0.3%	9.0%, 8.9%	30.8%, 31.0%	-
bis-2-GSH (**9**)	8.6% ± 0.4%	12.5%, 12.3%	-	24% ± 5%
dimer-3-GSH (**11**)	-	-	41.8%, 42.4%	-

Table 4-8. Consumption of BDA as measured by *bis*-semicarbazone trapping for the 5 mM GSH + 0.1 mM BDA and 100 mM GSH + 5 mM BDA reactions without amines.

	5 mM GSH + 0.1 mM BDA		100 mM GSH + 5 mM BDA	
GSH	Time (min)	*bis*-semicarbazone	Time (min)	*bis*-semicarbazone
-	0	100% (basis)	0	100% (basis)
+	0	15.3% ± 0.6%	0	77% ± 7%
+	1	5.0% ± 0.5%	5	25% ± 5%
+	2	2.0% ± 0.1%	10	6% ± 1%
+	3	0.73% ± 0.02%	15	2% ± 2%
+	4	0.294% ± 0.002%	20	1% ± 1%
+	5	0.12% ± 0.02%	25	0.17% ± 0.07%
+			30	0.08% ± 0.04%

5 mM GSH + 0.1 mM BDA: BDA hydrate (0.1 mM) was added to a solution of 5 mM GSH in 150 mM sodium phosphate, pH 7.4 containing 10% (v/v) D_2O at 37 °C. The reaction was quenched by the addition of semicarbazide monohydrochloride (1.4 mg, 13 μmol) and analyzed by HPLC-UV with detection at 311 nm. Averaged results for $N = 3$.
100 mM GSH + 5 mM BDA: BDA hydrate (5 mM) was added to a solution of 100 mM GSH in 80 mM sodium phosphate, pH 7.4 containing 10% (v/v) D_2O at 37 °C. The reaction was quenched by the addition of semicarbazide monohydrochloride (22 mg, 200 μmol) and analyzed by HPLC-UV with detection at 311 nm. Averaged results for $N = 3$.

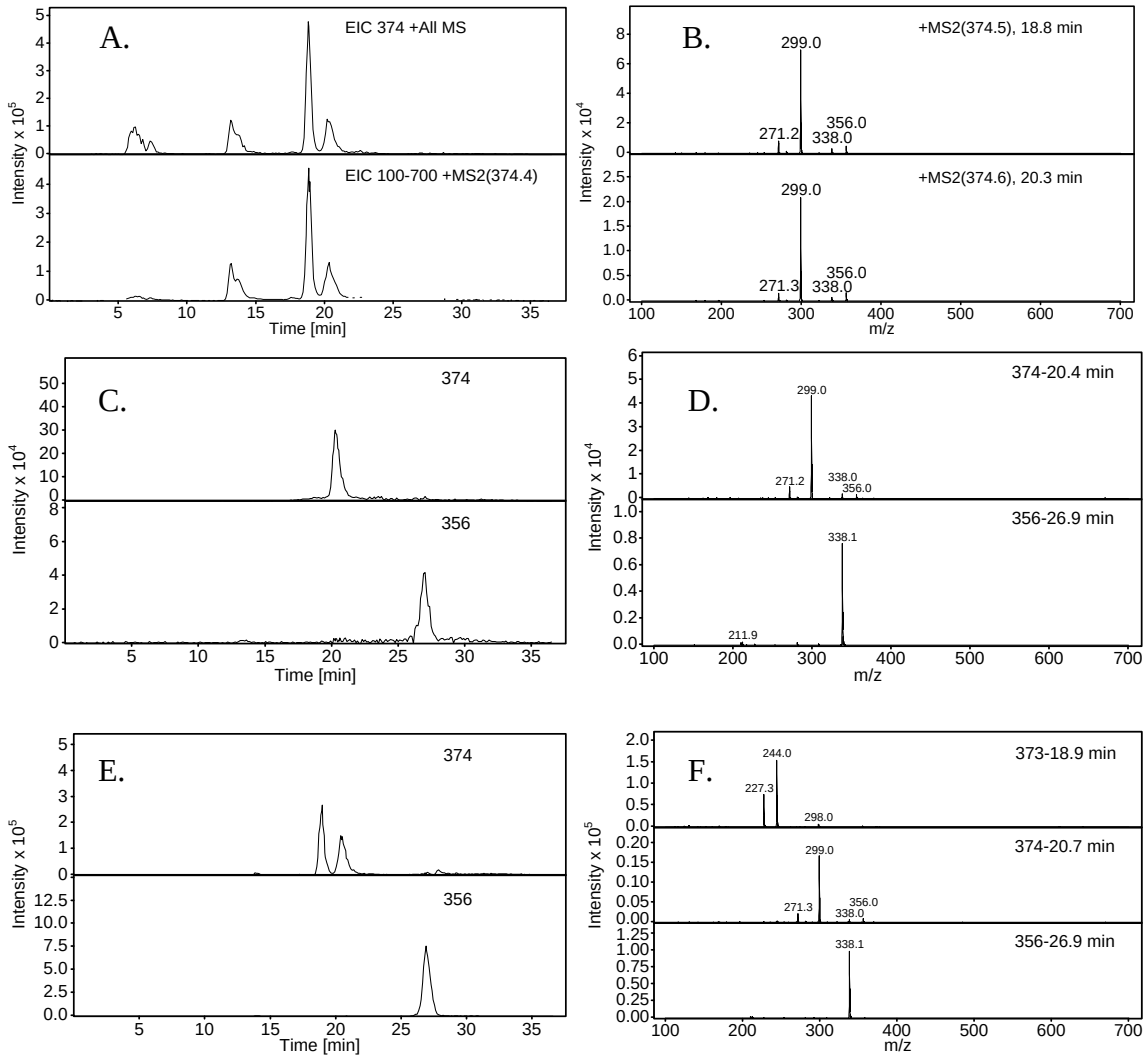

Figure 4-1. A) Extracted ion current of 374 *m/z* (top) and all MS^2 on 374 *m/z* (bottom) of the crude trapping reaction. Peak 1 has a retention time of 18.8 min, Peak 2 has a retention time of 20.3 min. B) Ion fragmentation spectra of Peak 1 (top, RT 18.8 min) and Peak 2 (bottom, RT 20.3 min). C) Extracted ion current of 374 *m/z* (top) and 356 *m/z* (bottom) for Peak 1 after isolation and reinjection on LC-MS/MS. D) Ion fragmentation spectra of the 374 *m/z* peak (top, RT 20.4 min) and 356 *m/z* peak (bottom, RT 26.9 min). The fragmentation of the 374 *m/z* peak matches that in the crude trapping reaction (shown in A and B). E) Extracted ion current of 374 *m/z* (top) and 356 *m/z* (bottom) for Peak 2 after isolation and reinjection on LC-MS/MS. F) Ion fragmentation spectra of the 374 *m/z* peaks (top, RT 18.9 min; middle, 20.7 min) and 356 *m/z* peak (bottom, RT 26.9 min). The fragmentation of the 374 *m/z* peak that elutes at 20.7 min matches that in the crude trapping reaction (shown in A and B).

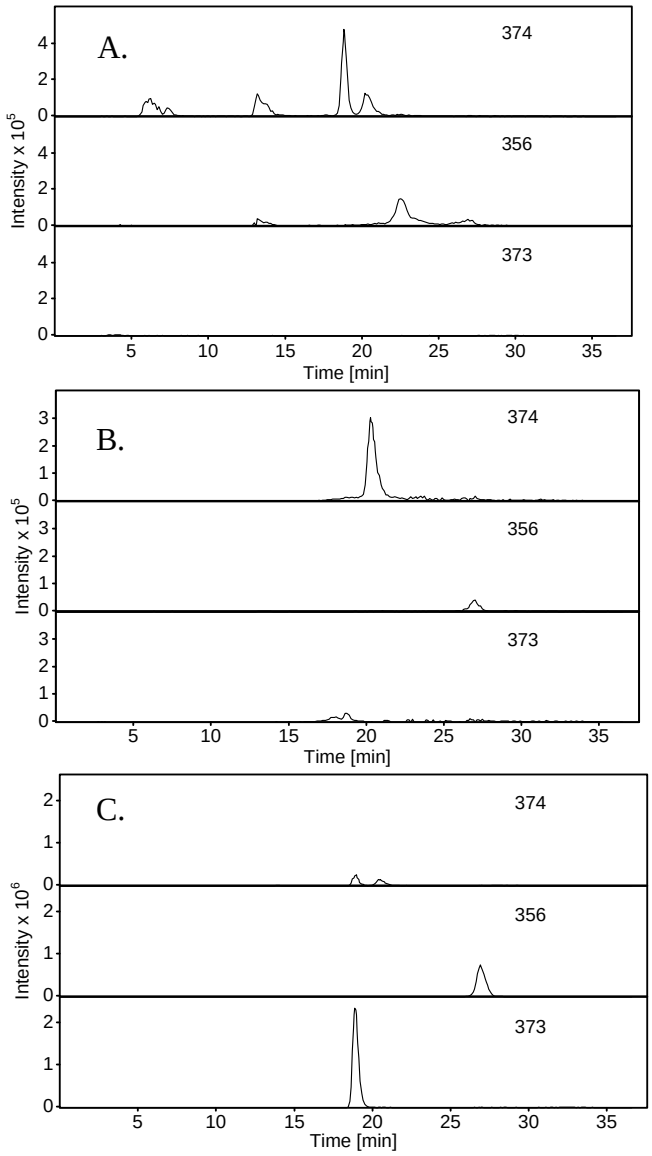

Figure 4-2. Relative amounts of the GSH-pyrrolinone (374 *m/z*), *mono*-3-GSH (**7**, 356 *m/z*), and the unknown (373 *m/z*) plotted on the same scale. A. Crude trapping reaction. B. Peak 1 after isolation and reinjection on LC-MS/MS. C. Peak 2 after isolation and reinjection on LC-MS/MS.

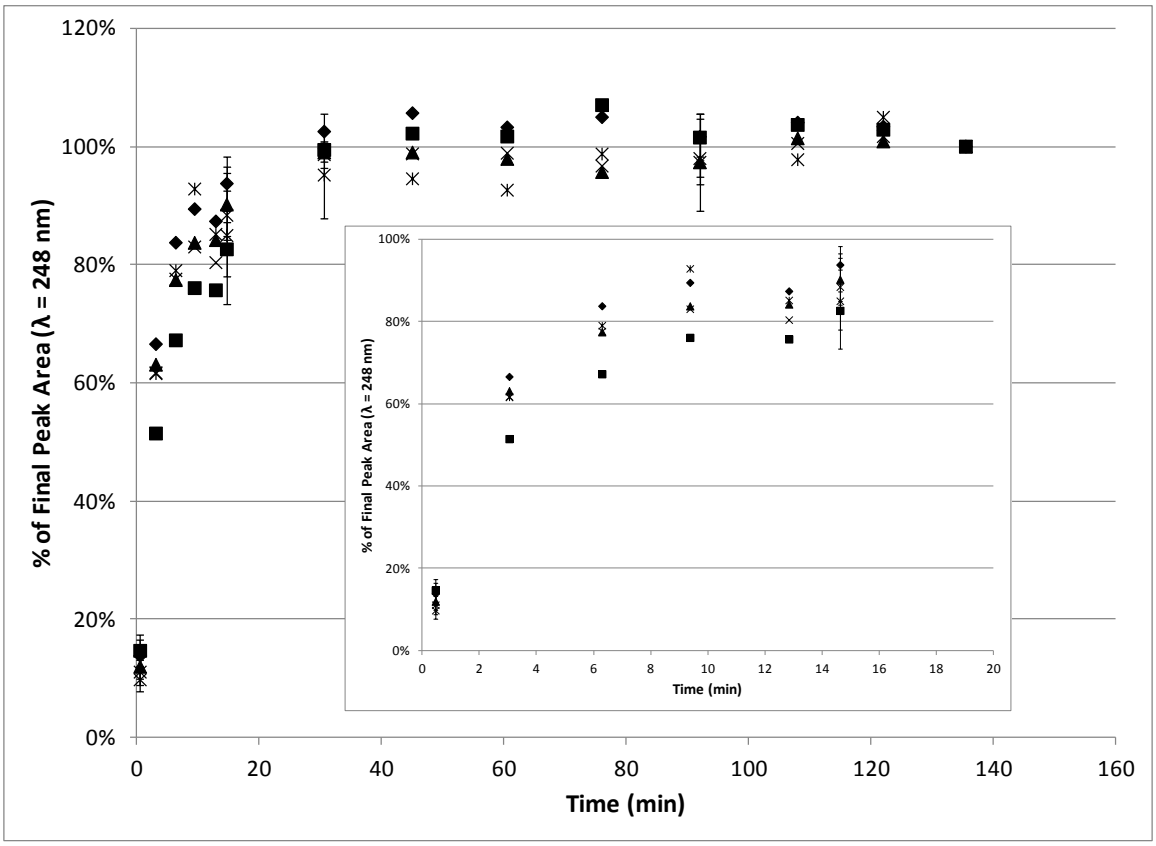

Figure 4-3. A representative plot of the HPLC time course of product formation in 150 mM sodium phosphate buffer. Inset figure shows the first 20 minutes of reaction. Retention times (in minutes using HPLC method 1 where solvent A was 50 mM ammonium formate, pH 2.8): *bis*-3-GSH: 40.2 (◆ **6**); *bis*-2-GSH (■ **9**): 39.7; GSH-BDA-Spermine (▲ **14**): 27.3; GSH-BDA-N^1-Spermidine (× **15**): 28.6; GSH-BDA-α-Ornithine: (× **16**) 31.4.

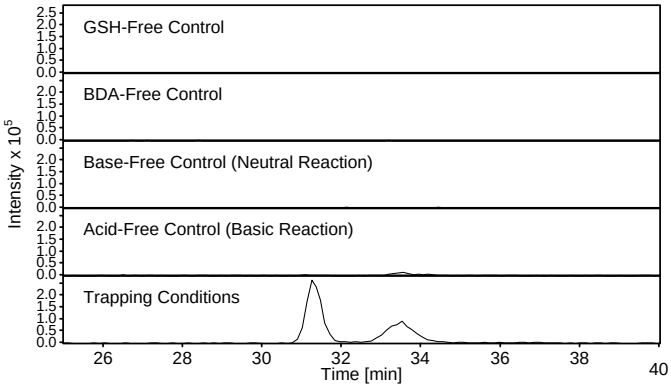

Figure 4-4. Sodium hydroxide/hydrochloric acid trapping of the GSH-BDA intermediate. Extracted ion current of 374 (*m/z*) corresponding to the [M+H$^+$] ion of the GSH-pyrrolinone.

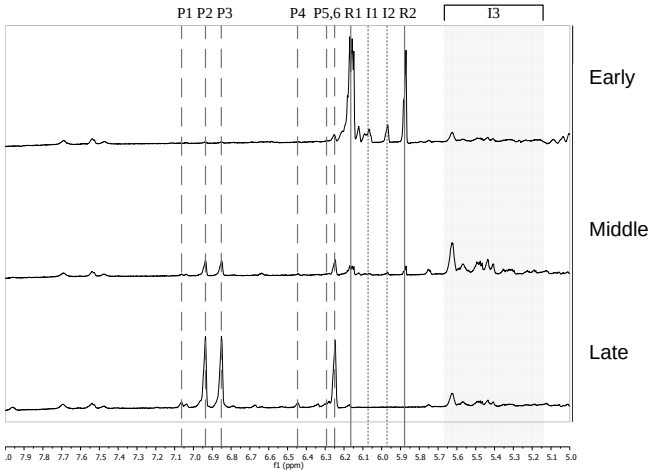

Figure 4-5. 1D-^{1}H traces of the NMR time course showing early (~4 min), middle (~16 min), and late (~80 min) time points. P1: *bis*-2-GSH (H5) P2: *bis*-3-GSH (H2), P3: *bis*-3-GSH (H5), P4: *bis*-2-GSH (H3), P5: *bis*-2-GSH (H4), P6: *bis*-3-GSH (H4), R1: BDA hydrate (both *trans*-protons and *cis*-vinylic proton), R2: BDA hydrate (*cis*-methine proton), I1: Int IB & Int IC (common resonance), I2: Int A, I3: Int II (mixture of isomers). Reactants decrease over time, products increase over time, and intermediates increase then decrease.

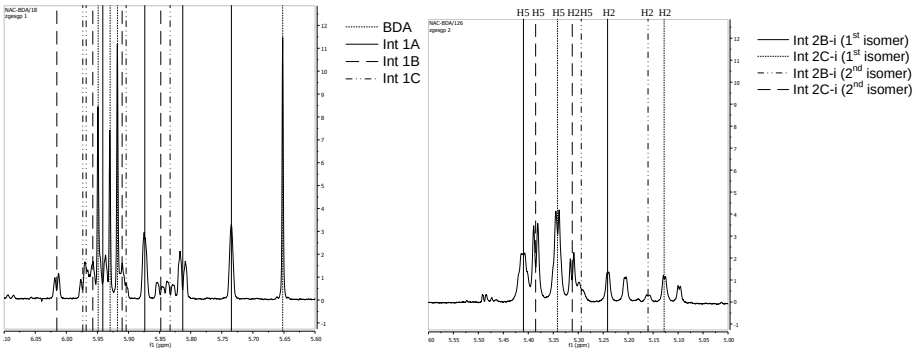

A. B.

Figure 4-6. 1D-^{1}H traces of the NAC + BDA reaction (5 mM both reactants). A. 5.6-4.8 ppm range. B. 6.18-5.58 ppm range.

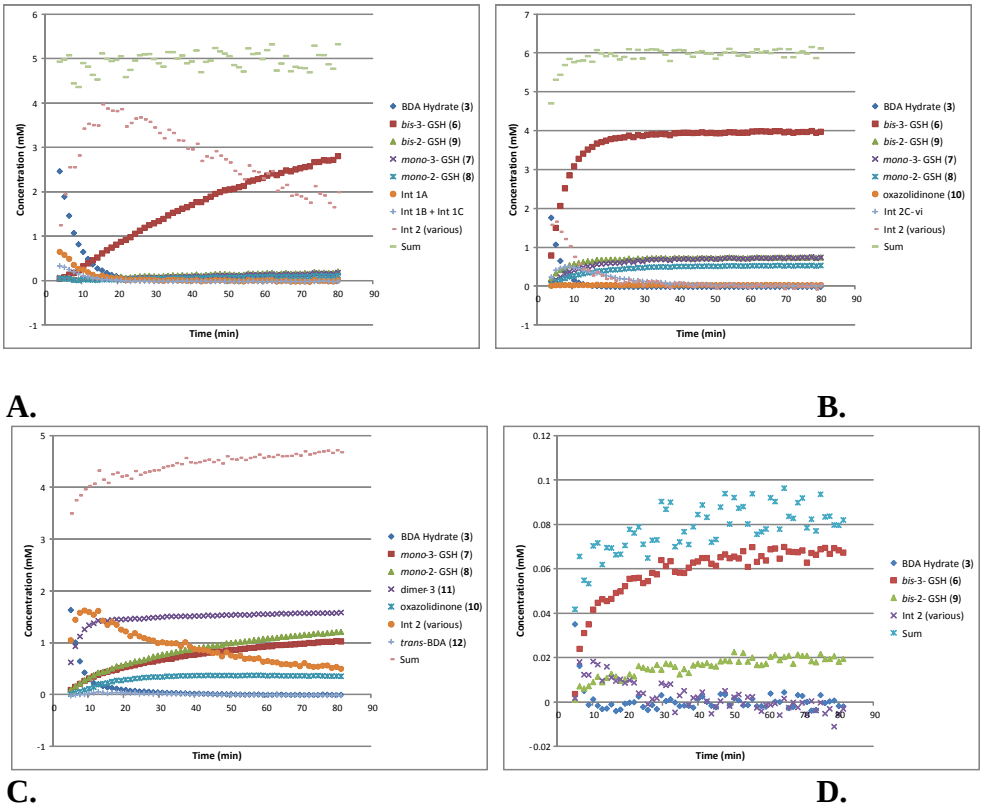

A. B.

C. D.

Figure 4-7. NMR time course showing concentration vs. time. A. 100 mM GSH + 5 mM BDA. B. 50 mM GSH + 5 mM BDA. C. 5 mM GSH + 5 mM BDA. D. 5 mM GSH + 0.1 mM BDA.

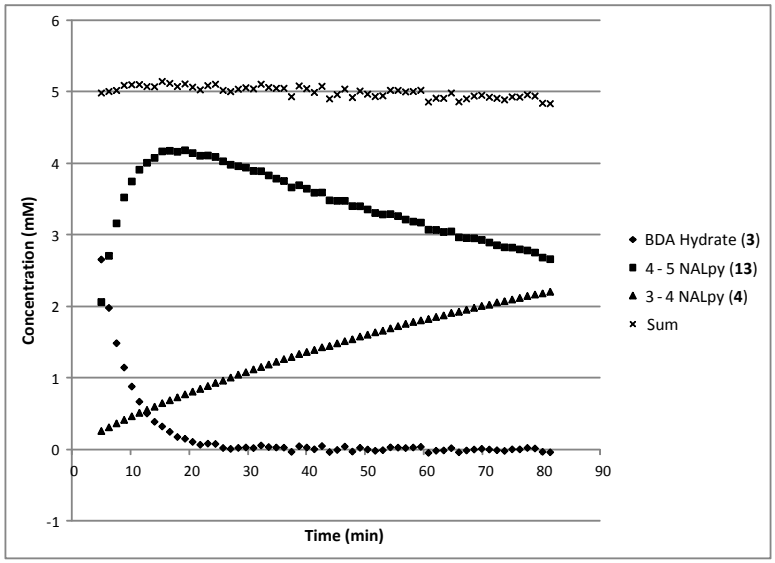

Figure 4-8. Representative NMR time course showing concentration vs. time for 100 mM NAL + 5 mM BDA.

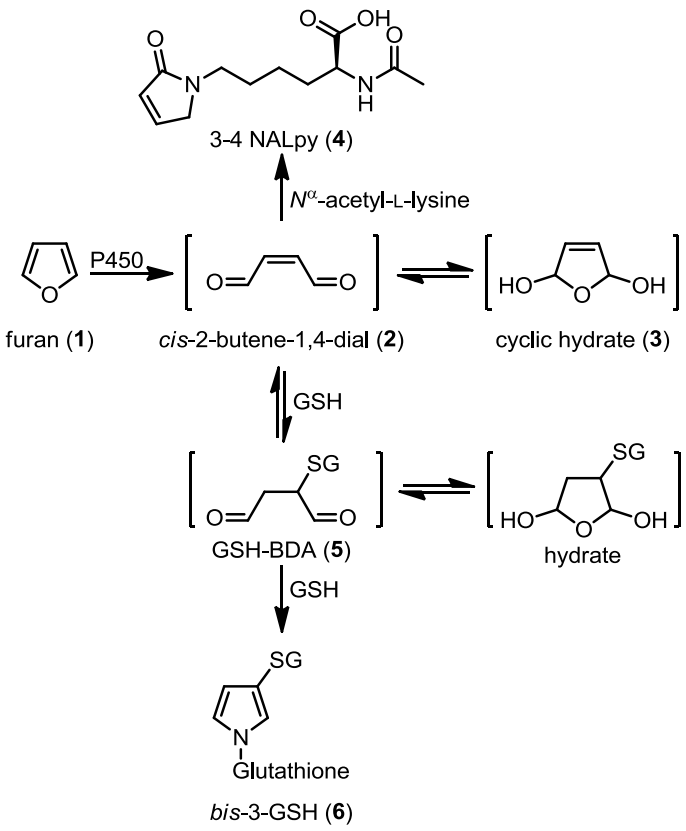

Scheme 4-1. Generalization of known furan metabolism.

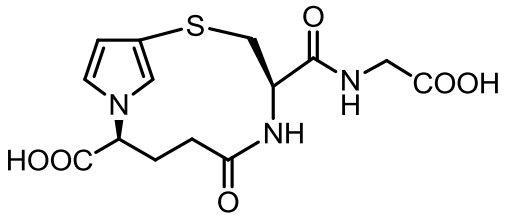

mono-3-GSH (**7**)

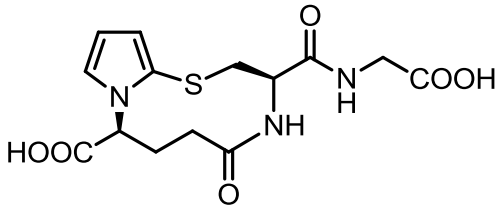

mono-2-GSH (**8**)

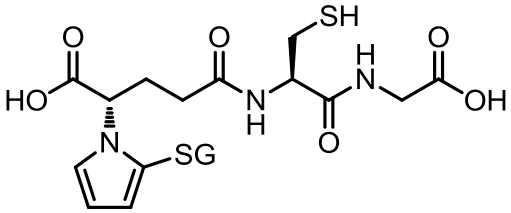

bis-2-GSH (**9**)

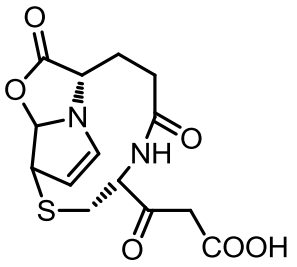

oxazolidinone product (**10**)

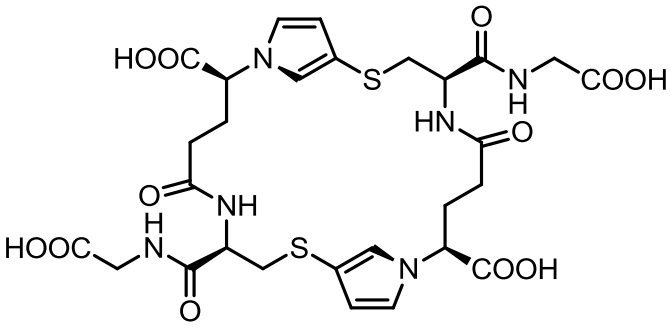

dimer product (**11**)

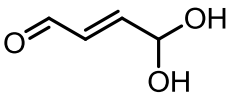

(*E*)-4,4-dihydroxybut-2-enal
(*trans*-BDA) (**12**)

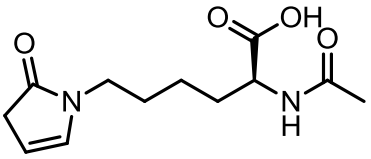

4-5 NALpy (**13**)

Scheme 4-2. Additional products of GSH-BDA reactions seen by NMR.

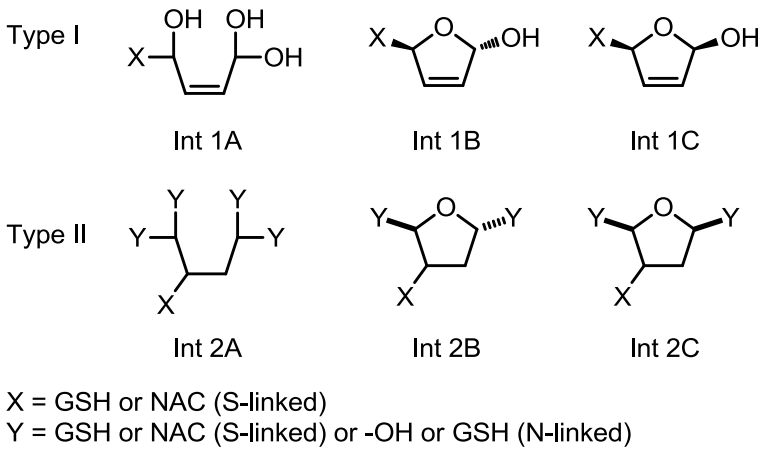

Scheme 4-3. Generalized naming system for intermediates.

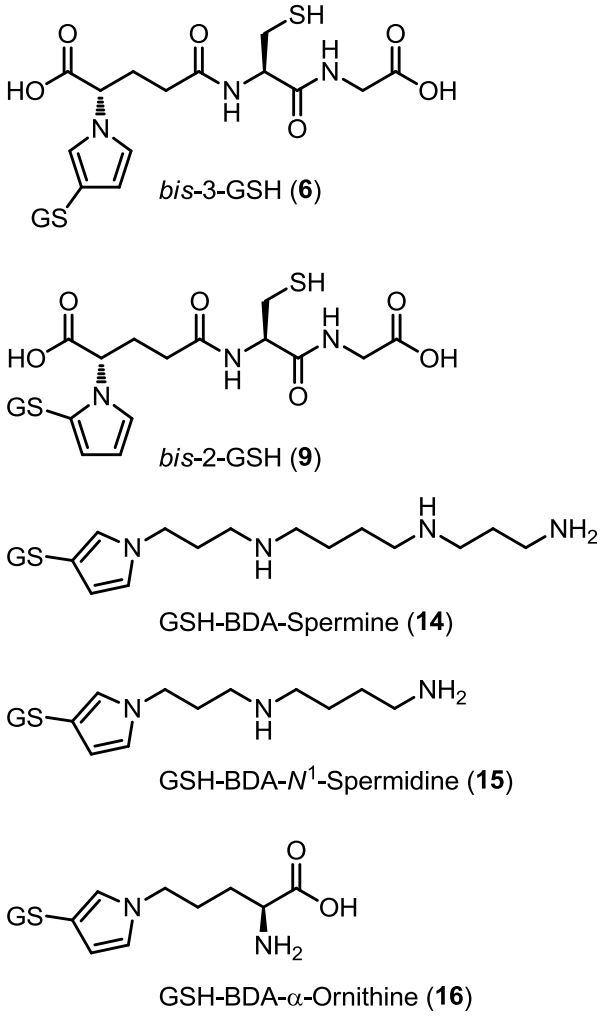

Scheme 4-4. Structures of furan metabolites monitored by HPLC/UV.

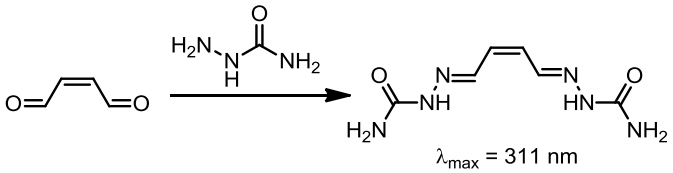

Scheme 4-5. Trapping of BDA with semicarbazide.

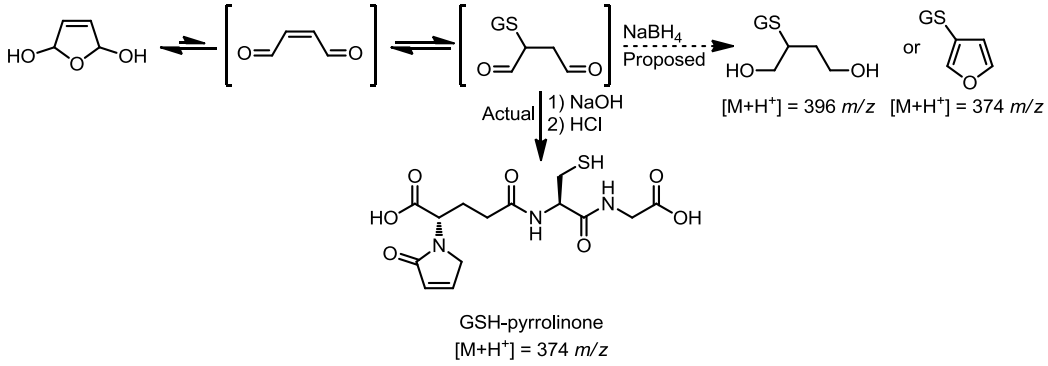

Scheme 4-6. Proposed and actual pathways for GSH-BDA trapping reactions.

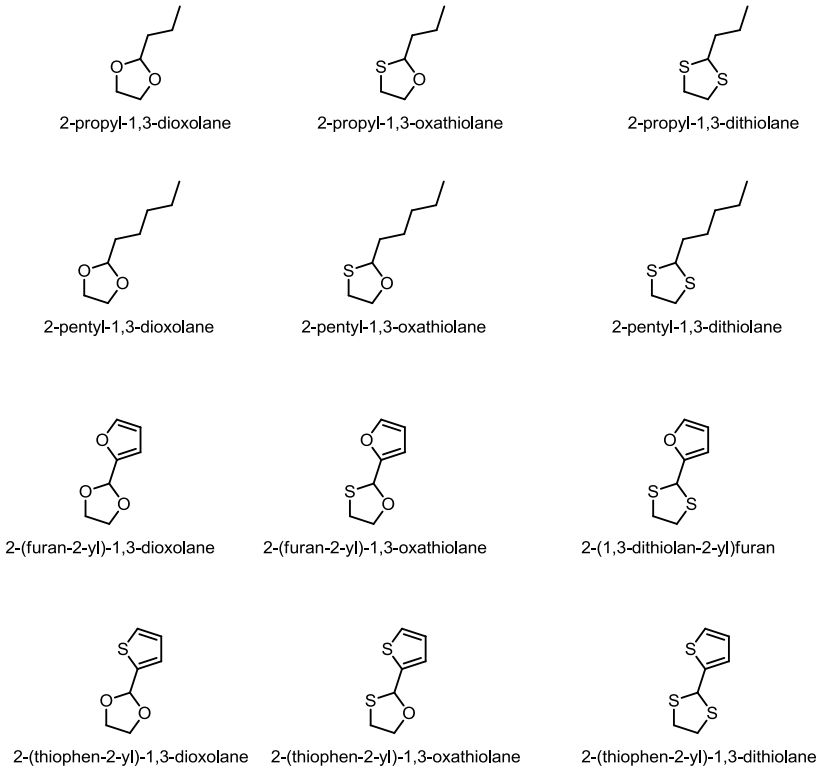

Scheme 4-7. Substituted dioxolanes, oxathiolanes, and dithiolanes.

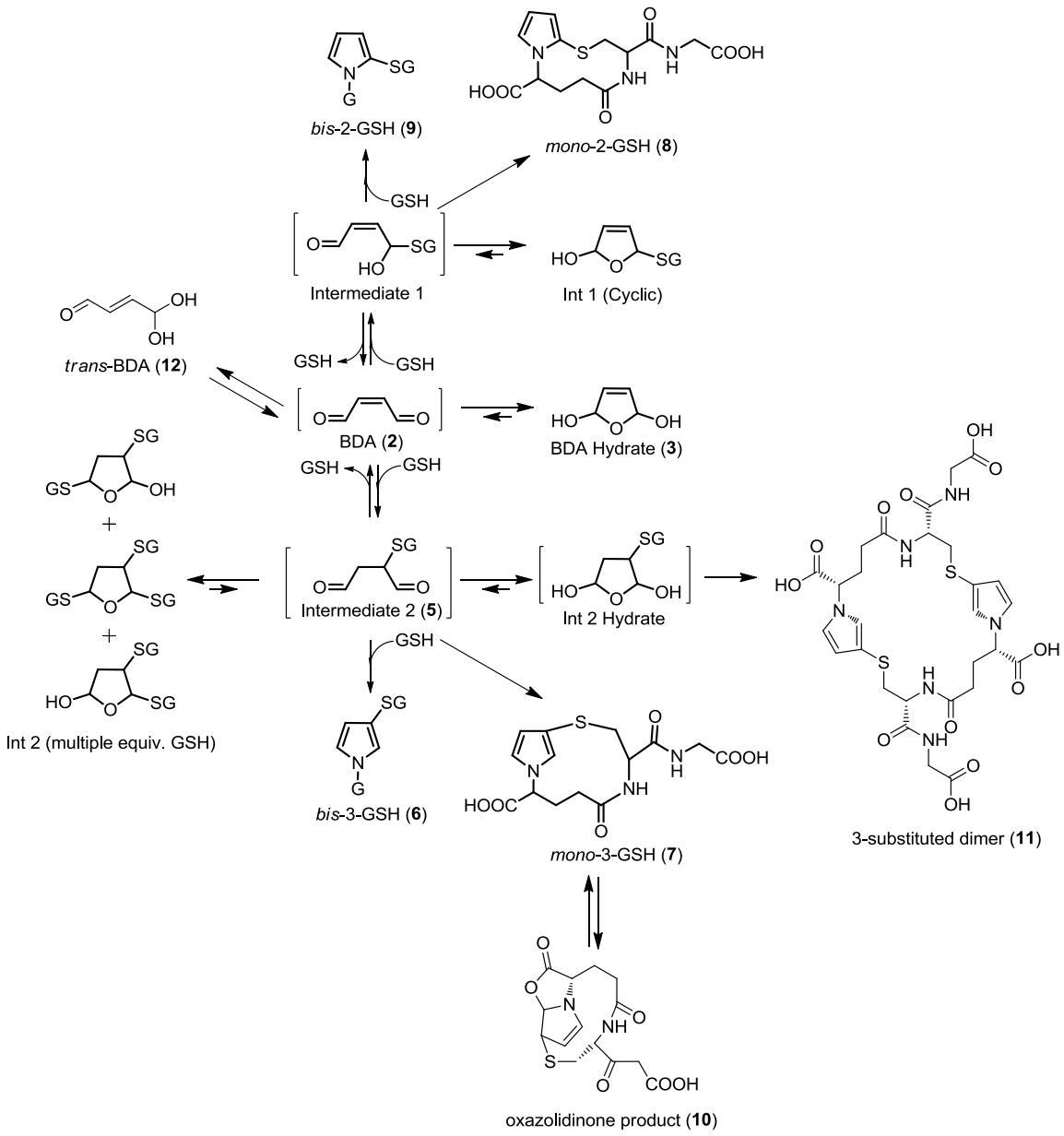

Scheme 4-8. Proposed reaction pathway for the GSH + BDA reaction including major intermediates and products.

Chapter 5: Covalent Cross-Linking of Glutathione to Cytochrome *c* by *cis*-2-Butene-1,4-dial, a Reactive Intermediate of Furan

Martin B. Phillips, Mathilde M. Sullivan, and Lisa A. Peterson

INTRODUCTION

Furan is a liver toxicant and carcinogen in rats and mice.[1] The mechanism of carcinogenesis is currently unknown, however widespread cell death followed by compensatory cellular proliferation has been implicated as a possibility.[42] This could either be through selection of pre-cancerous cells or through mutational events secondary to cell toxicity.[42] Protein adduct formation likely represents an important trigger of furan toxicity.[9] Approximately 13% of a carcinogenic dose of furan (8 mg/kg) was covalently bound to liver proteins in rats 24 h after treatment.[7] Furan is converted to a protein-binding reactive intermediate as a result of cytochrome P450 catalyzed oxidation, observed both *in vivo* and *in vitro*.[7,60] The reactive metabolite can be trapped with either semicarbazide or glutathione and has been identified as *cis*-2-butene-1,4-dial (BDA).[6,23,60] Chemical model studies indicate that BDA reacts with lysine residues to form pyrrolin-2-one adducts.[10] In addition, it is able to cross-link *N*-acetylcysteine or GSH to *N*-acetyllysine through pyrrole ring formation.[10] Studies in rat hepatocytes demonstrated that BDA cross-links glutathione (GSH) to a variety of amines, including proteins.[9,110] Analysis of furan urinary metabolites indicates that similar chemistry is occurring in rats *in vivo*; both lysine pyrrolin-2-one and cysteine-BDA-lysine pyrrole cross-links are precursors to these compounds.[9,26,28]

Based on these studies, one can propose two protein-reactive metabolites generated during furan metabolism, BDA and 2-(*S*-glutathionyl)succinaldehyde (GSH-BDA, Scheme 5-1). BDA can react directly with proteins to form pyrrolin-2-one lysine adducts (**1**). Alternatively, the reaction of BDA with GSH generates GSH-BDA, which is expected to react with protein lysine residues to form GSH-BDA-protein cross-links (**2**). Glutathionylation of proteins is thought to affect cellular energy metabolism and redox cycling.[126] To explore the relative protein reactivity of these two intermediates, a model protein, cytochrome *c*, was reacted with BDA in the presence and absence of glutathione. Similar studies have been performed with cytochrome *c* and other α,β-unsaturated carbonyl compounds, such as 4-hydroxy-2-nonenal.[127] The amount of alkylation was determined by MALDI mass spectral analysis whereas the amino acids targeted by BDA and GSH-BDA were determined by LC-MS/MS analysis of tryptic digests.

EXPERIEMENTAL PROCEDURES

Caution: *BDA is toxic and mutagenic in cell systems. It should be handled with proper safety equipment and precautions*.

Chemicals. Aqueous solutions of BDA were synthesized from the hydrolysis of 2,5-diacetoxy-2,5-dihydrofuran and quantified as the bis-semicarbazone as previously described.[43,46] Semicarbazide monohydrochloride was purchased from Acros Organics (Geel, Belgium). Optima® grade acetonitrile was purchased from Fisher Chemical (Fair Lawn, NJ). Sequencing grade modified trypsin was purchased from Promega (Fitchburg, WI). ZipTips were purchased from Millipore (Billerica, MA). All other reagents were purchased from Sigma-Aldrich (St. Louis, MO).

Protein Modification Reactions. Horse heart cytochrome *c* (250 μM) was reacted with BDA (0, 50, 100, or 500 μM) in the presence or absence of 1 mM GSH in 100 mM sodium phosphate, pH 7.4, at 37 °C for 2 h. The reaction mixtures were frozen at -20° C until tryptic digestion or MALDI-TOF-MS analysis.

Tryptic Digestion. Modified cytochrome *c* was diluted 1:4 in nanopure water and acetonitrile was added to a final concentration of 10% (v/v) MeCN. The pH of the solution was adjusted to 7.5-9.0 by adding 50 mM ammonium bicarbonate containing 1 mM $CaCl_2$. The lyophilized trypsin was solubilized in 50 mM acetic acid. Trypsin was added to the protein solution to a final concentration of ~1:60 protease:protein (w/w) and the digestion was allowed to proceed overnight at 37 °C. The samples were cooled to RT and the pH was adjusted to 3 with glacial acetic acid (1-5 μL). The digested samples were stored at -80 °C until analysis by LC-ESI^+-MS/MS.

MALDI-TOF-MS analysis. The digested sample (13 μL) was acidified with 0.7 μL of 10% (v/v) trifluoroacetic acid (TFA). A C4 ZipTip was wet by 50% (v/v) aqueous acetonitrile containing 0.1% (v/v) TFA and then equilibrated with 0.1% (v/v) TFA solution. The acidified sample (10 μL) was extracted with the prepared ZipTip and washed with 0.1% (v/v) TFA. Finally, the sample was eluted with 75% (v/v) aqueous acetonitrile containing 0.1% (v/v) TFA (1.2 μL). The protein sample was mixed on the stainless steel target with an equal volume of a saturated aqueous solution of sinapic acid containing 0.1% (v/v) TFA. MALDI-TOF mass spectra were acquired with a Bruker BiFlex III MALDI-TOF mass spectrometer (Bruker Daltonics) equipped with a pulsed nitrogen laser (2 ns pulse at 337 nm). All spectra were collected in the positive ion mode.

Spectra were acquired in either linear or reflectron modes. All data were processed with XMass (Bruker Daltonics). The MALDI-TOF mass spectrometer is located in the Center for Mass Spectrometry and Proteomics in the College of Biological Sciences, University of Minnesota.

LC-ESI$^+$-MS/MS. Reversed-phase LC was performed with an Eksigent nanoLC-Ultra 2D LC system (Dublin, CA) equipped with a 10-cm fused silica emitter (75 µm inner diameter from New Objective, Woburn, MA) in-house packed with reverse-phase Zorbax SB C18 5 µm resin (Agilent Technologies, Santa Clara, CA). The column was eluted at a constant flow rate of 300 nL/min with the following gradient: 25 min linear gradient from 95% A, 5% B to 80% A, 20% B; 25 min linear gradient to 10% A, 90 %B, 10 min hold at 10% A, 90% B; 5 min linear gradient to 95% A, 5% B, then a 15 min hold at 95% A, 5% B. Solvent A was 0.1% formic acid in water (v/v) and solvent B was acetonitrile containing 0.1% formic acid. ESI$^+$-MS/MS was performed with a Thermo Scientific LTQ-Orbitrap Velos instrument (Thermo Electron, Bremen, Germany) in positive ion mode. General mass spectrometric conditions were: electrospray voltage, 1.6 kV; capillary temperature, 275 °C; no sheath or auxiliary gas flow. Protein digests (1 µL) pre-acidified with glacial acetic acid were injected onto the column. MS data were acquired with the Orbitrap analyzer at a resolving power of 60,000 at 400 *m/z*. Nine scan events were used as follows: (Event 1) *m/z* 300-2000 full scan MS and (Events 2-9) data-dependent scan MS/MS on the eight most intense ions from event 1. An isolation window of 2.5 *m/z*, ion selection threshold of 500 counts, activation $q = 0.25$, and activation time of 30 ms were applied for MS^2 acquisitions. The spectra were recorded

using dynamic exclusion of previously analyzed ions for 0.5 min with two repeats and a repeat duration of 0.5 min. Ions with unassigned charge states or charge states of <2 were excluded. The MS/MS normalized collision energy was set to 35%. All data were processed with the Qual browser module of Xcalibur 2.1.0.1139 (Thermo Electron). The lock mass was enabled for accurate mass measurements. Polydimethylcyclosiloxane (*m/z*, 445.120024) ions were used for internal calibration. The mass spectrometer is located in the Analytical Biochemistry core facility of the Masonic Cancer Center, University of Minnesota.

Data Analysis. Tryptic digestion MS data was analyzed using Proteome Discoverer 1.3 and Xcalibur 2.1 (Thermo Electron). Peak lists and predicted CID fragmentation were generated using Proteome Discoverer, while peak areas and actual fragmentation were checked in Xcalibur. Precursor ions were required to have a mass tolerance of 5 ppm, while fragment ions were required to have a mass tolerance of 0.8 Da. Dynamic modifications were searched using Sequest on lysine and cysteine residues, as well as alanine residues (as a control). The monoisotopic modification masses were: 48.00000, 66.01056, 84.02113, or 355.08380 (Scheme 5-2). The peptide window for the peak list was set for 300-6000 Da (singly-charged equivalent). The search database consisted of the most recent sequence for horse heart cytochrome *c* (Equus caballus, NCBI accession: 1FI7_A, version GI: 159162308). Xcorr scores and mass deviations were used as significance cut-offs. Since alanine cannot be modified (it is not nucleophilic), the highest scoring peptide with a false alanine modification was used to set the minimum Xcorr score for an adducted peptide. In some cases, if the mass

deviation was great enough, a maximum mass deviation was set to exclude some high-scoring peptides with false alanine modifications. In reactions lacking GSH, mass deviation cut-offs were set to exclude false GSH-BDA adducts from consideration. Once a peptide was identified, its mass was searched in all of the samples. In order for a modification to be considered valid, the peptide must: 1) have been identified by the Proteome Discoverer software using the search criteria and significance cut-offs listed above in at least one sample, 2) be present as a peak in the chromatogram in both trials of the same condition and not in the controls, 3) have been chosen for fragmentation by the mass spectrometer in both trials, and 4) demonstrate at least two *y*- and two *b*-ions that match with the predicted fragmentation of that modified peptide.

RESULTS

Overview. To determine the extent of cytochrome *c* modification by BDA or GSH-BDA, the protein was incubated with 0-500 μM BDA in the presence or absence of 1 mM GSH. This allowed concentration-dependent changes in the extent and location of modifications to be detected, as well as determining the effect of GSH on the reactivity of BDA. Two different, complementary techniques were used to detect protein modification. MALDI-TOF was employed to measure overall extent of modification. This technique can be used to establish the number of modifications per protein along with the mass of each modification. The locations of the modifications were determined through high resolution LC-MS/MS analysis of tryptic digests.

Four different protein adduct structures were proposed for the BDA-only derived adducts detected in this experiment (Scheme 5-2). One possible protein adduct is the

addition of BDA to lysine residues to form a pyrrolin-2-one adduct, **1**.[10] This adduct will cause a mass shift to the protein or peptide of +66.01056 Da. A second possible structure is a cysteine-BDA-lysine pyrrole cross-link, **3**, which will increase the protein's weight by +48.00000 Da. Cytochrome *c* contains only two cysteine residues, so alkylation of cysteine is expected to play a minor role in overall adduct formation in this protein. Lysine-BDA-lysine pyrrole cross-links would also shift the protein's mass by 48 Da; however, this type of adduct is not expected because the side-chain nitrogen of lysine preferentially reacts through 1,2-direct addition.[10] Another possible adduct with this same mass is a double-Schiff base cross-link between two lysine residues (**4**). The double-Schiff base structure is likely reversible.[127] Finally, a fourth structure was considered in which BDA reacts with lysine to form a 4-ketoamide adduct (**5**), similar to what has been reported for 4-oxononenal.[128] This adduct would shift a protein or peptide mass by +84.02113 Da. When GSH is present in the reaction mixture the major product is expected to shift the mass by 355.08380 Da by analogy to the GSH-BDA-lysine metabolites seen in rat hepatocytes (**2**).[9]

MALDI-TOF analysis. MALDI-TOF analysis of the reaction mixtures indicated that reaction of cytochrome *c* with BDA increased the mass of the protein by 66 Da (Figure 5-1); this increase is consistent with the formation of pyrrolinone adducts **1** (Scheme 5-2). The number modifications per protein increased with higher BDA concentration, the majority of which appeared to be the addition of 66 Da; however, it is also possible that there was an increase in mass by 48 or 84 as well, since there were small peaks on either side of the plus 66 signal (Figure 5-1). At the highest BDA

concentration, there is no appreciable amount of unreacted protein left and as many as four modifications per protein are clearly seen. Based on the disappearance of this signal, the reaction with BDA was quite extensive.

The addition of GSH to the reaction mixtures reduced the overall extent of adduct formation and shifted the mass of the adducted protein by 355 Da (Figure 5-1). This increase in mass is consistent with the formation of GSH-BDA-lysine pyrrole cross-links (**2**). At the highest concentration of BDA, both GSH-BDA and BDA adducts were detected. The amount of GSH-BDA adducts was significantly greater than the BDA protein adducts.

LC-MS/MS Analysis of Tryptic Digests. The locations of the adducting fragments were determined by analyzing tryptic digests of the reaction mixtures by LC-MS/MS analysis on a LTQ-Orbitrap Velos mass spectrometer. Proteome Discoverer software was employed to determine the location of the various protein modifications caused by BDA treatment in the presence or absence of GSH. The BDA-modified peptides are displayed in Table 5-1 and the GSH-BDA-modified peptides are displayed in Table 5-2. Representative collision-induced dissociation (CID) spectra of a modified peptide are shown in Figure 5-2.

In the BDA-cytochrome *c* reaction mixtures, the most common peptide modification was a +66 Da increase at lysine residues occurring at K7, K8, K27, K39, K53, K55, K72, K73, or K86 at all BDA concentrations (Table 5-1); this mass shift occurred most likely because of pyrrolinone adduct formation. As the concentration of BDA increased, this modification was also detected at K60, K79, K87, and K99.

Alkylation of K88 was only observed at the lowest BDA concentration. Its absence at higher concentrations may be a result of interfering signals that prevent detection of this peptide. The +84 modification occurred at K39 and K53; this adduct was presumed to be the 4-ketoamide adduct **5**. Peptides containing two adducts were observed at the higher BDA concentrations. Mass shifts of +66 Da occurred in groups of two at positions K7 and K8, K39 and K53, and K86 and K87. At the highest BDA concentration, the peptide MIFAGIKKK had two molecules of BDA associated with it. The lysine at position K86 increased by +66 Da and the second was a presumed double-Schiff base cross-link (**4**, +48 modification) between K87 and K88. Sigolo, et al. suggest in their report regarding the reaction of cytochrome *c* with a related α,β-unsaturated aldehyde that when several lysines are found in sequence, such as the three consecutive lysines in MIFAGIKK(K), the high density of positive charge leads to deprotonation of the side chains, favoring Schiff base formation with electrophiles.[129] Overall, these data confirm the MALDI-TOF data that indicate that pyrrolinone adducts are the major product formed when BDA reacts with cytochrome *c*.

When GSH was included in the reaction, peptides containing K39, K79, K86, or K88 increased by +355 Da at all BDA concentrations; K8, K53, K72, and K73 were similarly modified at the highest BDA concentration (Table 5-2). These mass shifts are consistent with the formation of GSH-BDA-lysine crosslinks at these sites. GSH did not completely block the ability of BDA to directly alkylate cytochrome *c*. Peptides containing K39, K53, K55, K72, K73 or K86 were increased by +66 Da at all BDA concentrations. Peptides with K7, K8, K27, K87, K88 or K99 with +66 Da were also

detected at the highest BDA concentration. Double +66 Da modifications were observed in groups of two at positions K7 and K8 and K86 and K87 at the highest BDA concentration. A BDA-induced mass shift of +84 Da consistent with the formation of the 4-ketoamide **5** was detected at positions K39 and K53 in these reactions. The presumed double-Schiff base cross-link **4** between K87 and K88 was not detected in the presence of GSH.

DISCUSSION

The results show that both BDA and GSH-BDA may act as electrophiles, modifying cytochrome *c* in vitro. Both primarily targeted protein lysine residues with BDA reacting to form predominantly **1** and BDA-GSH undergoing Paal-Knorr condensation with lysine residues to form **2**. BDA is more reactive than GSH-BDA generating more adducts than GSH-BDA (Figure 5-1). In addition, BDA reacted with cytochrome *c* with less selectivity: fewer sites were modified by GSH-BDA than by BDA alone (Tables 5-1 and 5-2).

More protein is left unreacted in the presence of GSH-BDA in part because this electrophile can be diverted down a different pathway by reaction with the glutamyl α-amino group of the same or different glutathione molecule to form an intra- or intermolecular GSH-BDA-GSH cross-link.[6,10] Evidence of this is seen in biological assays: the protein-reactive metabolite of furan is efficiently trapped by GSH in microsomal incubations.[60] However, protein modification still occurs by GSH-BDA, both in our model system and in vivo[9] because the ε-amino group of lysine is more nucleophilic than the glutamyl α-amino group.[110]

A number of compounds demonstrate similar chemical properties to BDA. 4-Oxo-2-nonenal (ONE) is an α,β-unsaturated ketone while 4-hydroxy-2-nonenal (HNE) and *trans,trans*-2,4-decadienal (DDE) are both α,β-unsaturated aldehydes. 1,4-Benzoquinone is the archetypical quinone containing an α,β-unsaturated dicarbonyl. Finally, two model vinyl halides, vinylidene chloride (VDC) and 1,1-dichloroethylene (DCE), are metabolized to form electrophilic intermediates including aldehydes. ONE, HNE, and DDE are all endogenous electrophiles resulting from lipid peroxidation.[33] The reaction of these compounds with GSH and/or proteins has been investigated previously and may be compared to BDA.

ONE has been shown to cross-link GSH and cytochrome *c* in vitro.[130] When reacting ONE with cytochrome *c* in the absence and presence of GSH followed by analysis using MALDI-TOF a shift from +ONE to +(GSH-ONE) adducts was seen.[130] While GSH reduced the reactivity of BDA, it actually enhanced the reactivity of ONE with model proteins including cytochrome *c*, RNAse A and β-lactoglobulin.[130] The modification of lysine residues is a two-step process. The first is reversible addition of the primary amine to the carbonyl carbon or the β-carbon of the conjugated system, the second is rearrangement to form a stable, detectable adduct. While ONE reacts rapidly with thiols, the irreversible modification of lysine residues is slow.[128] In comparison, the irreversible reaction of BDA with lysine is relatively rapid (see Chapter 4). Therefore, while the aldehydes of both enediones react rapidly with lysine to form reversible Schiff base adducts, the next steps resulting in BDA-pyrrolinone adduct formation occur more

rapidly than those producing the ketoamide reaction product observed with 4-oxononenal.[128]

The location of the cytochrome *c* adducts of ONE and GSH-ONE was not reported.[130] However, this information is available for the aldehydic compounds HNE[127] and DDE.[129] Both compounds reacted with many of the same lysine residues in cytochrome *c* as BDA.[127,129] The exceptions were that HNE but not BDA reacted with K5 and K25 whereas BDA but not HNE alkylated K53.[127] HNE alkylated K86 even at a selective condition when its concentration was dropped relative to the protein.[127] At the more selective condition the K86 position was in the top five most modified lysines.[127] K86 plays a crucial role in the function of cytochrome *c*, discussed in detail below. K86 and K87 were two of the top eight sites modified by DDE and the doubly modified peptide was seen upon both tryptic and chymotryptic digestion.[129] When benzoquinone was used as the electrophile, K86-K87 and K25-K27 were the most predominant sites for formation of a cyclized diquinone adduct and K87 is one of the top five sites for a monoquinone adduct.[131]

Assuming the slight differences in reactivity do not result from differences in ion suppression or other interfering factors affecting detection, this would indicate that the substitution of the α,β-unsaturated carbonyl plays a role in determining adduction sites. This could be through steric mechanisms – BDA is the smallest, while HNE and DDE are both larger – or it could be due to the electronic effects of the subsitutents. The difference may also depend on each residue's susceptibility to modification. Nucleophilicity varies between lysines in a protein [132] and is influenced by the local

hydrophilicity/hydrophobicity, by the sequence context, and by local pH, which can differ from the solution pH in the microenvironment created by protein tertiary structure.

Some cytochrome *c* lysines (K72, K73, and K86) have been implicated in specific structure/function relationships. These three residues form crucial electrostatic interactions with negatively charged phospholipids in the mitochondrial membrane.[129,133] The consistent modification of these sites opens up the possibility of disrupting the function of cytochrome *c* through neutralization of the positive charge of the lysines and loss of the electrostatic interactions. Disruption of the interaction with the mitochondrial membrane could lead to accidental cytochrome *c* release, an event known to trigger apoptosis.[129,134] Another important residue for proper cytochrome *c* structure/function, K27, is thought to be important in the interaction of cytochrome *c* and cytochrome *c* oxidase, and modifications at this location may disrupt the interaction of cardiolipin vesicles.[129,135] This residue shows pyrrolinone modification under many of the conditions tested. K72, K73, and K86 have pyrrolinone modifications under all conditions tested (Table 5-1). When GSH is present, it cross-links with K86 at all concentrations of BDA and K72 & K73 are modified at the highest BDA concentrations. The benzoquinone adducts discussed above caused significant alterations in the structure of cytochrome *c* as determined by CD spectra and in silico modeling.[131]

Two vinyl halides, VDC and DCE, show some metabolic similarities to furan. They are bioactivated to reactive electrophilic intermediates, including aldehydes, which go on to cross-link GSH with proteins.[136,137] Disruption of mitochondria has been implicated as an early event in DCE-mediated cell death.[138] It is possible that the

electrophiles formed through vinyl halide metabolism lead to cytochrome *c* adducts that are similar to the ones discussed so far.

Since GSH-BDA-protein cross-links are more bulky than the BDA-only modifications, altered steric interactions could lead to disruption of protein structure and function. It is established that under some circumstances, the steric bulk of adducts can disrupt proper protein function.[139] Because degraded protein adducts are seen in vivo and are thought to contribute to furan's toxicology, it is important to investigate the protein adducts before degradation. Residues known to play a crucial role in cytochrome *c* electrostatic interactions (K72, K73, and K86) are among the most reactive. Alteration of cytochrome *c* structure and function may play a role in furan's mechanism of action.

Diethylpyrocarbonate reacts with histidine, lysine, and tyrosine residues based on factors including surface accessibility, pK_a, and involvement in hydrogen-bonding.[140] K86 was modified by this chemical despite having the lowest surface accessibility of any lysine in the protein at 11.5 $Å^2$ (as determined from molecular modeling using PDB 1AKK). K86 was one of three residues to show GSH-BDA-protein cross-linking at all BDA concentrations. Since K86 has the lowest surface accessibility of any lysine, and because of the steric bulk of the GSH-BDA electrophile, it is likely that the pK_a and/or the hydrogen bonding environment plays a crucial role in promoting reaction at this site.

While BDA is more reactive than GSH-BDA, there was significant overlap of target sites between these two electrophiles as well as the compounds mentioned above. K8, K39, K55, K72, K73, K79, and K86 were modified by both GSH-BDA and BDA. Of these, all but K8 and K79 reacted with BDA under every condition tested; K8 and

K79 were not alkylated at the lowest BDA concentration. This indicates that these sites are important targets in our system, and are top candidates to be confirmed by isolation from cells and/or tissues. K72, K73, and K86 are especially interesting because they play key roles in cytochrome *c* structure and function. Adaptation of the mass spectrometric techniques used for this model system will allow these protein adducts to be detected in more complex systems. Modification of vital sites on cytochrome *c* offers the potential for playing a crucial role in mediating furan's toxicity.

While GSH protects somewhat against the overall formation of protein adducts, specific protein glutathionylation by BDA may be important in understanding furan-related biological effects. The relative concentration of reactants in vivo is expected to be GSH > protein >> BDA,[130] similar to the lowest BDA concentration (50 μM) used in our study. Under this condition, the primary adducts were GSH-BDA-protein cross-links with insignificant levels of pyrrolinones formed. A proteomics study was recently published in which rats were administered a radiolabeled dose of furan and the modified liver proteins were separated using a 2D gel and detected via mass spectrometery.[8] The targeting of proteins was found to be selective, with distinct spots representing about 4-5% of the proteome.[8] While cytochrome *c* itself was not identified as a target for adduction, other mitochondrial proteins involved in energy production and maintenance of redox state were affected.[8] A recent review of protein glutathionylation also supports a link between this process and cellular energy production.[126] In addition, the proteins that were affected by furan treatment tended to have higher lysine but lower cysteine content than average.[8] This supports the hypothesis that GSH-BDA-protein cross-links

dominate in vivo. Because the concentration of the GSH thiol is much higher than that of protein thiols, the GSH-BDA electrophile is formed and then reacts with lysine sidechains. Understanding this process may be crucial to developing a realistic mechanism of action through which furan exerts its toxic and carcinogenic effects.

Table 5-1. Cytochrome *c* peptides modified with BDA.

Peptide Sequence	Position	Residue	Modification	Theoretical Mass	Avg. Observed Mass	μM BDA	50	100	500	50	100	500
						μM GSH	-	-	-	1000	1000	1000
							Modified peptide detected					
GkkIFVQK	6-13	K7 & K8	+66 x 2	1079.62482	1079.62401		X	X	X			X
kIFVQK	8-13	K8	+66	828.49782	828.49826		X	X	X		X	X
HkTGPNLHGLFGR	26-38	K27	+66	1499.78664	1499.78636		X	X	X			X
kTGQAPGFTYTDANK	39-53	K39	+66	1664.79152	1664.79256		X	X	X	X	X	X
kTGQAPGFTYTDANK	39-53	K39	+84	1682.80210	1682.80263				X		X	
kTGQAPGFTYTDANkNK	39-55	K39 & K53	+66 x 2	1972.93998	1972.94127				X			
TGQAPGFTYTDANkNK	40-55	K53	+66	1778.83446	1778.83547		X	X	X	X	X	X
TGQAPGFTYTDANkNK	40-55	K53	+84	1796.84502	1796.84434		X	X	X			X
KTGQAPGFTYTDANkNK	39-55	K53	+66	1906.92942	1906.93050				X			X
NkGITWK	54-60	K55	+66	912.49380	912.49327		X	X	X	X	X	X
GITWkEETLMEYLENPK	56-72	K60	+66	2147.03661	2147.03841				X			
GITWkEETLMEYLENPKK	56-73	K60	+66	2275.13157	2275.13304				X			
EETLMEYLENPkK	61-73	K72	+66	1689.80408	1689.80476		X	X	X	X	X	X
kYIPGTK	73-79	K73	+66	872.48764	872.48752		X	X	X	X	X	X
YIPGTkMIFAGIK	74-86	K79	+66	1504.82330	1504.82463				X	X	◦	X
MIFAGIkK	80-87	K86	+66	973.55398	973.55339		X	X	X	X	X	X
MIFAGIkkK	80-88	K86 & K87	+66 x 2	1167.65952	1167.65923				X			X
MIFAGIkkK	80-88	K86 & K87	+66; +48	1149.64896	1149.64914				X			
kTEREDLIAYLK	88-99	K88	+66	1544.83194	1544.83175		X					X
EDLIAYLkK	92-100	K99	+66	1158.64054	1158.64148			X	X			X

Table 5-2. Cytochrome *c* peptides modified with GSH-BDA.

Peptide Sequence	Position	Residue	Theoretical Mass	Avg. Observed Mass	μM BDA / μM GSH	**50** / **1000**	**100** / **1000**	**500** / **1000**
					Modified peptide detected			
kIFVQK	8-13	K8	1117.57107	1117.57176				X
kTGQAPGFTYTDANK	39-53	K39	1953.86475	1953.86472		X	X	X
TGQAPGFTYTDANkNK	40-55	K53	2067.90768	2067.90698				X
EETLMEYLENPkK	61-73	K72	1978.87732	1978.87953				X
kYIPGTK	73-79	K73	1161.56088	1161.56154				X
YIPGTkMIFAGIK	74-86	K79	1793.89654	1793.89779		X	X	X
MIFAGIkK	80-87	K86	1262.62722	1262.62728		X	X	X
kTEREDLIAYLK	88-99	K88	1833.90516	1833.90630		X	X	X

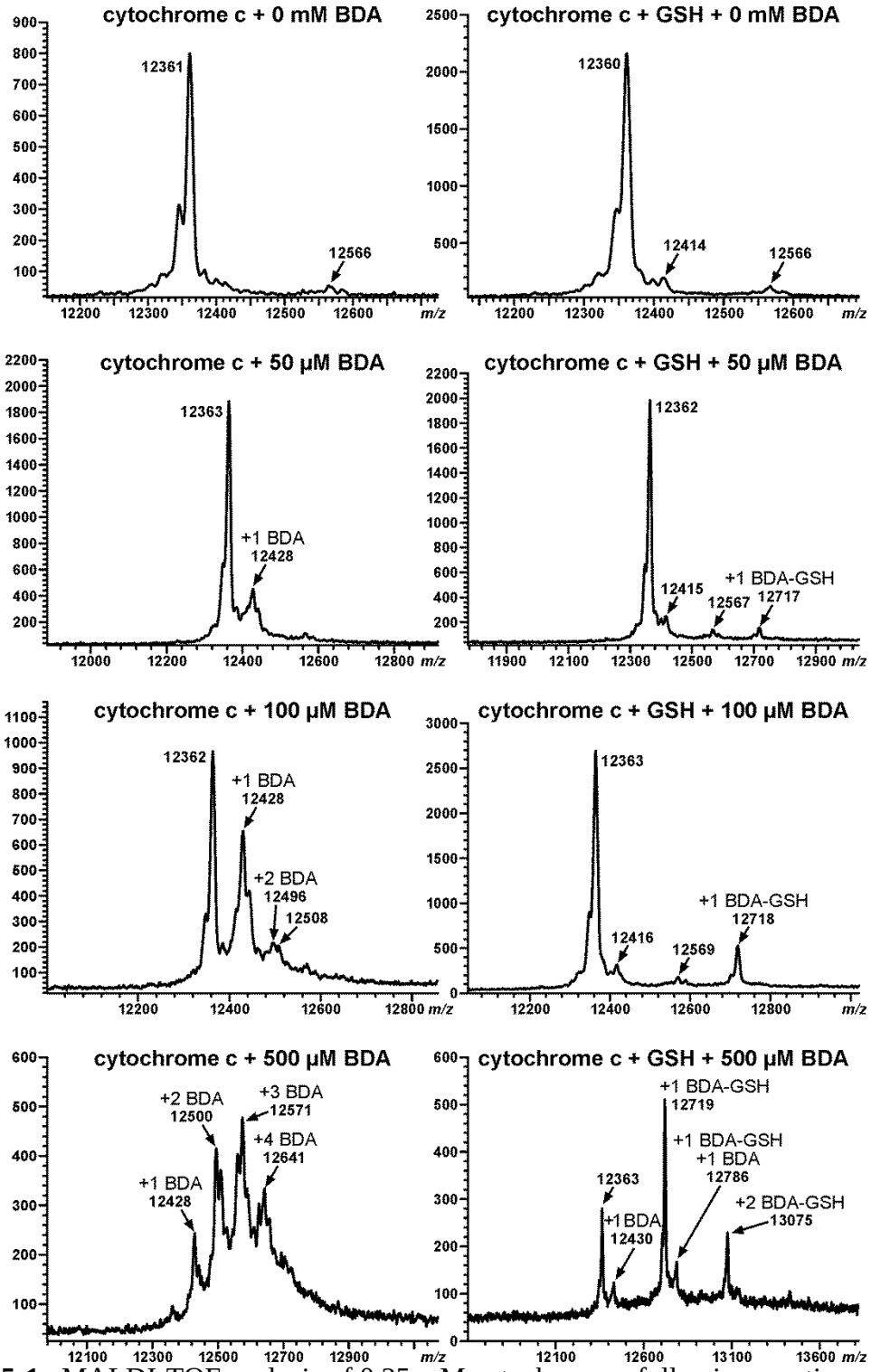

Figure 5-1. MALDI-TOF analysis of 0.25 mM cytochrome *c* following reaction with 0-0.5 mM BDA in the presence or absence of 1 mM GSH.

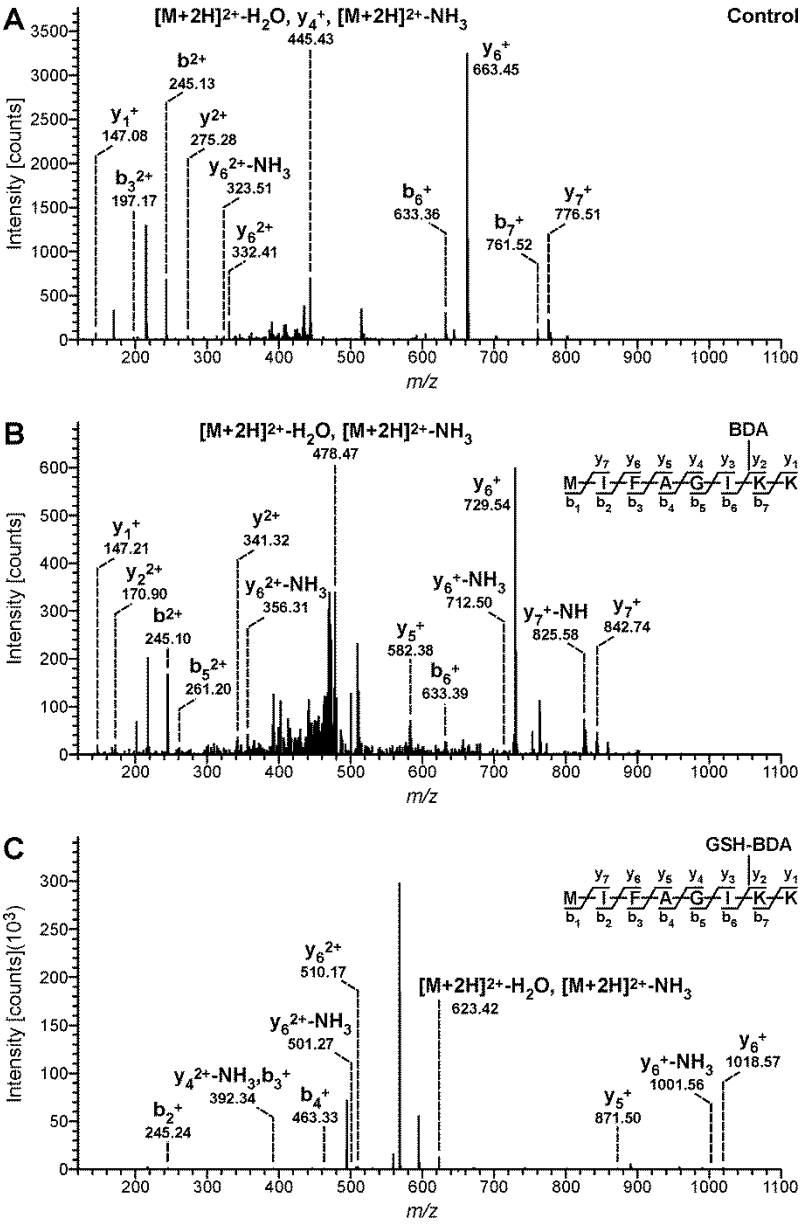

Figure 5-2. Example MS/MS spectra generated by Proteome Discoverer for the MIFAGIKK peptide from 0.25 mM cytochrome c reated with 0.1 mM BDA in the presence or absence of 1 mM GSH. A: Peptide from control reaction; B: Peptide from the reaction with cytochrome c and BDA; C: Peptide from reaction with cytochrome c, BDA and GSH.

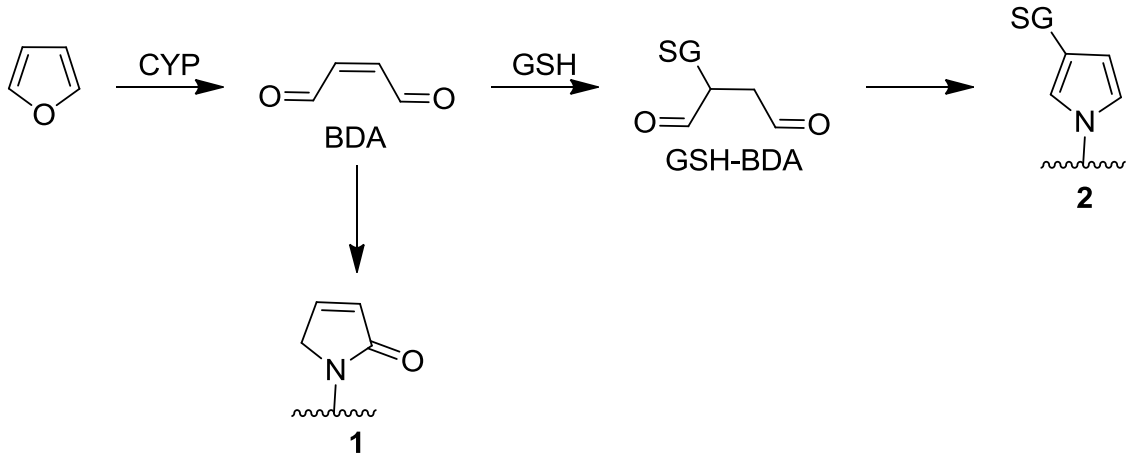

Scheme 5-1. Proposed pathways of protein adduct formation as a result of furan metabolism.

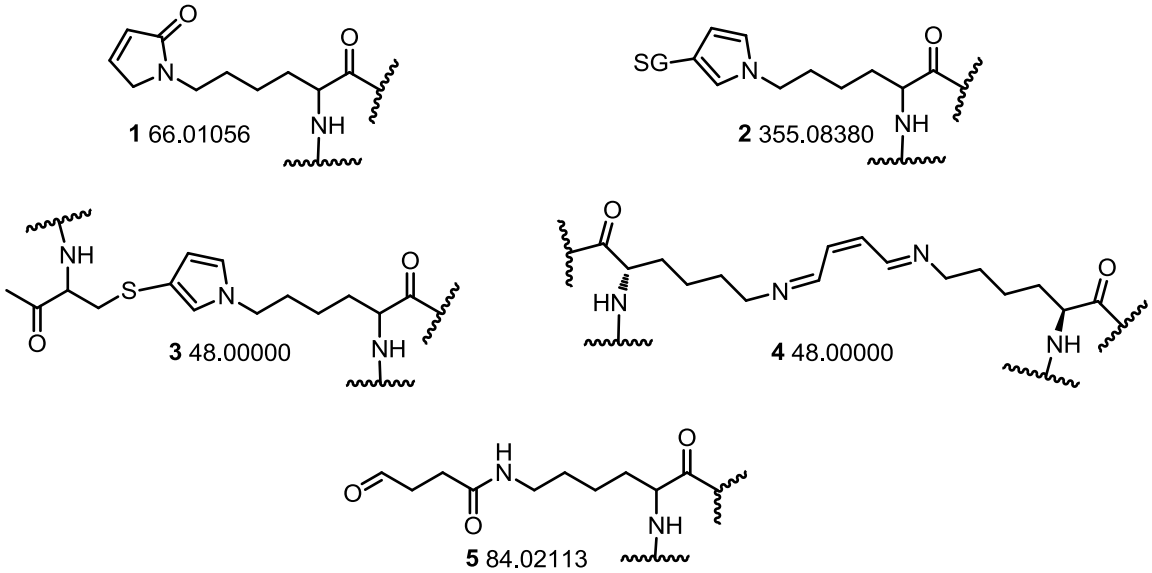

Scheme 5-2. Hypothesized structures of protein modifications and the monoisotopic mass shift corresponding to each.

Chapter 6: Discussion

Overview

The discipline of chemistry has developed powerful tools to allow for investigation of invisible events on the molecular level that have consequences on the macroscopic level. The common thread that connects the studies described in this dissertation is the application of these tools to understanding why furan exposure leads to toxicity and carcinogenicity. It is expected that the chemistry of furan's transformations in model biological systems can be applied to human biology as well, which may be used in hazard identification and risk assessment studies.

Protein adducts are formed as a result of furan exposure.[7-9] These adducts are formed because furan is oxidized in the liver by P450s to *cis*-2-butene-1,4-dial (BDA), an electrophile that can modify the nucleophilic sites of proteins.[9] The structure of these adducts is a natural result of the chemical properties of BDA. These adducts have been confirmed in rats in vivo through radiolabeling studies.[8] Degraded protein adducts have been detected in rat hepatocytes, bile, and urine.[9,27,28] These protein adducts are expected to play a central role in the toxicology of furan.

Polyamine adducts are also formed as a result of furan exposure.[110] Polyamines are known to be crucial to cell cycle control, proliferation, apoptosis, and other vital cell functions.[88] One leading theory of the mechanism of furan carcinogenesis is liver toxicity followed by compensatory cell proliferation.[8,42] This proliferation can lead to tumor formation through several mechanisms including converting DNA adducts into permanent mutations during DNA replication and encouraging proliferation of

precancerous or cancerous cells.[42] The exact role of polyamines in this process is unknown. Polyamine adducts secondary to xenobiotic exposure is an area that has received little attention in the literature. Because of the central role that polyamines play in cell regulation, the formation of polyamine adducts should be considered a primary candidate for understanding the toxicology of furan.

Most of furan's metabolites characterized to date contain either a glutathione (GSH) or an *N*-acetyl-L-cysteine (NAC) moiety.[9,26-28,110] Studies in our lab had indicated that GSH-BDA-amine cross-links were the predominant reaction products when the reaction mixture contained GSH before the addition of BDA.[110] Kinetics studies with GSH and N^{α}-acetyl-L-lysine showed that this observation was not due to kinetic effects, as BDA reacts with both nucleophiles in isolation at virtually identical rates (Chapter 4). Because of the frequency of GSH or GSH-derived moieties in the metabolites of furan, the GSH-BDA intermediates found in the kinetics study are important to consider when investigating the relationship between chemical properties and the ultimate structure of the eliminated compounds. Initial reaction of GSH with BDA was reasonably fast, with BDA being undetectable after ~15 min (Chapter 4). The second reaction with a primary amine to form stable pyrrole cross-links required 30-60 min for completion, depending on the relative concentrations of BDA and GSH as well as absolute concentration of the reactants (Chapter 4). This means that both BDA and GSH-BDA may have half-lives that are long enough for these electrophiles to migrate to sites distant from their formation.

Because furan is known to modify proteins, cytochrome *c* was used as a model protein in a mass spectrometry-based adduction study. The overall level of adduction was seen to be concentration dependent; however, GSH reduced the extent of reaction compared to BDA alone (Chapter 5). The target lysines were comparable to other electrophiles including the α,β-unsaturated carbonyl compounds generated by lipid peroxidation.[33] Some of the most reactive lysine residues also play a central role in the structure and function of cytochrome *c*, which is involved in the electron transfer chain and apoptosis.[133] Protein adducts resulting from furan exposure, possibly including cytochrome *c* adducts, are likely involved in the mechanisms of toxicity and/or carcinogenicity.

Future Studies – Metabolites of Furan

Many metabolites of furan have been identified in rat hepatocytes, bile, and urine.[9,26-28,110] However, it is known that within the first 24 hours 26% of a radioactive dose of furan is exhaled as carbon dioxide and 22% is eliminated in the feces.[7] A pathway between furan and CO_2 has been proposed but not been verified. Similarly, bile metabolites are not the same as fecal metabolites, and it is unknown if further processing occurs in the gut that may be toxicologically relevant. This is less likely because the colon is not a target tissue for furan toxicity, however it cannot be ruled out without more study.

It is likely that furan metabolites feed into the TCA cycle in order to generate CO_2. BDA could undergo two additional oxidations to give maleic acid. It could then isomerize to the *trans* form to give fumaric acid, a component of the TCA cycle and

eventually be transformed into CO_2. Radiolabel studies using ^{14}C[furan] could be used to identify metabolites along this pathway if it occurs in biological systems. The main technical difficulty would lie in separating the radiolabeled maleic, furmaric, and other acids from cell culture or from isolated tissue. A radioflow assay might have the sensitivity necessary to detect these metabolites since the endogenous counterparts would not generate a signal. ^{3}H[furan] has a much higher specific activity and would be easier to detect, but these protons would be subject to exchange and are certainly stripped from the carbon atoms by the time CO_2 is formed.

Another topic related to furan metabolites of perhaps even greater importance is their formation in different species of interest. The metabolites identified so far have been isolated from rat cell culture or from tissues of treated rats. It is known that furan is toxic and carcinogenic in mice as well, although there are important species differences.[2] Furthermore, it is humans that we are really interested in from a hazard identification and risk assessment perspective. Metabolites may be formed or not formed in different species, or even formed to different extents or in varying proportions. Investigating these inter-species differences in furan metabolism will aid us in generating a comprehensive picture of the pathway furan molecules take after entering the body. By comparing human metabolism to rat and mouse metabolism, parallels may be drawn between these rodent species that have served as the models in the toxicological studies to date, and humans, for which there is no strong toxicological data.

Comparative metabolism studies are possible using easily available cryopreserved hepatocytes. These are primary cells derived from a variety of organisms, including

humans, which have been collected and frozen for later use. The activity of enzymes of interest like CYP2E1 can be assayed after thawing to confirm that these bioactivation pathways are still active in the cell line. Western blotting can be used to complement activity information with protein levels. Gathering this information also allows for correlation of other experimental outcomes (i.e. extent of metabolite formation) with enzymes of interest. The major disadvantage of using cryopreserved hepatocytes is that they are not perfect substitutes for the in vivo environment, being only one cell type from a single tissue. Balanced against this are issues of cost, availability, and ethics (reducing animal usage and prohibitions on administering toxicants to human subjects). Since the liver is the target organ for both toxicity and carcinogenicity,[2] hepatocytes are a useful experimental model that can provide valuable insight into furan's toxicology.

The biological effects of furan's metabolites can be determined directly by synthesizing them and adding them to cell models like hepatocyte suspension culture. One obstacle is that the GSH-BDA-amine cross-links are hydrophilic. One way to overcome this obstacle is to synthesize a pro-metabolite (in analogy to a pro-drug) by using glutathione monoethyl ester instead of GSH. This molecule can cross cell membranes where the ethyl ester is cleaved by a non-specific cytosolic esterase to release GSH.[141] The ethyl ester analogue of the cross-link metabolites could be delivered into the cell and released, giving only ethanol as a by-product. The effects of metabolites can then be systematically tested one at a time to ascertain their impact on cellular proliferation, apoptosis, necrosis, and oncogenic transformation.

Future Studies – Polyamines

It is still undetermined what role polyamine adducts play in furan's mechanism of action. There are at least four ways that modification of polyamines might lead to the observed effects on the liver: by depleting polyamine pools with or without compensatory changes in polyamine levels; by interfering with the role polyamines play in stabilizing nucleic acids (both DNA and RNA); by modifying the ability of adducted polyamines to bind into enzyme active sites; or by leading to changes in expression of polyamine pathway enzymes, some of which are known oncoproteins.

Assays designed to quantitate polyamines in biological systems are available.[142-144] Most have some significant drawbacks. Because of the polycationic nature of the polyamines, they cannot be purified by reverse-phase liquid chromatography, which is standard for methods coupled to mass spectrometers. Aliphatic amines have essentially no UV absorbance, making spectrophotometric assays difficult to develop. As a result, many methods utilize complicated procedures to first derivatize the polyamines to make them more hydrophobic and sometimes to add a chromophore to simplify detection.[142-144] Quantifying the levels of polyamines before furan exposure and at several time points afterward would allow its effect on polyamine pool homeostasis to be determined. Polyamine levels would be expected to drop and stay low, or they might rebound as compensatory mechanisms are activated. Concentration of polyamine adducts could be assayed using extremely sensitive electrochemical detection due to the presence of a pyrrole moiety in the adducts but not in the unreacted polyamines.

Nucleic acids of all varieties are characterized by their negatively charged phosphate backbone. Polyamines form electrostatic associations with these backbones, which is believed to stabilize their conformations.[88] Adopting the correct conformation is crucial for nucleic acids to fulfill their cellular functions. Reaction of polyamines with furan-derived electrophiles like GSH-BDA neutralizes some of this positive charge, which may have a detrimental effect on nucleic acid stability. One way this could manifest is in decreased half lives of RNA molecules. This could be assayed using northern blotting, however since many factors can affect the half life of a particular transcript it would be necessary to take a global view to determine transcriptome-wide effects. As such, RNA microarrays might be better suited for this type of experiment, which are expensive and may be difficult to reproduce.

Altered enzyme binding caused by polyamine adduction would be much easier to determine. There are several important enzymes known to bind polyamines: spermidine synthase, spermine synthase, spermidine/spermine N^1-acetyltransferase, spermine oxidase, N^1-acetylpolyamine oxidase, and a handful of polyamine transporters.[88] Known polyamine metabolites of furan, such as the GSH-BDA-spermidine cross-link, could be synthesized and their binding to the various enzymes in the pathway could be investigated using methods like inhibition studies. This would provide insight into the effects of the adducts on the polyamine synthetic pathway and would complement other studies on the disruption of polyamine pools by furan. Once candidates have been identified, adduct binding could be confirmed using x-ray crystallography. The biological effects of modified polyamines should not be underestimated: some modified

polyamines have demonstrated nanomolar activity as medicinal agents and these are being pursued by drug researchers as a potentially novel scaffold for anti-cancer pharmaceuticals.[92]

Ornithine decarboxylase (OCD) is one of the most tightly regulated enzymes in the cell.[88] It is also the gateway enzyme to polyamine biosynthesis.[88] The polyamines can interconvert between each other thanks to a specialized enzyme network, but the decarboxylation of ornithine is rate-limiting and irreversible.[88] The expression of OCD is influenced by well known proto-oncogenes/proteins like *c*-myc.[145] Disruption of polyamine pools by reaction with furan-derived electrophiles may lead to compensatory changes in polyamine pathway enzyme expression, which may in turn lead to carcinogenic transformation. This could be determined using western and northern blot techniques coupled to enzyme activity assays. OCD and *c*-myc would be top candidates to test because of their previously studied role in oncogenesis.

Future Studies – Pathway Kinetics

We have described studies performed in vitro where reactions between BDA and model nucleophiles (GSH and NAL) were monitored by NMR, HPLC, and LC-MS (Chapter 4). One possible next step would be to monitor these kinetics in the cellular environment. The advent of cryoprobes has made it possible to detect extremely low concentrations of molecules by NMR. Using magic angle spinning NMR equipped with a carbon-enhanced cryoprobe, it might be possible to follow the fate of ^{13}C[furan] in a hepatocyte cell culture in real time. This would not only confirm the formation of intermediates previously only hypothesized based on the structures of end products, but

would also be a breakthrough in studying xenobiotic metabolism in situ. One of the conditions we tested showed that it was feasible to track the kinetics of 0.1 mM BDA in the presence of 5 mM GSH, which are comparable concentrations to those in our hepatocyte incubation studies (Chapter 4). The major hurdle to this approach is the expense of synthesizing ^{13}C[furan] and the lower sensitivity of this isotope compared to ^{1}H, even with a carbon-enhanced cryoprobe. ^{1}H-^{13}C coupling studies might be a practical alternative if ^{13}C-detection cannot provide the necessary sensitivity.

Future Studies – Protein Adduction

A natural next step for the cytochrome *c* study described in this dissertation would be to perform an immunoprecipitation of this protein from hepatocytes or liver tissue after furan treatment and use mass spectrometry to determine if these adducts are seen in a complete biological system. Even if cytochrome *c* adducts are not seen, a recent proteomics study identified a number of proteins that were modified by radiolabeled furan.[8] These proteins could be subjected to the same protocol of immunoprecipitation, digestion, and LC-MS/MS or MALDI-TOF to determine the structure and location of the adducts. The functions of the target proteins could then be re-examined in light of current knowledge of furan's toxicology.

Conclusions

Furan's toxicology is distinct from many structurally similar analogues. This difference is almost certainly due to the unique chemical properties of furan and its downstream metabolites. Our hypothesis was that the chemical properties of furan and its intermediates would define its cellular targets and help in the formulation of a

mechanism of toxicity. We have demonstrated that the primary amino groups of a) glutathione, b) amino acids, c) polyamines, and d) proteins are all targets for modification by BDA.

Initial reaction with GSH does not eliminate the reactive characteristics of BDA, but extends the lifetime of a different set of reactive intermediates grouped under the heading of "GSH-BDA." The results of the kinetics study in Chapter 4 indicate that BDA, by forming the BDA cyclic hydrate or by reacting once with GSH, may exist long enough without reacting to cause damage at sites distant from where furan is oxidized in the active site of CYP2E1. Reaction with amino acids and polyamine pools has the potential to disrupt cellular homeostasis and apoptosis signaling as discussed in Chapter 3. Modification of proteins could lead to alteration in structure and/or function. Both BDA and GSH-BDA can form adducts with cytochrome *c*, with certain crucial residues serving as particularly common targets. Because cytochrome *c* plays essential roles in cellular respiration and apoptosis as discussed in Chapter 5, this could be a potential mechanism of action. In this way, the greater understanding of the chemical properties of furan and its metabolic intermediates has allowed us to refine our hypotheses concerning its mechanism of action. Future work should focus on the consequences of the reactions of BDA, the disruption of cellular homeostasis, and the modification of protein structure and function.

Bibliography

(1) National Toxicology Program *Toxicology and carcinogenesis studies of furan in F344/N rats and B6C3F$_1$ mice* (1993) US Department of Health and Human Services, Public Health Service, National Institutes of Health, Research Triangle Park, NC.

(2) International Agency for Research on Cancer (1995) Furan. In *Dry Cleaning, Some Chlorinated Solvents and Other Industrial Chemicals* p 393, IARC, Lyon, France.

(3) National Toxicology Program *8th Report on Carcinogens* (1998) US Department of Health and Human Services, Washington DC.

(4) Carfagna, M. A., Held, S. D., and Kedderis, G. L. (1993) Furan-induced cytolethality in isolated rat hepatocytes: Correspondence with *in vivo* dosimetry. *Toxicol. Appl. Pharmacol. 123*, 265-273.

(5) Gates, L., Lu, D., and Peterson, L. A. (2012) Trapping of cis-2-butene-1,4-dial to Measure Furan Metabolism in Human Liver Microsomes by Cytochrome P450 Enzymes. *Drug Metab Dispos. 40*, 596-601.

(6) Peterson, L. A., Cummings, M. E., Vu, C. C., and Matter, B. A. (2005) Glutathione trapping to measure microsomal oxidation of furan to *cis*-2-butene-1,4-dial. *Drug Metab Dispos. 33*, 1453-1458.

(7) Burka, L. T., Washburn, K. D., and Irwin, R. D. (1991) Disposition of [^{14}C]furan in the male F344 rat. *J. Toxicol. Environ. Health 34*, 245-257.

(8) Moro, S., Chipman, J. K., Antczak, P., Turan, N., Dekant, W., Falciani, F., and Mally, A. (2012) Identification and pathway mapping of furan target proteins reveal mitochondrial energy production and redox regulation as critical targets of furan toxicity. *Toxicol. Sci. 126*, 336-352.

(9) Lu, D., Sullivan, M. M., Phillips, M. B., and Peterson, L. A. (2009) Degraded protein adducts of *cis*-2-butene-1,4-dial are urinary and hepatocyte metabolites of furan. *Chem. Res. Toxicol. 22*, 997-1007.

(10) Chen, L. J., Hecht, S. S., and Peterson, L. A. (1997) Characterization of amino acid and glutathione adducts of *cis*-2-butene-1,4-dial, a reactive metabolite of furan. *Chem. Res. Toxicol. 10*, 866-874.

(11) Kumar, S., Kokate, R. A., Sahu, M., Chaudhary, P., Sharma, R., Awasthi, S., and Awasthi, Y. C. (2011) Inhibition of mercapturic acid pathway-mediated

disposal of 4-hydroxynonenal causes complete and sustained remission of human cancer xenografts in nude mice. *Indian J. Exp. Biol. 49*, 817-825.

(12) Mally, A., Graff, C., Schmal, O., Moro, S., Hamberger, C., Schauer, U. M., Bruck, J., Ozden, S., Sieber, M., Steger, U., Schrenk, D., Hard, G. C., Chipman, J. K., and Dekant, W. (2010) Functional and proliferative effects of repeated low-dose oral administration of furan in rat liver. *Mol. Nutr. Food Res. 54*, 1556-1567.

(13) National Toxicology Program *NTP Research Concept: Furan* (2008) US Department of Health and Human Services, Washington DC.

(14) Moser, G. J., Foley, J., Burnett, M., Goldsworthy, T. L., and Maronpot, R. (2009) Furan-induced dose-response relationships for liver cytotoxicity, cell proliferation, and tumorigenicity (furan-induced liver tumorigenicity). *Exp. Toxicol. Pathol. 61*, 101-111.

(15) Vranová, J., and Ciesarová, Z. (2009) Furan in food - a review. *Czech J. Food Sci. 27*, 1-10.

(16) Perez, L. C., and Yaylayan, V. A. (2004) Origin and mechanistic pathways of formation of the parent furan--a food toxicant. *J. Agric. Food Chem 52*, 6830-6836.

(17) Morehouse, K. M., Nyman, P. J., McNeal, T. P., Dinovi, M. J., and Perfetti, G. A. (2008) Survey of furan in heat processed foods by headspace gas chromatography/mass spectrometry and estimated adult exposure. *Food Addit. Contam Part A Chem Anal. Control Expo. Risk Assess. 25*, 259-264.

(18) Goldmann, T., Perisset, A., Scanlan, F., and Stadler, R. H. (2005) Rapid determination of furan in heated foodstuffs by isotope dilution solid phase micro-extraction-gas chromatography--mass spectrometry (SPME-GC-MS). *Analyst 130*, 878-883.

(19) European Food Safety Authority. (2009) Technical report of EFSA prepared by Data Collection and Exposure Unit (DATEX) on "Monitoring of furan levels in food.". *The EFSA Scientific Report 304*, 1-23.

(20) National Toxicology Program *12th Report on Carcinogens* (2011) US Department of Health and Human Services, Washington DC.

(21) Hasnip, S., Crews, C., and Castle, L. (2006) Some factors affecting the formation of furan in heated foods. *Food Addit. Contam 23*, 219-227.

(22) Eschner, M. S., Selmani, I., Groger, T. M., and Zimmermann, R. (2011) Online comprehensive two-dimensional characterization of puff-by-puff resolved cigarette smoke by hyphenation of fast gas chromatography to single-photon ionization time-of-flight mass spectrometry: quantification of hazardous volatile organic compounds. *Anal. Chem 83*, 6619-6627.

(23) Chen, L. J., Hecht, S. S., and Peterson, L. A. (1995) Identification of *cis*-2-butene-1,4-dial as a microsomal metabolite of furan. *Chem. Res. Toxicol. 8*, 903-906.

(24) Kedderis, G. L., Carfagna, M. A., Held, S. D., Batra, R., Murphy, J. E., and Gargas, M. L. (1993) Kinetic analysis of furan biotransformation by F-344 rats *in vivo* and *in vitro*. *Toxicol. Appl. Pharmacol. 123*, 274-282.

(25) Franklin, M. R., and Hathaway, L. B. (2008) 2-Diethylaminoethyl-2,2-diphenylvalerate-HCl (SKF525A) revisited: comparative cytochrome P450 inhibition in human liver microsomes by SKF525A, its metabolites, and SKF-acid and SKF-alcohol. *Drug Metab Dispos. 36*, 2539-2546.

(26) Kellert, M., Wagner, S., Lutz, U., and Lutz, W. K. (2008) Biomarkers of furan exposure by metabolic profiling of rat urine with liquid chromatography-tandem mass spectrometry and principal component analysis. *Chem Res. Toxicol. 21*, 761-768.

(27) Hamberger, C., Kellert, M., Schauer, U. M., Dekant, W., and Mally, A. (2010) Hepatobiliary toxicity of furan: identification of furan metabolites in bile of male f344/n rats. *Drug Metab Dispos. 38*, 1698-1706.

(28) Lu, D., and Peterson, L. A. (2010) Identification of furan metabolites derived from cysteine-*cis*-2-butene-1,4-dial-lysine cross-links. *Chem. Res. Toxicol. 23*, 142-151.

(29) Peterson, L. A., Cummings, M. E., Chan, J. Y., Vu, C. C., and Matter, B. A. (2006) Identification of a *cis*-2-butene-1,4-dial-derived glutathione conjugate in the urine of furan-treated rats. *Chem Res. Toxicol. 19*, 1138-1141.

(30) Hochreuther, S., and van Eldik, R. (2012) Reactivity of a Cytostatic Active N,N-Donor-Containing Dinuclear Pt(II) Complex with Biological Relevant Nucleophiles. *Inorg. Chem 51*, 3025-3038.

(31) Reed, D. J. (1990) Glutathione: toxicological implications. *Annu. Rev. Pharmacol. Toxicol. 30*, 603-631.

(32) Bohme, A., Thaens, D., Schramm, F., Paschke, A., and Schuurmann, G. (2010) Thiol Reactivity and Its Impact on the Ciliate Toxicity of alpha,beta-Unsaturated Aldehydes, Ketones, and Esters. *Chem. Res. Toxicol.*

(33) Zhu, X., Tang, X., Zhang, J., Tochtrop, G. P., Anderson, V. E., and Sayre, L. M. (2010) Mass spectrometric evidence for the existence of distinct modifications of different proteins by 2(E),4(E)-decadienal. *Chem Res. Toxicol. 23*, 467-473.

(34) Bein, K., and Leikauf, G. D. (2011) Acrolein - a pulmonary hazard. *Mol. Nutr. Food Res. 55*, 1342-1360.

(35) Sun, X., Nair, J., Linseisen, J., Owen, R. W., and Bartsch, H. (2012) Lipid peroxidation and DNA adduct formation in lymphocytes of premenopausal women: Role of estrogen metabolites and fatty acid intake. *Int. J. Cancer*.

(36) Vermeire, T. G., Baars, A. J., Bessems, J. G. M., Blaauboer, B. J., Slob, W., and Muller, J. J. A. (2007) Toxicity Testing for Human Health Risk Assessment. In *Risk Assessment of Chemicals: An Introduction* (van Leeuwen, C. J., and Vermeire, T. G., Eds.) pp 227-280, Springer, Dordrecht, The Netherlands.

(37) Mortelmans, K., Haworth, S., Lawlor, T., Speck, W., Tainer, B., and Zeiger, E. (1986) *Salmonella* mutagenicity tests. II. Results from the testing of 270 chemicals. *Environmental Mutagenesis 7 (suppl)*, 1-119.

(38) McGregor, D. B., Brown, A., Cattanach, P., Edwards, I., McBride, D., Riach, C., and Caspary, W. J. (1988) Responses of the L5178Y tk^+/tk^- mouse lymphoma cell forward mutation assay: III. 72 coded chemicals. *Environ. Mol. Mutagen. 12*, 85-154.

(39) Stich, H. F., Rosin, M. P., Wu, C. H., and Powrie, W. D. (1981) Clastogenicity of furans found in food. *Cancer Let. 13*, 89-95.

(40) Foureman, P., Mason, J. M., Valencia, R., and Zimmering, S. (1994) Chemical mutagenesis testing in *Drosophila*. X. Results of 70 coded chemicals tested for the National Toxicology Program. *Environ. Mol. Mutagen. 23*, 208-227.

(41) Ronto, G., Fekete, A., Grof, P., Bilger, C., Buisson, J. P., Tromelin, A., and Demerseman, P. (1989) Genotoxicity testing: phage T7 inactivation test of various furan and arenofuran derivatives. *Mutagenesis 4*, 471-475.

(42) Wilson, D. M., Goldsworthy, T. L., Popp, J. A., and Butterworth, B. E. (1992) Evaluation of genotoxicity, pathological lesions, and cell proliferation in livers of rats and mice treated with furan. *Environ. Mol. Mutagen. 19*, 209-222.

(43) Peterson, L. A., Naruko, K. C., and Predecki, D. (2000) A reactive metabolite of furan, *cis*-2-butene-1,4-dial, is mutagenic in the Ames assay. *Chem. Res. Toxicol. 13*, 531-534.

(44) Kellert, M., Brink, A., Richter, I., Schlatter, J., and Lutz, W. K. (2008) Tests for genotoxicity and mutagenicity of furan and its metabolite cis-2-butene-1,4-dial in L5178Y tk+/- mouse lymphoma cells. *Mutat. Res. 657*, 127-132.

(45) Byrns, M. C., Predecki, D. P., and Peterson, L. A. (2002) Characterization of nucleoside adducts of *cis*-2-butene-1,4-dial, a reactive metabolite of furan. *Chem. Res. Toxicol. 15*, 373-379.

(46) Byrns, M. C., Vu, C. C., and Peterson, L. A. (2004) The formation of substituted 1,N^6-etheno-2'-deoxyadenosine and 1,N^2-etheno-2'-deoxyguanosine adducts by *cis*-2-butene-1,4-dial, a reactive metabolite of furan. *Chem. Res. Toxicol. 17*, 1607-1613.

(47) Byrns, M. C., Vu, C. C., Neidigh, J. W., Abad, J. L., Jones, R. A., and Peterson, L. A. (2006) Detection of DNA adducts derived from the reactive metabolite of furan, *cis*-2-butene-1,4-dial. *Chem. Res. Toxicol. 19*, 414-420.

(48) Terrell, A. N. (2012) The mutagenic potential of furan and its metabolite *cis*-2-butene-1,4-dial. University of Minnesota,

(49) McDaniel, L. P., Ding, W., Dobrovolsky, V. N., Shaddock, J. G., Jr., Mittelstaedt, R. A., Doerge, D. R., and Heflich, R. H. (2012) Genotoxicity of furan in Big Blue rats. *Mutat. Res. 742*, 72-78.

(50) Qiu, Y., Benet, L. Z., and Burlingame, A. L. (1998) Identification of the hepatic protein targets of reactive metabolites of acetaminophen in vivo in mice using two-dimensional gel electrophoresis and mass spectrometry. *J Biol Chem 273*, 17940-17953.

(51) Manyike, P. T., Kharasch, E. D., Kalhorn, T. F., and Slattery, J. T. (2000) Contribution of CYP2E1 and CYP3A to acetaminophen reactive metabolite formation. *Clin. Pharmacol. Ther. 67*, 275-282.

(52) Hickling, K. C., Hitchcock, J. M., Oreffo, V., Mally, A., Hammond, T. G., Evans, J. G., and Chipman, J. K. (2010) Evidence of oxidative stress and associated DNA damage, increased proliferative drive, and altered gene expression in rat liver produced by the cholangiocarcinogenic agent furan. *Toxicol. Pathol. 38*, 230-243.

(53) Ding, W., Petibone, D. M., Latendresse, J. R., Pearce, M. G., Muskhelishvili, L., White, G. A., Chang, C. W., Mittelstaedt, R. A., Shaddock, J. G., McDaniel, L. P., Doerge, D. R., Morris, S. M., Bishop, M. E., Manjanatha, M. G., Aidoo, A., and Heflich, R. H. (2012) In vivo genotoxicity of furan in F344 rats at cancer bioassay doses. *Toxicol. Appl. Pharmacol. 261*, 164-171.

(54) Chen, T., Mally, A., Ozden, S., and Chipman, J. K. (2010) Low doses of the carcinogen furan alter cell cycle and apoptosis gene expression in rat liver independent of DNA methylation. *Environ. Health Perspect. 118*, 1597-1602.

(55) Chen, T., Williams, T. D., Mally, A., Hamberger, C., Mirbahai, L., Hickling, K., and Chipman, J. K. (2012) Gene expression and epigenetic changes by furan in rat liver. *Toxicology 292*, 63-70.

(56) Maga, J. (1979) Furans in foods. *Crit. Rev. Food Sci. Nutr. 11*, 355-366.

(57) Capurro, P. U. (1973) Effects of exposure to solvents caused by air pollution with special reference to CCl_4 and its distribution in air. *Clin. Toxicol. 6*, 109-124.

(58) Crews, C., and Castle, L. (2007) A review of the occurrence, formation and analysis of furan in heat-processed foods. *Trends Food Sci. Technol. 18*, 365-372.

(59) National Toxicology Program *9th Report on Carcinogens* (2000) US Department of Health and Human Services, Washington DC.

(60) Parmar, D., and Burka, L. T. (1993) Studies on the interaction of furan with hepatic cytochrome P-450. *J. Biochem. Toxicol. 8*, 1-9.

(61) Peterson, L. A. (2006) Electrophilic intermediates produced by bioactivation of furan. *Drug Metabolism Reviews 38*, 615-626.

(62) Vu, C. C., and Peterson, L. A. (2005) Synthesis of [$^{13}C_4$]furan. *J. Label. Compounds Radiopharm. 48*, 117-121.

(63) Berry, M. N., and Friend, D. S. (1969) High-yield preparation of isolated rat liver parenchymal cells: a biochemical and fine structural study. *J. Cell Biol. 43*, 506-520.

(64) Burns, J. A., Butler, J. C., Moran, J., and Whitesides, G. M. (1991) Selective reduction of disulfides by tris(2-carboxyethyl)phosphine. *J. Org. Chem. 56*, 2648-2650.

(65) Krijt, J., Vackova, M., and Kozich, V. (2001) Measurement of homocysteine and other aminothiols in plasma: Advantages of using tris(2-carboxyethyl)phosphine as reductant compared with tri-n-butylphosphine. *Clin. Chem. 47*, 1821-1828.

(66) Henchoz, Y., Schappler, J., Geiser, L., Prat, J., Carrupt, P. A., and Veuthey, J. L. (2007) Rapid determination of pKa values of 20 amino acids by CZE with UV and capacitively coupled contactless conductivity detections. *Anal. Bioanal. Chem 389*, 1869-1878.

(67) Kedderis, G. L., Batra, R., and Koop, D. R. (1993) Epoxidation of acrylonitrile by rat and human cytochromes P450. *Chem. Res. Toxicol. 6*, 866-871.

(68) Gerlo, E., Van Coster, R., Lissens, W., Winckelmans, G., De Meirleir, L., and Wevers, R. (2006) Gas chromatographic-mass spectrometric analysis of N-acetylated amino acids: the first case of aminoacylase I deficiency. *Anal. Chim. Acta 571*, 191-199.

(69) Liebich, H. M., and Forst, C. (1985) Urinary excretion of *N*-acetylamino acids. *J. Chromatogr. 338*, 187-191.

(70) Anders, M. W. (2008) Chemical toxicology of reactive intermediates formed by the glutathione-dependent bioactivation of halogen-containing compounds. *Chem Res. Toxicol. 21*, 145-159.

(71) Ikehata, K., Duzhak, T. G., Galeva, N. A., Ji, T., Koen, Y. M., and Hanzlik, R. P. (2008) Protein targets of reactive metabolites of thiobenzamide in rat liver in vivo. *Chem Res. Toxicol. 21*, 1432-1442.

(72) National Toxicology Program *11th Report on Carcinogens* (2005) US Department of Health and Human Services, Washington DC.

(73) Mugford, C. A., Carfagna, M. A., and Kedderis, G. L. (1997) Furan-mediated uncoupling of hepatic oxidative phosphorylation in Fischer-344 rats: an early event in cell death. *Toxicol. Appl. Pharmacol. 144*, 1-11.

(74) Igarashi, K., and Kashiwagi, K. (2010) Modulation of cellular function by polyamines. *Int J. Biochem. Cell Biol. 42*, 39-51.

(75) Gerner, E. W., and Meyskens, F. L., Jr. (2004) Polyamines and cancer: old molecules, new understanding. *Nat. Rev. Cancer 4*, 781-792.

(76) Casero, R. A., Jr., and Marton, L. J. (2007) Targeting polyamine metabolism and function in cancer and other hyperproliferative diseases. *Nat. Rev. Drug Discov. 6*, 373-390.

(77) Casero, R. A., and Pegg, A. E. (2009) Polyamine catabolism and disease. *Biochem. J. 421*, 323-338.

(78) Wilkinson, C. F., Hetnarski, K., Denison, M. S., and Guengerich, F. P. (1983) Selectivity of 1-phenylimidazole as a ligand for cytochrome P-450 and as an inhibitor of microsomal oxidation. *Biochem. Pharmacol. 32*, 997-1003.

(79) Sava, I. G., Battaglia, V., Rossi, C. A., Salvi, M., and Toninello, A. (2006) Free radical scavenging action of the natural polyamine spermine in rat liver mitochondria. *Free Radic. Biol. Med. 41*, 1272-1281.

(80) Tadolini, B. (1988) Polyamine inhibition of lipoperoxidation. The influence of polyamines on iron oxidation in the presence of compounds mimicking phospholipid polar heads. *Biochem. J. 249*, 33-36.

(81) Lovaas, E., and Carlin, G. (1991) Spermine: an anti-oxidant and anti-inflammatory agent. *Free Radic. Biol. Med. 11*, 455-461.

(82) Ha, H. C., Sirisoma, N. S., Kuppusamy, P., Zweier, J. L., Woster, P. M., and Casero, R. A., Jr. (1998) The natural polyamine spermine functions directly as a free radical scavenger. *Proc. Natl. Acad. Sci. U. S. A 95*, 11140-11145.

(83) Rider, J. E., Hacker, A., Mackintosh, C. A., Pegg, A. E., Woster, P. M., and Casero, R. A., Jr. (2007) Spermine and spermidine mediate protection against oxidative damage caused by hydrogen peroxide. *Amino. Acids 33*, 231-240.

(84) Belle, N. A., Dalmolin, G. D., Fonini, G., Rubin, M. A., and Rocha, J. B. (2004) Polyamines reduces lipid peroxidation induced by different pro-oxidant agents. *Brain Res. 1008*, 245-251.

(85) Norikura, T., Kojima-Yuasa, A., Opare, K. D., and Matsui-Yuasa, I. (2007) Protective effect of gamma-aminobutyric acid (GABA) against

cytotoxicity of ethanol in isolated rat hepatocytes involves modulations in cellular polyamine levels. *Amino. Acids 32*, 419-423.

(86) Yoshida, M., Tomitori, H., Machi, Y., Hagihara, M., Higashi, K., Goda, H., Ohya, T., Niitsu, M., Kashiwagi, K., and Igarashi, K. (2009) Acrolein toxicity: Comparison with reactive oxygen species. *Biochem. Biophys. Res. Commun. 378*, 313-318.

(87) Pignatti, C., Tantini, B., Stefanelli, C., and Flamigni, F. (2004) Signal transduction pathways linking polyamines to apoptosis. *Amino. Acids 27*, 359-365.

(88) Pegg, A. E. (2009) Mammalian polyamine metabolism and function. *IUBMB. Life 61*, 880-894.

(89) Toninello, A., Salvi, M., and Mondovi, B. (2004) Interaction of biologically active amines with mitochondria and their role in the mitochondrial-mediated pathway of apoptosis. *Curr. Med. Chem 11*, 2349-2374.

(90) Wu, C., Kennedy, D. O., Yano, Y., Otani, S., and Matsui-Yuasa, I. (1999) Thiols and polyamines in the cytoprotective effect of taurine on carbon tetrachloride-induced hepatotoxicity. *J. Biochem. Mol. Toxicol. 13*, 71-76.

(91) Schipper, R. G., Penning, L. C., and Verhofstad, A. A. (2000) Involvement of polyamines in apoptosis. Facts and controversies: effectors or protectors? *Semin. Cancer Biol. 10*, 55-68.

(92) Casero, R. A., Jr., and Woster, P. M. (2009) Recent advances in the development of polyamine analogues as antitumor agents. *J. Med. Chem 52*, 4551-4573.

(93) Clements, R. L., Holt, A., Gordon, E. S., Todd, K. G., and Baker, G. B. (2004) Determination of rat hepatic polyamines by electron-capture gas chromatography. *J. Pharmacol. Toxicol. Methods 50*, 35-39.

(94) Marce, M., Brown, D. S., Capell, T., Figueras, X., and Tiburcio, A. F. (1995) Rapid high-performance liquid chromatographic method for the quantitation of polyamines as their dansyl derivatives: application to plant and animal tissues. *J. Chromatogr. B Biomed. Appl. 666*, 329-335.

(95) Statter, M., and Russel, A. (1978) Competitive interrelationships between lysine and arginine in rat liver under normal conditions and in experimental hyperammonemia. *Life Sci. 22*, 2097-2101.

(96) Yamashita, K., and Ashida, K. (1969) Lysine metabolism in rats fed lysine-free diet. *J. Nutr. 99*, 267-273.

(97) Wahllander, A., Soboll, S., Sies, H., Linke, I., and Muller, M. (1979) Hepatic mitochondrial and cytosolic glutathione content and the subcellular distribution of GSH-S-transferases. *FEBS Lett. 97*, 138-140.

(98) Zhou, S., and Decker, E. A. (1999) Ability of carnosine and other skeletal muscle components to quench unsaturated aldehydic lipid oxidation products. *J. Agric. Food Chem 47*, 51-55.

(99) Smith, M. B., and March, J. (2007) Effects of Structure and Medium on Reactivity. In *March's Advanced Organic Chemistry: Reactions, Mechanisms, and Structure* pp 395-416, John Wiley & Sons, Hoboken, NJ.

(100) Wang, Y., and Casero, R. A., Jr. (2006) Mammalian polyamine catabolism: a therapeutic target, a pathological problem, or both? *J. Biochem. 139*, 17-25.

(101) Prior, R. L., Clifford, A. J., and Visek, W. J. (1970) Tissue amino acid concentrations in rats during acute ammonia intoxication. *Am. J. Physiol 219*, 1680-1683.

(102) Prior, R. L., and Visek, W. J. (1972) Effects of urea hydrolysis on tissue metabolite concentrations in rats. *Am. J. Physiol 223*, 1143-1149.

(103) Dawson, R. M. C., Elliott, D. C., Elliott, W. H., and Jones, K. M. *Data for Biochemical Research* (1986) Clarendon Press, Oxford, U.K.

(104) Cochon, A. C., Gonzalez, N., and San Martin de Viale LC. (2002) Effects of the porphyrinogenic compounds hexachlorobenzene and 3,5-diethoxycarbonyl-1,4-dihydrocollidine on polyamine metabolism. *Toxicology 176*, 209-219.

(105) Watanabe, S., Sato, S., Nagase, S., Shimosato, K., and Ohkuma, S. (1999) Effects of methotrexate and cyclophosphamide on polyamine levels in various tissues of rats. *J. Drug Target 7*, 197-205.

(106) Andersson, A. C., Henningsson, S., and Rosengren, E. (1979) Formation of cadaverine in the pregnant rat. *Acta Physiol Scand. 105*, 508-512.

(107) Aikens, D., Bunce, S., Onasch, F., Parker, R., III, Hurwitz, C., and Clemans, S. (1983) The interactions between nucleic acids and polyamines. II. Protonation constants and 13C-NMR chemical shift assignments of spermidine, spermine, and homologs. *Biophys. Chem 17*, 67-74.

(108) Sies, H., Gerstenecker, C., Menzel, H., and Flohe, L. (1972) Oxidation in the NADP system and release of GSSG from hemoglobin-free perfused rat liver during peroxidatic oxidation of glutathione by hydroperoxides. *FEBS Lett. 27*, 171-175.

(109) Sies, H., Brigelius, R., and Akerboom, T. P. M. (1983) Intrahepatic Glutathione Status. In *Functions of Glutathione: Biochemical, Physiological, Toxicological and Clinical Aspects* (Larsson, A., Orrenius, S., Holmgren, A., and Mannervik, B., Eds.) pp 51-64, Raven Press, New York, NY.

(110) Peterson, L. A., Phillips, M. B., Lu, D., and Sullivan, M. M. (2011) Polyamines are traps for reactive intermediates in furan metabolism. *Chem. Res. Toxicol. 24*, 1924-1936.

(111) Ruan, C. Q., Chi, Y. J., and Zhang, R. D. (2010) Kinetics of Hydrolysis of Egg White Protein by Pepsin. *Czech J. Food Sci. 28*, 355-363.

(112) Gottlieb, H. E., Kotlyar, V., and Nudelman, A. (1997) NMR Chemical Shifts of Common Laboratory Solvents as Trace Impurities. *J. Org. Chem. 62*, 7512-7515.

(113) Kirby, A. J. *Stereoelectronic Effects* (2011) Oxford University Press, USA, New York, NY.

(114) Wu, J., and Serianni, A. S. (1991) Ring-opening kinetics of the D-pentofuranuronic acids. *Carbohydr. Res. 211*, 207-217.

(115) Sokolowski, A., Burczyk, B., and Oles, J. (1984) Acetals and ethers. 11. Solubility of alkyl-substiuted 1,3-dioxolanes and 1,3-dioxanes in water. *J. Phys. Chem. 88*, 807-809.

(116) Katritzky, A. R., Odens, H. H., and Voronkov, M. V. (2000) Masked Formylation with 2-Benzotriazolyl-1,3-dioxolane, a Novel Formyl Cation Equivalent. *J. Org. Chem 65*, 1886-1888.

(117) Jo, S., Tanimoto, S., Oida, T., and Okano, M. (1981) The Reaction of 2-Ethoxy-1,3-dithiolane with Carbonyl Compounds. *Bull. Chem. Soc. Japan 54*, 1434-1436.

(118) Mandal, P. K., and Roy, S. C. (1995) Ceric Ammonium Nitrate as a Convenient Catalyst for Chemoselective Thioacetalisation. *Tetrahedron 51*, 7823-7828.

(119) Bandgar, B. P., and Bettigeri, S. V. (2004) Organic reactions in aqueous media: I2-in-water-catlysed rapid and chemoselective oxathioacetalisation of aldehydes under mild conditions. *J. Chem. Res. 2004*, 389-391.

(120) Electronegativity (2012) In *CRC Handbook of Chemistry and Physics* (Haynes, W. M., and Lide, D. R., Eds.) pp 9-99, CRC Press/Taylor and Francis, Boca Raton, FL.

(121) Mohrig, J. R., Hammond, C. N., and Schatz, P. F. (2006) Nuclear Magnetic Resonance Spectroscopy. In *Techniques in Organic Chemistry: Miniscale, Standard Taper Microscale, and Williamson Microscale* (Marshall, C., Anderson, V., Thorne, A., Crawford, J., Wright, C., and Hull, P., Eds.) pp 267-341, W.H. Freeman and Company, New York, NY.

(122) Barbasiewicz, M., and Makosza, M. (2006) Intermolecular reactions of chlorohydrine anions: acetalization of carbonyl compounds under basic conditions. *Org. Lett. 8*, 3745-3748.

(123) Ranu, B. C., and Das, A. (2004) Molten Salt as a Green Reaction Medium: Efficient and Chemoselective Dithioacetalization and Oxathioacetalization of Aldehydes Mediated by Molten Tetrabutylammonium Bromide. *Austral. J. Chem. 57*, 605-608.

(124) Li, Y., Zhang, X., Ren, T., and Zhou, J. (2006) New Catalytic Methods for the preparation of Acetals from Alcohols and Aldehydes. *Synthetic Communications 36*, 1679-1685.

(125) Chen, L. J., DeRose, E. F., and Burka, L. T. (2006) Metabolism of furans in vitro: ipomeanine and 4-ipomeanol. *Chem. Res. Toxicol. 19*, 1320-1329.

(126) Cooper, A. J., Pinto, J. T., and Callery, P. S. (2011) Reversible and irreversible protein glutathionylation: biological and clinical aspects. *Expert. Opin. Drug Metab Toxicol. 7*, 891-910.

(127) Tang, X., Sayre, L. M., and Tochtrop, G. P. (2011) A mass spectrometric analysis of 4-hydroxy-2-(E)-nonenal modification of cytochrome c. *J. Mass Spectrom. 46*, 290-297.

(128) Zhu, X., and Sayre, L. M. (2007) Long-lived 4-oxo-2-enal-derived apparent lysine michael adducts are actually the isomeric 4-ketoamides. *Chem Res. Toxicol. 20*, 165-170.

(129) Sigolo, C. A., Di Mascio, P., and Medeiros, M. H. (2007) Covalent modification of cytochrome c exposed to trans,trans-2,4-decadienal. *Chem. Res. Toxicol. 20*, 1099-1110.

(130) Zhu, X., Gallogly, M. M., Mieyal, J. J., Anderson, V. E., and Sayre, L. M. (2009) Covalent cross-linking of glutathione and carnosine to proteins by 4-oxo-2-nonenal. *Chem. Res. Toxicol. 22*, 1050-1059.

(131) Fisher, A. A., Labenski, M. T., Malladi, S., Chapman, J. D., Bratton, S. B., Monks, T. J., and Lau, S. S. (2011) The frequency of 1,4-benzoquinone-lysine adducts in cytochrome c correlate with defects in apoptosome activation. *Toxicol. Sci. 122*, 64-72.

(132) Xu, K. Y. (1989) Acid dissociation constant and apparent nucleophilicity of lysine-501 of the alpha-polypeptide of sodium and potassium ion activated adenosinetriphosphatase. *Biochemistry 28*, 6894-6899.

(133) Diaz-Moreno, I., Garcia-Heredia, J. M., Diaz-Quintana, A., and De la Rosa, M. A. (2011) Cytochrome c signalosome in mitochondria. *Eur. Biophys. J. 40*, 1301-1315.

(134) Martinou, J. C., Desagher, S., and Antonsson, B. (2000) Cytochrome c release from mitochondria: all or nothing. *Nat. Cell Biol. 2*, E41-E43.

(135) Kawai, C., Prado, F. M., Nunes, G. L., Di Mascio, P., Carmona-Ribeiro, A. M., and Nantes, I. L. (2005) pH-Dependent interaction of cytochrome c with mitochondrial mimetic membranes: the role of an array of positively charged amino acids. *J. Biol. Chem. 280*, 34709-34717.

(136) Liebler, D. C., Meredith, M. J., and Guengerich, F. P. (1985) Formation of glutathione conjugates by reactive metabolites of vinylidene chloride in microsomes and isolated hepatocytes. *Cancer Res. 45*, 186-193.

(137) Liebler, D. C., Latwesen, D. G., and Reeder, T. C. (1988) S-(2-chloroacetyl)glutathione, a reactive glutathione thiol ester and a putative metabolite of 1,1-dichloroethylene. *Biochemistry 27*, 3652-3657.

(138) Martin, E. J., and Forkert, P. G. (2005) 1,1-Dichloroethylene-induced mitochondrial damage precedes apoptotic cell death of bronchiolar epithelial cells in murine lung. *J. Pharmacol. Exp. Ther. 313*, 95-103.

(139) Welch, W., Ahmad, S., Airey, J. A., Gerzon, K., Humerickhouse, R. A., Besch, H. R., Jr., Ruest, L., Deslongchamps, P., and Sutko, J. L. (1994) Structural determinants of high-affinity binding of ryanoids to the vertebrate skeletal muscle ryanodine receptor: a comparative molecular field analysis. *Biochemistry 33*, 6074-6085.

(140) Hnizda, A., Santrucek, J., Sanda, M., Strohalm, M., and Kodicek, M. (2008) Reactivity of histidine and lysine side-chains with diethylpyrocarbonate --

a method to identify surface exposed residues in proteins. *J. Biochem. Biophys. Methods 70*, 1091-1097.

(141) Thornalley, P. K. (1991) Esterification of reduced glutathione. *Biochem. J. 275 (Pt 2)*, 535-539.

(142) Mayr, C. M., and Schieberle, P. (2012) Development of stable isotope dilution assays for the simultaneous quantitation of biogenic amines and polyamines in foods by LC-MS/MS. *J. Agric. Food Chem 60*, 3026-3032.

(143) Chen, G. G., Fiori, L. M., Mamer, O. A., and Turecki, G. (2011) High-resolution capillary gas chromatography in combination with mass spectrometry for quantification of three major polyamines in postmortem brain cortex. *Methods Mol. Biol. 720*, 427-436.

(144) La Torre, G. L., Saitta, M., Giorgia, P. A., Di Bella, G., and Dugo, G. (2010) High performance liquid chromatography coupled with atmospheric pressure chemical ionization mass spectrometry for sensitive determination of bioactive amines in donkey milk. *J. Chromatogr. A 1217*, 5215-5224.

(145) Bello-Fernandez, C., Packham, G., and Cleveland, J. L. (1993) The ornithine decarboxylase gene is a transcriptional target of c-Myc. *Proc. Natl. Acad. Sci. U. S. A 90*, 7804-7808.